**UNIVERSITY OF SOUTHAMPTON**

FACULTY OF ENGINEERING, SCIENCE AND MATHEMATICS

SCHOOL OF ELECTRONICS AND COMPUTER SCIENCE

# PERFORMANCE ENHANCEMENT OF FREQUENCY HOPPING SYSTEMS IN THE PRESENCE OF INTERFERENCE

*by*

Sohail Ahmed

B.E. (Avionics), M. S. E. E.

*A thesis submitted in partial fulfilment of the requirements for the award of Doctor of Philosophy at the University of Southampton*

August 2007

SUPERVISORS:

Professor Lajos Hanzo, Dip Ing, MSc, PhD, FIEEE, DSc, FREng

and Dr. Lie-Liang Yang, MSc, PhD, SMIEEE

School of Electronics and Computer Science

University of Southampton, United Kingdom

"You see things; and you say, 'Why?' But I dream things that never were; and I say, 'Why not?'"

George Bernard Shaw in "Back to Methuselah" (1921), part 1, act 1.

Dedicated

to my loving and caring wife, my adorable son, my parents and my siblings,
and to all those less fortunate people of my country for the betterment of whom I am expected to work after I complete my education in this university.

UNIVERSITY OF SOUTHAMPTON

ABSTRACT

Faculty of Engineering, Science and Mathematics

School of Electronics and Computer Science

Doctor of Philosophy

**PERFORMANCE ENHANCEMENT OF FREQUENCY HOPPING SYSTEMS IN THE PRESENCE OF INTERFERENCE**

by Sohail Ahmed

Frequency hopping (FH) constitutes a powerful spread spectrum technique historically used for combatting intentional jamming or interference. In FH systems, the carrier frequency is hopped in a pseudo-random fashion across a large set of legitimate frequencies under the control of a random sequence generator. This perpetual hopping of the transmitted frequency renders the system robust against interference and jamming. The motivation of this thesis is to present a study of various performance enhancement techniques used in frequency hopping assisted non-coherent $M$-ary frequency shift keying (MFSK) systems encountering interference or jamming. The first three chapters focus on the performance investigation of FH in the presence of jamming, while the enhancement of the multiple access capability of FH is the subject of fourth and fifth chapters.

In Chapter 1, the basic philosophy of frequency hopping is introduced and two main types of FH systems, namely slow frequency hopping (SFH) and fast frequency hopping (FFH) are discussed. Furthermore, a comparative study of various diversity combining techniques used in FFH assisted MFSK systems is presented, when the system is exposed to partial band noise jamming (PBNJ) and multitone jamming (MTJ).

In Chapter 2, the performance of Reed Solomon (RS) coded SFH-MFSK systems using various low-complexity erasure insertion (EI) schemes is investigated, when communicating over Rayleigh fading channels in the presence of MTJ. Three different EI schemes are considered, which are based on the output threshold test (OTT), on the ratio threshold test (RTT) and on the joint maximum output-ratio threshold test (MO-RTT). The relevant statistics of these EI schemes are investigated mathematically and based on these statistics, the performance of the EI schemes is evaluated in the context of error-and-erasure RS decoding and compared to the performance of error-correction only decoding.

In Chapter 3, a novel method of bit error ratio (BER) analysis of product combining (PC) used in FFH-MFSK has been proposed. This method employs Mellin transform which is a convenient tool for determining the probability density function of a product of random variables. The relevant decision statistics have been derived in semi-closed form when the system operates in a Rayleigh fading channel contaminated by PBNJ. Derivation of these statistics facilitates computation of the system's BER. This method facilitates for the first time the analysis of the FFH PC receiver using modulation orders higher than 2.

In Chapter 4, the FFH-MFSK system is considered in a land mobile communication system, where a

base station (BS) supports multiple users. The ability of a range of diversity combining schemes to combat multi-user interference is evaluated. Furthermore, two successive interference cancellation techniques have been proposed for multi-user detection at the BS receiver. These techniques employ various reliability tests to carry out symbol detection in multiple stages. Our simulation results show that an attractive BER performance can be achieved when these techniques are employed in a FFH-MFSK system operating in multiple access scenarios.

In Chapter 5, iterative decoding designed for FFH-MFSK is investigated. The soft information generated by the FFH demodulator and passed to the outer decoder is derived for various channel models. The convergence behaviour of the iterative scheme is investigated employing Extrinsic Information Transfer (EXIT) charts, casting light on the various parameters that influence its iterative gain. Furthermore, a novel interference cancellation scheme that operates in conjunction with a soft-input-soft-output decoder is proposed. Our simulation results demonstrate that this scheme significantly enhances the multiple access capability of the FFH system.

In Chapter 6, the findings of the thesis have been summarised and future research ideas have been proposed. Specifically, a novel ultra-wideband (UWB) system based on multistage FFH is proposed as an alternative to the classical impulse-radio UWB systems. This FFH-based UWB scheme allows multiple users to access a wide bandwidth and offers the advantages of reduced interference and improved performance for a high number of users. Furthermore, in Chapter 5 a FFH-assisted differential space time block coded (DSTBC) system has been proposed, which amalgamates the attractive aspects of both the FFH and the DSTBC systems, benefitting from both spatial as well as frequency diversity. A few other research ideas have also been discussed briefly.

# Acknowledgement

First of all, I would like to thank my supervisors, Professor Lajos Hanzo and Dr. Lie-Liang Yang, for their invaluable guidance and inspiration during my work. I consider myself very fortunate to be a student of these learned men and have greatly benefitted from their vast experience, meticulous methods of research and their sincerity towards pursuit of knowledge.

Many thanks are also due to the academic staff of the Communications Research Group, especially Dr. Stephan Weiss, for their useful guidance in my research. I also owe many personal thanks to all my colleagues of the Communications Group, particularly to Dr. Soon Xin Ng, Dr. Jos Akhtman, Dr. Ming Jiang, Dr. Osamah Alamri, Mr. Andreas Wolfgang, Mr. Muhammad El-Hajjar, Dr. Jin Wang, Dr. Xiang Liu, Mr. Qasim Zeeshan Ahmed and Mr. Raja Ali Riaz for their timely help, whenever I needed it. Special thanks are due to Mr. Nan Wu and Mr. Rob Maunder with whom I collaborated to produce research work that resulted in IEEE publications and that became part of my thesis.

I also wish to thank the Higher Education Commission (HEC), Pakistan, the EPSRC, UK and EU under the auspices of the Phoenix and Newcom projects and the School of ECS, University of Southampton for the financial support I received from them.

Finally I would like to thank my parents, sisters and brothers back in Pakistan for their love and prayers for me. And I owe special gratitude to my beloved wife, Tallat, who is more concerned about my success and well being than I am, and to my adorable son, Saalaar, for being a beautiful part of my life.

# List of Publications

1) S. Ahmed, L. L. Yang and L. Hanzo, "Erasure Insertion in RS-Coded SFH MFSK Subjected to Tone Jamming and Rayleigh Fading", in *Proceedings of IEEE Vehicular Technology Conference '05 Fall*, (Dallas, US), September 2005, Volume 2, Page(s):917 - 921.

2) S. Ahmed, L. L. Yang and L. Hanzo, "Erasure Insertion in RS-Coded SFH MFSK Subjected to Tone Jamming and Rayleigh Fading", accepted for publication as Letter to *IEEE Transactions on Vehicular Technology.*

3) S. Ahmed, L. L. Yang and L. Hanzo,"Diversity Combining for Fast Frequency Hopping Multiple Access Systems Subjected to Nakagami-m Fading", in *Proceedings of Sixth International Conference on 3G and Beyond - 3G 2005*, Savoy Place, London UK), 4-6th November 2005.

4) S. Ahmed, L. L. Yang and L. Hanzo,"Successive Interference Cancellation in Clipped and Product Combining aided FFH Multi-User Systems", *IEEE 64th Vehicular Technology Conference, 2006. VTC '06 Spring*, Melbourne, May 2006, Volume 5, Page(s):2188 - 2192.

5) S. Ahmed, L. L. Yang and L. Hanzo,"Mellin Transform Based Performance Analysis of Fast Frequency Hopping Using Product Combining", *IEEE 64th Vehicular Technology Conference, 2006. VTC '06 Spring*, Melbourne, May 2006, Volume 4, Page(s):1635 - 1639.

6) S. Ahmed, L. L. Yang and L. Hanzo, "Mellin Transform Based Performance Analysis of FFH $M$-ary FSK Using Product Combining for Combatting Partial Band Noise Jamming", submitted in October, 2006 for publication as Letter to *IEEE Transactions on Vehicular Technology.*

7) N. Wu, S. Ahmed, O. Alamri, L. L. Yang and L. Hanzo, "A Sphere-Packing Modulated Space-Frequency Diversity Aided FFH-Assisted DSTBC System", *IEEE Wireless Communications and Networking Conference*, (Las Vegas, USA), Volume 4, 3-6 April 2006 Page(s):1881 - 1886.

8) S. Ahmed, S. X. Ng, L. L. Yang and L. Hanzo, "Iterative Decoding and Soft Interference Cancellation in Fast Frequency Hopping Multiuser System Using Clipped Combining", accepted for publication in *Proceedings of the IEEE Wireless Communications and Networking Conference, WCNC 2007, March 2007 Page(s):723 - 728 . The paper was awarded the "First runner up" award in the PHY/MAC layer track.*

9) S. Ahmed, L. L. Yang and L. Hanzo,"Mellin Transform Based Performance Analysis of FFH M-ary FSK Using Product Combining Against Partial Band Noise Jamming", in *Vehicular Technology Conference, 2007. VTC2007-Spring. IEEE 65th*, April 2007 Page(s):1901 - 1905.

10) S. Ahmed, R. G. Maunder, L. L. Yang, S. X. Ng and L. Hanzo, "Joint Source Coding, Unity Rate Precoding and FFH-MFSK Modulation using Iteratively Decoded Irregular Variable Length Coding", accepted for publication in *IEEE 66th Vehicular Technology Conference, 2007. VTC '07 Fall*, Baltimore, 30 September - 3 October 2007.

11) S. Ahmed, L. L. Yang, L. Hanzo and F. Guo, "Soft Decoding Assisted Interference Cancellation in a Non-binary LDPC Coded Fast Frequency Hopping Multiuser System Using Product Combining", accepted for publication in *IEEE 66th Vehicular Technology Conference, 2007. VTC '07 Fall*, Baltimore, 30 September - 3 October 2007.

12) S. Ahmed, L. L. Yang and L. Hanzo, "Iterative Decoding and Soft Information Assisted Interference Cancellation in FFH-MA Communicating over Nakagami-$m$ Channels", submitted in May, 2007 to *IEEE Transactions on Wireless communications.*

13) S. Ahmed, R. G. Maunder, L. L. Yang, and L. Hanzo, "Iterative Detection of Three-Stage Concatenated FFH-MFSK", submitted in July, 2007 to *IEEE Transactions on Wireless communications.*

# Glossary

| | |
|---|---|
| **AWGN** | Additive White Gaussian Noise |
| **BER** | Bit Error Ratio |
| **BFSK** | Binary Frequency Shift Keying |
| **BS** | Base-Station |
| **CDF** | Cumulative Distribution Function |
| **CDMA** | Code Division Multiple Access |
| **CD** | Conventional Detection |
| **CF** | Characteristic Function |
| **CSI** | Channel State Information |
| **EED** | Error-and-Erasure Decoding |
| **EI** | Erasure Insertion |
| **EXIT** | EXtrinsic Information Transfer |
| **FFH** | Fast Frequency Hopping |
| **FH** | Frequency Hopping |
| **HDD** | Hard Decision Decoding |
| **HDMV** | Hard Decision Majority Vote |
| **HLMV** | Hard Limiting Majority Vote |
| **ID** | Iterative Decoding |
| **IrVLC** | Irregular variable length coding |

**LLR** Log-Likelihood Ratio

**MA** Multiple Access

**MFSK** $M$-ary Frequency Shift Keying

**MIMO** Multiple Input Multiple Output

**MO-RTT** Maximum Output-Ratio Threshold Test

**MRC** Maximum Ratio Combining

**MS** Mobile Station

**MTJ** Multitone Jamming

**MUD** Multi User Detection

**MUI** Multi-User Interference

**NED** Normalized Envelope Detection

**NSC Code** Non-Systematic Convolutional Code

**OS-NED** Order Statistics Normalized Envelope Detection

**OTT** Output Threshold Test

**PBNJ** Partial Band Noise Jamming

**PC-SLC-SIC** Product Combining and Soft Limiting Combiner based Successive Interference Cancellation

**PDF** Probability Density Function

**PSK** Phase Shift Keying

**QAM** Quadrature Amplitude Modulation

**RSC Code** Recursive, Systematic Convolutional Code

**RS** Reed Solomon code

**RTT** Ratio Threshold Test

**SDD** Soft Decision Decoding

**SFH** Slow Frequency Hopping

**SIC** Successive Interference Cancellation

**SISO** Soft-Input-Soft-Output

**SLC-SIC** Soft Limiting Combiner based Successive Interference Cancellation

**SLC** Soft Limiting Combiner

**Soft-PC-SIC** Soft Information and Product Combiner based Successive Interference Cancellation

**Soft-SLC-SIC** Soft Information and Soft Limiting Combiner based Successive Interference Cancellation

**STBC** Space-Time Block Code

**SUD-ID** Single User Detection-Iterative Decoding

**SUD** Single User Detection

**UWB** Ultra-Wideband

**VLC** Variable Length Coding

# List of Symbols

- $\mathbf{a}_k$: PN address vector of the $k$th user, in the context of the FFH-MA system.
- $b$: Number of bits per transmitted symbol;
- $B$: Bandwidth of an FSK tone;
- $C$: Threshold corresponding to the clipped diversity combining;
- $\mathbf{D}^{(k)}$: The dehopped received matrix of the $k$th user in the context of HLMV combining;
- $E_b$: Transmitted energy per bit;
- $E_h$: Transmitted energy per hop;
- $E_j$: Tone jammer energy per hop;
- $E_s$: Transmitted symbol energy;
- $f_c$: Carrier frequency;
- $f_l$: Hopping frequency during the $l$th hop;
- $f_m$: Frequency corresponding to the $m$th FSK tone;
- $f(U_{ml})$: A function of the square-law detector output corresponding to the $l$the hop and the $m$th FSK tone;
- $(G, G_r)$: Generator polynomial of a convolutional code;
- $h(t)$: Channel induced time dependent gain;
- $I_{M,a}$, $I_{M,p}$, $I_{M,e}$: *a priori*, *a posteriori* and extrinsic mutual information of the MFSK based demodulator;
- $I_{D,a}$, $I_{D,p}$, $I_{D,e}$: *a priori*, *a posteriori* and extrinsic mutual information of the outer decoder;
- $I_{P,a}$, $I_{P,p}$, $I_{P,e}$: *a priori*, *a posteriori* and extrinsic mutual information of the unity-rate decoder (precoder);
- $I_{V,a}$, $I_{V,p}$, $I_{V,e}$: *a priori*, *a posteriori* and extrinsic mutual information of the VLC decoder;
- $(j)$: When used as a subscript with any symbol indicates the presence of jamming;
- $j_m(t)$: Gaussian distributed noise interference in the $m$th FSK tone;

- $j_{mc}(t)$: Cosine component of the noise interference at the square-law detector output, corresponding to the $m$th FSK tone;
- $j_{ms}(t)$: Sine component of the noise interference at the square-law detector output, corresponding to the $m$th FSK tone;
- $J_m$: Component of the noise interference at the end of square-law detector corresponding to the $m$th FSK tone;
- $(k)$: When used as a superscript with any symbol denotes the $k$th user;
- $K$: Number of information bits (or symbols) in a block of coded bits (or symbols);
- $K_s$: Alphabet size of the IrVLC source symbol;
- $l$: Index of the frequency hops, $l = 0, 1, \ldots, L-1$
- $L$: Number of hops per symbol of the FFH system, also referred to as diversity order;
- $\max(\cdot)$: Maximum or largest;
- $\max 2(\cdot)$: Second largest;
- $M$: Modulation order;
- $n_m$: Component of the AWGN at the square-law detector output corresponding to the $m$th FSK tone;
- $n_m(t)$: Gaussian distributed thermal noise in the $m$th FSK tone;
- $n_{mc}(t)$: Cosine component of the AWGN at the square-law detector output;
- $n_{ms}(t)$: Sine component of the AWGN at the square-law detector output;
- $N_0$: AWGN power spectral density;
- $N_b$: Number of FH bands in the total FH bandwidth;
- $N_{ID}$: Number of iterative decoding iterations between the inner and outer components;
- $N_{IN}$: Number of LDPC decoder's inner iterations;
- $N_J$: Jamming signal power spectral density;
- $N_{SIC}$: Number of SIC iterations;
- $N_U$: Number of users in a multiple access system;
- $N_v$: Number of VLC components in an IrVLC scheme (Chapter 5);
- $O(.)$: Landau symbol denoting asymptotes;

- $P$: Transmitted signal power;
- $P_b$: Probability of bit error;
- $P_e$: Probability of erasure;
- $P_J$: Power of a single jamming tone ;
- $P_{NJ}$: Total power of noise jammer;
- $P_s$: Probability of symbol error;
- $P_t$: Probability of error after erasure;
- $P_{TJ}$: Total power of tone jammer;
- $q$: MTJ duty factor - the ratio of the number of interference tones to the number of MFSK bands in the total hopping bandwidth;
- $q_0$: Worst-case MTJ duty factor
- $Q$: Number of interference tones in the spread spectrum bandwidth;
- $r(t)$: Received signal;
- $r_i$: Rank or index, in the context of the order statistics and non-parametric diversity combining methods;
- $\mathcal{R}[\cdot]$: Residue of a complex integral;
- $R_b$: Number of bits per second, the bit rate;
- $R_c$: Code rate;
- $R_h$: Number of hops per second, the hop rate;
- $R_s$: Number of symbols per second, the symbol rate;
- $\mathbf{R}$: Received signal matrix at the output of the square-law detector before de-hopping; the element $R_{ml}$ represents the square-law detector output corresponding to the $m$th FSK tone and the $l$th hop;
- $\mathbf{R}^{(th)}$: Received signal matrix at the output of the square-law detector before de-hopping and after thresholding in the context of HLMV combining; the element $R_{ml}^{(th)}$ represents the square-law detector output corresponding to the $l$th hop and the $m$th FSK tone;
- $S_k$: Transmitted symbol vector of the $k$th user, in the context of the FFH-MA system;
- $s_k(t)$: Frequency hopping transmitted signal corresponding to the $k$th user;

- $s_m(t)$: MFSK modulated signal corresponding to the $m$th FSK tone;
- $T_h$: Time duration of one hop;
- $T_s$: Time duration of one symbol;
- $\mathbf{U}$: The dehopped received signal matrix at the square-law detector output; the element $U_{ml}$ represents the square-law detector output corresponding to the $m$th FSK tone and the $l$th hop, after de-hopping;
- $U_{ml}^{(r)}$: Ranked square-law detector output corresponding to the $m$th FSK tone and the $l$th hop, in the context of order statistics diversity combining;
- $v$: Constraint length of a convolutional code;
- $W_{ss}$: Spread spectrum bandwidth;
- $w_i$: Multiplicative factor corresponding to the $i$th index, in the context of the non-parametric diversity combining methods;
- $X_k$: $M$-ary information symbol of the $k$th user, in the context of the FFH-MA system;
- $Y_1$: Largest of the $M$ detection decision variables in the context of MFSK-based demodulation schemes;
- $Y_2$: Second largest of the $M$ detection decision variables in the context of MFSK-based demodulation schemes;
- $\mathbf{Z}$: Diversity combiner output vector; the element $Z_m$, also referred to as the decision variable, corresponds to the $m$th FSK tone;
- $\alpha$: Random variable representing the channel induced attenuation factor;
- $\alpha_j$:Random variable representing the channel induced attenuation factor corresponding to the jamming tone signal;
- $\alpha_s$: Random variable representing the channel induced attenuation factor associated with the desired signal;
- $\eta$: Spectral efficiency;
- $\gamma_b$: Signal to noise power ratio per transmitted bit, same as bit energy to noise power spectral density ratio $E_b/N_0$;
- $\gamma_c$: Signal to noise power ratio per coded symbol;
- $\gamma_j$: Signal to noise power ratio per transmitted symbol;
- $\Gamma(\cdot)$: Gamma function [1];

- $\delta$: Detection threshold in the context of the HLMV combining scheme;
- $\delta_c$: Cancellation coefficient in the context of SIC schemes;
- $\epsilon$: Ratio of the 2nd largest to the largest of symbol probabilities, in the context of the Soft SIC schemes of Chapter 5;
- $\epsilon_T$: Reliability test threshold, in the context of the Soft SIC schemes of Chapter 5;
- $\Phi(a, b, c)$; Hypergeometric function [1];
- $\lambda$: Ratio of the largest to the second largest (or of the second largest to the largest) in the context of ratio threshold test (RTT);
- $\lambda^{(cc)}$: Appropriately chosen RTT threshold when FFH-MFSK receiver employs clipped combining;
- $\lambda^{(pc)}$: Appropriately chosen RTT threshold when FFH-MFSK receiver employs product combining;
- $\Lambda_{M,a}$, $\Lambda_{M,p}$, $\Lambda_{M,e}$: *a priori*, *a posteriori* and extrinsic LLRs of the MFSK based demodulator;
- $\Lambda_{D,a}$, $\Lambda_{D,p}$, $\Lambda_{D,e}$: *a priori*, *a posteriori* and extrinsic LLRs of the outer decoder;
- $\Lambda_{P,a}$, $\Lambda_{P,p}$, $\Lambda_{P,e}$: *a priori*, *a posteriori* and extrinsic LLRs of the unity-rate decoder (precoder);
- $\Lambda_{V,a}$, $\Lambda_{V,p}$, $\Lambda_{V,e}$: *a priori*, *a posteriori* and extrinsic LLRs of the VLC decoder;
- $\Pi$ or $\pi$: Interleaver;
- $\Pi^{-1}$ or $\pi^{-1}$: De-interleaver;
- $\rho$: PBNJ duty factor;
- $\rho_0$: Worst case PBNJ duty factor;
- $\sigma_J$: Standard deviation of the noise jammer;
- $\sigma_N$: Standard deviation of the AWGN;
- $\tau$: Time delay;
- $\theta$: Channel induced phase;
- $\theta_j$: Phase associated with the jamming tone signal;
- $\theta_m$: Phase associated with the $m$th FSK tone, resulting from the effects of MFSK and frequency hopping;
- $\theta_s$: Phase associated with the desired signal;
- $\varrho_{ij}$: Measure of correlation between $i$th and $j$th component;

- $\varphi_k(t)$: Phase associated with the $k$th frequency hopping tone;
- $\varphi_m$: Phase associated with the $m$th FSK tone, resulting from the effects of MFSK;
- $\xi_{km}$: $k$th order moment of the square-law detector outputs corresponding to the $m$th FSK tone;

# Contents

Chapter 1

# Diversity Combining Methods Used in Fast Frequency Hopping Systems

## 1.1 Introduction

Over the past few decades spread spectrum (SS) systems have attracted considerable attention in the field of wireless communications, owing to their ability to simultaneously support multiple users within a given band [2–8]. The family of SS systems has found applications in wireless networks, cellular telephony, satellite communications and wide area networks [9–14]. Typical SS systems are characterised by the use of a very wide bandwidth, which is significantly wider than that required for narrowband transmission. More importantly, all users share the same bandwidth by employing user-specific codes often aimed at minimising the inter-user interference. The family of ubiquitous code division multiple access (CDMA) schemes, which is based on the SS techniques, is capable of supporting higher number of users than less sophisticated multiple access systems, such as frequency division multiple access (FDMA) and time division multiple access (TDMA). There are other advantages of SS or CDMA as well. For instance, they provide higher immunity to multipath effects; in fact, they actively benefit from multipath propagation with the aid of diversity combining. They are also more difficult to jam owing to transmission over a wide bandwidth and their performance degrades gracefully upon increasing the number of users in comparison to FDMA and TDMA [7, 8, 11–14].

The SS systems are broadly categorised into two main types: direct sequence (DS) SS and frequency hopping (FH) SS. In DS spreading, the information-bearing signal is multiplied by a spreading code sequence consisting of very low-duration chips compared to the symbol interval. The resultant signal is spread across a very wide bandwidth at a low power. Consequently, it appears *noise-like* to receivers which cannot despread it since they do not possess knowledge of the specific spreading code. By contrast, the intended receiver can decode the information signal with the aid of the knowledge of the DS code sequence. Thus,

DS spreading exhibits a certain grade of secrecy as well as efficient use of the spectrum. The family of DS-CDMA systems is the more commercially popular type of SS system. In 1993, DS-CDMA was adopted for Interim Standard (IS) 95 systems for the third generation cellular systems. It is also likely to find more applications in the future generations of wireless communications systems [14].

In contrast to the DS-CDMA, in FHSS, the carrier frequency is hopped in a pseudo-random fashion across a large set of legitimate frequencies spread over a wide bandwidth. The frequency pattern is controlled by a random sequence generator. This perpetual change of the transmitted frequency renders the system robust against jamming of the desired signal. Furthermore, since the transmitted signal utilizes a particular frequency for a short duration only, the interference to/from another transmitter is experienced for a brief interval of time, rendering the FH system attractive in terms of employment in multiuser scenarios.

Historically, owing to their attractive anti-jamming properties and low probability of interception, FH systems were initially employed in military communications [2–5, 15–17]. However, FH systems have also been considered as an alternative to DS-CDMA [18–22]. Moreover, they have been considered for other applications such as satellite communications [17, 23], as an alternative to Ultra Wideband (UWB) systems [24] and as personal communications systems [25–27].

A number of researchers have carried out the comparison of DS and FH based CDMA systems [21, 27–30]. There are certain advantages that FH has over DS-CDMA. For example, it is far less vulnerable to the near-far problem and is more immune to multipath effects [11, 28]. Moreover, in [29] it has been argued that creating a DS-based synchronous communication system is more challenging compared to a FH-based one, because in DS system the synchronization has to be maintained to the level of chip duration, which is typically orders of magnitude smaller than a FH dwell interval. Finally, owing to its frequency agility, FH is better equipped against noise jamming. However, FH systems are more prone to narrowband interference and are less bandwidth efficient. In order to exploit the advantages of both, hybrid systems employing both DS and FH have also been investigated [31–33].

**Fast Frequency Hopping:** The number of times a FH system changes its frequency in a second is referred to as the *hop rate*. On the basis of the relation between the hop rate and symbol rate, FH systems may be classified into two basic types [2–5, 34]. In one of the types, which is referred to as *slow frequency hopping* (SFH), one or several data symbols are transmitted per frequency hop. That is, if $T_h$ is the hop duration which is defined as the time for which one of the many possible frequencies is transmitted, and $T_s$ is the symbol duration, then in SFH systems, we have $T_s = LT_h$ and $R_h = LR_s$, where $R_h = 1/T_h$ and $R_s = 1/T_s$ are the hop rate and the symbol rate respectively and $L \leq 1$. The second type of FH systems is constituted by the family of *fast frequency hopping* (FFH). In FFH, in contrast to SFH, a single data symbol is transmitted using several frequencies. Hence, in FFH, the relationship between the hop duration $T_h$ and symbol duration $T_s$ may still be represented by the same equation of $T_s = LT_h$, but with $L > 1$. Therefore, in FFH, the frequency is hopped $L$ times within one data symbol duration. This process may be viewed as the repetition of each symbol $L$ number of times for a total duration of $T_s$.

It can be inferred from its basic definition that a FFH based system has two important advantages over a SFH system. The first advantage is that the probability of jamming a FFH signal, or what is generally referred to as the probability of interception, is reduced considerably. This is because, the transmitted signal uses a certain frequency for a significantly shorter duration of time, compared to the case of SFH. That is, we have $T_h \ll T_s$ in FFH. Therefore, FFH systems are more robust against so-called follower or repeat-back jammers [3].

The second advantage of using FFH schemes is that the same symbol is replicated during several hops, each of which corresponds to a different time slot and a different frequency. This lends both time and frequency diversity to the system and provides the receiver with replicas of the same signal. In fading channels, the various replicas of the signal will experience independent fading, if the spacing between adjacent FFH frequencies is at least equal to the channel's coherence bandwidth [34]. In this case, there is a high probability that at least one of the replicas will suffer from less severe fading as compared to the case when there is no diversity. Hence, when the signals received in various hops are combined in the receiver, the detrimental effects of the fading channel are considerably reduced. Consequently, diversity reduces the error probability under fading conditions. In other words, the signal to noise ratio (SNR) required for achieving a certain bit error ratio (BER) is reduced compared to a system dispensing with diversity reception. This reduction of the required SNR to achieve a certain BER is usually referred to as *diversity gain*. The inherent time and frequency diversity of FFH systems is also an effective anti-jamming measure.

The signal energy received during the various hops can, hence, be combined using one of the numerous established diversity combining techniques designed for FFH systems [35–45]. It is well known that the performance of FFH, especially in the presence of jamming or interference, is dependent upon the type of diversity combining scheme employed in the receiver.

There are certain other advantages of FFH systems. First, they are immune to correlated fading and to the problems associated with it. This is because each symbol is transmitted using a different frequency in FFH systems, and hence the fading experienced by the FFH symbols becomes uncorrelated, regardless of the degree of fading correlation. Consequently, burst errors do not dramatically affect the performance of coded FFH systems and hence no channel interleaving is needed. For the same reason, FFH systems are almost immune to multipath effects. To elaborate a little further, since a transmitted symbol hops to another frequency in every hop interval, copies of the symbol arriving from multiple paths after a delay in excess of one hop duration do not interfere with the original signal. However, in this treatise we will focus our attention on the advantages FFH systems enjoy by virtue of the inherent diversity.

Naturally, there are also certain problems associated with the use of FFH systems. Firstly, FFH requires a higher bandwidth than an equivalent SFH system. This is because in order to maintain orthogonality between FH tones, the bandwidth of a single FH frequency should at least equal the hop rate, which is higher in FFH than in SFH. The issue of orthogonality between FH tones will be discussed in greater detail in Section 1.3.1. Thus, for a given transmission rate, FFH systems are less spectrally efficient than SFH systems and their

bandwidth requirements increase in proportion to their hop rate. Secondly, the implementation of a FFH transmitter and receiver requires frequency synthesizers whose switching speed should be able to support the hop rate. The higher the number of hops per symbols, the higher is the switching speed that the synthesizer should support. The implementation of a frequency synthesizer capable of high switching speeds can be challenging. However, it ought to be borne in mind that the hop rate is a function of both the symbol rate and the number of hops per symbols. Thus, if the symbol rate is low, the associated hop rate will be correspondingly low.

Lastly, we mention that a range of FH systems have been proposed which are more spectrally efficient owing to use of nonorthogonal FH tones [46, 47]. However, nonorthogonal FH tones lead to increased interference between adjacent tones, thereby yielding inferior error rates. Likewise, phase shift keying (PSK) or differential phase shift keying (DPSK) considered in conjunction with FH [18, 48–51] impose less stringent bandwidth requirements as compared to $M$-ary frequency shift keying (MFSK) based FH. However, PSK systems are coherent by nature while DPSK schemes are suited to slowly fading channels only. Hence, FH systems, and in particular the FFH systems in which hop duration is very small, prohibit the use of coherently detected modulation schemes and are therefore typically implemented in conjunction with noncoherent MFSK. That is because MFSK is typically suitable for fast fading channels or for schemes where channel estimation may not be practicable. Therefore, in this treatise unless otherwise stated, we assume the employment of MFSK modulation and completely orthogonal FH tones.

**Overview of the Thesis:** In this treatise, we will be focusing our attention on the family of FHSS systems, with special emphasis on FFH systems. The thesis can be conceptually divided into two parts: the first part, consisting of the first three chapters, focuses on the investigation of the performance of SFH and FFH in the presence of jamming, while the investigation of FFH communicating in multi-user scenarios is the subject of fourth and fifth chapters. In both parts, we will investigate both uncoded as well as coded FH systems. A brief overview of all the chapters is given below.

This chapter presents a comparison of the various diversity combining methods used in FFH assisted non-coherent FSK receivers. The structure of the rest of this chapter is as follows. In Section 1.2, a brief summary of the state-of-the-art is presented. Section 1.3 contains a description of the FFH assisted MFSK transmitter, the corresponding receiver using linear combining, and a discussion on the nature of jamming signals typically encountered by FFH systems. Section 1.4 discusses various nonlinear diversity combining techniques, briefly highlighting their operating principles. Section 1.5 contains a more detailed discussion, complemented by our simulation results, on some of the more important nonlinear diversity combining techniques. Finally, Section 1.6 presents a summary of this chapter.

In Chapter 2, the performance of Reed Solomon (RS) coded SFH-MFSK system using various low-complexity erasure insertion (EI) schemes is investigated, when communicating over Rayleigh fading channels in the presence of tone jamming. The relevant statistics of the EI schemes considered are investigated mathematically and the performance of the EI schemes is evaluated in the context of error-and-erasure RS

decoding and compared to the performance of error-correction only decoding.

In Chapter 3, a novel method of BER analysis of product combining (PC) scheme used in FFH-MFSK systems has been discussed. This method is based on the Mellin transform which assists us in determining the probability density function of the product of the received signals during various hops. Relevant statistics have been derived in semi-closed form when the system operates in a Rayleigh fading channel contaminated by noise jamming. With the aid of these statistics the BER expression of the system can be computed.

In Chapter 4, the FFH-MFSK is considered in a multiuser communications system. In this scenario, the performance of a range of diversity combining schemes is evaluated from the viewpoint of combatting multi-user interference. Furthermore, two novel interference cancellation techniques are proposed for further enhancing the multiple access capability of FFH.

In Chapter 5, iterative decoding designed for FFH-MFSK is investigated. The soft information generated by the FFH demodulator and passed to the outer decoder is derived for various channel models. The convergence behaviour of the iterative scheme is investigated employing Extrinsic Information Transfer (EXIT) charts. Furthermore, a novel interference cancellation scheme that operates in conjunction with soft-input-soft-output decoders is proposed.

Finally, in Chapter 6, our findings are summarised and future research areas are discussed.

## 1.2 Review of Previous Works

This section discusses the contributions of various researchers in the field of diversity combining schemes designed for FFH systems combatting jamming. Although, the principles behind the diversity combining schemes will be outlined in greater detail later in this chapter, a brief comment about each of them has been made in this section.

One of the earliest notable contributions on FFH diversity combining was provided by Lee *et al.* [35–37]. The researchers analyzed linear combining, noise-normalization combining and clipping based combining when used in non-coherent binary FSK (BFSK) receivers operating in additive white Gaussian noise (AWGN) channel, when exposed to partial band noise jamming (PBNJ). Linear combining constitutes a simple summing of the energy detector outputs corresponding to each MFSK tone received during all hops of a transmitted symbol. By contrast, in the context of noise-normalization combining, the received energy components are normalized by the associated noise power received during each hop before they are combined, implying that a highly noise-contaminated energy component is de-weighed [36]. Finally, in the context of the clipping based combining, energy detector outputs received during all hops are clipped at a certain level before combining [36]. Lee *et al.* [35–37] concluded that whereas linear combining provides no diversity gain, noise-normalization and clipping based combining schemes do enhance the achievable performance of FFH BFSK receiver in the presence of AWGN and PBNJ. Their analysis, however, as-

sumed perfect noise power estimation in case of noise normalization combining and perfect clipping level information in case of clipping based combining. Robertson *et al.* [52, 53] improved upon the analysis of noise-normalization combining when used in an MFSK receiver by taking into account the effect of errors in the noise power measurement under various fading conditions. The authors concluded that the performance of this receiver is satisfactory against PBNJ even in conjunction with 50% error in the noise power estimation. In [54], Li *et al.* investigated a so-called maximum likelihood diversity combining scheme which required the knowledge of received SNR as well as of which hops are jammed. The authors [54] however demonstrated that the noise-normalization combining yields performance very close to the maximum likelihood diversity combining scheme. An analysis of the clipped based combining, also known as clipper combiner or soft limiter combiner (SLC) was performed by Yue [48] for FFH operating in multiuser scenario.

Lee *et al.* [37] also analysed the self-normalization based FFH BFSK receiver albeit under no fading conditions and showed that this combining scheme constitutes an effective tool against partial-band noise interference. In self-normalization combining, the energy received corresponding to each MFSK tone is divided by the sum of the energy detector outputs corresponding to all the MFSK tones for each hop. The energy detector outputs thus normalized are combined at the end of all hops. A significant advantage that self-normalization combining has over many other schemes is that it does not need side information which is required, for example, in the case of clipping based combining and noise-normalization combining. Robertson *et al.* [39, 40] analyzed the self-normalization combining scheme when used in FFH assisted BFSK and MFSK under Rician fading conditions in partial band interference. It was shown in these contributions that while self-normalization combining is quite effective in combatting partial band interference, its performance degrades if severe fading is encountered.

March and Ritcey [55] have contributed by providing the analysis of the order statistics based diversity combining method when used in FFH assisted non-coherent BFSK in the presence of PBNJ. In the context of this method, the approach used is to sort the energy detector outputs received in all the hops corresponding to each MFSK tone in ascending order of their magnitude. This scheme has been found to be very effective since it allows to identify jammed hops to a significant extent.

One diversity combining scheme that has attracted considerable attention is the product combining scheme. In the context of product combining, a product of the energy components, rather than the sum as in linear combining, corresponding to each MFSK tone received in all the hops is used in detection process. In [56–61], various methods have been employed to analyze the FFH-BFSK scheme using product combining under various channel conditions contaminated by PBNJ.

Let us now review some of the contributions in the open literature made towards analysis of various diversity combining schemes when FFH operates in the presence of multitone jamming (MTJ). Wang and Jiang [65] have analyzed the performance of the linear combining FFH assisted MFSK receiver communicating in fading channels under multitone jamming. Orr and Rice [70] analyzed the performance of

the self-normalization combining FFH-MFSK receiver communicating under multitone jamming. Teh *et al.* [63] have investigated self-normalization combining based BFSK receiver in Rician fading conditions in the presence of MTJ, while Wang and Jiang [66] have extended the analysis of this combining scheme to MFSK-based FFH receivers. The findings of these authors show that self-normalization combining scheme is capable of providing useful performance improvement in the context of FFH assisted non-coherent MFSK receivers operating in MTJ.

Teh *et al.* [42, 71] have compared the achievable performance of linear and clipping based combining BFSK receivers, while Chang and Lee [67] analyzed the clipping based combining aided MFSK receiver under fading conditions. In multiple tone jamming, product combining based BFSK receiver has also been analyzed at length by some researchers. Teh *et al.* have contributed the mathematical analysis for BFSK receiver employing product combining, both in AWGN [43] and in Rician fading conditions [64]. Product combining scheme is particularly suitable in MTJ because it provides the ability to reject tone interference and also because it does not need side information.

| Researcher(s) | Contribution | | | | Year | References |
|---|---|---|---|---|---|---|
| | Modulation | Combining Scheme | Jamming Type | Channel | | |
| Lee *et al.* | BFSK | Linear | PBNJ | AWGN | 1984 | [35] |
| Lee *et al.* | BFSK | AGC, SLC | PBNJ | AWGN | 1984 | [36] |
| Lee *et al.* | BFSK | NED | PBNJ | AWGN | 1986 | [37] |
| Robertson,Ha | BFSK | NED | PBNJ | Rician | 1992 | [39] |
| Robertson,Lee | MFSK | Linear, NED | PBNJ | Rician | 1992 | [40] |
| Robertson *et al.* | MFSK | AGC | PBNJ | Rician | 1992,1998 | [52,53] |
| Robertson *et al.* | MFSK | RSC | PBNJ | Rician | 1992 | [62] |
| Huo and Alouini | BFSK | PCR | PBNJ | Rayleigh | 2000-01 | [59–61] |
| Lim *et al.* | BFSK | PCR | PBNJ | Nakagami | 1998 | [57] |
| Chang and Tu | BFSK | PCR | PBNJ | Rician | 2005 | [58] |
| Teh *et al.* | BFSK | NED | MTJ | Rician | 2000 | [63] |
| Teh *et al.* | BFSK | SLC | MTJ | Rician | 1998 | [42] |
| Teh *et al.* | BFSK | PCR | MTJ | AWGN | 1999 | [43] |
| Teh *et al.* | BFSK | PCR | MTJ | Rician | 2000 | [64] |
| Teh *et al.* | BFSK | PCR | PBNJ | Rayleigh | 1997 | [56] |
| Wang, Jiang | MFSK | Linear | MTJ | Rician | 2000 | [65] |
| Jiang, Wang | MFSK | NED | MTJ | Rician | 2002 | [66] |
| March, Ritcey | BFSK | OSC | PBNJ | AWGN | 1989 | [55] |
| Chang, Lee | MFSK | Linear, SLC | MTJ | AWGN | 1994 | [67] |
| Shen, Su | BFSK | RSC | MTJ | Rician | 2003 | [45] |
| Gulliver, Felstead | MFSK | Moments | PBNJ, MTJ | AWGN | 1993 | [68] |
| Gulliver, Felstead | MFSK | Non-Parametric | PBNJ, MTJ | AWGN | 1995 | [69] |

Linear=Linear combining, NED=Self-normalization combining, SLC=Soft limiter or clipper based combining, PCR=Product combining receiver, AGC=Noise normalization combining, OSC=Order statistics based combining, RSC=Ratio statistics based combining, Moments=Moments based combining, Non-Parametric=Non-parametric combining method
PBNJ=Partial band noise jamming, MTJ=Multitone jamming.

**Table 1.1:** Summary of contributions of various researchers towards analysis of diversity combining techniques used in FFH assisted MFSK systems to combat jamming.

Gulliver *et al.* [72] proposed new methods for analyzing the linear combining receiver when FFH-MFSK operates under the multitone jamming. Gulliver *et al.* [44] have also compared performance of various diversity combining techniques. Han and Teh have also analyzed the FFH-MFSK receiver using maximum likelihood combining [73, 74]. In pursuit of better performance under MTJ, Gulliver and Felstead [68] have also analyzed the moments based diversity combining methods which involve the moments of various orders of the energy detector outputs and some non-parametric methods based diversity combining [69], which use sorting of these outputs followed by various operations which will be discussed in detail in Section 1.4. A summary of major contributions in the area of diversity combining for FFH systems has been tabulated in Table 1.1.

## 1.3 FFH Assisted Non-Coherent MFSK System

Having provided a brief overview of a range of diversity combining techniques, let us now consider FFH-assisted non-coherent MFSK in more detail. We commence our discourse by outlining the basic philosophy of FFH assisted non-coherent MFSK systems in this section. In Section 1.3.1, a brief introduction to the principles of FFH-MFSK transmitter in comparison with its SFH counterpart with characterization of the corresponding transmitted signal is given. This discussion is followed in Section 1.3.2 by the description of the jamming signals. The received signal is characterised in Section 1.3.3, when the transmitted signal is contaminated by jamming and corrupted by various channel impairments. The receiver configuration designed for detection of the resultant signal is also described in this section. The linear combining scheme is discussed in Section 1.3.4 and a brief discussion on some related issues are included in Sections 1.3.5 and 1.3.6.

### 1.3.1 FFH-MFSK Transmitter

In FH systems, the instantaneous carrier frequency is hopped across a set of legitimate frequencies under the control of a *pseudo-noise* (PN) sequence generator. In FH systems typically non-coherent data modulation schemes are employed because the carrier phase is difficult to estimate within the hop duration, which is typically a small fraction of the symbol duration. The most common non-coherent modulation scheme used in conjunction with FH systems is MFSK. Let us first consider a SFH transmitter using MFSK modulation. The operation of a SFH-MFSK transmitter may be understood by referring to Figures 1.1 and 1.2. As shown in Figure 1.1, the MFSK modulated signal [34] $s_m(t)$ modulates a carrier $\cos(2\pi f_l t)$ having a frequency $f_l$, which is generated by a frequency synthesizer working under the control of a PN sequence. The transmitted signal during one symbol duration may be expressed as

$$s(t) = \sqrt{2P} P_{T_s}(t - iT_s - lT_h) \cos\left\{2\pi \left[f_m + f_l\right] t + \varphi_m + \varphi_l\right\} \tag{1.1}$$

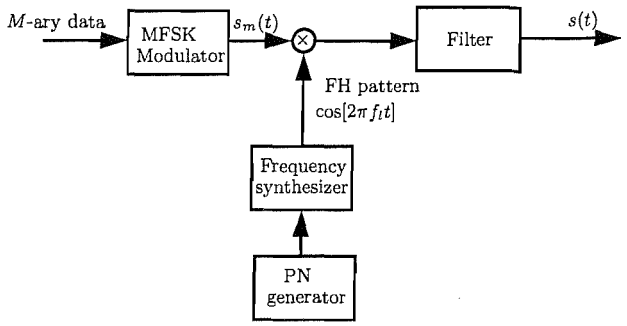


**Figure 1.1:** Transmitter schematic of FH SS systems using MFSK data modulation

where $P$ is the power of the transmitted signal, $f_m$ is the MFSK tone's frequency, $f_l$ is the $l$th frequency in the frequency hopping sequence during the time interval $lT_h \leq t < (l+1)T_h$ and $T_h$ represents the FH dwell interval or the hop duration. Furthermore, in Equation (1.1), $P_{T_s}(t)$ denotes a rectangular signalling waveform associated with one symbol duration and $\varphi_l$ and $\varphi_m$ represent the phases associated with the $l$th hopping tone and the $m$th MFSK tone, respectively. In this treatise, we will refer to the transmitted or activated MFSK tone as the *signal* tone and all other ($M$-1) tones as *non-signal* tones.

In Figure 1.2, the operating principle of a SFH SS system using MFSK modulation is shown in a graphical form, where it is assumed that the FH system employs six frequency slots for hopping and 8FSK data modulation. Furthermore, it is assumed that the FH dwell time $T_h$ is twice the MFSK symbol duration $T_s$, i.e. we have $T_h = 2T_s$, which implies that two MFSK symbols are transmitted within each FH dwell time. The FH pattern used in Figure 1.2 is $\{1, 3, 2, 6, 4, 5; 1, 3, 2, \cdots\}$, which is a periodic sequence. As shown in Figure 1.2, the FH signal transmitted within an MFSK symbol duration constitutes a narrow-band signal, whose frequency is determined by the current FH frequency controlled by the FH pattern, while the frequency of the current MFSK tone is determined by the transmitted data.

Now let us consider an FFH system where a single MFSK symbol is transmitted with the aid of several FH frequencies. This FFH system has the same transmitter schematic as the SFH system of Figure 1.1. However, in this type of FH SS systems, we have $L = T_s/T_h > 1$, where $L$ is an integer which is also termed as the diversity order of the system since the value of $L$ determines the number of times the symbol transmission is repeated. In contrast to Equation (1.1), in the context of the FFH-MFSK, the transmitted signal during the $i$th symbol duration may be expressed as

$$s(t) = \sum_{l=0}^{L-1} \sqrt{2P} P_{T_h}(t - iT_s - lT_h) \cos\left\{2\pi \left[f_m + f_l\right] t + \varphi_m + \varphi_l)\right\} \tag{1.2}$$

where all parameters are the same as in Equation (1.1), but $P_{T_h}(t)$ denotes a rectangular signalling waveform associated with one hop duration. The corresponding transmitted signal during the $l$th hop duration

$$s_l(t) = \sqrt{2P} P_{T_h}(t - iT_s - lT_h) \cos\left\{2\pi \left[f_m + f_l\right] t + \varphi_m + \varphi_l)\right\}. \tag{1.3}$$

Note that in this treatise we characterise a FFH system with $L > 1$ number of hops per symbol. Correspondingly, $L \leq 1$ implies a SFH system.

The graphical representation of a FFH scheme using six FH slots and 8FSK data modulation is shown in Figure 1.3, where we assume that one 8FSK symbol is transmitted using two FH slots, i.e. we assume that $T_s = 2T_h$. The FH pattern used in Figure 1.3 is the same as that used in Figure 1.2, namely $\{1, 3, 2, 6, 4, 5; 1, 3, 2, \cdots\}$.

**Orthogonality of FFH tones:** Assuming that $L = T_s/T_h$ is an integer, in FFH systems the frequencies are designed to be orthogonal for satisfying the zero coherence condition, i.e.

$$\begin{aligned} \varrho_{ij} &= \frac{L}{E_s}\int_0^{T_h} s_i(t)s_j(t)dt \\ &= \frac{1}{T_h}\int_0^{T_h} \cos\left[2\pi(f_i - f_j)t + \varphi_i - \varphi_j\right] dt \\ &= 0,\ i \neq j \end{aligned} \tag{1.4}$$

where $s_i(t)$ and $s_j(t)$ are the signals transmitted during $i$th and $j$th hop durations, respectively, and expressed in Equation (1.3) and $E_s = PT_s$ represents the transmitted symbol energy. Therefore, the frequency spacing between two frequencies must obey [34]

$$f_i - f_j = \frac{n}{T_h},\ n = 1, 2, \ldots \tag{1.5}$$

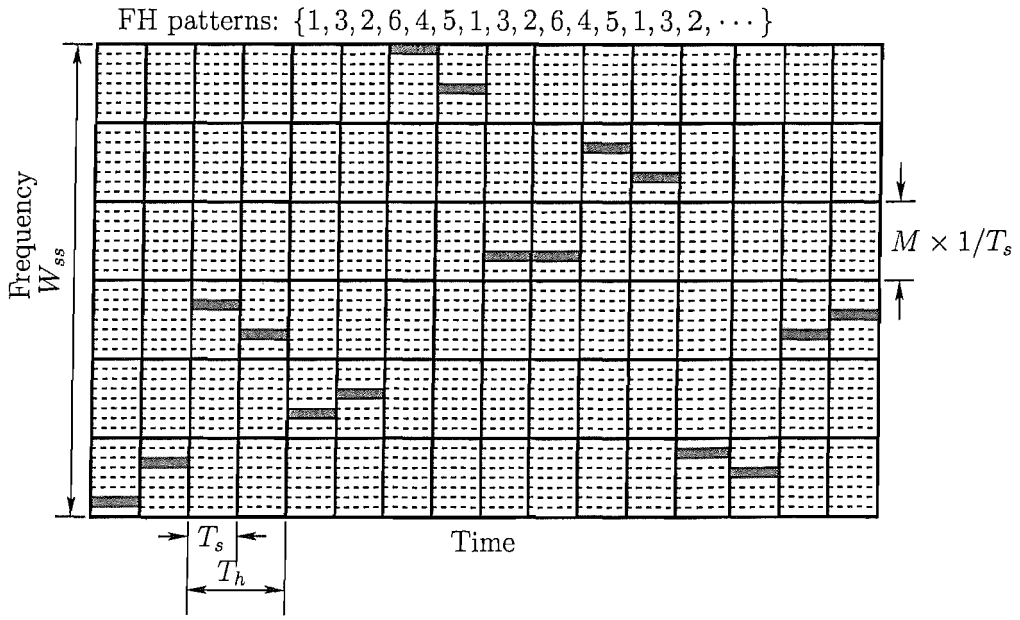


**Figure 1.2:** Graphical representation of SFH SS signals using six frequency slots and 8FSK data modulation, where two 8FSK symbols are transmitted within one FH slot, i.e. we have $T_h = 2T_s$. The transmitted symbols are given by $\{2, 6, 6, 3, 3, 5, 8, 4, 3, 3, 6, 3, 7, 5, 3, 5\}$, assuming they take on values from $1, \ldots, 8$.

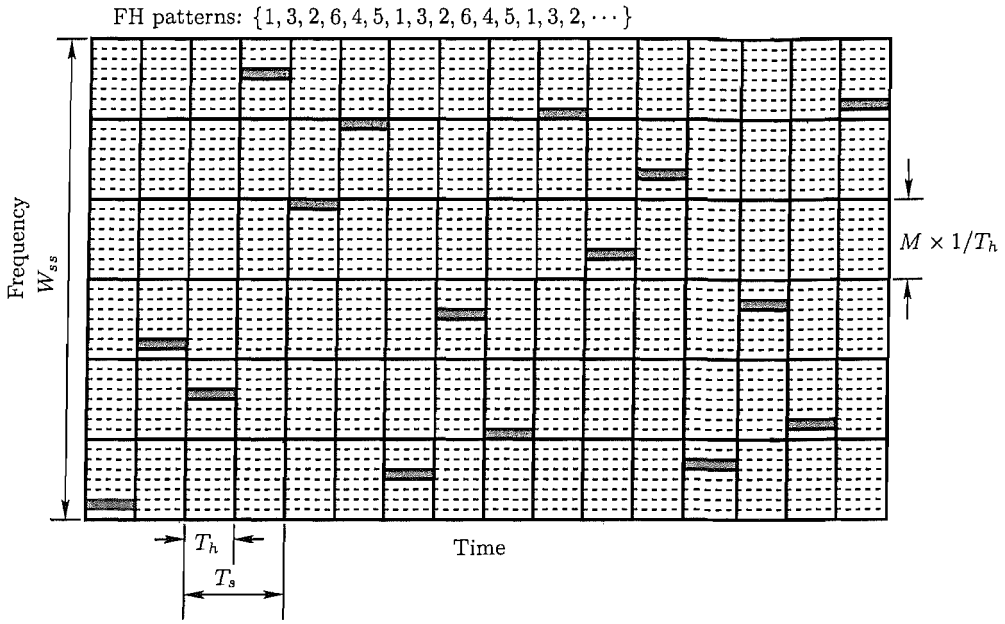


**Figure 1.3:** Graphical representation of FFH (FFH)SS signals using six frequency slots and 8FSK data modulation, where one 8FSK symbol is transmitted within two FH slots, i.e. we have $T_s = 2T_h$. The transmitted symbols are given by $\{2, 5, 7, 5, 1, 3, 6, 2\}$.

Given a minimum frequency spacing of $1/T_h$, the frequency set of

$$\mathbf{F} = \left\{ \frac{0}{T_h}, \frac{1}{T_h}, \cdots, \frac{M-1}{T_h} \right\} \tag{1.6}$$

is capable of guaranteeing the creation of an orthogonal MFSK scheme. The bandwidth of one FSK tone $B$, which is also equal to the bandwidth of one hop, is hence given by $B = 1/T_h$.

**Spread spectrum bandwidth:** The FFH-MFSK signal is hopped randomly over a SS bandwidth of $W_{ss}$ which is significantly larger than the signal bandwidth. The ratio $W_{ss}/B$ is generally referred to as the FH *spreading gain* or *spread factor*. The bandwidth $W_{ss}$ is divided into $N_b$ MFSK bands, each of which is divided into $M$ bins corresponding to $M$ FSK tones, where $M$ is the order of modulation. This implies that there are a total of $M \times N_b$ hopping frequencies. Mathematically, we can say that $W_{ss} = M \times N_b \times B$. When the transmitted signal hops, it may acquire any one of the $M$ bins in that band, depending upon which FSK tone has been chosen. It should be noted that in this chapter, the term *bin* corresponds to a frequency or tone and frequency *band* or hop band defines a set of $M$ bins or tones.

### 1.3.2 Jamming Signals

Before we discuss the noncoherent FFH-MFSK receiver, we provide a brief discussion in the section on the key types of jamming signals encountered by FH systems. Any undesired signal that happens to be present, whether intentionally or not, at the same frequency (or in the same frequency band) as the desired transmitted signal constitutes a *jamming* signal or *interference*. The presence of a jamming signal degrades

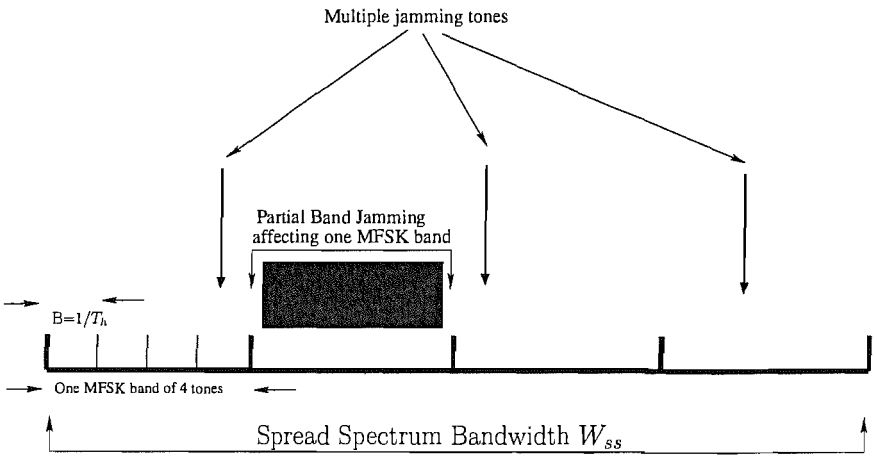


**Figure 1.4:** Graphical representation of frequency hopping bands, partial band noise jamming and multiple jamming tones; modulation level $M = 4$, number of FH bands $N_b = 4$ and number of jamming tones $Q = 3$

the achievable performance of a receiver system impairing its ability to correctly demodulate the transmitted symbols. The strategy of an intentional jammer is usually to concentrate enough power in one specific frequency band or tone and, at the same time, improve the probability of jamming by covering as much of the total spread spectrum bandwidth as possible.

Two important types of jamming/interference will be discussed in this section [2, 3, 34, 38]. The first type of jamming is referred to as *partial band noise jamming* (PBNJ), while the second type is referred to as as *multitone jamming* (MTJ). A graphical representation of the SS bandwidth and the jamming signals is shown in Figure 1.4.

**PBNJ:** In the context of PBNJ, the jamming signal has typically a flat spectrum similar to that of Gaussian noise, but it may affect only part of the system's bandwidth. The source of noise jamming may be intentional as in the case of military communication systems [2–5, 15–17] where enemy jammers try to disrupt the friendly communication. But it may be caused by microwave sources and lighting devices operating adjacent to a FH network such as Bluetooth radio system [19, 20]. The military communication systems usually operate using a significant part of the frequency spectrum. Similarly, a number of commercial FH networks utilize the Industrial Scientific Medical (ISM) band. Thus both types of communication systems are susceptible to partial-band or full-band noise from intentional or unintentional jammers.

The fraction of bandwidth jammed is generally referred to as the jammer's *duty factor* and is denoted by $\rho$; hence, $\rho W_{ss}$ is the bandwidth affected by the jamming signal [38]. The fraction $\rho$ also represents the probability of a tone being jammed. When we have $\rho = 1$, the entire system bandwidth is affected by interference and hence the probability of being jammed is 1, i.e. 100%. If the total noise jammer power is denoted by $P_{NJ}$, then the single sided power spectral density of PBNJ is $P_{NJ}/W_{ss}$.

It can be seen that although increasing $\rho$ improves the chances of jamming a signal from the jammer's point of view, the power of the jamming signal is, however, spread over a larger bandwidth. Consequently, the power concentrated on a single frequency is low. Based on the above arguments it may be stated that,

from the jammers' point of view, a trade off exists between the jamming duty factor $\rho$ and the effective jamming power, assuming a fixed total jammer power. A high value of $\rho$ increases the probability of jamming the transmitted signal but the resultant jamming power becomes relatively low. By contrast, using a low $\rho$ reduces the probability of jamming the transmitted signal; however, in this case, more power will be concentrated in a specific bandwidth. Generally, an optimum value of $\rho$, which is often referred to as the worst-case $\rho$, denoted by $\rho_0$, can be chosen in order to result in the worst detection performance and, hence, in the highest probability of error for the desired receiver [2,3,34,38,39]. The value of worst-case $\rho$ depends on the signal to jamming power ratio $E_b/N_J$, the SNR $E_b/N_0$ and the diversity order $L$. It has been shown that the value of $\rho_0$ tends to unity as $L$ is increased and as the fading becomes more severe [38,39,75].

**MTJ:** In the context of MTJ, the jamming power is concentrated in a few continuous-wave tones instead of being spread over a large bandwidth. The frequency of the jamming tone may coincide with that of any of the MFSK tones transmitted by the desired transmitter. Again, the MTJ may be intentional or accidental. In the former case, the jamming may result from an intentional jammer transmitting continuous-wave tones at the same frequency as that employed by the target communications system in order to degrade its performance. In the latter case, the interference source may be other users of the same communications network or of an adjacent network.

The number of jamming tones, which is denoted by $Q$, is an important parameter of MTJ signal that aims to jam an FFH assisted MFSK system. Generally, two broad categories of MTJ are defined. The first category is referred to as the band MTJ [75,76] and corresponds to the scenario when the jammer distributes the jamming tones according to the MFSK band structure and may assign exactly $n = 1, 2, \ldots, M-1$ tones within an MFSK band. In case of the other category of MTJ, known as the independent MTJ [77], the jammer spreads the jamming tones all over the SS bandwidth independent of the band structure of the MFSK.

A specific sub-category of band MTJ, which is often referred to as *$n$=1-band MTJ*, has been termed as the worst-case jamming by Houston [38, 75] since it results in the poorest desired signal detection performance. In the context of $n = 1$-band MTJ, at the most one jamming tone is present in a band of $M$ FSK tones. To elaborate further, whenever an MFSK band is jammed, it will contain exactly $n = 1$ jamming tone in the context of $n = 1$-band MTJ; however, certain bands may not be jammed at all and would contain no jamming tone. This concept can be understood with the aid of Figure 1.4 where 3 of the 4 MFSK bands contain one jamming tone each. Thus the MTJ in Figure 1.4 is a case of $n$=1-band MTJ. It can be intuitively seen why $n$=1-band MTJ is the worst case jamming. This is because it allows the jamming power to be spread more or less evenly over the entire hopping bandwidth instead of concentrating it to a narrower band. Note that to cause a detection error, the jammer has to coincide its frequency with that of any of the non-signal tones. Since each hopping band contains a single signal tone and $M-1$ non-signal tones, it is wasteful from the jammer's perspective to distribute its power across more than one jamming tones in a hopping band. It can be readily seen that $0 \leq Q \leq N_b$ for $n = 1$-band MTJ and $0 \leq Q \leq N_b \times M$ for

independent MTJ. We will consider only the case of $n = 1$-band MTJ in this chapter, since it constitutes the worst-case jamming.

Although various definitions of the MTJ duty factor have been put forward [75–77], we define it as the ratio of the jamming tones to the number of the MFSK bands in the total $W_{ss}$ bandwidth. That is MTJ duty factor is given by $q = Q/N_b$. Thus, $q = 3/4$ in Figure 1.4.

Similar to $\rho$ in case of PBNJ, a high value of $q$ increases the probability of jamming the transmitted signal but the resultant jamming power becomes low whereas a low value of $q$ reduces the probability of jamming the transmitted signal but results in a higher power being concentrated in the jamming tone. A suitable value of $Q$ (from the jammer's perspective) has to be based on an attractive compromise between achieving sufficiently high probability of jamming the target hop band and concentrating sufficient power in the jamming signal. This specific compromise will correspond to the worst-case $q$ usually referred to as $q_0$, the role of which is analogous to the value of $\rho_0$ in PBNJ. The related literature suggests that $q_0$ also tends towards unity when the fading becomes severe or when the associated diversity order increases [75–77].

The distribution of jamming power in MTJ may be *contiguous* or *non-contiguous*. In the contiguous case, the jamming tones are co-located or, in other words, lie in adjacent slots. Whereas, when tones are non-contiguous, they are dispersed randomly and widely over the hopping bandwidth [38]. In Figure 1.4, the three jamming tones are non-contiguous in relation to each other. As mentioned previously, in PBNJ, the jamming is usually assumed to be contiguous, since it is technically challenging to spread the noise jamming power non-contiguously. Furthermore, for the sake of convenience in the analysis, it is generally assumed that if one tone is noise jammed in a hop band, then all the other MFSK tones in the hop band are also affected by the noise jamming [38]. In other words, the jamming signal completely covers the hop band having a bandwidth of $M \times B$.

In closing we note that there are other types of jamming techniques which often may be deemed to be special cases or variations of the MTJ or the PBNJ discussed above. For example, the case of $\rho = 1$ in the context of PBNJ corresponds to wideband noise jamming.

### 1.3.3 FFH Non-Coherent MFSK Receiver

In this section, we discuss the configuration of an FFH assisted non-coherent MFSK receiver employing linear combining used for detecting the transmitted signal discussed in Section 1.3.1. Figure 1.5 shows the block diagram of such a receiver. If the transmitted signal given by Equation (1.3) passes through a noise- and interference-free channel, the signal at the input to this receiver during the $l$th hop of duration $T_h$ can be expressed as

$$r_l(t) = \sqrt{2P}\cos\left\{2\pi\left[f_m + f_l\right](t-\tau) + \theta_m\right\}, \tag{1.7}$$

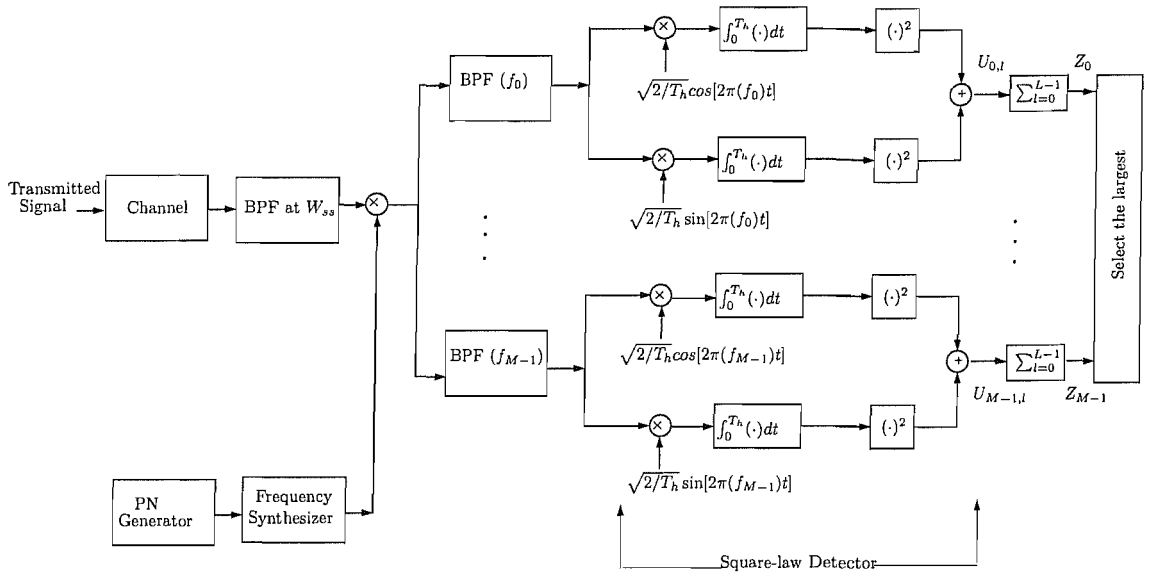


**Figure 1.5:** Block diagram of a FFH assisted non-coherent MFSK Receiver using linear combining

where $\theta_m$ is the phase resulting from the joint effects of MFSK and frequency hopping, while $\tau$ is the transmission delay. The receiver is made up a bandpass filter (BPF), a frequency de-hopper, $M$ branches of the demodulator and finally a decision device [2, 34]. The BPF at $W_{ss}$ filters out any frequency that is not part of the SS bandwidth. The de-hopper consists of a PN generator, that is identical to and aligned to the PN generator used in the transmitter shown in Figure 1.1, a frequency synthesizer and a multiplier. We will assume throughout this treatise that the transmitter's and the receiver's frequency hopping sequences are perfectly synchronized. When this assumption holds, the de-hopper is able to remove the hopping frequency from the received signal. Each of the $M$ demodulator branches corresponds to one MFSK tone and consists of a BPF set at that tone frequency, followed by a square-law detector [34] and then a diversity combiner. In Figure 1.5, a linear combiner is shown which performs linear summation of the signals received in all hops. The $M$ outputs of the diversity combiners constitute the decision variables. The detection decision is made on the basis of maximum likelihood principle in favour of the decision variable having the highest magnitude [34]. The index of the chosen decision variable, hence, yields the estimate of the transmitted symbol. A detection error occurs if magnitude of the decision variable corresponding to any of the non-signal tones exceeds the one corresponding to the transmitted signal tone.

The resultant filtered and dehopped baseband MFSK signal corresponding to the $m$th FSK tone, $m = 0, 1 \ldots, M-1$, at the input of the square law detector during the $l$th hop is given by

$$r_m(t) = \sqrt{2P}\cos\left\{2\pi\left(f_m\right)t + \theta_m\right\}. \tag{1.8}$$

Now let us consider the effects of the presence of AWGN and both types of jamming discussed in Section 1.3.2 on the detection process.

#### 1.3.3.1 Effects of PBNJ and AWGN

If the transmitted signal is corrupted both by AWGN as well as PBNJ, the received signal given in Equation (1.8) may be expressed in the following modified form as:

$$r_m(t) = \sqrt{2P}\cos\{2\pi\,(f_m)\,t + \theta_m\} + n_m(t) + j_m(t), \tag{1.9}$$

where $n_m(t)$ is zero-mean AWGN having a power $\sigma_N^2 = BN_0$, $N_0$ is the one-sided power spectral density of the AWGN, FH tone bandwidth is given by $B = 1/T_h$ and $j_m(t)$ is the PBNJ interference which, like AWGN, is Gaussian but jamming a portion $\rho$ of the SS bandwidth $W_{ss}$. The signal to noise ratio may be expressed as $E_b/N_0$, where $E_b = E_s/b$ is the energy per bit, $b = \log_2 M$ is the number of bits per symbol while $E_s = PT_s$ is the energy per transmitted symbol. Similarly, $E_h = E_s/L = PT_h$ may be defined as the energy per symbol per hop.

Let us focus our attention on the energy of the transmitted signal relative to the PBNJ signal. Let $P_{NJ}$ be the total noise jamming power and $N_J = P_{NJ}/W_{ss}$ its power spectral density. Then, the jamming noise power concentrated on one FH tone is given by [2,3,35–38]

$$\sigma_J^2 = \frac{N_J B}{\rho}. \tag{1.10}$$

The effective signal to jammer power ratio (SJR) is given by $E_b/N_J$. Now we are in a position to express the signal power to total interference (thermal noise plus PBNJ) power ratio in a single FH tone as [35–37]

$$SIR = \frac{P}{\sigma_N^2 + \sigma_J^2} = \frac{E_s/T_s}{BN_0 + BN_J/\rho} = \frac{E_s}{LN_0 + LN_J/\rho}, \tag{1.11}$$

where we have used the relation of $B = L/T_s = 1/T_h$.

Let us now investigate the noncoherent detection of the signal contaminated by PBNJ. In the square-law detector of Figure 1.5, the received signal is multiplied in parallel by both the sine and cosine of the MFSK tone. More precisely, the square law detector consists of two branches, one where the input signal is multiplied by $\sqrt{2/T_h}\cos(2\pi f_m t)$ and the other where it is multiplied by $\sqrt{2/T_h}\sin(2\pi f_m t)$. The products are integrated over the duration of one hop in the two separate correlators as seen in Figure 1.5. Thus, assuming that the first tone $m = 0$ is the transmitted one and using the expression for the dehopped signal from Equation (1.9), we can express the output of the cosine based correlator as

$$r_{0,c} = \int_0^{T_h} r_0(t)\sqrt{2/T_h}\cos(2\pi f_0 t) = \sqrt{PT_h}\cos\theta_0 + n_{0c} + j_{0c}, \tag{1.12}$$

where $n_{0c}$ and $j_{0c}$ represent the outputs of the cosine based correlator corresponding to the first tone, when AWGN $n(t)$ and $j(t)$ respectively are present at its input. Similarly, the output of the correlator correspond-

ing to the sine branch is given by

$$r_{0,s} = \int_0^{T_h} r_0(t)\sqrt{2/T_h}\sin(2\pi f_0 t) \quad = \quad \sqrt{PT_h}\sin\theta_0 + n_{0s} + j_{0s}, \tag{1.13}$$

where $n_{0s}$ and $j_{0s}$ represent the outputs of the sine based correlator corresponding to the first tone, when AWGN $n(t)$ and $j(t)$ respectively are present at its input. The sine and cosine components are squared and added to yield a variable corresponding to the $m$th tone during the $l$th hop, which denoted here by $U_{ml}$, can be expressed as

$$U_{0l} = (r_{0,c})^2 + (r_{0,s})^2 \quad = \quad PT_h + n_0 + J_0 = E_h + n_0 + J_0, \tag{1.14}$$

where $n_0 = n_{0c}^2 + n_{0s}^2$ and $J_0 = j_{0c}^2 + j_{0s}^2$ are the AWGN and PBNJ components respectively at the output of the square-law detectors of Figure 1.5. Equation (1.14) represents the output of the square-law detector corresponding to the transmitted signal tone. For the remaining ($M$-1) square-law detectors that correspond to non-signal tones, it can be shown that the output consists of superposition of thermal noise and the jamming signal. Thus we have

$$U_{ml} = n_m + J_m, \quad m > 0. \tag{1.15}$$

Finally, note that Equations (1.9), (1.14) and (1.15) assume that the noise jamming is present and is interfering with all the $M$ tones of a band. If the band is unimpaired by jamming, the jammer's contribution will be absent from both of these equations, resulting in

$$U_{0l} = E_h + n_0 \tag{1.16}$$

and

$$U_{ml} = n_m, \quad m > 0. \tag{1.17}$$

We can infer from Equations (1.14) to (1.17) that when PBNJ is present in the band used by the desired signal, the effective noise power spectral density is increased due to the additive nature of the PBNJ. In this way, the presence of PBNJ increases the probability of detection error. However, in the context of FFH systems, the probability that all hops experience jamming is low. Therefore in comparison to SFH, FFH is more robust against PBNJ. Nevertheless, PBNJ can still degrade the performance of the FFH receiver employing linear combining.

### 1.3.3.2 Effects of MTJ and AWGN

The MTJ signal is in the form of $Q$ number of continuous wave tones having the same frequency as the $M$ MFSK tones. Although tone jamming may not be treated the same way as noise jamming, the concept of an equivalent spectral density has been defined in [75]. Let $P_{TJ}$ be the total MTJ power and $P_J = P_{TJ}/Q$ be the MTJ power in one of the jamming frequency tones. Then, the effective transmitted signal to jamming power is given by [2,3,38,65,66]

$$\begin{aligned} SJR = \frac{E_b}{P_{TJ}/W_{ss}} &= \frac{E_s}{b}\frac{MN_b}{T_h}\frac{1}{QP_J} \\ &= \frac{E_s}{P_J}\frac{N_b}{Q}\frac{M}{bT_h} = \frac{E_h}{E_j}\frac{LM}{qb}, \end{aligned} \tag{1.18}$$

where $E_j = P_J T_h$ is the energy associated with the jamming tone per hop and we have used the relations $W_{ss} = N_b MB = N_b M/T_h$ and $q = Q/N_b$. If a jamming tone corresponds to the same frequency as the transmitted MFSK tone, which we assumed as the first tone, then the signal at the input to the square-law detector is given by

$$r_0(t) = \sqrt{2P}\cos\{2\pi\,(f_0)\,t + \theta_0\} + \sqrt{2P_J}\cos\{2\pi\,(f_0)\,t + \theta_j\} + n_0(t), \tag{1.19}$$

where $\theta_j$ represents the phase associated with the jamming tone frequency. The operations performed by the square-law detector on this signal are the same as discussed in the context of PBNJ contaminated signal in Section 1.3.3.1. Thus we can express the output of the cosine based correlator as

$$\begin{aligned} r_{0,c} &= \int_0^{T_h} r_0(t)\sqrt{2/T_h}\cos(2\pi f_0 t) \\ &= \sqrt{PT_h}\cos\theta_0 + \sqrt{P_J T_h}\cos\theta_j + n_{0c} \end{aligned} \tag{1.20}$$

and that of the sine based correlator as

$$\begin{aligned} r_{0,s} &= \int_0^{T_h} r_0(t)\sqrt{2/T_h}\sin(2\pi f_0 t) \\ &= \sqrt{PT_h}\sin\theta_0 + \sqrt{P_J T_h}\sin\theta_j + n_{0s}. \end{aligned} \tag{1.21}$$

Thus, the output of the detector corresponding to the first tone and the $l$th hop is given by

$$U_{0l} = E_h + E_j + 2\sqrt{E_h E_j}\cos(\theta_0 - \theta_j) + n_0. \tag{1.22}$$

Equation (1.22) represents the output of the square-law detector of Figure 1.5 corresponding to the signal tone, corrupted by a jamming tone and AWGN. If the same signal is not contaminated by jamming, the output of the square-law detector may be represented by substituting $E_j = 0$ in Equation (1.22), resulting in $U_{0l} = E_h + n_0$. The output of any square-law detector corresponding to non-signal MFSK tone, cor-

responding to $m > 0$, may be represented by $U_{ml} = E_j + n_m$, if corrupted by the jamming tone and by $U_{0l} = n_0$, if uninterfered by jamming. It can be inferred from the above discussion that a jamming tone is more likely to cause detection error in the context of MFSK systems, if the jamming tone coincides with one of the non-signal tones rather than with the signal tone. Since the distribution of jamming tones may be assumed independent and random, the probability of occurrence of the jamming tone frequency coinciding with the signal tone frequency is only $1/M$, while the probability of the jamming tone hitting any of the non-signal tones is $1 - 1/M$, in the context of $n = 1$-band MTJ. Hence, despite the inherent diversity of the FFH system, MTJ can still degrade its performance considerably, thereby necessitating the employment of effective anti-jamming measures.

### 1.3.4 Linear Diversity Combining

This section discusses the basic principles of the diversity combiner referred to as the *linear diversity combiner* that forms part of the FFH assisted MFSK receiver shown in Figure 1.5. As mentioned earlier, this type of scheme simply adds the outputs of the square-law detectors received in all the hops corresponding to a transmitted symbol. Thus for each of the receiver branch corresponding to an MFSK tone, a decision variable given by [34,35,44]:

$$Z_m = \sum_{l=0}^{L-1} U_{ml}, \qquad m = 0, 1, \ldots, M-1 \tag{1.23}$$

is obtained upon completing $L$ hops where $U_{ml}$ is the output of the $m$th square-law detector during the $l$th hop. As mentioned above, the outputs $Z_m$, $m = 0, 1, \ldots, M-1$ of all the $M$ combiners constitute the detection decision variables.

The most attractive property of the linear diversity combining is that its inherent time and frequency diversity constitutes an effective tool against frequency selective fading [34]. To elaborate, since in the context of FFH, each symbol is transmitted using $L$ different frequencies, hence the signal in each hop experiences independent fading, provided two adjacent hopping frequencies are separated by at least the coherence bandwidth of the channel [39,40,78]. Consequently, BER performance of the FFH-MFSK system is superior to that of SFH-MFSK. We will augment this argument mathematically. Suppose that a BFSK modulated signal $s(t)$ is transmitted over a Rayleigh fading channel. Then, the received signal is given by

$$r(t) = \alpha e^{-j\theta} s(t) + n(t) \tag{1.24}$$

where $\alpha$ is the Rayleigh distributed attenuation factor, $\theta$ is the channel-induced phase shift in the transmitted signal and $n(t)$ is the Gaussian distributed noise. The probability of error $P_b$ for a non-coherently detected SFH assisted BFSK system in Rayleigh fading, which is the same as that of a non-hopping non-coherent BFSK scheme, assuming perfect synchronization of hopping between the transmitter and the receiver, is

given by [34]

$$P_b = \frac{1}{2+\gamma_b} \tag{1.25}$$

where $\gamma_b = \alpha^2 E_b/N_0$ is the average signal to noise ratio per bit. By contrast, the probability of error for FFH assisted non-coherent BFSK using linear combining in Rayleigh fading is also given by [34] and can be expressed as

$$P_b(L) = (\frac{1}{2+\gamma_l})^L \sum_{k=1}^{L-1} \binom{L-1+k}{k} \left(\frac{1+\gamma_l}{2+\gamma_l}\right)^k \tag{1.26}$$

where $\gamma_l = \gamma_b/L$ is the average signal to noise ratio per diversity path. As can be seen, substituting $L = 1$ in Equation (1.26) gives us Equation (1.25) confirming that no diversity implies SFH system. Proakis [34] has shown both mathematically and graphically that the BER expressed by Equation (1.26) for $L > 1$ is superior to that given by Equation (1.25). We can conclude that the frequency diversity resulting from FFH yields improvement in the BER performance of MFSK system when communicating in Rayleigh fading channels. This conclusion will be verified in Section 1.5.1 with the aid of our simulation results. The comparison of the linear combining scheme with self-normalization based scheme will also be presented in Section 1.5.1.

The results found in the literature show that in the absence of jamming, a linear square law diversity combining receiver performs reasonably well [35–37] under fading conditions. However, when jamming or interfering signals are present, the performance of FFH assisted MFSK receiver using linear combining is degraded. The detrimental effects of PBNJ and MTJ have already been discussed in Section 1.3.3.

### 1.3.5 Combining Losses Versus Diversity Gain

In this section, we will continue our discourse by discussing the advantages and drawbacks of FFH compared to SFH in the context of a non-coherent MFSK system. Proakis [34] has shown that if a signal is split into $L$ diverse and independent propagation paths and the signal components received in the $L$ paths are then combined coherently in the receiver, no loss of transmitted energy results, provided the estimate of the fading parameters (attenuation and phase) are perfect. Such a type of diversity combining, where signal components are weighed appropriately by channel coefficients of each path, is referred to as *optimum combining*. If the said estimates are imperfect, some losses may however result. By contrast, in the context of non-coherent detection, no attempt is made to estimate the channel, and estimates of the channel coefficients are not available. When signals received over diverse path are combined without weighting, the combining method is often referred to as *equal gain combining* (EGC). Proakis [34] has shown that non-coherent combining of the signal components received through diverse propagation paths results in losses. In other words, EGC yields inferior performance than that afforded by OC. These losses also occur because, the squaring operation seen in Figure 1.5 performed on the received sum of energy and noise in the context

of non-coherent MFSK detection enhances the noise power.

Let us follow this intuitive reasoning with mathematical results. We compare the error probability in case of non-coherent MFSK using SFH with the same demodulation system using FFH. It is readily seen that error probability of SFH assisted non-coherent BFSK system is identical to that of the non-hopping system, assuming perfect synchronization of hopping between the transmitter and receiver. In AWGN , this bit error ratio (BER) is given by [34]

$$P_b = \frac{1}{2} e^{-\gamma_b/2} \tag{1.27}$$

By contrast, the probability of error for FFH non-coherent BFSK under AWGN can be expressed using [34] for non-coherent BFSK to get

$$P_b(L) = \frac{1}{2^{2L-1}} e^{-\gamma_l/2} \sum_{n=0}^{L-1} c_n (\gamma_l/2)^n \tag{1.28}$$

where

$$c_n = \frac{1}{n!} \sum_{i=0}^{L-1-n} \binom{2L-1}{i}. \tag{1.29}$$

It can be verified that Equation (1.28) reduces to Equation (1.27) if we substitute $L = 1$ in the former. Equations (1.27) and (1.28) have been plotted in Figure 1.6. It can be seen from this figure that the BER degrades as the diversity order is increased when FFH assisted BFSK communicates in AWGN. We may conclude that BER performance of SFH aided non-coherent BFSK is superior to that of the same system invoking FFH with linear combining in AWGN. In fact, SFH enjoys this superiority over FFH in the context of $M$-ary FSK with $M > 2$ [34]. Consequently, we may conclude that no improvement is to be gained in the BER performance of non-coherent FSK by using linear diversity combining under conditions of no fading.

Nevertheless, there are certain aspects in which the inherent time diversity of FFH system makes it superior to the SFH counterpart. Firstly, diversity constitutes an effective anti-jamming measure. In the context of FFH system, the transmitted symbol is repeated in multiple hops and the probability of jamming more than one hops is low, since, if probability of jamming a single hop is $p$, that of jamming all hops of an $L$ order diversity system is $p^L$. Hence, when a symbol is transmitted using FFH, there is a high probability that at least one of the hops is unjammed. A suitable non-linear diversity combining scheme may be employed to further exploit the benefits of diversity. Numerous non-linear diversity combining techniques may be invoked for aiding the FFH assisted MFSK receiver to combat PBNJ and MTJ effectively and, hence, achieve an improved BER performance compared to that of the SFH system. We will demonstrate in Section 1.5 with the aid of simulation results that, by employing a suitable diversity combining technique, FFH yields superior performance compared to SFH even in AWGN in the presence of jamming. This is because in the

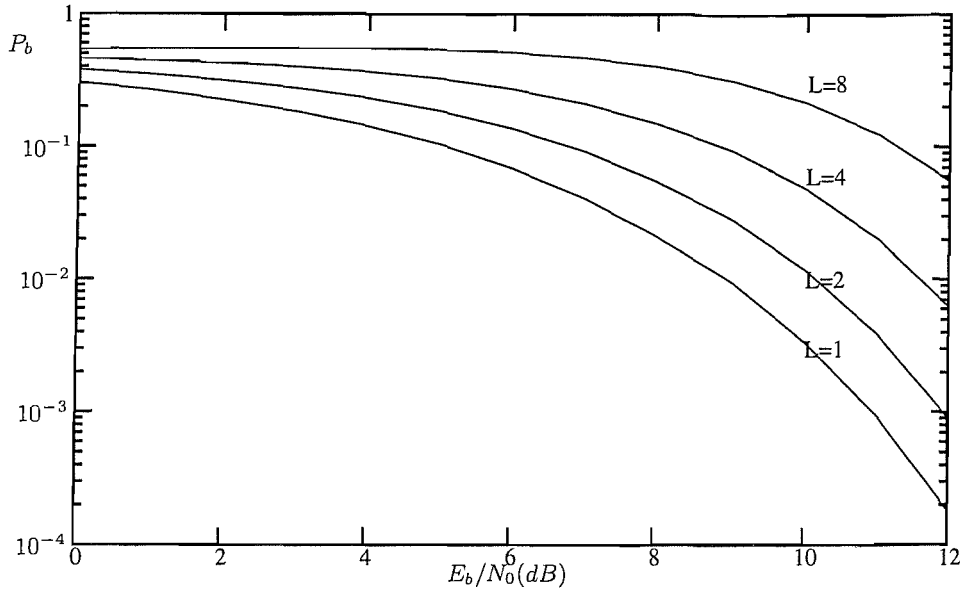


**Figure 1.6:** Degradation of the BER of FFH assisted BFSK in AWGN with increasing diversity order, plotted using Equations (1.27) and (1.28) extracted from [34].

presence of jamming, the disadvantage of the combining losses in the context of FFH is offset by its superior performance against jamming.

The second advantage that FFH systems enjoy over SFH systems is that the $L$th order frequency diversity of FFH systems proves to be an effective mechanism in combatting fading. This aspect has already been discussed in Section 1.3.4.

The above-mentioned two advantages of the FFH based system over its SFH aided counterpart results in reduced SNR requirement when aiming for a fixed BER in the presence of jamming, which is referred to as *diversity gain.*

### 1.3.6 Fixed Hop Rate Versus Fixed Symbol Rate

Having considered the effects of combining losses and diversity, let us now focus our attention on the impact of the hopping rate on the achievable system performance. We know that the number of hops per second, referred to as the *hop rate*, is related to symbol rate in FFH by the relation $R_h = LR_s$. We have already mentioned in Section 1.3.5 that under fading conditions, increasing the diversity order $L$ results in improvement of achievable BER. Now, if the diversity order has to be increased for the sake of achieving better diversity gain, either the hop rate or the symbol rate has to be modified. A variable hop rate may be used to achieve a fixed data rate but it was found that this scheme led to some problems [79]. Firstly, the total hopping bandwidth is related to hop rate by the relation $W_{ss} = MN_b/T_h$. For a fixed hopping bandwidth, increasing the hop rate by reducing $T_h$ to achieve higher diversity will reduce the value of $N_b$, which will render the system more vulnerable to multitone jamming, and especially to $n = 1$-band MTJ. Secondly, since the hop rate determines the FSK tone spacing according to $B = R_h = 1/T_h$, increasing hop rate will make the assumption of a frequency flat channel less valid although, at the same time, it will make

the assumption of a slowly fading channel more applicable. Thirdly, having a variable hop rate coupled with large number of hops per second makes synchronization more difficult especially in multi-user scenario. Due to these reasons, using high diversity orders is prohibitive and attaining low error rates with the advent of high diversity gains constitutes a grave technical challenge, in the context of variable hop rate systems.

These problems of the family of variable hop rate systems can be circumvented by having a fixed hop rate and using high diversity orders. Fixed hop rate systems were initially investigated in the context of military communication systems [79]. In conjunction with a fixed hop rate $R_h$, increasing $L$ reduces the symbol rate $R_s$, since we have $R_h = LR_s$. Nonetheless, at the cost of decreasing the data rate, one can achieve a more reliable transmissions. Most researchers assume having a fixed hop rate [4-31] and in this treatise, the same assumption applies.

## 1.4 Non-Linear Diversity Combining Techniques

In this section, a brief introduction to various non-linear combining methods has been provided [5-31]. Before we begin, it is relevant to mention that, broadly speaking, there are three main categories of diversity combining techniques. This categorization has been done in the context of diversity achieved through other means as well, e.g spatial and multipath diversity [80–90]. In the context of the first category, referred to as the *optimum combining* (OC) or *maximum-ratio combining* (MRC), the signals received in various diverse paths are weighed in proportion to the gains of the individual paths before they are combined. This scheme is considered to be the optimum, since it caters for the channel impairments imposed on the signal in each individual path. However, it requires the knowledge of the channel gains. Another category is referred to as the *selection or switched combining* (SC), in the context of which the receiver chooses the path yielding the maximum SNR. This scheme gives reasonably good performance but results in poor performance under low SNR conditions. Finally, in the context of EGC, the signals in all the diverse paths are merely summed without any weightage. We can see that EGC is another name for linear combining discussed above. In fact, majority of the non-linear diversity combining schemes we will consider in this section may be deemed as sub-classes of the EGC scheme, since they operate without applying any weights to the various received signals. Indeed, some of them do apply various de-emphasis mechanisms but they are not based on the knowledge of the channel gains. This is attractive from the viewpoint of implementation in noncoherent FFH-MFSK receiver where channel estimation may not be feasible.

Note that in [54], the authors have investigated a so-called maximum likelihood diversity combining scheme which is shown to yield superior performance to all other known diversity combining schemes when FFH-MFSK encounters PBNJ. However, besides the side information about the received SNR, this scheme requires the knowledge of which hops are jammed. By contrast, our emphasis in this treatise is on low-complexity schemes. Hence, we will consider only those diversity combining schemes which do not require extensive side information, such as the knowledge about which hops are jammed or about the channel gains.

Furthermore, it has been shown in [54] that the noise-normalization combining yields performance very close to the maximum likelihood diversity combining scheme.

As discussed in Section 1.3.3, an error in detection decision occurs if the output $Z_m$ of the diversity combiner, seen in Figure 1.5, corresponding to any of the $M$-1 non-signal MFSK tones exceeds that corresponding to the signal tone, i.e. if the first tone corresponding to $m = 0$ is transmitted, then a detection error occurs if $Z_m > Z_0, m = 1, 2, \ldots, M-1$. In the presence of thermal noise and especially jamming, the probability of this erroneous decision is quite high. Linear combining of various signals received from multiple propagation paths results in poor performance, because the receiver has neither any means of distinguishing between square-law detector outputs corresponding to jammed non-signal tones and that corresponding to unjammed signal tone, nor any method of suppressing the effects of jamming. Now we will discuss the methodology employed by non-linear combining methods to combat the effects of jamming or interference.

For each transmitted symbol, after the square-law detector stage of Figure 1.5, the receiver has $M \times L$ variables corresponding to the $M$ tones and the $L$ hops of a symbol. The combining principle of most non-linear diversity combining schemes is that the $M \times L$ variables are weighed down before they are combined [44]. Thus, the effects of interferences may be reduced before superimposing them. This is equivalent to applying a specific function to the variables before adding them. Let one of these variables be represented by $U_{ml}$, $m = 0, 1, \ldots, M-1$, $l = 0, 1, \ldots L-1$. Then, the decision metric $Z_m$ of a non-linear combining scheme is given by [44]:

$$Z_m = \sum_{l=0}^{L-1} f(U_{ml}), \qquad m = 0, 1, \ldots, M-1. \tag{1.30}$$

As shown in Equation (1.30), the decision metric is not simply the linear sum of all the variables $U_{ml}$ but that of some specific function of these variables. We can see from Equations (1.23) and (1.30) that for the linear combining receiver, we have $f(U_{ml}) = U_{ml}$. Alternatively, some diversity combining schemes, such as a few order-statistics based and non-parametric schemes (to be discussed in Sections 1.4.7 and 1.4.8), do not use the decision variable determined by Equation (1.30) and are instead based on other algorithms applied to the variables $U_{ml}$. Some of the key non-linear diversity combining techniques have been discussed in Sections 1.4.1 to 1.4.9. Figure 1.7 shows schematics of the various diversity combining operations that may be performed on the outputs of the $M$ square-law detectors in a FFH assisted MFSK system. The combining principles of these schemes have been summarised in Table 1.2.

### 1.4.1 Majority Vote Combining

One of the simplest of all non-linear combining methods is the hard decision majority vote (HDMV) based diversity combining. For this scheme, the highest square-law detector output in each hop is assigned a logical 1 and the remaining outputs are assigned logical 0. The assigned values are added for all $L$

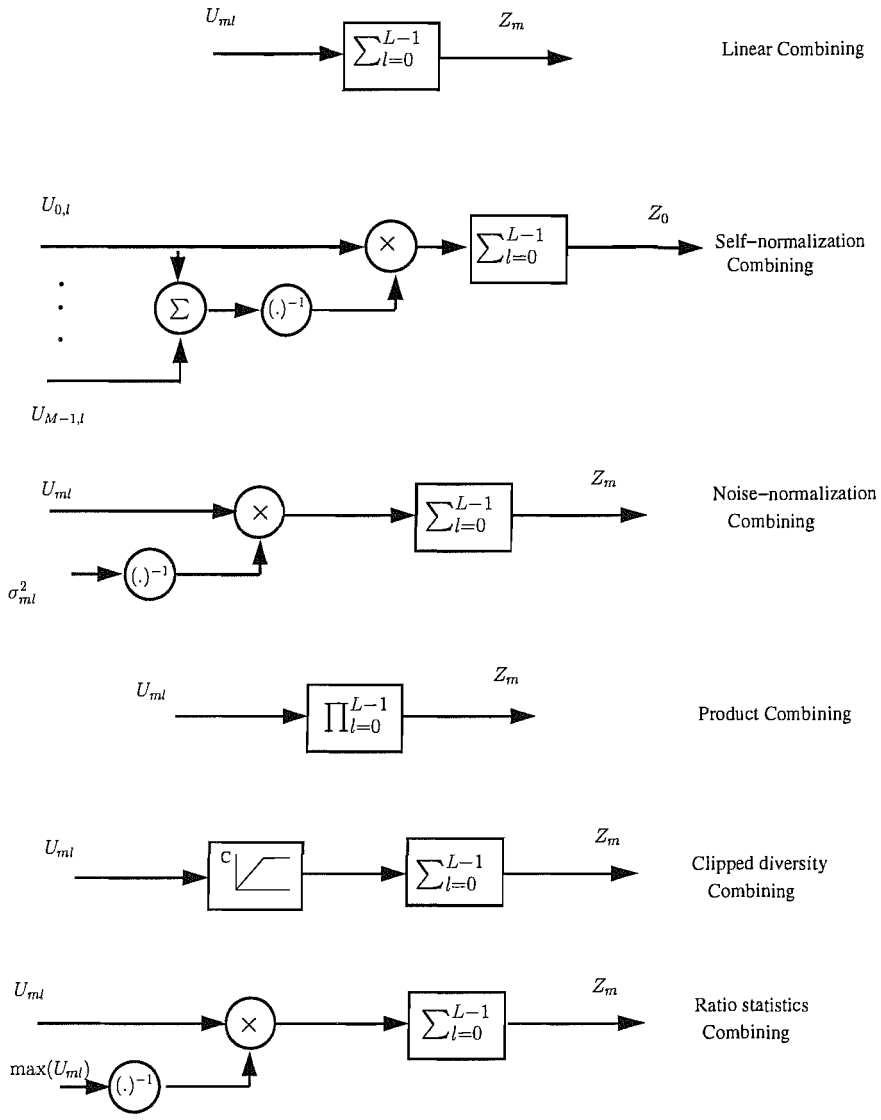


**Figure 1.7:** Block diagrams of various diversity combiners used in FFH assisted non-coherent MFSK Receiver; $U_{ml}$ denotes the square-law detector output corresponding to the $m$th tone during the $l$th hop and $Z_m$ is the decision variable for the $m$th tone.

hops corresponding to each MFSK tone. The decision metric given by Equation (1.30) is based on the function [44].

$$f(U_{ml}) = \begin{cases} 1 & U_{ml} \geq U_{kl} \text{ for all } k \\ 0 & \text{otherwise,} \end{cases} \qquad \begin{matrix} k, m = 0, 1, \ldots, M-1, \\ l = 0, 1, \ldots L-1. \end{matrix} \tag{1.31}$$

The summation is equivalent to counting the number of 1s corresponding to each frequency tone. Comparison between the MFSK tones is based on the number of logical 1s in all the hops. The specific frequency tone and the corresponding symbol that achieves the maximum number of logical 1s in all hops is assumed to be the transmitted one.

It was reported in [44] that this technique is poor especially under jamming conditions because the receiver discards a lot of potentially useful information by making hard decisions i.e., by assigning logical

1 to the highest detector output and logical 0 to any detector output that has a lower magnitude than the maximum.

A similar diversity combiner scheme proposed in [91] for FFH systems operating in multiple access (MA) channels is referred to as the *hard limiting majority vote* (HLMV) combiner [48, 93, 94], and can be considered as an improved variation of HDMV scheme. In the context of this combining scheme, at the end of each hop, the output of a square-law detector is assigned a value of 1, if it exceeds a pre-set threshold or 0, if it does not. Hence, when employing the HLMV combiner, we have

$$f(U_{ml}) = \begin{cases} 1 & U_{ml} \geq \delta \\ 0 & \text{otherwise}, \end{cases} \qquad m = 0, 1, \ldots, M-1; l = 0, 1, \ldots L-1, \tag{1.32}$$

where $\delta$ is an appropriately chosen pre-set threshold. At the end of the $L$ hops, the assigned values are summed. Thus the decision variable corresponding to each FSK tone can be found by inserting $f(U_{ml})$

| Combining Method | Combining Operation | | Comments |
|---|---|---|---|
| | Function $f(U_{ml})$ | Decision Variable $Z_m$ | |
| Linear [35] | $U_{ml}$ | $\sum_{l=0}^{L-1} f(U_{ml})$ | Sum of $L$ outputs |
| HDMV [44] | 1 for the largest<br>0 for others | $\sum_{l=0}^{L-1} f(U_{ml})$ | Sum of<br>assigned 1s or 0s |
| HLMV [91] | $f(U_{ml}) = 1$ if $U_{ml} \geq \delta$<br>0 otherwise | $\sum_{l=0}^{L-1} f(U_{ml})$ | Sum of<br>assigned 1s or 0s |
| NED [37] | $U_{ml} / \sum_{m=1}^{M} U_{ml}$ | $\sum_{l=0}^{L-1} f(U_{ml})$ | Sum of $L$ outputs normalized by the sum of $M$ outputs |
| AGC [36, 52] | $U_{ml}/\sigma_{ml}^2$ | $\sum_{l=0}^{L-1} f(U_{ml})$ | Sum of $L$ outputs normalized by noise power |
| Clipper [44, 48] receiver | $C$ if $U_{ml} \geq C$<br>else $U_{ml}$ | $\sum_{l=0}^{L-1} f(U_{ml})$ | Sum of $L$ clipped outputs |
| PCR [44] | $U_{ml}$ | $\prod_{l=1}^{L} f(U_{ml})$ | Product of $L$ outputs |
| Moments based [44, 68] | $\eta_{km} = \frac{1}{L}\sum_{l=0}^{L-1} U_{ml}^k$ | <br>$2\eta_{2m}^2 - \eta_{4m}$<br>$2\eta_{1m}^2 - \eta_{2m}$ | Moments of outputs<br>4-2M method<br>2-1M method |
| Order Statistics [44, 55, 92] | $U_{lmi}^{(r)}, i = 1, \ldots L$<br><br><br><br>$\frac{U_{lmi}^{(r)}}{\sum_{m=0}^{M-1} U_{lmi}^{(r)}}$ | <br>$\sum_{i=1}^{L_n} U_{lmi}^{(r)}$<br>$U_{lmL-1}^{(r)}$<br>$U_{lmL/2}^{(r)}$<br>$\sum_{l=0}^{L-1} f(U_{ml})$ | Ordering of $L$ outputs<br>Sum of $L_n = L-1$ outputs<br>Selection of 2nd maximum<br>Selection of middle value<br>OS-NED |
| Nonparametric [44, 69] | $r_i, i = 1, \ldots L \times M$<br>$w_i, i = 1, \ldots L \times M$<br>$r_i, i = 1, \ldots M$ | $\sum_{l=0}^{L-1} f(U_{ml})$<br>$\sum_{l=0}^{L-1} f(U_{ml})$<br>$\sum_{l=0}^{L-1} f(U_{ml})$ | Ordering of $L \times M$ outputs<br>Sum of assigned ranks<br>Sum of weighted ranks<br>Ordering of $M$ outputs and sum of $L$ ranks |
| Ratio Statistics [44, 62] | $U_{ml}/\max(U_{ml})$ | $\sum_{l=0}^{L-1} f(U_{ml})$ | Sum of $L$ outputs normalized by the largest |

HDMV=Hard decision majority vote, HLMV=Hard limiting majority vote, NED=Self-normalization combining, AGC=Noise-normalization combining, OS-NED=Order statistics-normalized envelope detection, PCR=Product combining receiver.

**Table 1.2:** Summary of the functions performed on the square-law detector outputs $f(U_{ml})$ to compute the decision variables $Z_m$, in the context of various diversity combining techniques used in FFH assisted MFSK receivers.

given by Equation (1.32) into Equation (1.30). We will consider HLMV based combining scheme in MA application in Chapter 4.

### 1.4.2 Self-Normalization Combining

This class of diversity combining schemes is also referred to as *Normalized envelope detection (NED)* arrangement. When using this combining scheme, for each hop, the output of each square law detector is divided by the sum of the outputs of all the $M$ detectors before they are combined for all hops corresponding to an $M$-ary symbol, as seen in Figure 1.7. The corresponding decision function is given by [37,39,40,44]:

$$f(U_{ml}) = \frac{U_{ml}}{\sum_{m=0}^{M-1}(U_{ml})}, \qquad l = 0, 1, ...L-1, \tag{1.33}$$

where $U_{ml}$ represents the outputs of the square-law detectors for the $l$th hop and $m$th MFSK tone. The decision variable is determined by substituting Equation (1.33) in Equation (1.30).

The self-normalization process has the effect of reducing the contribution of heavily jammed signal paths and thus the jammed signals are de-emphasized. The FFH assisted MFSK receiver using self-normalizing diversity combining has been discussed in more detail in Section 1.5.1.

### 1.4.3 Noise-Normalization Combining

In the context of this technique, the outputs of all square-law detectors are normalized by the channel noise power which is measured separately for each hop and each MFSK tone, as seen in Figure 1.7, before they are summed. The associated decision variable is based on the function [36,44,52,53,95]:

$$f(U_{ml}) = \frac{U_{ml}}{\sigma_{ml}^2}, \qquad m = 0, 1, \ldots, M-1, \qquad l = 0, 1, ...L-1, \tag{1.34}$$

where $\sigma_{ml}^2$ is the noise power in the $l$th diversity path of the $m$th transmitted tone, $U_{ml}$ represents the outputs of the square-law detectors for the $l$th hop and $m$th MFSK tone and the decision variable is determined by substituting Equation (1.34) in Equation (1.30). The FFH assisted non-coherent MFSK receiver based on noise-normalization diversity combining is also referred to as *automatic gain control (AGC) based receiver*, Owing to the noise-normalization effect, this type of receiver is especially effective in additive noise and hence, against PBNJ, it is capable of even outperforming the self-normalization based receiver. However, this receiver is not very resilient against tone jamming and its performance under MTJ has not been considered in the open literature.

Although this type of diversity combining requires additional information often referred to as 'side information', Robertson *et al.* [53] have shown that the noise power measurement does not have to be very accurate for attaining acceptable performance results. Even in conjunction with 50% errors in the noise power estimation, the system performance is not much different from that assuming ideal noise estimate.

However, in general, over-estimation of noise rather than under estimation yields better results [53].

### 1.4.4 Clipped Diversity Combining

In the context of this technique [36, 42, 44, 67], the outputs of the square-law detectors, seen in Figure 1.7, are clipped at a certain value before combining them for all hops. Hence, for the clipped diversity combining receiver, the decision variable is based on the function

$$f(U_{ml}) = \begin{cases} C & \text{for } U_{ml} \geq C \\ U_{ml} & \text{otherwise,} \end{cases} \qquad m = 0, 1, \ldots, M-1, \qquad l = 0, 1, \ldots L-1, \tag{1.35}$$

where $U_{ml}$ represents the outputs of the square-law detectors for the $l$th hop and $m$th MFSK tone while the final decision variable $Z_m$ is determined by substituting Equation (1.35) in Equation (1.30) [42,44,67]. The value of $C$, usually referred to as the *clipping threshold*, is adjusted during each hop based on the estimate of the noise power and fading conditions. The philosophy governing this technique is that since jammed signals may appear to have power which might be unrealistically high, any received energy in excess of a certain level may be attributable to jamming or interference. This is particularly true in the case of MTJ. It has been reported that the clipper receiver is capable of performing as well as the NED based receiver under PBNJ and outperforms it in MTJ [36,42,67].

In [48], an optimum diversity combiner designed for FFH-MA systems has been derived based on the maximum likelihood criterion, which operates on the principle of linearly combining a non-linear function of the energy detector outputs. Owing to the complexity of the derived combining scheme, it was suggested [48] that the optimum non-linearity may be approximated by a clipping function, as expressed in Equation (1.35). This approximate optimum combiner, which is identical to the clipped diversity combiner discussed above, is termed as the *soft limiting combiner* (SLC) in [48]. In the context of an FFH-MA system, the SLC constitutes the best diversity combining scheme proposed in [48, 96–98]. However, the SLC requires side information of the SNR and of the number of active users in order to accurately set the clipping threshold. The results of [96] demonstrate that even without accurate knowledge of the number of active users, the performance of the SLC is not significantly different from that achieved assuming perfect side information. However, again, the measurement of the noise power is mandatory in order to accurately adjust the clipping threshold. In Chapter 4, we will consider the use of SLC in order to combat multiuser interference.

### 1.4.5 Product Diversity Combining

As the terminology suggests, in the context of this type of diversity combining, the decision variable $Z_m$ corresponding to each MFSK tone, as seen in Figure 1.7, is obtained by multiplying the outputs of the

corresponding square-law detector for all hops, which can be expressed mathematically as [43,44,64]:

$$Z_m = \prod_{l=0}^{L-1} (U_{ml}), \qquad m = 0, 1, \ldots, M-1, \tag{1.36}$$

where $U_{ml}$ represents the outputs of the square-law detectors for the $l$th hop and $m$th MFSK tone. The idea behind this technique is that the received signal corresponding to a non-signal tone will carry low power in at least one of the $L$ hops, with a high probability. Consequently, when the product of the detector outputs corresponding to that particular tone for all hops is computed, the decision variable $Z_m$ corresponding to the non-signal tone yields a low value. By contrast, in the context of the signal tone, the product of the detector outputs generated for all hops will yield a significantly higher value, owing to the presence of the signal power in addition to any noise and jamming power. Thus, a correct decision is facilitated using this diversity combining scheme. The performance of the product combining receiver (PCR) in the presence of MTJ has been discussed with the aid of simulation results in Section 1.5.2, while a complete mathematical analysis of this receiver in the presence PBNJ is the subject of Chapter 3.

### 1.4.6 Moments Based Diversity Combining Methods

This class of diversity combining schemes [44,68] utilizes various moments of the outputs of the square-law detectors. The $p$th moment of the detector outputs corresponding to the $m$th tone is defined as [44,68]:

$$\xi_{pm} = \frac{1}{L} \sum_{l=0}^{L-1} U_{ml}^p, \qquad m = 0, 1, \ldots, M-1, \tag{1.37}$$

where $U_{ml}$, $m = 0, 1, \ldots, M-1$, $l = 0, 1, \ldots L-1$, represents the outputs of the square-law detectors for the $l$th hop and the $m$th MFSK tone, as seen in Figure 1.5. The decision variable is then based on a particular function of these moments. In the open literature, first, second, fourth and one-half order of moments have been suggested and investigated in the context of this scheme. In the context of the so-called 4-2M method [44,68], the decision variable is given by [68]

$$Z_m = 2\xi_{2m}^2 - \xi_{4m}, \tag{1.38}$$

which is a function of both the second and fourth order moments. In the context of another type referred to as 2-1M method, the decision variable can be expressed [68]

$$Z_m = 2\xi_{1m}^2 - \xi_{2m}, \tag{1.39}$$

which is based on both the first and second order moments. It has been shown in the literature [44, 68] that the 4-2M technique performs well both in partial and full-band noise jamming, but offers modest BER performance improvement when the system operates under MTJ. The performance of the 2-1M method is

comparable to that of the NED based method when the system operates in PBNJ and significantly better than the same technique under MTJ. The performance of the 1-1/2M based diversity combining is slightly better than that of the 2-1M technique in MTJ, but slightly worse in PBNJ. Hence, the 2-1M based diversity combining method may be considered a suitable choice for use in conjunction with a FFH assisted MFSK receiver, in both PBNJ and MTJ environments [44, 68].

### 1.4.7 Order Statistics Based Diversity Combining

In the context of order statistics (OS) based diversity combining [44, 55, 92], the $L$ outputs of each of the $M$ square law detector are first ranked in ascending order of magnitude. The ranked square-law detector outputs $U_{ml}$, $m = 0, 1, \ldots, M-1, l = 0, 1, \ldots L-1$, seen in Figure 1.5, may be represented by $U_{mli}^{(r)}$, where $i$, $i = 1, 2, \ldots L$, represents the rank of that output in the ordered list. The rank value is typically set to 1 for the smallest and $L$ for the largest of the square-law detector outputs. Mathematically, we have

$$U_{ml1}^{(r)} \leq U_{ml2}^{(r)} \leq U_{ml3}^{(r)} \leq, \ldots, U_{mlL}^{(r)}.$$

The basic idea behind the ordering is to identify the higher square-law detector outputs, thus aiding in identifying the jammed signals. A number of methods have been suggested in literature to generate the decision variable following this sorting operation. The decision variable may be based on the selection of a particular ranked detector output. Usually the highest detector output is to be avoided [44, 55], because it is likely to correspond to the jammed tone. Selecting the next highest detector output, instead, has been suggested by March and Ritcey [55] in which case the decision metric is given by

$$Z_m = \max 2[U_{mli}^{(r)}] = U_{mlL-1}^{(r)}, \tag{1.40}$$

where $\max 2[.]$ is used here to denote the second highest of set of values. The same researchers have suggested summing of the first $L_n$ outputs of the $L$ outputs corresponding to each MFSK tone in order to determine the decision variable, where $L_n < L$. In that case, we have [55]

$$Z_m = \sum_{i=1}^{L_n} U_{mli}^{(r)}, \qquad m = 0, 1, \ldots, M-1, \qquad l = 0, 1, \ldots L-1. \tag{1.41}$$

Typically the specific choice of $L_n = L - 1$ is suggested [55], thus leaving out the highest detector output. The selection of the middle value in the set of $L$ outputs has also been suggested in literature [44], whereby the decision variable can be expressed as

$$Z_m = U_{mlL/2}^{(r)}. \tag{1.42}$$

In the context of order statistics-normalized envelope detection (OS-NED) based diversity combining [98], self-normalization operation, as expressed in Equation (1.33), is performed on the ordered values.

Thus, in the context of the OS-NED, we have [98]

$$f(U_{ml}) = \frac{U_{lmi}^{(r)}}{\sum_{m=0}^{M-1} U_{lmi}^{(r)}}, \qquad l = 0, 1, ...L-1, \tag{1.43}$$

and the decision variable is determined by substituting Equation (1.43) into Equation (1.30). The ordering and normalization in OS-NED result in stronger de-emphasis of the energy detector outputs corresponding to the interference-infested tones. Thus, the effects of interferences are substantially reduced.

The numerous variations of OS based diversity combining yield diversity gain in the context of both PBNJ and MTJ, resulting in better performance compared to the linear combining method [44] . However, we can see that by rejecting one or more of the signals received in different hops, the receiver based on this combining method is discarding a part of the potentially useful received energy. As a result, the BER performance of the FFH assisted MFSK system achievable by using this combining scheme is inferior to that of the same system using other combining schemes such as self-normalization combining, noise-normalization combining and clipper based combining [44]. In Chapter 4, OS-NED will be considered for use in FFH in multiuser channels.

### 1.4.8 Non-parametric Diversity Combining Methods

Non-parametric diversity combining methods are similar to the family of order statistics method discussed in previous section. But, whereas in OS based combining, the detector outputs of $L$ hops corresponding to each MFSK tone are ranked in a separate list, thus resulting in $M$ lists of $L$ elements each, in the non-parametric combining method, all the $M \times L$ outputs of the correlators corresponding to $M$ tones and $L$ hops per symbol are ranked in a single list. Additionally, the ranked detector outputs are then assigned values in proportion to their rank. Thus the ranked square-law detector outputs represented by $U_{lmi}^{(r)}$ are given by [44, 69]

$$U_{lmi}^{(r)} = r_i, \tag{1.44}$$

where $r_i$ represents the ranked value and $i = 1, 2, ...L \times M$, represents the indexing variable.

Following the ranking of the detector outputs, a number of methods have been suggested to generate the decision variable [69]. We will discuss briefly some of these methods.

One of the simplest of the non-parametric combining methods is the rank sum combining [69]. In the context of this combining method, the lowest detector output is assigned a value of 1, while the highest is assigned a value equal to $L \times M$. In other words, the ranked $L \times M$ detector outputs are indexed and their values are replaced by their index values. Thus $r_1 = 1$ corresponds to the lowest detector output and and $r_{LM} = L \times M$ represents the highest detector output amongst all the $L \times M$ detector outputs. The decision variable corresponding to each MFSK tone is obtained by summing the indexed values assigned to each detector output given in Equation (1.44) over the $L$ hops of a symbol. It is worth comparing this philosophy

with that of the linear combining where the actual detector output values corresponding to all hops are added to arrive at a decision variable corresponding to each tone, whereas in rank sum combining, the index values assigned to them are added instead of the actual detector outputs. Hence, the decision function is given by [69]

$$f(U_{ml}) = U_{lmi}^{(r)} = r_i = i \tag{1.45}$$

and the decision variable $Z_m$ is determined by substituting Equation (1.45) in Equation (1.30).

Here, we will illustrate the concept of rank sum combining with the aid of an example. Suppose that we have 4 MFSK tones (4-ary FSK) and 3 hops per symbol ($L = 3$). Then, corresponding to each transmitted symbol we have 12 detector outputs at the end of the three hops. Using the rank sum combining method, we construct a list of these 12 values and then rank them in ascending order of their magnitudes. Next, we will replace the detector output variables $U_{ml}$, $l = 0, 1, \ldots, L-1$ corresponding to the $m$th tone by the index value they were assigned in the list of 12 we created. Then, the new values corresponding to each MFSK tone are summed to get the decision variables $Z_m$.

In a specific variant of the rank sum combining technique referred to as the list rank sum (LRS) combining, the values assigned to the $L \times M$ outputs are not their indices but they are chosen from a list [44, 69] i.e.

$$f(U_{ml}) = r_i = w_i, \tag{1.46}$$

where $w_i$ is a weighting factor and its value is different for each of the $i$ values. The decision variable $Z_m$ is determined by substituting Equation (1.46) in Equation (1.30) similar to the case of rank sum combining. The purpose of this multiplicative factor $w_i$ is to provide more weightage to some detector outputs as compared to others. Thus, the detector outputs corresponding to the signals that are likely to be contaminated by interference are given less weight in order to de-emphasize them. The multiplicative factor and the list values are usually adapted according to the fading and interference conditions during each hop. The efficacy of this method, thus, depends upon reliability of the side information. Amalgamation of this scheme with self-normalization combining has also been suggested [69]. This combined method, which is referred to as the *list rank sum-normalized envelope detection* (LRS-NED) first applies the ranking and weighting operations, as explained in the context of the LRS technique, and then normalizes them, as follows [69]:

$$Z_m = \sum_{l=0}^{L-1} \left( \frac{w_i}{\sum_{m=1}^{M} (U_{ml})} \right), \qquad i = 1, 2, \ldots L \times M. \tag{1.47}$$

In another type of non-parametric combining method, referred to as hop rank sum (HRS) combining, only the $M$ values of the square-law detector outputs corresponding to each hop are ranked and their values are replaced by their rank [69]. That is, corresponding to each received symbol, we have $L$ lists of $M$ elements each. Following this, the assigned index values are summed for all hops. It should be noted that this method is different from the OS method discussed in Section 1.4.7 in the context of which the ranking is done separately for the $L$ values of each MFSK tone resulting in $M$ lists of $L$ elements each. HRS combining

method was suggested in literature [69] because for higher modulation orders and diversity orders, the product $L \times M$ becomes too large and rank sum combining may become too cumbersome to handle.

Gulliver and Felstead [69] have shown that, if the side information is reliable, the BER performance achieved using non-parametric combining methods under MTJ is superior than that achievable using most of the other linear and non-linear combining methods. Rank sum combining and the LRS-NED methods, hence, merit consideration.

### 1.4.9 Ratio Statistics Based Diversity Combining

In the context of the ratio statistics based diversity combining method [44,45,62], the output of each square-law detector, as seen in Figure 1.5, is normalized by the largest value amongst the $M$ values corresponding to a particular hop and then the normalized values are summed for all hops. Let $\max(U_l)$ be the largest of the $m = 0, 1, \ldots, M-1$, values for the $l$th hop. Thus, according to this method, the decision variable $Z_m$ is based on the function:

$$f(U_{ml}) = \frac{U_{ml}}{\max(U_l)}, \qquad m = 0, 1, \ldots, M-1, \qquad l = 0, 1, ...L-1 \tag{1.48}$$

and is determined by substituting Equation (1.48) in Equation (1.30), where $U_{ml}$ represents the outputs of the square-law detectors for the $l$th hop and the $m$th MFSK tone. This type of combining scheme is more efficient than the linear combining scheme of Section 1.3.4 in the presence of PBNJ or MTJ. However, the BER performance achievable using this scheme is inferior to that using some of the diversity combining schemes, which will be discussed in Section 1.5.

### 1.4.10 Performance Criteria of Diversity Combining Methods

In the Sections 1.4.1 to 1.4.9, a range of major non-linear diversity combining methods used in FFH assisted non-coherent MFSK receivers have been discussed. Except for the HDMV method, all of the combining schemes discussed perform better than the linear combining scheme, discussed in Section 1.3.4, when the communication system is subjected to jamming, provided the fading is not severe [44]. The choice of any diversity combining technique for use in conjunction with FFH is made based on certain parameters. The most important of these parameters is the performance of the combining scheme when the FFH assisted MFSK communicates in the presence of interference. Moreover, other factors like performance under fading conditions and thermal noise, simplicity of implementation and whether or not any side information is needed also have to be considered. Each of these factors may become significant depending upon the propagation conditions. For instance, there are combining methods such as noise-normalization combining, clipper based combining and LRS-NED that perform very well in the presence of interference but are dependent for successful operation upon the side information concerning the channel and interference conditions [36,44,69]. When side information cannot be made available or is unreliable, some simpler but less

efficient methods may have to be favoured.

## 1.5 Performance of FFH-MFSK using Non-Linear Diversity Combining

[1] In this section, the performance of two promising non-linear diversity combining schemes will be characterised with the aid of Monte Carlo simulation results. Specifically, the performance of FFH assisted non-coherent MFSK receiver using self-normalization combining will be discussed in Section 1.5.1, while the same system using product combining is the topic of Section 1.5.2. Further discussions based on the open literature related to these two combining methods have also been included along with the relevant comparisons. Let us focus our attention on the self-normalization combining scheme.

### 1.5.1 Self-Normalization Combining Based FFH MFSK

The self-normalization combining scheme may be considered to be a benchmark arrangement in the context of diversity combining schemes used in FFH assisted MFSK systems. Although it may not perform as well as some of the other diversity combining techniques characterised in Section 1.4 under certain conditions, it constitutes an attractive combining scheme because it does not require side information for its operation. We will analyze different aspects of this combining scheme in the forthcoming sections. For the purpose of all simulations, unless otherwise stated, we have used $E_b/N_0 = 13.35$dB in AWGN channel, which corresponds to the value of bit energy to noise power spectral density needed to achieve a BER of $10^{-5}$ using BFSK [34], and slightly higher signal energy, i.e. $E_b/N_0 = 16$dB in Rayleigh fading channel.

#### 1.5.1.1 Performance in the Presence of PBNJ

**Worst-case PBNJ Duty Factor:** As discussed in Section 1.3.2, an intentional jammer may use the worst-case duty factor of PBNJ, termed as $\rho_0$, which will inflict maximum damage upon the receiver and, hence, result in the poorest error rate. This trend is observable in the performance of NED based receiver also. In Figures 1.8 and 1.9, the BER of the NED based receiver has been plotted against the PBNJ duty factor $\rho$ for $L$=2 and increasing values of $E_b/N_J$ under AWGN and uncorrelated Rayleigh fading respectively. It can be seen that while $\rho = 1$ is the best strategy from the jammer's viewpoint at lower $E_b/N_J$ values, lower values of $\rho$ become preferable as signal to jammer power increases. In other words, it is beneficial for the jammer to concentrate its power to as small a fraction of the bandwidth as possible when its power is low in comparison to that of the transmitted signal. This trend becomes more clear in the case of contamination with AWGN in Figure 1.8, while in Rayleigh fading, it is less pronounced as evidenced by Figure 1.9. We can see in Figure 1.9 that for $E_b/N_J \geq 25$dB the performance of the NED based receiver is nearly constant for all values of $\rho$. This means that when fading is severe and when jammer signal power is low, full-band

[1] The simulation results of this section are based on reconstructing the range of solutions found in the published work cited in Table 1.1, in order to calibrate the accuracy of the investigations and infer the generic performance trends.

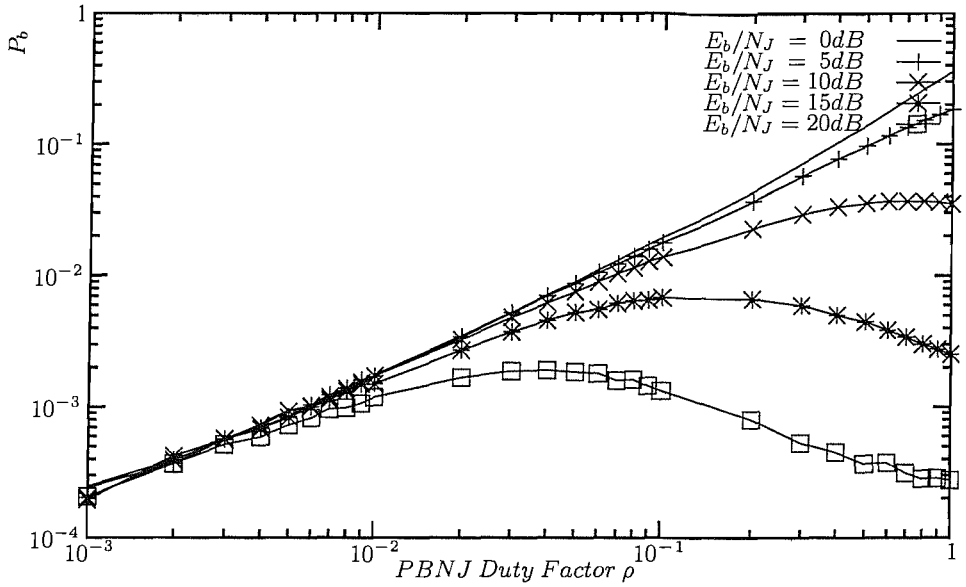


**Figure 1.8:** BER $P_b$ versus PBNJ duty factor $\rho$ curves for the self-normalization based FFH assisted non-coherent BFSK receiver in AWGN for various values of $E_b/N_J$ and for diversity order of $L = 2$ at $E_b/N_0 =$ 13.35dB

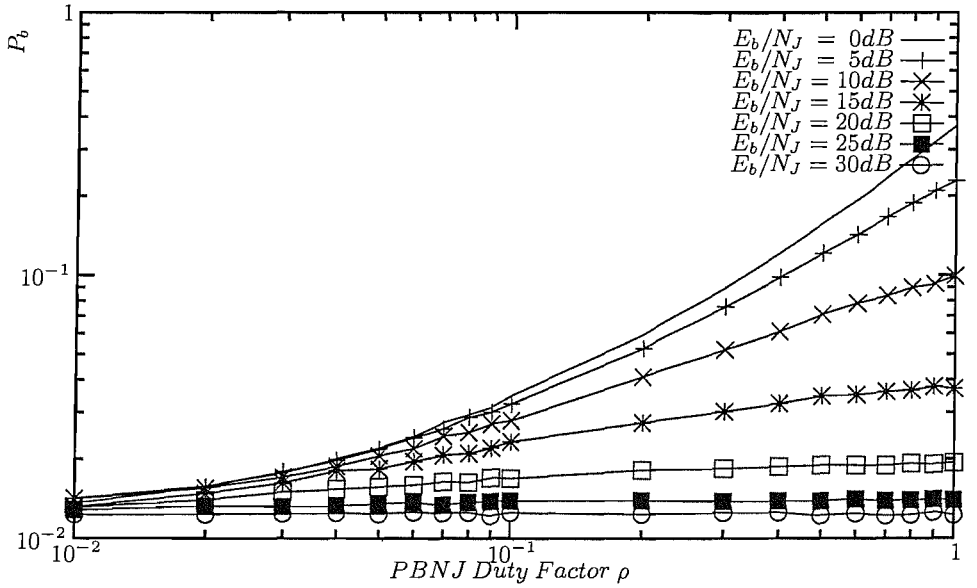


**Figure 1.9:** BER $P_b$ versus PBNJ duty factor $\rho$ curves for the self-normalization based FFH assisted non-coherent BFSK receiver in Rayleigh fading for various values of $E_b/N_J$ and for diversity order of $L = 2$ at $E_b/N_0 =$ 16dB

jamming is more effective. Crepeau [78] has shown that for any fading less severe than that introduced by Rayleigh fading channel, a partial band jamming strategy is better from the jammer's point of view.

Simulation results also confirm that for higher orders of diversity, $\rho_0 = 1$ is the best jamming strategy and the worst-case duty factor values for lower diversity orders are lower [37]. Various values of worst-case PBNJ duty factor $\rho_0$ for partial band noise jamming of the NED based receiver in both AWGN and Rayleigh fading obtained through simulation results have been summarised in Table 1.3. It can be seen from Table 1.3 that for most values of $E_b/N_J$ in case of Rayleigh fading with $L = 3$, we have $\rho_0 = 1$. Also, in the case of AWGN, $\rho_0 = 1$ for $E_b/N_J \leq$ 4dB when $L = 1$ whereas $\rho_0 = 1$ for $E_b/N_J \leq$ 10dB when $L = 3$. These

| $E_b/N_J(dB)$ | $\rho_0$ | | | |
|---|---|---|---|---|
| | L=1 | | L=3 | |
| | AWGN | Rayleigh | AWGN | Rayleigh |
| 0 | 1.0 | 1.0 | 1.0 | 1.0 |
| 2 | 1.0 | 1.0 | 1.0 | 1.0 |
| 4 | 1.0 | 1.0 | 1.0 | 1.0 |
| 6 | 0.8 | 1.0 | 1.0 | 1.0 |
| 8 | 0.4 | 1.0 | 1.0 | 1.0 |
| 10 | 0.3 | 1.0 | 1.0 | 1.0 |
| 12 | 0.2 | 0.8 | 0.7 | 1.0 |
| 14 | 0.09 | 0.5 | 0.5 | 1.0 |
| 16 | 0.07 | 0.4 | 0.3 | 1.0 |
| 18 | 0.05 | 0.3 | 0.2 | 0.9 |
| 20 | 0.03 | 0.2 | 0.09 | 0.8 |

**Table 1.3:** Worst-case duty factor $\rho_0$ values of PBNJ for self-normalization based FFH non-coherent BFSK in conjunction with $L$=1 and 3 in both AWGN and Rayleigh fading channel, at $E_b/N_0 = 13.35$dB

observations also imply that wide band jamming is more suitable from jammer's point of view when either diversity order is high, signal power is low or fading is severe.

**Diversity Gain:** Having studied the effects of the PBNJ duty factor on the NED based receiver, we have used the worst-case PBNJ duty factor values in all subsequent simulations. First, let us compare this system's achievable performance with that of linear combining FFH assisted BFSK receiver in AWGN from the point of view of partial band jamming rejection. In contrast to the linear combining receiver, the NED based receiver is capable of providing diversity gain even under no fading conditions. This can be seen from Figure 1.10 in which performance of the two types of receivers under worst-case PBNJ namely, using worst-case $\rho$ values for each value of $E_b/N_J$ and $L$ in AWGN, is shown for different diversity orders. As can be seen in Figure 1.10, while the performance of the linear combining based BFSK degrades, that of the NED based BFSK system improves upon increasing the order of diversity.

A comparison of the FFH BFSK receiver's performance in conjunction with these two types of diversity combining schemes under uncorrelated Rayleigh fading can be seen in Figure 1.11. The figure shows that in Rayleigh fading, the attainable performance of both the receivers is much poorer than that in AWGN although both types of combining schemes do provide a diversity gain. In fact, the linear combining method outperforms the self-normalization combining when $E_b/N_J \geq 8$dB with $L = 2$ and when $E_b/N_J \geq 16$dB with $L = 4$. The fact that the linear combining based receiver provides diversity gain when fading is severe has been mentioned in Section 1.3.5. The reason why self-normalization combining is not as powerful as the linear combining in Rayleigh fading channels is because, owing to the self-normalization operation in the former case, the net signal energy at the output of the diversity combiner is considerably reduced compared to the latter case. Moreover, since self-normalization in the NED receiver is basically an anti-jamming means, this receiver outperforms the linear combining receiver when signal to jammer power ratio is not high. But when $E_b/N_J$ exceeds a certain value, the anti-jamming mechanism becomes almost redundant and most of the errors occur due to fading. Therefore at high $E_b/N_J$ values, the linear combiner outperforms the NED receiver in Rayleigh fading. The performance degradation of the the NED based receiver compared

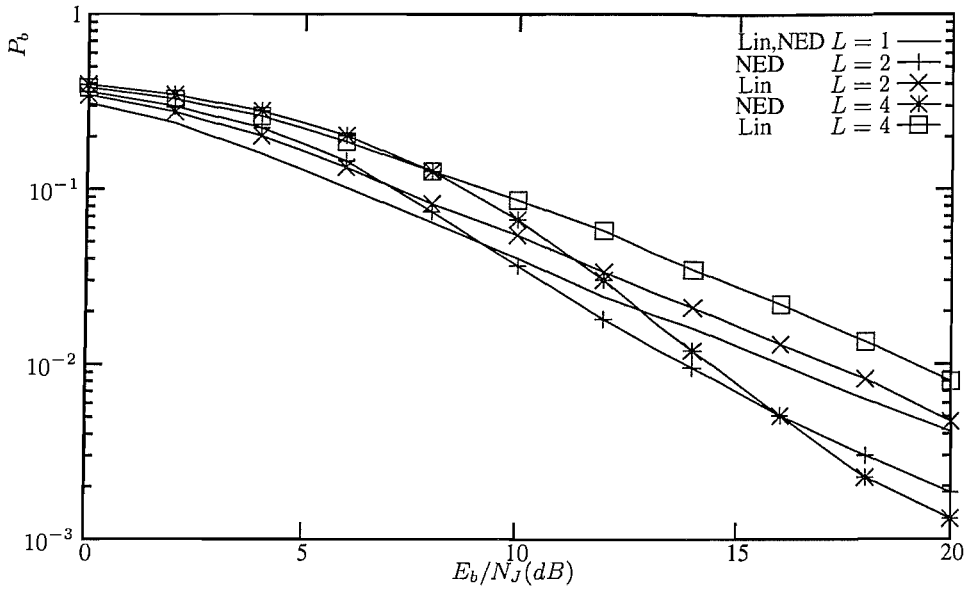


**Figure 1.10:** BER $P_b$ versus $E_b/N_J$ performance of the self-normalization (*NED*) and linear combining (*Lin*) based FFH assisted non-coherent BFSK receivers under the worst-case PBNJ in AWGN at $E_b/N_0 = 13.35$dB

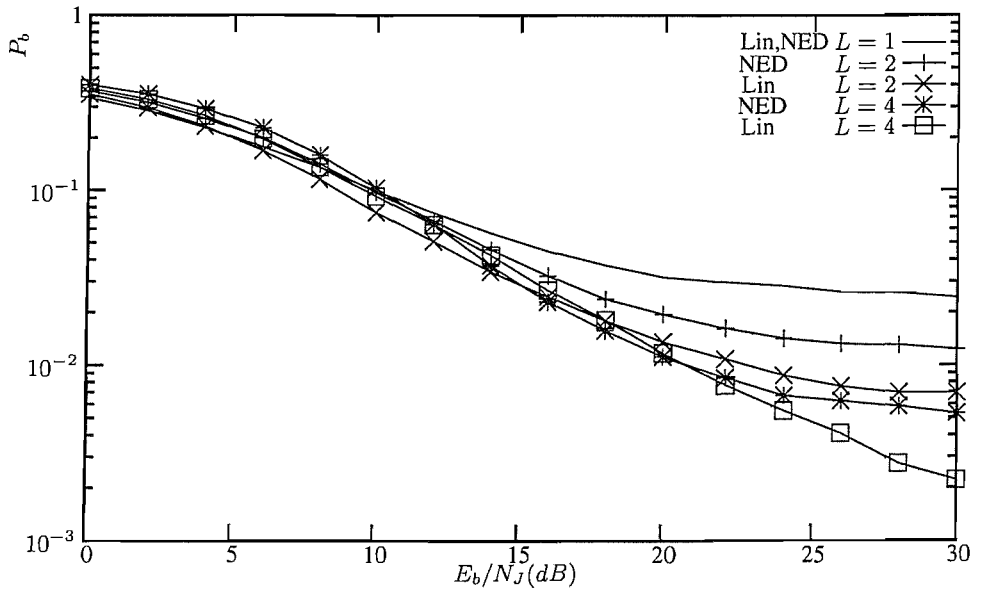


**Figure 1.11:** BER $P_b$ versus $E_b/N_J$ performance of the self-normalization based (*NED*) and linear combining (*Lin*) based FFH assisted non-coherent BFSK receivers under the worst-case PBNJ in uncorrelated Rayleigh fading at $E_b/N_0 = 16$dB

to the linear combining scheme in Rayleigh fading has been demonstrated by other researchers in [39,63,66]. Furthermore, it has been shown that, for less severe fading, as that characterised by Rician channel, the NED receiver maintains its superiority over the linear combining receiver [39,40].

Figures 1.12 and 1.13 show the advantage of using a high order of diversity in the NED based receiver. Due to the fact that non-coherent combining losses also increase upon increasing diversity level, as seen in Figure 1.6 and discussed in Section 1.3.5, an optimum diversity order exists for the NED based receiver the value of which depends upon the absence or presence of fading and $E_b/N_0$ value experienced. Thus, diversity gain is not attained and instead losses may result by using $L$ greater than the optimum value.

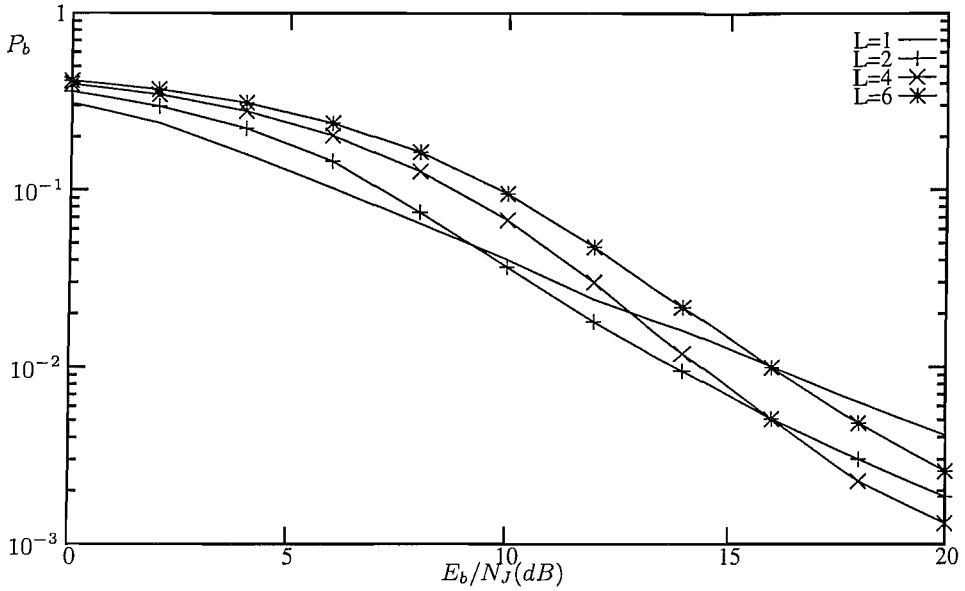


**Figure 1.12:** BER $P_b$ versus $E_b/N_J$ performance of the self-normalization based FFH assisted non-coherent BFSK receiver under the worst-case PBNJ in AWGN for increasing diversity order $L$ at $E_b/N_0 = 13.35$dB

Figure1.12 shows that although diversity provides performance gain for the NED based receiver in AWGN channels, the performance of the receiver associated with $L = 6$ is poorer than that in conjunction with $L = 4$. Similarly, Figure1.13 shows that under Rayleigh fading conditions, the performance of the same receiver using $L = 10$ is hardly better than that in conjunction with $L = 8$. Thus, at $E_b/N_0 = 13.35$dB, in AWGN $L$=4 (or perhaps $L$=5) appears to be an attractive design choice, while in Rayleigh fading at $E_b/N_0 = 16$dB, $L = 8$ may be deemed as the optimum diversity order. More importantly, it can be deduced from these two figures that diversity is more helpful under Rayleigh fading conditions. Hence, the optimum value of $L$ is higher for Rayleigh fading than for AWGN.

The fact that non-linear diversity combining schemes provide diversity gain both in non-fading and fading conditions is verified from Figures 1.12 and 1.13 in the context of the NED based receiver. These figures also demonstrate that the FFH assisted BFSK receiver employing non-linear diversity combining outperforms the SFH based MFSK system, where no diversity, i.e. $L = 1$ implies SFH.

Another observation that can be made from Figures 1.10 to 1.13 is that the achievable diversity gain does not manifest itself until a certain $E_b/N_J$ is reached. This is because for low values of $E_b/N_J$, the non-coherent combining losses dominate. Thus, the performance curve of NED based receiver shown in Figure 1.10 associated with $L$=2 drops below the curve recorded for $L$=1 beyond $E_b/N_J = 8$dB approximately, and similarly the curve corresponding to $L$=4 crosses that associated with $L$=2 when $E_b/N_J = 16$dB approximately. The values of these cross-over points depend upon the diversity order, on the type of channel and on $E_b/N_0$ value. Although this has not been depicted in the figures, the results of various researchers [36, 37, 39, 63, 66] show that the higher the $E_b/N_0$, the lower the $E_b/N_J$ value at which the diversity gain dominates the combining losses.

**Modulation Order:** It is well-known that the BER performance of FSK system improves with increase in modulation order [34]. This is because demodulation and detection decision in FSK receiver is based

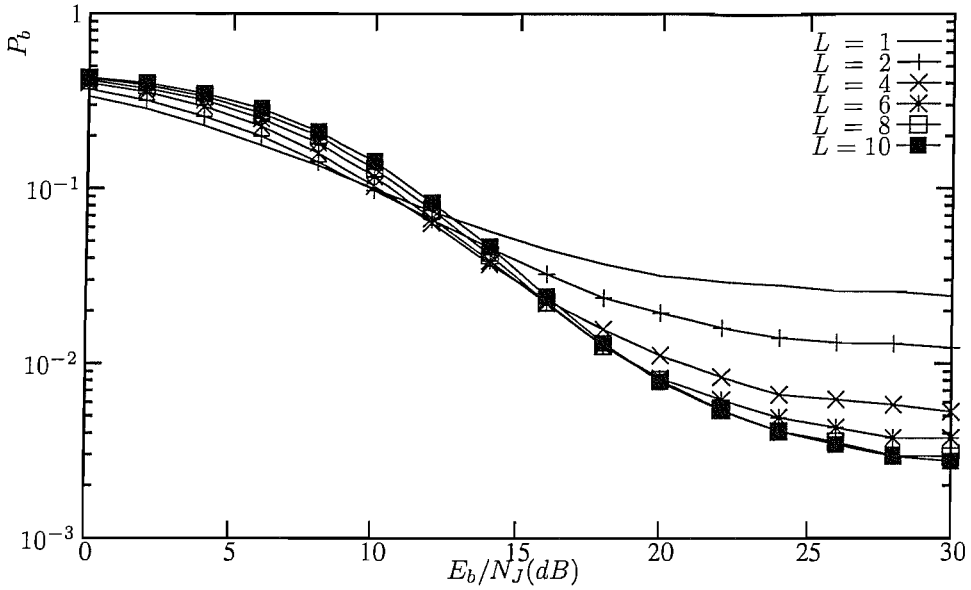


**Figure 1.13:** BER $P_b$ versus $E_b/N_J$ performance of the self-normalization based FFH assisted non-coherent BFSK receiver under the worst-case PBNJ in uncorrelated Rayleigh fading for increasing diversity order $L$ at $E_b/N_0 = 16$dB

on the energy received corresponding to all the FSK tones, and increasing modulation order enhances the symbol energy by a factor of $b = \log_2 M$, where $b$ is the number of bits per symbol and $M$ is the modulation order. Hence, energy per symbol is related to energy per bit by the relation: $E_s = bE_b$. Consequently, increasing the modulation order improves the achievable performance of the NED based receiver [40], as shown in Figures 1.14 and 1.15 where the performance of this receiver has been plotted in Rayleigh fading channels under worst case PBNJ for various values of modulation and diversity orders. It can be seen from these figures that the gain in BER performance achieved through higher value of $M$ becomes more significant with increasing diversity order. Thus, the gap between the curves corresponding to $M = 4$ and 8 widens when $L$ =4 as seen in Figure 1.15 compared to the case when $L = 2$ in Figure 1.14. Thus, the use of higher modulation order in conjunction with higher diversity level promises significant BER performance gain against PBNJ in non-coherent MFSK.

In summary, the key to achieving good performance using the NED based receiver against PBNJ is to maintain a sufficiently high $E_b/N_0$ (which is in excess of 13dB), choose an optimum diversity order such as $L = 2$ or 4 in case of AWGN and higher values of $L$ for fading channels, and maintain an appropriate value of $E_b/N_J$. The use of higher $L$ would also force the jammer to adopt a wide-band jamming strategy, thus lowering the jammer power as evidenced by the $\rho_0$ values seen in Table 1.3. Furthermore, use of higher modulation order also yields improved performance, although the bandwidth requirements also increase.

### 1.5.1.2 Performance in the Presence of MTJ

Let us now focus our attention on the performance of the NED based receiver in the presence of MTJ. We present here a brief analysis of this type of receiver under MTJ, focusing our attention primarily on the

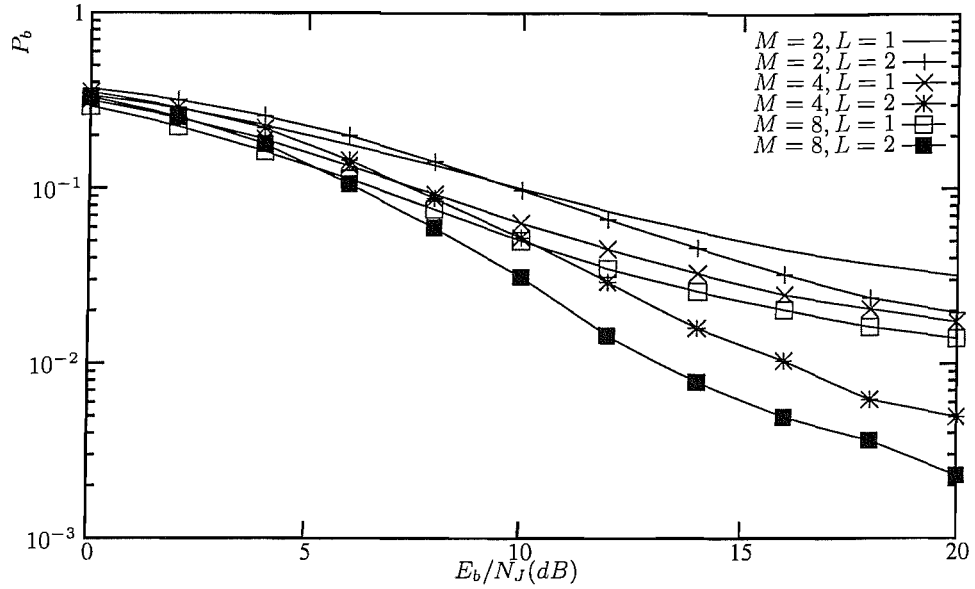


**Figure 1.14:** BER $P_b$ versus $E_b/N_J$ performance of the self-normalization based FFH assisted non-coherent BFSK receiver under the worst-case PBNJ in uncorrelated Rayleigh fading with diversity order $L$ and modulation order $M$ as parameters at $E_b/N_0 = 16$dB

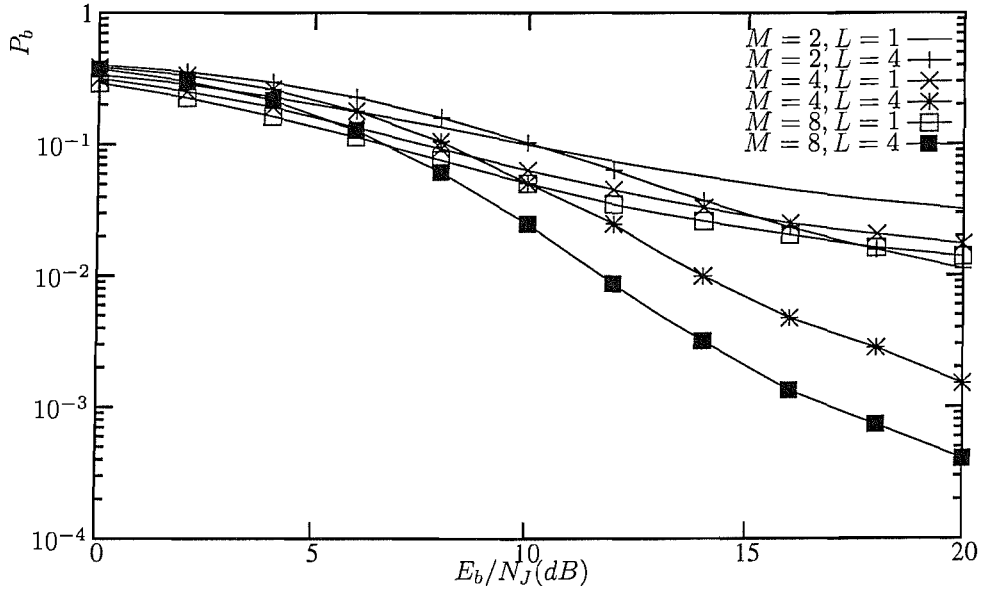


**Figure 1.15:** BER $P_b$ versus $E_b/N_J$ performance of the self-normalization based FFH assisted non-coherent BFSK receiver under the worst-case PBNJ in uncorrelated Rayleigh fading with diversity order $L$ and modulation order $M$ as parameters at $E_b/N_0 = 16$dB

comparison of the system performance under MTJ to that under PBNJ. To begin with, just as in the case of PBNJ, worst-case values of $q$ have been determined for $E_b/N_0 = 13.35$dB and various values of $E_b/N_J$ and $L$ which were summarised in Table 1.4. We can see from the table that $q_0$ shows trends similar to $\rho_0$. More specifically, its value tends to be closer to 1 when the fading is severe and the diversity order is high.

Study of the open literature suggests that MTJ is, in general, more effective than PBNJ in terms of degrading any receiver's performance [38, 63, 65]. Figures 1.16 and 1.17 show the performance of the self-normalization BFSK receiver under worst-case PBNJ and MTJ in AWGN and uncorrelated Rayleigh fading, respectively. It can be seen from Figure 1.16 that the performance of this receiver under PBNJ is

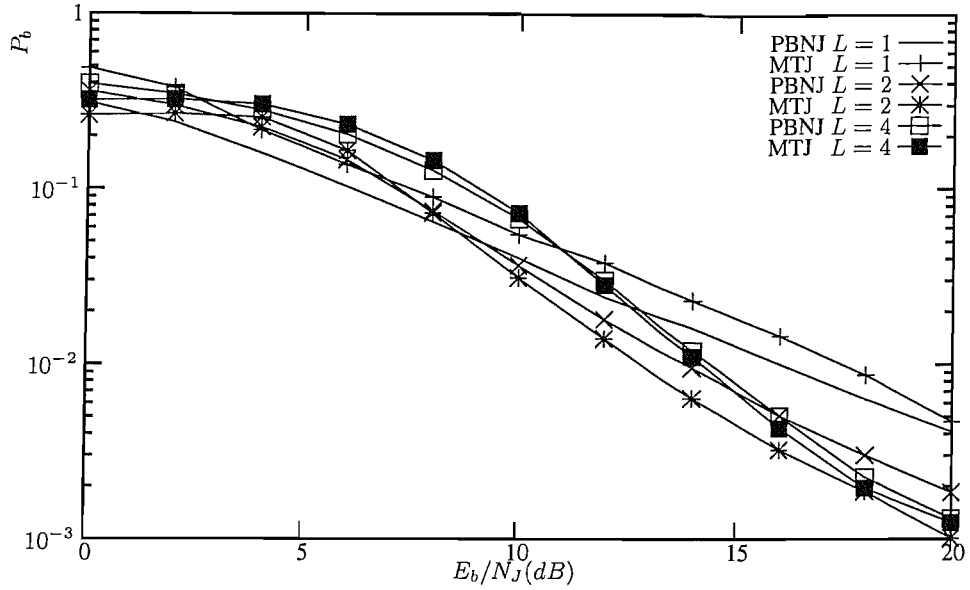


**Figure 1.16:** BER $P_b$ versus $E_b/N_J$ performance of the self-normalization based FFH assisted non-coherent BFSK receiver under worst-case PBNJ and MTJ in AWGN at $E_b/N_0 = 13.35$dB

better than that under MTJ in AWGN for $L = 1$. However, with increasing diversity order and sufficiently high signal to jammer noise power ratio, the difference between the two types of jamming is negligible. In fact, for $L = 2$ and 4, the performance under MTJ is slightly superior in comparison to that under PBNJ for a wide range of $E_b/N_J$ values. Figure 1.17 shows that the performance of self normalized BFSK receiver in uncorrelated Rayleigh fading is similar under worst-case PBNJ and MTJ for all the values of diversity orders shown. These results are similar to those recorded by Teh *et al.* in [63].

In Figures 1.18 and 1.19, we have made a similar comparison of the BER performance under worst case PBNJ and worst case MTJ for 4-ary and 8-ary FSK respectively. From these figures, we can see a significant performance difference for the receiver under the two different types of jamming and MTJ is seen to be markedly more detrimental in terms of degrading the BER performance of the receiver. Furthermore, we can see that for $M = 8$, the gaps between the curves corresponding to PBNJ and MTJ are even wider as

| $E_b/N_J(dB)$ | $q_0$ | | | |
|---|---|---|---|---|
| | L=1 | | L=3 | |
| | AWGN | Rayleigh | AWGN | Rayleigh |
| 0 | 1.0 | 1.0 | 1.0 | 1.0 |
| 2 | 1.0 | 1.0 | 1.0 | 1.0 |
| 4 | 0.6 | 1.0 | 1.0 | 1.0 |
| 6 | 0.5 | 1.0 | 1.0 | 1.0 |
| 8 | 0.3 | 1.0 | 1.0 | 1.0 |
| 10 | 0.2 | 0.9 | 1.0 | 1.0 |
| 12 | 0.09 | 0.8 | 0.8 | 1.0 |
| 14 | 0.06 | 0.7 | 0.4 | 1.0 |
| 16 | 0.04 | 0.6 | 0.1 | 1.0 |
| 18 | 0.02 | 0.4 | 0.08 | 0.9 |
| 20 | 0.008 | 0.2 | 0.06 | 0.7 |

**Table 1.4:** Worst-case duty factor $q_0$ values of MTJ for self-normalized non-coherent BFSK in conjunction with $L$=1 and 3 in both AWGN and Rayleigh fading channel at $E_b/N_0 = 13.35$dB

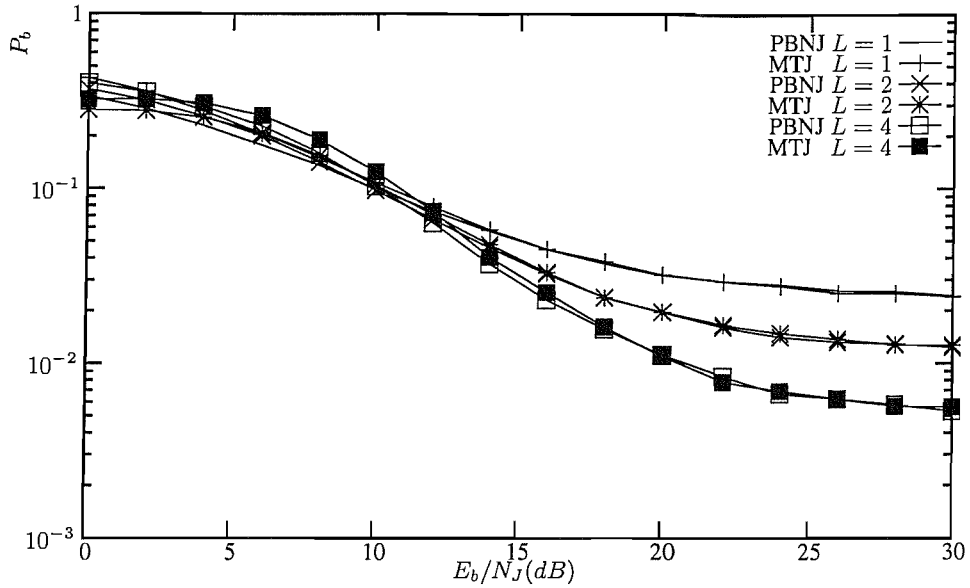


**Figure 1.17:** BER $P_b$ versus $E_b/N_J$ performance of the self-normalization based FFH assisted non-coherent BFSK receiver under worst-case PBNJ and MTJ in uncorrelated Rayleigh fading of both signal and jammer tones, at $E_b/N_0 = 16$dB

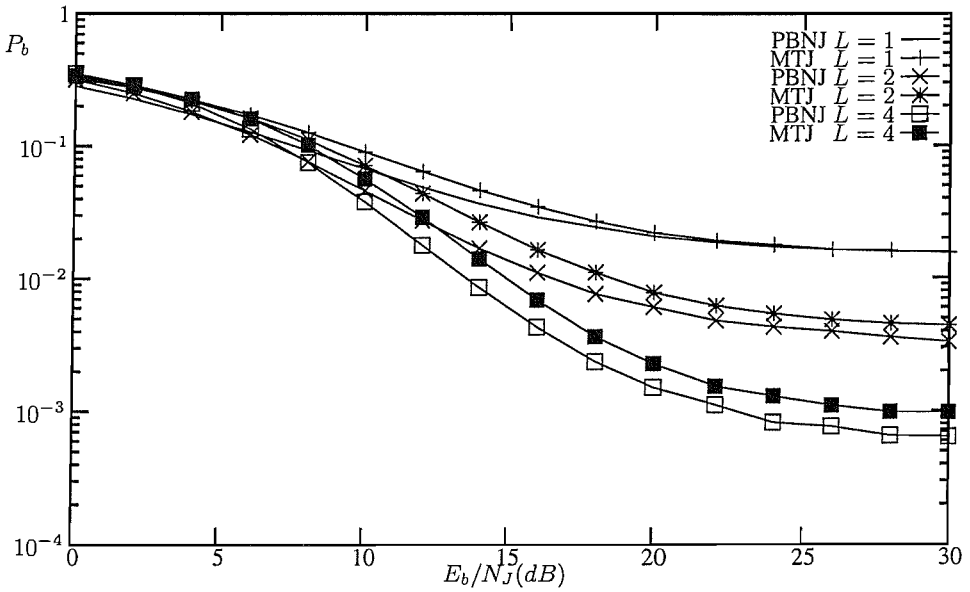


**Figure 1.18:** BER $P_b$ versus $E_b/N_J$ performance of the self-normalization FFH assisted non-coherent 4-ary FSK receiver under worst-case PBNJ and MTJ in uncorrelated Rayleigh fading of both signal and jammer tones, at $E_b/N_0 = 16$dB

compared to that for $M = 4$, when considering a given diversity order. From Figures 1.16 to 1.19, we can conclude that, while for $M = 2$ both types of jamming are almost equally detrimental against FFH assisted FSK, with increasing value of $M$ the detrimental effects of MTJ increase as compared to those of PBNJ in degrading the BER of the system. These simulation results agree with the findings of other researchers [38, 65, 66, 77].

There are two reasons for the increasing detrimental effects of MTJ with increase in modulation order. We elaborate these reasons in the context of $n = 1$-band MTJ, which is the worst-case MTJ [38]; the extension of the concept to the case of multiple jamming tones is straightforward. Firstly, when the jammer

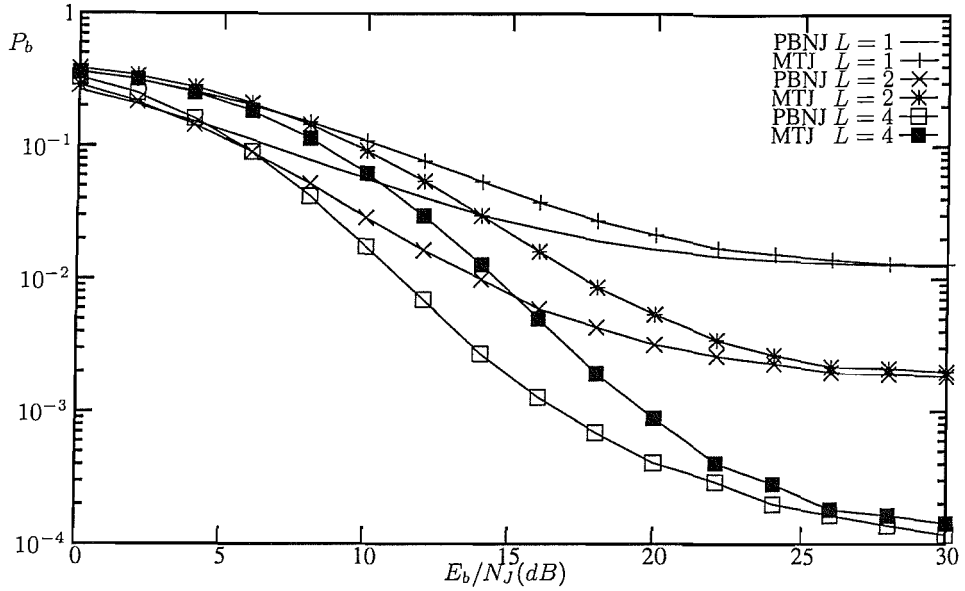


**Figure 1.19:** BER $P_b$ versus $E_b/N_J$ performance of the self-normalization based FFH assisted non-coherent 8-ary FSK receiver under worst-case PBNJ and MTJ in uncorrelated Rayleigh fading of both signal and jammer tones, at $E_b/N_0 = 16$dB

tones coincides with the signal tone, the jammer power, in fact, may aid the correct decisions, since the power of the jamming tone is added to that of the desired signal as shown in Section 1.3.3.2. Although the phases of the desired signal and the MTJ signal also play a part but they are uniformally distributed from 0 to $2\pi$. Conversely, the jamming tone results in detection error when it coincides with one of the non-signal tones. For low values of $M$, the probability of the jamming tone coinciding with the signal tone is high. This probability is 1/2 for BFSK, 1/4 for 4-ary FSK and $1/M$ for $M$-ary FSK, assuming the presence of a single jammer tone in each MFSK band. Likewise, the probability of jamming tone hitting the non-signal tine is 1/2 for BFSK, 3/4 for 4-ary FSK and $(M-1)/M$ for $M$-ary FSK, which means that it increases upon increasing the value of $M$. Secondly, a large value of $M$ reduces the total number of hopping bands for a fixed SS bandwidth ($N_b = W_{ss}/BM$) which will, in turn, increase the hit probability given by $q = Q/N_b$. Thus, as the modulation order of FSK system is increased, MTJ becomes more detrimental while the effects of PBNJ do not vary.

In general, the performance of the NED based receiver interfered by MTJ exhibits trends similar to that shown under PBNJ, apart from a few differences. As in the case of PBNJ, when FFH assisted MFSK communicates in the presence of MTJ, diversity is, as expected, more effective when fading is severe [63, 66]. Analogous to the case of PBNJ discussed in PBNJ in Section 1.5.1.1, combining losses also come into play with diversity combining when the system encounters MTJ. Therefore, an optimum diversity order may be determined, the value of which is typically higher for Rayleigh fading as compared to that for Rician fading and AWGN. Increasing $M$ to 4 and 8 improves receiver's performance but increasing it beyond 8 degrades performance [66]. Hence, optimum modulation order and diversity order have to be maintained to effectively combat MTJ in Rician channels, whereas in Rayleigh fading, higher $L$ always improves performance against MTJ, although overall performance is poor.

Since MTJ signals consist of pure tones which are assumed to be at the same frequency as the hopping tones, jamming signals may also experience fading just like the desired signal. Moreover, it is reasonable to assume that the fading of jamming tones is independent of that of the desired signal. Teh *et al.* [63] have shown that the performance of most receivers is only moderatley affected by the type of fading experienced by the jamming tones. The results shown in Figures 1.16 to 1.19 have been obtained from simulations assuming uncorrelated Rayleigh fading of both the signal and the jammer tones.

### 1.5.2 Product Combining Based FFH-MFSK Receiver

As discussed in Section 1.4.5, in the FFH assisted non-coherent MFSK receiver using product combining, the product of the outputs of each square-law detectors during all hops is computed to arrive at the decision variable, based on which the detection decision is made. The product combining receiver achieves good performance against MTJ, which many other receivers do not tolerate as well as they do PBNJ. The reason is that because of the multiplication operation, any non-signal branch yields very low value whatever be the power of the jamming signal in any of the jammed hops.

Teh *et al.* [43, 56, 64] have analyzed the BER performance of FFH assisted non-coherent BFSK using product combining under both MTJ and PBNJ. The researchers have shown that, since it is more robust against MTJ, the performance of this receiver is better in worst-case MTJ than in worst-case PBNJ, which is in contrast to most other receivers. Its performance has been found to be better than that of the linear combining receiver and nearly as good as that of the self-normalizing receiver in MTJ when operating in AWGN. Moreover, as compared to many other combining schemes, product combining has the advantage of not requiring any side information. Furthermore, a specific drawback of the product combining based scheme is that the performance of the system becomes severely degraded, when fading is severe and in Rayleigh fading, the performance achieved by this scheme is poorer than that attained using some other schemes, such as, for example, self-normalization combining [43, 64]. This is because the $M$ decision variables $Z_m, m = 0, 1, \ldots, M-1$, attain low values when the system operates in Rayleigh fading owing to the associated multiplication operation. Note that if one of two multiplicative variables is less than 1, then their product becomes lower than the larger of the two. Thus, under severe fading conditions, energy is lost owing to the product combining.

Figure 1.20 compares the achievable performance of the product combining scheme to that of the self-normalizing scheme when used in FFH assisted non-coherent BFSK under worst-case MTJ in AWGN channel. The difference in the performance of the two types of receivers corresponding to a diversity order of 2 is negligible, while when we have $L = 4$, the product combining scheme results in slightly better BER for $E_b/N_J \leq$ 10dB, beyond which the performance of self-normalization based system becomes slightly better than its product combining based counterpart. We also note from Figure 1.20 that for a wide range of $E_b/N_J$, the performance achieved by both types of combining schemes corresponding to $L = 2$ is better than that with $L = 4$, thus indicating that an optimum diversity order also exists for the product combining

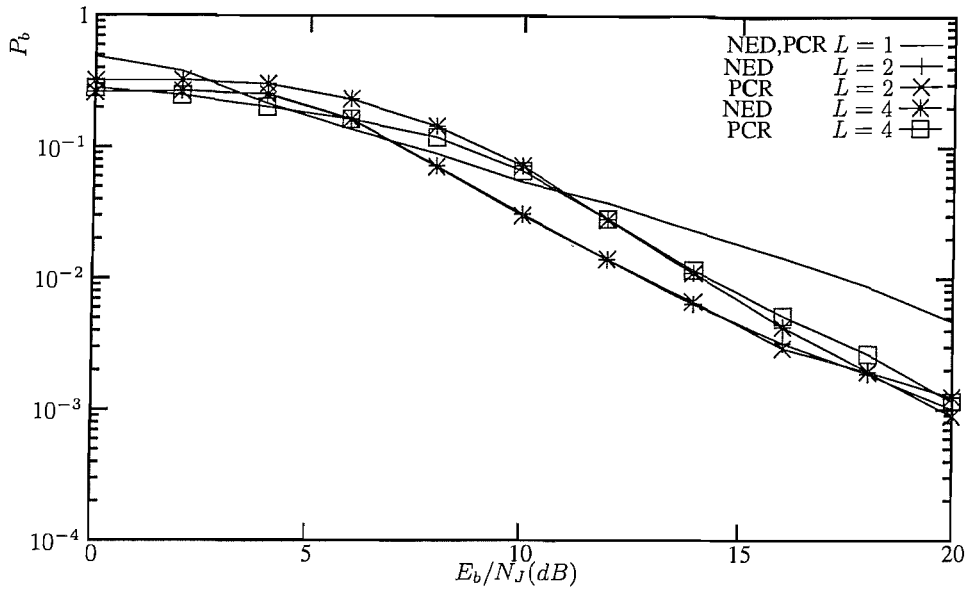


**Figure 1.20:** BER $P_b$ versus $E_b/N_J$ performance of the self-normalization (*NED*) and product combining (*PCR*) based FFH assisted non-coherent BFSK receivers under worst-case MTJ in AWGN at $E_b/N_0 = 13.35$dB

based non-coherent MFSK system.

Figure 1.21 makes a similar comparison between the achievable performance of the product combining scheme and that of the self-normalizing scheme used in FFH assisted BFSK under worst-case MTJ, in conjunction with uncorrelated Rayleigh fading of both the signal and jamming tones. It can be seen from this figure that the performance of the product combining receiver is better that of the self-normalization based receiver when $E_b/N_J \leq 15$dB and poorer than it beyond this value of $E_b/N_J$; however, the performance difference is not significant. Assuming the same experimental conditions as in Figure 1.21 but with the modulation order increased to 4, the difference in the BER of FFH assisted FSK achieved using product combining and self-normalization combining increases, as shown in Figure 1.22. More significantly, this difference increases for $L = 4$ and also, the product combining based receiver achieves better BER than its NED based counterpart when $E_b/N_J \leq 15$dB.

It is seen from Figures 1.20 to 1.22 that the product combining scheme also results in satisfactory performance for the FFH assisted non-coherent FSK system, especially when there is no fading. In Rayleigh fading channel, this scheme results in better achievable performance than NED based system for low values of $E_b/N_J$. However, beyond a value of $E_b/N_J \approx 15$dB, the NED based receiver outperforms the product combining based system.

## 1.6 Summary and Conclusion

In this chapter, FH system was introduced and its two main types, namely SFH and FFH, were compared. Furthermore, various diversity combining techniques that can be used in conjunction with FFH assisted non-coherent MFSK receivers have been discussed. The basic principle of diversity combining used in each of

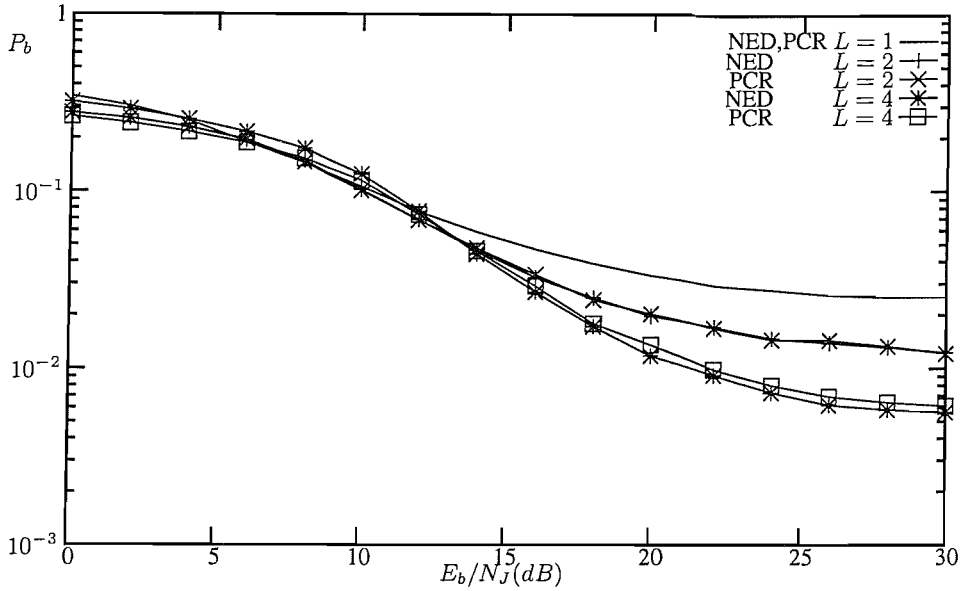


**Figure 1.21:** BER $P_b$ versus $E_b/N_J$ performance of the self-normalizing (*NED*) and product combining (*PCR*) based FFH assisted non-coherent BFSK receivers under worst-case MTJ in uncorrelated Rayleigh fading of both signal and jammer tones at $E_b/N_0 = 16$dB

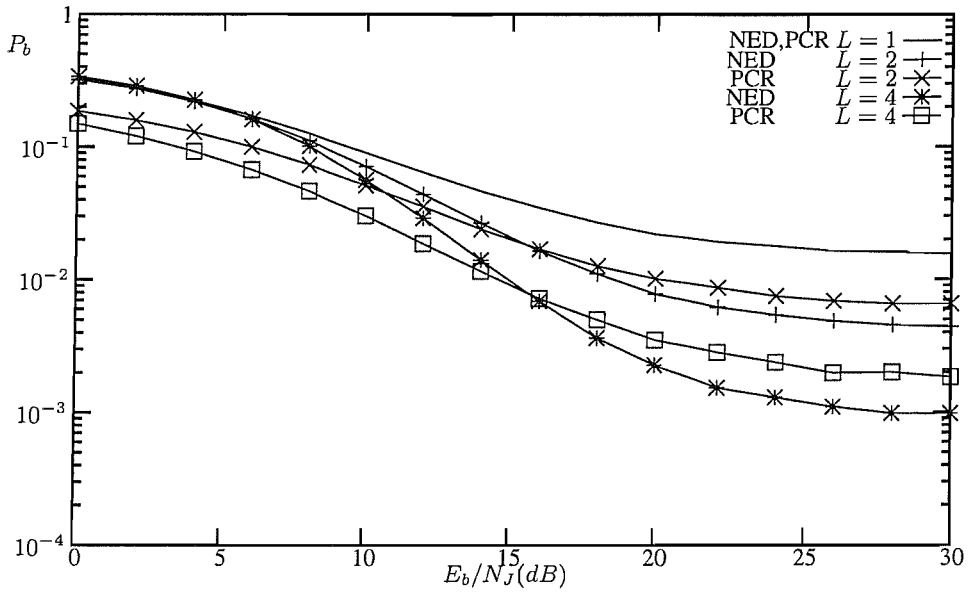


**Figure 1.22:** BER $P_b$ versus $E_b/N_J$ performance of the self-normalizing (*NED*) and product combining (*PCR*) based FFH assisted non-coherent 4-ary FSK receivers under worst-case MTJ in uncorrelated Rayleigh fading of both signal and jammer tones at $E_b/N_0 = 16$dB

these techniques has been discussed briefly. One of these combining schemes, namely the self-normalization diversity combining scheme, has been investigated using simulations results given in Figures 1.8 to 1.19 when used in a FFH non-coherent MFSK receiver under various channel and jamming conditions. Comparisons of its performance with that of the linear combining scheme have been given in Figures 1.10 and 1.11. A few simulation results have also been provided for the product combining based scheme in Figures 1.20 to 1.22. These combining schemes have been chosen as representative schemes for detailed investigation because of their attractive performance and low complexity. Based on the investigation of these diversity combining schemes, generalized conclusions can be drawn about linear and other non-linear diversity com-

bining schemes, which are summarised below.

Study of the contributions of a large numbers of researchers summarised and discussed in Sections 1.2 and 1.4 and results obtained from simulations, given in Section 1.5 demonstrate that:

1) The jamming duty factor, which is a measure of the fraction of the SS bandwidth affected by the jamming, is a key parameter that governs the detrimental effects inflicted by PBNJ or MTJ.

2) Most of the discussed non-linear diversity combining methods provide appreciable performance gain compared to the linear diversity combining method, when the receiver operates in AWGN under the influence of interference [44] (Figures 1.10 and 1.11).

3) Self-normalization, the noise-normalization and the clipped diversity methods rank amongst the best diversity combining methods, when used in FFH assisted non-coherent MFSK [39, 40, 42, 44, 52]. Using these diversity combining schemes, useful BER performance gain for MFSK may be obtained and the achievable performance gain increases upon increasing the diversity order (Figures 1.10 to 1.22).

4) An optimum value of the diversity order has to be determined for all types of combining schemes, as seen in Figures 1.11 and 1.12 in the context of self-normalization combining. This is because non-coherent combining losses also come into play in non-coherent MFSK receiver, owing to which little performance gain is attained through using high $L$ values. The value of the optimum diversity level depends upon the fading conditions and the values of $E_b/N_J$, $E_b/N_0$ and the modulation order.

5) Due to the associated combining losses, the diversity gain manifests itself only beyond a certain value of $E_b/N_J$, and little performance gain is attained when the signal power is either too low or too high in comparison to the jammer power.

6) Increasing the modulation order of the MFSK system improves the performance of all MFSK receivers, although in MTJ conditions, a high value of $M$ ($M \geq 8$) increases the detrimental effect of the jamming. Thus, when operating under MTJ, a suitable modulation order, for example 4 or 8, has to be chosen [66]. Hence, to achieve the best BER performance in the context of most diversity combining schemes, an intermediate range of the signal to interference power ratio has to be maintained, together with the optimum diversity and, in case of MTJ, the optimum modulation order.

7) The performance of NED based receiver is poor in Rayleigh fading conditions, as seen in Figures 1.11, 1.13 to 1.15, 1.17 to 1.19, 1.21 and 1.22. Similar trends have been recorded about a number of other diversity combining schemes in [39,40]. This is a consequence of the various normalization operations performed by the receiver on the received signals when using the non-linear combining methods of Section 1.4. Consequently, in Rayleigh fading, the performance improvement of NED combining over linear combining scheme is not significant and using linear combining is the better option, when the SJR is high enough. The achievable diversity gain is more substantial, however, in Rayleigh fading,

as seen for example in Figure 1.13. Moreover, the study of published literature demonstrates that in less severe fading conditions, non-linear combining schemes constitute better option than the linear combiner [39, 40, 43, 63].

The performance of FFH-MFSK receiver employing various combining schemes under different channel conditions have been tabulated in Tables 1.5, 1.6 and 1.7.

We have seen in this chapter that although the inherent diversity of FFH systems results in improvement of the MFSK system performance in fading and interference conditions, two areas remain of concern: one, performance in severe fading, i.e in Rayleigh fading, is poor, and two, MTJ can severely degrade the performance of the FFH assisted MFSK receiver, also prohibiting the use of higher modulation order. To circumvent these problems, a suitable diversity combining scheme can be used in conjunction with some form of forward error correction coding, if fading is severe [39]. Employing erasure insertion techniques has the potential of further assisting in combatting interference in coded FFH-MFSK and is an area which merits research [99]. In the next chapter, use of error-and-erasure Reed Solomon decoding is considered with SFH assisted MFSK system encountering MTJ and Rayleigh fading.

| | SFH (L=1) | Linear combining | NED combining |
|---|---|---|---|
| AWGN, $L = 2$, $E_b/N_0 = 13.35$dB | 16.1 | 17.2 | 14.1 |
| Rayleigh, $L = 4$, $E_b/N_=16$dB | NA | 20.8 | 20.8 |

NA means 'not achieved'.

**Table 1.5:** $E_b/N_J$ values in dBs required to achieve a BER of $10^{-2}$ by FFH-BFSK receiver encountering PBNJ and using various configurations. The results were extracted from Figures 1.10 and 1.11.

| M | $L = 1$ | | $L = 2$ | | $L = 4$ | |
|---|---|---|---|---|---|---|
| | PBNJ | MTJ | PBNJ | MTJ | PBNJ | MTJ |
| 2 | NA | NA | NA | NA | 20.9 | 20.9 |
| 4 | NA | NA | 16.2 | 18.4 | 13.9 | 15.0 |
| 8 | NA | NA | 13.6 | 17.1 | 11.7 | 14.5 |

NA means 'not achieved'.

**Table 1.6:** $E_b/N_J$ values in dBs required to achieve a BER of $10^{-2}$ by FFH-MFSK NED receiver encountering PBNJ and MTJ, assuming Rayleigh fading channel and $E_b/N_0 = 16$dB. The results were extracted from Figures 1.17 to 1.19.

| | $M$ | SFH (L=1) | PCR | NED combining |
|---|---|---|---|---|
| AWGN, $L = 2$, $E_b/N_0 = 13.35$dB | 2 | 17.5 | 12.8 | 12.8 |
| Rayleigh, $L = 4$ | 2 | NA | 21.6 | 20.9 |
| $E_b/N_0 = 16$dB | 4 | NA | 14.6 | 15 |

NA means 'not achieved'.

**Table 1.7:** $E_b/N_J$ values in dBs required to achieve a BER of $10^{-2}$ by FFH-MFSK receiver encountering MTJ and using various configurations. The results were extracted from Figures 1.17 to 1.22.

Chapter 2

# Erasure Insertion in RS-Coded SFH MFSK Subjected to Tone Jamming

## 2.1 Introduction

In the last chapter, we investigated the anti-jamming capabilities of the uncoded fast frequency hopping $M$-ary frequency shift keying (FFH-MFSK) employing various diversity combining schemes. In this chapter, we look into another technique of combatting jamming in FH-MFSK. Specifically, we consider how error and erasure decoding (EED) can aid SFH-MFSK in mitigating the effects of multitone jamming (MTJ). Erasure insertion (EI) implies that, based on certain criteria, a symbol which is deemed to be unreliable owing to fading, interference or both is erased. Consequently, the erasure of the unreliable symbols allows the decoder to make better decoding decisions [100, 101], since, the decoder can correct more errors with erasures then it can when employing error-correcting-only (ECO) decoding.

Since slow frequency hopping (SFH) does not benefit from diversity inherently available to FFH, its performance is severely degraded in the presence of jamming, necessitating the use of some form of forward error correction (FEC) [100–105]. In SFH assisted MFSK using Reed Solomon (RS) coding, typically EED is employed for enhancing the achievable system performance when encountering interference and/or jamming. Various EI schemes designed for supporting EED in conjunction with SFH assisted MFSK receivers have been proposed in open literature [99, 106, 107]. The pioneering contribution on erasure of unreliable symbols in MFSK systems was made by Viterbi [106], who suggested the well-known ratio threshold test (RTT) based EI scheme. Baum and Pursley [107–109] proposed an EI criterion based on the Bayesian method which outperforms Viterbi's RTT [106]. However, the Bayesian method requires the knowledge of all of the $M$ FSK decision variables and the associated complexity increases exponentially with $M$. Su and Jeng have considered both the Bayesian and the RTT based methods in conjunction with RS-coded SFH assisted MFSK in [96]. When using RS coding, EI can also be achieved by attaching parity-check bits to

each of the RS coded symbols [110–112], for checking whether the symbol was correctly received. However, this type of EI is achieved at the cost of reducing the overall throughput. Furthermore, similar to other channel coded schemes, this type of EI degrades the achievable performance in the low SNR region, due to the increased redundancy. This is because the increased redundancy reduces the transmitted energy per symbol, as a result of which the achievable uncoded error rate increases, which may therefore exceed the error-correcting capability of the RS code, when the SNR is low. EI methods have also been employed in SFH communicating in multiple access (MA) scenario [109, 113–115].

In [99], two low complexity EI methods namely, the output threshold test (OTT) and the maximum output-ratio threshold test (MO-RTT) have been proposed and investigated, when the RS-coded SFH assisted MFSK system is considered in conjunction with Nakagami-$m$ fading channels in the presence of partial band noise jamming (PBNJ). Like the RTT, these two EI schemes belong to the class of low-complexity EI schemes. Specifically, the OTT-based EI observes the maximum of the $M$ decision variables, while the joint MO-RTT-based EI observes both the maximum and the second maximum of the $M$ decision variables of the MFSK demodulator. It has been shown in [99] that the OTT-based EI is resilient against fading, while the joint MO-RTT is robust against both fading and PBNJ. Note that the RTT-assisted EI [106] is capable of mitigating PBNJ, but it is not particularly resilient against fading.

It is well recognized that in general tone jamming is more detrimental in terms of degrading the performance of MFSK based communication systems [38]. We verified this fact with the aid of simulation results in Chapter 1. However, in literature, the investigation of the SFH assisted MFSK system employing EED and encountering both fading and tone jamming has received little attention. Therefore, in this chapter, we extend the results of [99] by investigating the performance of the SFH assisted MFSK system when communicating over Rayleigh fading channels in the presence of tone jamming. In our analysis three different types of low complexity EI schemes are considered, which include Viterbi's RTT [106], as well as the OTT and the MO-RTT techniques which were proposed in [99]. The statistics associated with these EI schemes are derived, when we assume that both the desired signal and the interfering tones experience Rayleigh fading. With the aid of these statistics, we then compute the codeword error probability after erasure insertion. Finally, the bit error ratio (BER) performance of the SFH assisted MFSK system is evaluated and analyzed. We will demonstrate that these EI schemes are capable of providing useful information for improving the performance of EED.

The rest of this chapter is structured as follows. In Section 2.2, we briefly describe the communication system, the channel model and the characteristics of the tone jamming. In Section 2.3, the performance of the uncoded SFH assisted MFSK system is analyzed, while in Section 2.4, the EI schemes considered are discussed and their relevant statistics are derived. Section 2.5 provides a range of performance results and finally in Section 2.6 we provide our conclusions.

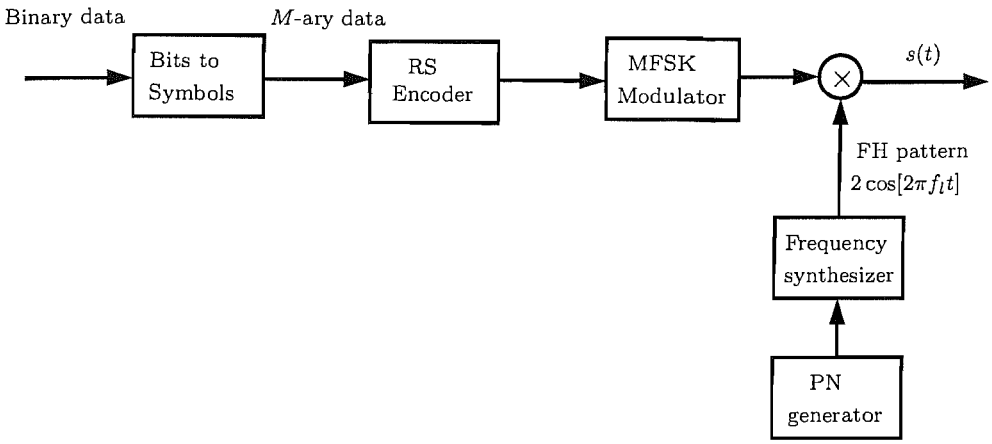


**Figure 2.1:** Transmitter block diagram of the SFH assisted MFSK system using RS coding

## 2.2 System Description

The system under consideration is similar to that considered in [96]. The block diagram of the transmitter for the SFH assisted MFSK system is shown in Figure 2.1. As shown in this figure, after the bit-to-symbol mapping, the $M$-ary data are RS-encoded before MFSK modulation, where the RS encoder converts each block of $K$ $M$-ary information symbols into $N$ coded symbols. We assume that $N = M-1 = 2^b-1$, where $b = \log_2 M$ represents the number of bits per symbol. We also assume that the coded symbols are perfectly interleaved. However, we assume in this particular scenario that every symbol is transmitted in a separate hop, hence interleaving may be dispensed with. As shown in Figure 2.1, the frequency synthesizer is under the control of a pseudo-noise (PN) generator in order to form a sequence of random hopping frequencies, one of which is activated during each hop interval of duration $T_h$, for implementation of the frequency hopping. Finally, as shown in Figure 2.1, assuming that the $m$th FSK tone $f_m$ is activated, the MFSK modulated SFH signal may be expressed as:

$$s(t) = \sqrt{2PR_c}\cos\left\{2\pi\left[f_m + f_l\right]t + \varphi_m + \varphi_l\right\}, \tag{2.1}$$

where $P$ represents the power of the transmitted signal, $R_c = K/N$ is the code rate, $f_l$ is the FH frequency during the time interval of $lT_h \leq t < (l+1)T_h$, while $T_h$ represents the FH dwell time. Furthermore, in Equation (2.1), $\varphi_l$ and $\varphi_m$ represent the phases associated with the $l$th FH frequency and the $m$th MFSK tone, respectively, both of which are assumed to be constant within a symbol duration. We assume that there is only one hop per symbol, i.e. diversity order $L = 1$. Thus, we have $T_h = T_s$, which is the symbol duration. Furthermore, we assume that bandwidth of one FSK tone $B = 1/T_h$, which is the minimum frequency spacing required to maintain orthogonality amongst FSK tones and FH tones. Thus, the FH signal hops randomly over a total spread spectrum bandwidth of $W_{ss} = MN_bB$, where $N_b$ is the number of hop bands each consisting of $M$ FSK tones.

For each FH tone, the signal given by Equation (2.1) is transmitted over a channel which is modeled as

frequency non-selective fading obeying Rayleigh distribution. We assume that the fading is sufficiently slow so that its amplitude and phase remain constant within a symbol duration. Moreover, we assume that fading is independent for each symbol. Consequently, when assuming Rayleigh fading, the probability density function (PDF) of the amplitude attenuation factor is given by [34]

$$p_\alpha(r) = \frac{2r}{\Omega} e^{-r^2/\Omega}, \qquad r \geq 0 \tag{2.2}$$

where $\Omega = E[\alpha^2]$.

In addition to the channel's fading, the transmitted signal is also assumed to be interfered by a tone jamming signal, which is assumed to have $Q$ equal-power continuous wave tones, each of which has a frequency equal to that of one of the $M$-ary tones. The ratio $q = Q/N_b$ is termed as the jamming duty factor of the MTJ signal. We consider the case of $n = 1$-band multitone jamming (MTJ), which has been investigated in [75], and is regarded as the worst case tone jamming scenario [38, 75]. In the context of this type of jamming, as discussed in Section 1.3.2, the intentional jammer places at the most one interfering tone in a MFSK band, defined by the bandwidth occupied by the $M$ FSK signalling tones. Furthermore, it has been shown and also verified by our simulation results in Section 1.5 that for Rayleigh fading a jammer associated with a jamming duty factor of unity causes the most detrimental interference of the FH system [76, 78]. Then, the above assumptions imply that the number of jamming tones obeys $Q = N_b$ or $q = 1$ and there is exactly one interfering tone in each of the MFSK bands. This also implies that the probability that a specific MFSK tone is interfered is given by $1/M$. The total spread spectrum bandwidth is assumed fixed. Moreover, we assume that the intentional jammer has knowledge of the parameters of the communication system and, thus, can adjust the number of jamming tones accordingly, keeping the total MTJ power fixed. This implies that, if the modulation order $M$ is increased, $Q = N_b = W_{ss}/MB$ reduces allowing the jammer to spread its total power in fewer, higher power tones in comparison with a lower modulation order system. We can define the signal energy to jammer power spectral density as [65, 75]

$$SJR = \frac{E_b}{P_{TJ}/W_{ss}} = \frac{E_b}{P_J}\frac{N_b}{Q}\frac{M}{T_h}, \tag{2.3}$$

where $E_s = PT_h = bE_b$ represents the energy per $M$-ary symbol and $E_b$ is the energy per bit. Furthermore, in Equation (2.3), $P_{TJ} = P_J Q$ is the total MTJ power, $P_J$ is the power of a single MTJ tone, and we also define the MTJ power spectral density as $N_J = P_{TJ}/W_{ss}$. Thus, from Equation (2.3) we have [65]

$$SJR = \frac{E_s}{E_j}\frac{M}{b}, \tag{2.4}$$

where $E_j = P_J T_h$ represents the energy of the interfering tone per symbol duration. We further assume that the interfering tones also experience Rayleigh fading. Furthermore, the fading processes of the signal and interfering tones are assumed to be independent of each other.

The receiver block diagram of the SFH assisted MFSK system is shown in Figure 2.2. The receiver

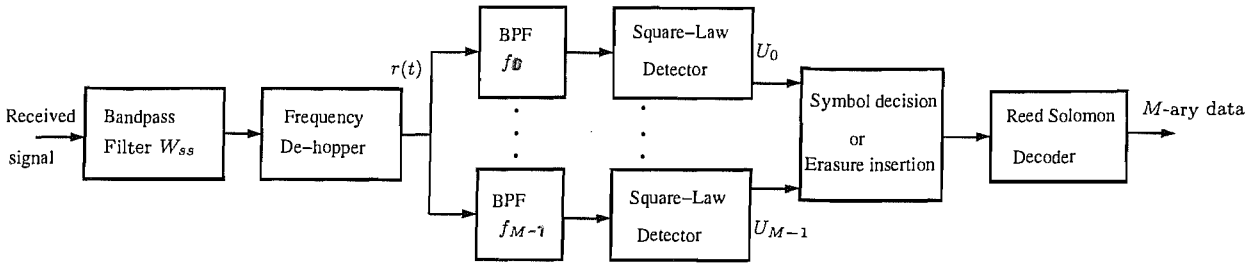


**Figure 2.2:** Receiver block diagram of SFH assisted non-coherent MFSK system employing erasure insertion and RS decoding.

consists of a bandpass filter, a frequency de-hopper, a non-coherent MFSK demodulator, a decision device and finally an RS decoder. The bandpass filter removes any frequency that falls outside the FH bandwidth $W_{ss}$. The frequency de-hopper consists of a PN generator and a frequency synthesizer that are identical to those used in the transmitter shown in Figure 2.1. The frequency de-hopper removes the FH frequency from the received signal. As shown in Figure 2.2, following frequency de-hopping, the signal is demodulated using a non-coherent MFSK detection scheme, yielding $M$ number of variables at the outputs of the square law detectors. These variables are then input to the decision device which, based on the reliability of the corresponding symbol, either outputs a symbol based on hard maximum likelihood decision or generates an erasure , as will be discussed in Section 2.4. Finally, as shown in Figure 2.2, when the receiver has collected $N = M-1$ symbols of a full RS code, the $N$ symbols are decoded using the error-and-erasure RS decoding, in order to recover the $K$ information symbols.

**PDFs of the Energy Detector Outputs:** Without loss of generalization, we assume that the first FSK tone is activated, which is referred to as the desired signal tone, whereas all the other FSK tones are referred to as non-signal tones. Then, after the FH dehopping scheme as shown in Figure 2.2, the signal at the input of the square law detectors, when no interference tone is present, can be expressed as

$$r(t) = \alpha_s \sqrt{2PR_c} \cos\left\{2\pi\left(f_0\right)t + \theta_s\right\} + n_0(t), \tag{2.5}$$

where $\alpha_s$ represents the amplitude attenuation factor due to Rayleigh fading, $\theta_s$ includes all the phases in the received signal, including those due to FH, carrier modulation and MFSK modulation as well as that induced by the fading channel. Furthermore, in Equation (2.5), $n_0(t)$ represents the AWGN with zero mean and double-sided power spectral density of $N_0/2$. By contrast when an interference tone coincides with the signal tone, the signal at the input of the square law detector may be expressed as

$$r(t) = \alpha_s \sqrt{2PR_c} \cos\left\{2\pi\left(f_0\right)t + \theta_s\right\} + \alpha_j \sqrt{2P_J} \cos\left\{2\pi\left(f_0\right)t + \theta_j\right\} + n_0(t), \tag{2.6}$$

where $\alpha_j$ and $\theta_j$ are the amplitude attenuation factor and the phase of the MTJ signal, respectively.

Let us denote the output of the square-law detector corresponding to the signal tone by $U_0$, when it

is uninterfered, and by $U_{0(j)}$ when the frequency of the interfering tone coincides with that of the signal tone. Similarly, let $U_m$ and $U_{m(j)}$ denote the output of the square-law detector corresponding to the $m$th non-signal tone when it is unaffected by jamming and when it is jammed, respectively. When the interfering tone frequency coincides with that of the signal tone, the outputs of the square-law detectors, using our discussion in Section 1.3.3.2, can be expressed as

$$U_{0(j)} = |\alpha_s\sqrt{R_cE_s}e^{j\theta_s} + \alpha_j\sqrt{E_j}e^{j\theta_j} + n_0|^2 \tag{2.7}$$

and

$$U_m = |n_m|^2 \qquad m = 1, 2, \ldots, M-1, \tag{2.8}$$

where $n_m$ represents the AWGN imposed on the $m$th tone, $m = 0, 1, \ldots, M$. By contrast, when the jamming signal coincides with one of the non-signal tones, the output of the square-law detector corresponding to the signal tone is given by

$$U_0 = |\alpha_s\sqrt{R_cE_s}e^{j\theta_s} + n_0|^2 \tag{2.9}$$

and that of the square-law detector corresponding to the jammed non-signal tone is

$$U_{m(j)} = |\alpha_j\sqrt{E_j}e^{j\theta_j} + n_m|^2. \tag{2.10}$$

Since we assume that both the desired signal and the jamming signal experience independent Rayleigh fading, the variables $\alpha_s\sqrt{R_cE_s}e^{j\theta_s}$, $\alpha_j\sqrt{E_j}e^{j\theta_j}$, as well as $n_m$, obey the complex Gaussian distribution. Thus, $U_{0(j)}$, $U_0$, $U_m$ and $U_{m(j)}$ in Equations (2.7) to (2.10) respectively, are central Chi-squared distributed with double degrees of freedom or exponentially distributed [34]. More specifically, the PDF of $U_{0(j)}$ can be expressed as [34]

$$f_{U_{0(j)}}(U_{0(j)}) = \frac{1}{2\sigma^2_{0(j)}} \exp\Big(-U_{0(j)}/2\sigma^2_{0(j)}\Big), \tag{2.11}$$

where $2\sigma^2_{0(j)} = E[U_{0(j)}] = \Omega_s R_c E_s + \Omega_j E_j + N_0$, $E[x]$ represents the estimate of the variable $x$, while $\Omega_s = E[\alpha_s^2]$ and $\Omega_j = E[\alpha_j^2]$. Similarly, the PDF of $U_m$ of Equation (2.8) is given by

$$f_{U_m}(U_m) = \frac{1}{2\sigma_m^2} \exp\Big(-U_m/2\sigma_m^2\Big), \qquad m = 1, 2, \ldots, M-1, \tag{2.12}$$

where $2\sigma_m^2 = E[U_m] = N_0$. Similarly, the PDFs of $U_0$ in Equation (2.9) and $U_{m(j)}$ in Equation (2.10) can be expressed as

$$f_{U_0}(U_0) = \frac{1}{2\sigma_0^2} \exp\Big(-U_0/2\sigma_0^2\Big) \tag{2.13}$$

and

$$f_{U_{m(j)}}(U_{m(j)}) = \frac{1}{2\sigma^2_{m(j)}} \exp\Big( - U_{m(j)}/2\sigma^2_{m(j)}\Big), \qquad m = 1, 2, \ldots, M-1, \tag{2.14}$$

where $2\sigma_0^2 = E[U_0] = \Omega_s R_c E_s + N_0$ and $2\sigma^2_{m(j)} = E[U_{m(j)}] = \Omega_j E_j + N_0$.

Let us define $\gamma_c = \Omega_s R_c E_s / N_0$ and $\gamma_j = \Omega_j E_j / N_0$. Thus, upon normalizing the decision variables by $2\sigma_m^2 = N_0$ it can be shown that

$$f_{U_{0(j)}}(y) = \frac{1}{1+\gamma_{cj}} \exp\left[ - \frac{y}{1+\gamma_{cj}}\right], \qquad y \geq 0, \tag{2.15}$$

$$f_{U_m}(y) = \exp(-y), \qquad y \geq 0, m > 1, \tag{2.16}$$

$$f_{U_0}(y) = \frac{1}{1+\gamma_c} \exp\left[ - \frac{y}{1+\gamma_c}\right], \qquad y \geq 0 \tag{2.17}$$

and

$$f_{U_{m(j)}}(y) = \frac{1}{1+\gamma_j} \exp\left[ - \frac{y}{1+\gamma_j}\right], \qquad y \geq 0, m > 1, \tag{2.18}$$

where $\gamma_{cj} = \gamma_c + \gamma_j$. Moreover, we can express $\gamma_j$ in terms of the SNR, given by $E_b/N_0$, and the SJR, represented by $E_b/N_J$. From Equation (2.4), we have

$$\gamma_j = \Omega_j E_j / N_0 = \Omega_j M \frac{SNR}{SJR}. \tag{2.19}$$

Having derived the PDFs of the decision variables, let us now derive the corresponding probability of error expressions.

## 2.3 Error Probability of the Uncoded System

In order to determine the probability of the symbol error of the uncoded SFH assisted MFSK system in the presence of $n = 1$-band MTJ, both the cases of the desired signal tone being jammed as well as that of the non-signal tones being jammed need to be considered. Let $H_1$ represent the hypothesis that the transmitted symbol is detected correctly and $H_0$ denote the hypothesis that the transmitted symbol is detected incorrectly, when using hard decisions. The probability of occurrence of these events is denoted by $P(H_1)$ and $P(H_0)$, respectively. Consequently, the probability $P_c$ of a correct decision can be expressed as

$$P_c = P(H_1) \;=\; \frac{1}{M} P[U_1 < U_{0(j)}, U_2 < U_{0(j)}, \ldots, U_{M-1} < U_{0(j)}]$$

$$+\frac{M-1}{M}P[U_1 < U_0, U_2 < U_0, \ldots, U_{m(j)} < U_0, \ldots, U_{M-1} < U_0], \quad (2.20)$$

where the first term on the right hand side of the above equation corresponds to the scenario when the signal tone is jammed while the second term caters for the case when a non-signal jamming tone is jammed. Upon substituting the PDFs of Equation (2.15) to Equation (2.18) into Equation (2.20), we arrive at

$$\begin{aligned}
P_c &= \frac{1}{M}\int_0^\infty f_{U_{0(j)}}(y)\left[\int_0^y f_{U_m}(x)dx\right]^{M-1} dy \\
&+ \left(\frac{M-1}{M}\right)\int_0^\infty f_{U_0}(y)\int_0^y f_{U_{m(j)}}(x)dx\left[\int_0^y f_{U_m}(x)dx\right]^{M-2} dy \\
&= \frac{1}{M}\int_0^\infty \frac{1}{1+\gamma_{cj}}\exp\left[-\frac{y}{1+\gamma_{cj}}\right]\left[\int_0^y e^{-x}dx\right]^{M-1} dy \\
&+\left(\frac{M-1}{M}\right)\int_0^\infty \frac{1}{1+\gamma_c}\exp\left[-\frac{y}{1+\gamma_c}\right] \\
&\times\left[\int_0^y \frac{1}{1+\gamma_j}\exp\left(-\frac{x}{1+\gamma_j}\right)dx\right]\left[\int_0^y e^{-x}dx\right]^{M-2} dy. \quad (2.21)
\end{aligned}$$

By carrying out the integrations and then invoking the binomial expansion [1], Equation (2.21) can be expressed as

$$\begin{aligned}
P_c &= \frac{1}{M}\sum_{n=0}^{M-1}(-1)^n\binom{M-1}{n}\frac{1}{1+n(1+\gamma_{cj})} \\
&+ \left(\frac{M-1}{M}\right)\sum_{n=0}^{M-2}(-1)^n\binom{M-2}{n}\left[\frac{1}{1+n(1+\gamma_c)}\right. \\
&\left.-\frac{1+\gamma_j}{2+\gamma_{cj}+n(1+\gamma_c)(1+\gamma_j)}\right]. \quad (2.22)
\end{aligned}$$

For the specific case of binary FSK, i.e. for $M = 2$, the above equation is reduced to the simple form of

$$P_c = \frac{1}{2}\left[\frac{2+\gamma_c+\gamma_{cj}}{2+\gamma_{cj}}\right]. \quad (2.23)$$

The corresponding probability $P_s$ of symbol error can, hence, be expressed as

$$P_s = P(H_0) = 1 - P_c. \quad (2.24)$$

Finally the BER of the uncoded system can be determined by using the relation

$$P_b = \frac{2^{b-1}}{M-1}P_s. \quad (2.25)$$

Figure 2.3 shows the BER of the uncoded SFH assisted MFSK system, when communicating over

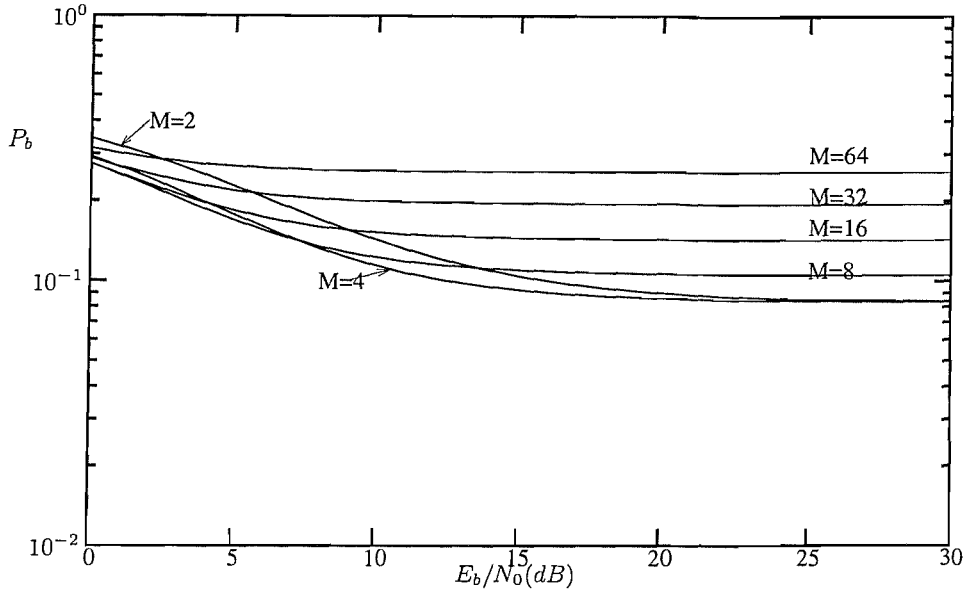


**Figure 2.3:** BER $P_b$ versus $E_b/N_0$ performance of SFH assisted uncoded non-coherent MFSK, when communicating over Rayleigh fading channels in the presence of $n = 1$-band MTJ at $E_b/N_J = 10$dB. $P_b$ is computed using Equations (2.22), (2.24) and (2.25).

Rayleigh fading channels, in the presence of $n = 1$-band MTJ. The BER evaluation is based on Equations (2.22), (2.24) and (2.25) and we have assumed $E_b/N_J = 10$dB as well as $M = 2, 4, 8, 16, 32$ and 64. It can be seen from Figure 2.3 that single tone jamming associated with each MFSK band severely degrades the BER performance of the system. Furthermore, the performance of the MFSK system deteriorates as $M$ increases, when a jamming tone is present in each MFSK band. This observation has also been reported in [38, 75, 116] and was also discussed in Section 1.5. From the results of Figure 2.3, it can be seen that the MFSK system corresponding to $M = 4$ achieves the best BER performance for most values of $E_b/N_0$. Note however that $M = 4$ is only optimum under the conditions assumed in Figure 2.3. When other conditions, for example other values of $E_b/N_0$ and $E_b/N_J$ are considered, the optimum value of $M$ might be different. Let us now focus our attention on the RS-coded SFH system.

## 2.4 RS-Coded System using Error-and-Erasure Decoding

In this section, we investigate the performance of the SFH assisted MFSK system when EED is considered. Three types of EI schemes are considered, namely, OTT, RTT and MO-RTT [99, 106]. We derive the PDFs associated with these EI schemes, in the context of the SFH assisted MFSK system. Based on these PDFs, the probability of erasure corresponding to a given EI scheme can be derived. Finally, based on the probability of erasures, the probability of codeword EED can be computed. Below we provide a brief overview of these EI schemes.

### 2.4.1 Overview of the EI Schemes

In this section three EI schemes associated with noncoherent $M$-ary orthogonal demodulation are reviewed. Let $Y_1$ and $Y_2$ denote the maximum and second maximum of the square-law detector outputs $U_m, m = 0, 1, 2, \ldots, M$ shown in Figure 2.2. Then we have

$$Y_1 = \max[U_0, U_1, \ldots, U_{M-1}] \tag{2.26}$$

and

$$Y_2 = \max 2[U_0, U_1, \ldots, U_{M-1}]. \tag{2.27}$$

The principles of the three EI schemes considered are explained below.

**OTT:** In the context of the OTT, the decision variable subjected to an erasure insertion is $Y_1$, i.e. the actual demodulator output is observed. Let $f_{Y_1}(y|H_1)$ and $f_{Y_1}(y|H_0)$ be the associated conditional PDFs, given that the associated demodulated symbol is correct ($H_1$) and incorrect ($H_0$), respectively. Let $Y_T$ be a threshold associated with making an erasure decision based on the OTT. Then, if $Y_1 \leq Y_T$, the associated demodulated symbol should be erased. Otherwise, if $Y_1 > Y_T$, the demodulator outputs a RS code symbol. The objective of employing this EI scheme is to erase symbols which are rendered unreliable due to deep fading.

**RTT:** The ratio involved in Viterbi's RTT is defined as the ratio of the maximum to the 'second' maximum [106], or equivalently, it can be defined as the ratio of the 'second' maximum to the maximum, which can be expressed as

$$\lambda = \frac{Y_2}{Y_1}, \; 0 \leq \lambda \leq 1. \tag{2.28}$$

Let $f_\lambda(r|H_1)$ and $f_\lambda(r|H_0)$ be the associated conditional PDFs under the hypotheses of $H_1$ and $H_0$, respectively. Consequently, a pre-set threshold $\lambda_T$ can be invoked, in order to erase these low-reliability symbols, whenever $\lambda \geq \lambda_T$. This scheme was proposed in [106] to combat interference or jamming.

**MO-RTT:** In the context of the joint MO-RTT, the erasure insertion is based on the observation of both the maximum $Y_1$ of Equation (2.26) and the ratio $\lambda$ of Equation (2.28). Specifically, let $f_{Y_1,\lambda}(y, r|H_1)$ and $f_{Y_1,\lambda}(y, r|H_0)$ be the joint two-dimensional (2D) PDFs of the maximum $Y_1$ and the ratio $\lambda$ associated with the MO-RTT, conditioned on both the correct detection and erroneous detection of $M$-ary symbols. The properties of the MO-RTT can be studied with the aid of the 2D PDFs of $f_{Y_1,\lambda}(y, r|H_1)$ and $f_{Y_1,\lambda}(y, r|H_0)$. Consequently, in order to erase the low-reliability RS coded symbols, we assume that $Y_T$ and $\lambda_T$ are two thresholds, which activate an EI, whenever we have $Y_1 \leq Y_T$ and $\lambda \geq \lambda_T$. As we can see, this scheme is an integration of both the OTT and the RTT.

### 2.4.2 Statistics of the EI Schemes

In this subsection, we determine the expressions for the PDFs of $Y_1$ in the context of the OTT, of $\lambda = Y_2/Y_1$ in the context of the RTT as well as the joint PDF of $Y_1$ and $\lambda = Y_2/Y_1$ in the context of the MO-RTT, when the SFH assisted MFSK system operates in Rayleigh fading in the presence of $n = 1$-band MTJ. With the aid of these PDFs, we are then capable of determining the probabilities of erasures and of errors after erasures. Finally, we can compute the probability of error for SFH assisted MFSK employing OTT, RTT and MO-RTT aided EED.

**OTT:** The PDF of $Y_1$ of Equation (2.26), conditioned on the correct decision hypothesis of $H_1$, can be derived as follows:

$$\begin{aligned} f_{Y_1}(y_1|H_1) &= \frac{d}{dy_1}P[Y_1 \le y_1|H_1] = \frac{1}{P(H_1)}\frac{d}{dy_1}P\Big[Y_1 \le y_1, H_1\Big] \\ &= \frac{1}{P(H_1)}\frac{d}{dy_1}\Bigg[\frac{1}{M}P\Big[U_{0(j)} = Y_1 \le y_1, (U_m \le U_{0(j)})_{m=2}^{M}\Big] \\ &+ \left(1-\frac{1}{M}\right)P\Big[U_0 = Y_1 \le y_1, U_{m(j)} \le U_0, (U_m \le U_0)_{m=2,m(j)\neq m}^{M}\Big]\Bigg] \\ &= \frac{1}{P(H_1)}\frac{d}{dy_1}\Bigg[\frac{1}{M}\int_0^{y_1} f_{U_{0(j)}}(x)dx\Big[\int_0^x f_{U_m}(y)dy\Big]^{M-1} \\ &+ \left(1-\frac{1}{M}\right)\int_0^{y_1} f_{U_0}(x)dx\Big[\int_0^x f_{U_{m(j)}}(y)dy\Big]\Big[\int_0^x f_{U_m}(y)dy\Big]^{M-2}\Bigg]. \end{aligned} \quad (2.29)$$

Upon substituting the corresponding PDFs given in Equations (2.15) to (2.18) into the above equation, it can be shown that the PDF of $Y_1$ can be expressed as

$$\begin{aligned} f_{Y_1}(y_1|H_1) &= \frac{1}{P(H_1)}\frac{1}{M}\Bigg[\frac{1}{1+\gamma_{cj}}\exp\left(\frac{-y_1}{1+\gamma_{cj}}\right)(1-e^{-y_1})^{M-1} \\ &+(M-1)\frac{1}{1+\gamma_c}\exp\left(\frac{-y_1}{1+\gamma_c}\right)(1-e^{-y_1})^{M-2}\Big[1-\exp\left(\frac{-y_1}{1+\gamma_j}\right)\Big]\Bigg], \end{aligned} \quad (2.30)$$

where we have $P(H_1) = P_c$, which was given in Equation (2.22).

When deriving the PDF $f_{Y_1}(y_1|H_0)$, we should consider the fact that if a non-signal tone is jammed, the largest of the square-law detector outputs, i.e. $Y_1$, may correspond to either the jammed non-signal tone or to one of the unjammed non-signal tones. Hence, the union of all of the following events must be considered:

1) The signal tone is jammed and $U_m = Y_1, U_n < U_m$ for $m, n = 0, 1, \ldots, M-1, n \neq m$;

2) A non-signal tone is jammed and

- $U_m = Y_1, U_{m(j)} < U_m, U_n < U_m$ for $n \neq m$;
- $U_{m(j)} = Y_1, U_m < U_{m(j)}$ for $m \neq m(j)$.

Upon considering all these events, we have

$$
\begin{aligned}
f_{Y_1}(y_1|H_0) &= \frac{d}{dy_1}P[Y_1 \le y_1|H_0] = \frac{1}{P(H_0)}\frac{d}{dy_1}P[Y_1 \le y_1, H_0] \\
&= \frac{1}{P(H_0)}\frac{d}{dy_1}\left[\frac{1}{M}(M-1)P\left[U_m = Y_1 \le y_1, U_{0(j)} \le U_m, (U_n \le U_m)_{n=3,n\neq m}^{M}\right]\right. \\
&+ \left(\frac{M-1}{M}\right)\left\{(M-2)P\left[U_m = Y_1 \le y_1, U_0 \le U_m, U_{m(j)} \le U_m, (U_n \le U_{m(j)})_{n=4,n\neq m}^{M}\right]\right. \\
&+ \left.\left.P\left[U_{m(j)} = Y_1 \le y_1, U_0 \le U_{m(j)}, (U_n \le U_{m(j)})_{n=2,n\neq m(j)}^{M}\right]\right\}\right] \\
&= \frac{1}{P(H_0)}\frac{d}{dy_1}\left[\frac{1}{M}(M-1)\int_0^{y_1} f_{U_m}(x)dx\left[\int_0^x f_{U_{0(j)}}(y)dy\right]\left[\int_0^x f_{U_m}(y)dy\right]^{M-2}\right. \\
&+ \left(\frac{M-1}{M}\right)\left\{(M-2)\int_0^{y_1} f_{U_m}(x)dx\left[\int_0^x f_{U_0}(y)dy\right]\left[\int_0^x f_{U_{m(j)}}(y)dy\right]\left[\int_0^x f_{U_m}(y)dy\right]^{M-3}\right. \\
&+ \left.\left.\int_0^{y_1} f_{U_{m(j)}}(x)dx\left[\int_0^x f_{U_0}(y)dy\right]\left[\int_0^x f_{U_m}(y)dy\right]^{M-2}\right\}\right] \qquad (2.31)
\end{aligned}
$$

Upon substituting the corresponding PDFs into the above equation, we obtain

$$
\begin{aligned}
f_{Y_1}(y_1|H_0) &= \frac{1}{P(H_0)}\left(\frac{M-1}{M}\right)\left[\left[1-\exp\left(\frac{-y_1}{1+\gamma_{cj}}\right)\right]\left(1-e^{-y_1}\right)^{M-2}e^{-y_1}\right. \\
&+\left[1-\exp\left(\frac{-y_1}{1+\gamma_c}\right)\right]\left\{(M-2)e^{-y_1}(1-e^{-y_1})^{M-3}\left[1-\exp\left(\frac{-y_1}{1+\gamma_j}\right)\right]\right. \\
&+\left.\left.\frac{1}{1+\gamma_j}\exp\left(\frac{-y_1}{1+\gamma_j}\right)(1-e^{-y_1})^{M-2}\right\}\right]. \qquad (2.32)
\end{aligned}
$$

**MO-RTT:** In order to determine the joint PDF of $Y_1$ and $Y_2$, under the hypothesis $H_1$, the following events have to be considered:

1) The signal tone is jammed, $U_{0(j)} = Y_1$, $U_m = Y_2$, $U_n < U_m$, for $m, n = 0, 1, \ldots, M-1$, $n \neq m$;

2) A non-signal tone is jammed, $U_0 = Y_1$ and

   - $U_m = Y_2$, $U_{m(j)} < U_m$, $U_n < U_m$, $n \neq m$;
   - $U_{m(j)} = Y_2$, $U_n < U_m(j)$, $n \neq m(j)$.

Thus, the joint PDF of $Y_1$ and $Y_2$, conditioned on the hypothesis $H_1$ can be expressed as

$$
\begin{aligned}
f_{Y_1,Y_2}(y_1, y_2|H_1) &= \frac{\partial^2}{\partial y_1 \partial y_2}P\left[Y_1 \le y_1, Y_2 \le y_2|H_1\right] = \frac{1}{P(H_1)}\frac{\partial^2}{\partial y_1 \partial y_2}P\left[Y_1 \le y_1, Y_2 \le y_2, H_1\right] \\
&= \frac{1}{P(H_1)}\frac{\partial^2}{\partial y_1 \partial y_2}\left[\frac{M-1}{M}\int_0^{y_2} f_{U_m}(x)dx\left[\int_x^{y_1} f_{U_{0(j)}}(y)dy\right]\left[\int_0^x f_{U_m}(y)dy\right]^{M-2}\right.
\end{aligned}
$$

$$+ \frac{M-1}{M}\Bigg\{(M-2)\int_0^{y_2} f_{U_m}(x)dx\Big[\int_x^{y_1} f_{U_0}(y)dy\Big]\Big[\int_0^{x} f_{U_{m(j)}}(y)dy\Big]\Big[\int_0^{x} f_{U_m}(y)dy\Big]^{M-3}$$
$$+ \int_0^{y_2} f_{U_{m(j)}}(x)dx\Big[\int_x^{y_1} f_{U_0}(y)dy\Big]\Big[\int_0^{x} f_{U_m}(y)dy\Big]^{M-2}\Bigg\}\Bigg] \tag{2.33}$$

After performing the required differentiation, the above equation can be written as

$$\begin{aligned} f_{Y_1,Y_2}(y_1,y_2|H_1) &= \frac{1}{P(H_1)}\left(\frac{M-1}{M}\right)\Bigg[f_{U_{0(j)}}(y_1)f_{U_m}(y_2)\Big[\int_0^{y_2} f_{U_m}(y)dy\Big]^{M-2} \\ &+ f_{U_0}(y_1)\Bigg\{(M-2)\int_0^{y_2} f_{U_{m(j)}}(y)dy\Big[\int_0^{y_2} f_{U_m}(y)dy\Big]^{M-3} \\ &\times f_{U_m}(y_2)+f_{U_{m(j)}}(y_2)\Big[\int_0^{y_2} f_{U_m}(y)dy\Big]^{M-2}\Bigg\}\Bigg]. \end{aligned} \tag{2.34}$$

Now, let $Y = Y_1$ and $\lambda = Y_2/Y_1$. Then, upon using the expressions for the corresponding PDFs, it can be shown that the joint PDF of $Y$ and $\lambda$, which is the PDF associated with the MO-RTT based EI scheme, conditioned on the hypothesis $H_1$, can be expressed as [34, 99]

$$\begin{aligned} f_{Y,\lambda}(y,r|H_1) &= \left(\frac{M-1}{M}\right)y\frac{1}{P(H_1)}\Bigg[\frac{1}{1+\gamma_{cj}}\exp\left(\frac{-y}{1+\gamma_{cj}}\right)e^{-yr}(1-e^{-yr})^{M-2} \\ &+\frac{1}{1+\gamma_c}\exp\left(\frac{-y}{1+\gamma_c}\right)\Bigg\{(M-2)e^{-yr}\Big[1-\exp\left(\frac{-yr}{1+\gamma_j}\right)\Big] \\ &\times(1-e^{-yr})^{M-3}+\frac{1}{1+\gamma_j}\exp\left(\frac{-yr}{1+\gamma_j}\right)(1-e^{-yr})^{M-2}\Bigg\}\Bigg]. \end{aligned} \tag{2.35}$$

For the joint PDF of $Y_1$ and $Y_2$ conditioned on the hypothesis $H_0$, we have to consider the following events:

1) The signal tone is jammed and

- $U_m = Y_1, U_{0(j)} = Y_2, U_n < U_{0(j)}$ for $m, n = 0, 1, \ldots, M-1, n \neq 0, m$;
- $U_m = Y_1, U_n = Y_2, U_{0(j)} < U_n, U_k < U_n$, for $k \neq 0, m, n$;

2) A non-signal tone is jammed and

- $U_m = Y_1, U_0 = Y_2, U_{m(j)} < U_0, U_n < U_0$, for $n \neq 0, m$;
- $U_m = Y_1, U_{m(j)} = Y_2, U_0 < U_{m(j)}, U_n < U_{m(j)}$ for $n \neq 0, m$;
- $U_m = Y_1, U_n = Y_2, U_0 < U_n, U_{m(j)} < U_n, U_k < U_n$, for $k \neq 0, m, n$;
- $U_{m(j)} = Y_1, U_0 = Y_2, U_m < U_0$, for $m \neq 0, m(j)$;
- $U_{m(j)} = Y_1, U_m = Y_2, U_0 < U_m, U_n < U_m$, for $n \neq 0, m$.

Therefore, the joint PDF of $Y_1$ and $Y_2$, conditioned on the hypothesis $H_0$, can be expressed as

$$f_{Y_1,Y_2}(y_1,y_2|H_0) = \frac{\partial^2}{\partial y_1 \partial y_2}P[Y_1 \leq y_1, Y_2 \leq y_2|H_0] = \frac{1}{P(H_0)}\frac{\partial^2}{\partial y_1 \partial y_2}P[Y_1 \leq y_1, Y_2 \leq y_2, H_0]$$

$$
\begin{aligned}
&= \frac{1}{P(H_0)}\frac{\partial^2}{\partial y_1 \partial y_2}\Bigg[\frac{1}{M}(M-1)\Bigg\{\int_0^{y_2} f_{U_{0(j)}}(x)dx\Big[\int_x^{y_1} f_{U_m}(y)dy\Big]\Big[\int_0^{x} f_{U_m}(y)dy\Big]^{M-2} \\
&+ (M-2)\int_0^{y_2} f_{U_m}(x)dx\Big[\int_x^{y_1} f_{U_m}(y)dy\Big]\Big[\int_0^{x} f_{U_{0(j)}}(y)dy\Big]\Big[\int_0^{x} f_{U_m}(y)dy\Big]^{M-3}\Bigg\} \\
&+ \Big(\frac{M-1}{M}\Big)\Bigg\{\int_0^{y_2} f_{U_0}(x)dx\Big\{\Big[\int_x^{y_1} f_{U_{m(j)}}(y)dy\Big]\Big[\int_0^{x} f_{U_m}(y)dy\Big]^{M-2} \\
&+ (M-2)\Big[\int_x^{y_1} f_{U_m}(y)dy\Big]\Big[\int_0^{x} f_{U_{m(j)}}(y)dy\Big]\Big[\int_0^{x} f_{U_m}(y)dy\Big]^{M-3}\Big\} \\
&+ (M-2)\int_0^{y_2} f_{U_m}(x)dx\Big[\int_x^{y_1} f_{U_{m(j)}}(y)dy\Big]\Big[\int_0^{x} f_{U_0}(y)dy\Big]\Big[\int_0^{x} f_{U_m}(y)dy\Big]^{M-3} \\
&+ (M-2)\int_0^{y_2} f_{U_{m(j)}}(x)dx\Big[\int_x^{y_1} f_{U_m}(y)dy\Big]\Big[\int_0^{x} f_{U_0}(y)dy\Big]\Big[\int_0^{x} f_{U_m}(y)dy\Big]^{M-3} \\
&+ (M-3)\int_0^{y_2} f_{U_m}(x)dx\Big[\int_x^{y_1} f_{U_m}(y)dy\Big]\Big[\int_0^{x} f_{U_{m(j)}}(y)dy\Big] \\
&\times \Big[\int_0^{x} f_{U_0}(y)dy\Big]\Big[\int_0^{x} f_{U_m}(y)dy\Big]^{M-4}\Bigg\}\Bigg]. \qquad (2.36)
\end{aligned}
$$

After partial differentiation, the above equation can be written as

$$
\begin{aligned}
f_{Y_1,Y_2}(y_1,y_2|H_0) &= \frac{1}{P(H_0)}\Big(\frac{M-1}{M}\Big)\Big[f_{U_{0(j)}}(y_2)f_{U_m}(y_1)\Big[\int_0^{y_2} f_{U_m}(y)dy\Big]^{M-2} \\
&+ (M-2)f_{U_m}(y_2)f_{U_m}(y_1)\int_0^{y_2} f_{U_{0(j)}}(y)dy\Big[\int_0^{y_2} f_{U_m}(y)dy\Big]^{M-3} \\
&+ f_{U_0}(y_2)f_{U_{m(j)}}(y_1)\Big[\int_0^{y_2} f_{U_m}(y)dy\Big]^{M-2} \\
&+ (M-2)f_{U_0}(y_2)f_{U_m}(y_1)\int_0^{y_2} f_{U_{m(j)}}(y)dy\Big[\int_0^{y_2} f_{U_m}(y)dy\Big]^{M-3} \\
&+ (M-2)f_{U_m}(y_2)f_{U_{m(j)}}(y_1)\int_0^{y_2} f_{U_0}(y)dy\Big[\int_0^{y_2} f_{U_m}(y)dy\Big]^{M-3} \\
&+ (M-2)f_{U_m}(y_1)\int_0^{y_2} f_{U_0}(y)dy\Big\{f_{U_{m(j)}}(y_2)\Big[\int_0^{y_2} f_{U_m}(y)dy\Big]^{M-3} \\
&+ (M-3)f_{U_m}(y_2)\int_0^{y_2} f_{U_{m(j)}}(y)dy\Big[\int_0^{y_2} f_{U_m}(y)dy\Big]^{M-4}\Big\}\Big]. \qquad (2.37)
\end{aligned}
$$

Finally, after changing the variables from $Y_1$ and $Y_2$ to $Y$ and $\lambda = Y_2/Y_1$ [34, 99], we obtain the corresponding joint PDF, which is the PDF associated with the MO-RTT based EI scheme, conditioned on the hypothesis $H_0$. We have

$$
\begin{aligned}
f_{Y,\lambda}(y,r|H_0) &= \Big(\frac{M-1}{M}\Big)y\frac{1}{P(H_0)}\Big[e^{-y}\frac{1}{1+\gamma_{cj}}\exp\Big(\frac{-yr}{1+\gamma_{cj}}\Big)(1-e^{-yr})^{M-2} \\
&+(M-2)e^{-y(r+1)}\Big[1-\exp\Big(\frac{-yr}{1+\gamma_{cj}}\Big)\Big](1-e^{-yr})^{M-3}
\end{aligned}
$$

$$+\frac{1}{1+\gamma_c}\exp\left(\frac{-yr}{1+\gamma_c}\right)\left\{\frac{1}{1+\gamma_j}\exp\left(\frac{-y}{1+\gamma_j}\right)(1-e^{-yr})^{M-2}\right.$$
$$\left.+(M-2)e^{-y}\left[1-\exp\left(\frac{-yr}{1+\gamma_j}\right)\right](1-e^{-yr})^{M-3}\right\}+(M-2)\left[1-\exp\left(\frac{-yr}{1+\gamma_c}\right)\right]$$
$$\times\left\{(1-e^{-yr})^{M-3}\frac{1}{1+\gamma_j}\exp\left(\frac{-y}{1+\gamma_j}\right)e^{-yr}+e^{-y}\frac{1}{1+\gamma_j}\exp\left(\frac{-yr}{1+\gamma_j}\right)(1-e^{-yr})^{M-3}\right.$$
$$\left.\left.+(M-3)e^{-y(r+1)}(1-e^{-yr})^{M-4}\left[1-\exp\left(\frac{-yr}{1+\gamma_j}\right)\right]\right\}\right]. \tag{2.38}$$

**RTT:** Finally, we derive the PDFs corresponding to the ratio $\lambda = Y_2/Y_1$, in the context of the RTT assisted EI scheme. These PDFs can be readily obtained from Equation (2.35) and Equation (2.38) by integrating them in terms of $Y$ from 0 to $\infty$, yielding

$$\begin{aligned}
f_\lambda(r|H_1) &= \int_0^\infty f_{Y,\lambda}(y,r|H_1)dy \\
&= \left(\frac{M-1}{M}\right)\frac{1}{P(H_1)}\left[\sum_{n=0}^{M-2}(-1)^n\binom{M-2}{n}\frac{1+\gamma_{cj}}{[1+r(n+1)(1+\gamma_{cj})]^2}\right. \\
&\quad +(M-2)\sum_{n=0}^{M-3}(-1)^n\binom{M-3}{n}\left\{\frac{1+\gamma_c}{[1+r(n+1)(1+\gamma_c)]^2}-\right. \\
&\quad \left.\frac{(1+\gamma_c)(1+\gamma_j)^2}{[1+\gamma_j+r(1+\gamma_c)\{1+(n+1)(1+\gamma_j)\}]^2}\right\} \\
&\quad \left.+\sum_{n=0}^{M-2}(-1)^n\binom{M-2}{n}\frac{(1+\gamma_c)(1+\gamma_j)}{[1+\gamma_j+r(1+\gamma_c)\{1+n(1+\gamma_j)\}]^2}\right]
\end{aligned} \tag{2.39}$$

and

$$f_\lambda(r|H_0)=\int_0^\infty f_{Y,\lambda}(y,r|H_0)dy=(M-1)\frac{1}{P(H_0)}\left[\sum_{n=0}^{M-2}(-1)^n\binom{M-2}{n}\right.$$
$$\times\left\{\frac{1+\gamma_{cj}}{[r+(nr+1)(1+\gamma_{cj})]^2}+\frac{(1+\gamma_c)(1+\gamma_j)}{[1+\gamma_c+r(1+\gamma_j)\{1+n(1+\gamma_c)\}]^2}\right\}$$
$$+(M-2)\sum_{n=0}^{M-3}(-1)^n\binom{M-3}{n}\left\{\frac{1}{[1+r(n+1)]^2}-\frac{(1+\gamma_{cj})^2}{[r+\{1+r(n+1)\}(1+\gamma_{cj})]^2}\right.$$
$$+\frac{1+\gamma_c}{[r+(rn+1)(1+\gamma_c)]^2}+\frac{1+\gamma_j}{[r+(rn+1)(1+\gamma_j)]^2}$$
$$+\frac{1+\gamma_j}{[1+r(n+1)(1+\gamma_j)]^2}-\frac{(1+\gamma_c)^2(1+\gamma_j)}{[1+\gamma_c+r(1+\gamma_j)\{1+(n+1)(1+\gamma_c)\}]^2}$$
$$\left.-\frac{(1+\gamma_c)(1+\gamma_j)(2+\gamma_c+\gamma_j)}{[(1+nr)(1+\gamma_c)(1+\gamma_j)+r(2+\gamma_c+\gamma_j)]^2}\right\}$$
$$+(M-2)(M-3)\sum_{n=0}^{M-4}(-1)^n\binom{M-4}{n}\left\{\frac{1}{[1+r(n+1)]^2}\right.$$
$$\left.+\frac{(1+\gamma_c)^2(1+\gamma_j)^2}{[\{1+r(n+1)\}(1+\gamma_c)(1+\gamma_j)+r(2+\gamma_c+\gamma_j)]^2}\right.$$

$$-\frac{(1+\gamma_j)^2}{[r+\{1+r(n+1)\}(1+\gamma_j)]^2}-\frac{(1+\gamma_c)^2}{[r+\{1+r(n+1)\}(1+\gamma_c)]^2}\Bigg\}\Bigg]. \tag{2.40}$$

### 2.4.3 Symbol, Word and Bit Error Probabilities

From the PDFs derived in the previous section, it is straightforward to derive the probabilities of error or erasure for a chosen threshold corresponding to a certain EI scheme. The required relations have been extracted from [99].

We commence with the RTT based EI scheme. Let $\lambda_T$ represent a preset threshold corresponding to the RTT based scheme. Then, whenever we have $\lambda = Y_2/Y_1 \geq \lambda_T$, the corresponding symbol is unreliable and, hence, it is replaced by an erasure. Consequently, the corresponding probability of erasure can be expressed as [99]

$$P_e(\lambda_T) = P(H_1)\int_{\lambda_T}^{1} f_\lambda(r|H_1)dr + P(H_0)\int_{\lambda_T}^{1} f_\lambda(r|H_0)dr, \tag{2.41}$$

where $f_\lambda(r|H_1)$ is given in Equation (2.39) and $f_\lambda(r|H_0)$ in Equation (2.40). The error probability after erasure insertion, denoted by $P_t$, can be expressed as [99]

$$\begin{aligned} P_t(\lambda_T) &= P(H_0)\int_{0}^{\lambda_T} f_\lambda(r|H_0)dr \\ &= P(H_0)\left[1-\int_{\lambda_T}^{1} f_\lambda(r|H_0)dr\right]. \end{aligned} \tag{2.42}$$

In a similar manner, corresponding to OTT, if $Y_1$ is less than a preset threshold $Y_T$, the corresponding symbol is replaced by an erasure. The probability of erasure for this specific threshold $Y_T$ is given by

$$P_e(Y_T) = P(H_1)\int_{0}^{Y_T} f_{Y_1}(y|H_1)dy + P(H_0)\int_{0}^{Y_T} f_{Y_1}(y|H_0)dy, \tag{2.43}$$

where $f_{Y_1}(y_1|H_1)$ is given in Equation (2.30) and $f_{Y_1}(y_1|H_0)$ in Equation (2.32). The associated error probability after erasure insertion is expressed by

$$\begin{aligned} P_t(Y_T) &= P(H_0)\int_{Y_T}^{\infty} f_{Y_1}(y|H_0)dy \\ &= P(H_0)\left[1-\int_{0}^{Y_T} f_{Y_1}(y|H_0)dy\right]. \end{aligned} \tag{2.44}$$

Finally, in the context of the MO-RTT, let $\lambda_T$ and $Y_T$ be the preset thresholds. Then, an erasure is inserted, whenever we have $\lambda \geq \lambda_T$ and $Y \leq Y_T$. The probabilities of erasure and error after erasure are given by

$$P_e(Y_T,\lambda_T) = P(H_1)\int_{0}^{Y_T}\int_{\lambda_T}^{1} f_{Y,\lambda}(y,r|H_1)drdy + P(H_0)\int_{0}^{Y_T}\int_{\lambda_T}^{1} f_{Y,\lambda}(y,r|H_0)drdy \tag{2.45}$$

and

$$\begin{aligned} P_t(Y_T, \lambda_T) &= P(H_0) \int_{Y_T}^{\infty} \int_{0}^{\lambda_T} f_{Y,\lambda}(y, r|H_0) dr dy \\ &= P(H_0) \left[ 1 - \int_{0}^{Y_T} \int_{\lambda_T}^{1} f_{Y,\lambda}(y, r|H_0) dr dy \right], \end{aligned} \tag{2.46}$$

where $f_{Y,\lambda}(y, r|H_1)$ is given in Equation (2.35) and $f_{Y,\lambda}(y, r|H_0)$ in Equation (2.38). The final expressions of $P_e$ and $P_t$ in the context of the three schemes considered are given in Appendix 2.A.

Having derived the probability of erasure and the probability of random error after erasure, it is possible to determine the symbol error ratio of the SFH assisted MFSK system after error-and-erasure RS decoding. Specifically, the probability of not decoding the codeword correctly, i.e. *codeword error probability* $P_w$ can be expressed as [99–101]

$$P_w = \sum_{i=0}^{N} \sum_{j=j_0(i)}^{N-i} \binom{N}{i} \binom{N-i}{j} (P_t)^i (P_e)^j (1 - P_t - P_e)^{N-i-j}, \tag{2.47}$$

where we have $j_0(i) = \max\{0, N - K + 1 - 2i\}$. The symbol error ratio, after the error-and-erasure RS decoding can be expressed as [117]

$$P_s \approx \frac{1}{N} \sum_{i=0}^{N} \sum_{j=j_0(i)}^{N-i} (i+j) \binom{N}{i} \binom{N-i}{j} (P_t)^i (P_e)^j (1 - P_t - P_e)^{N-i-j}. \tag{2.48}$$

The BER of the SFH assisted MFSK system employing error-and-erasure RS decoding can be determined from the symbol error ratio expression of Equation (2.48) with the aid of Equation (2.25).

## 2.5 Analytical Results and Discussion

Having derived the BER expressions of the RS-coded system employing one of the three EI schemes considered in this chapter, we are now capable of studying the properties of these EI schemes in the context of a SFH assisted MFSK system. Usually, a good EI scheme allows us to choose the thresholds such that the maximum possible fraction of the incorrectly detected symbols are erased, while erasing the minimum possible number of correct symbols. The PDFs of $Y_1$ in the context of OTT, of $\lambda = Y_2/Y_1$ in the context of the RTT and the joint PDF of $Y_1$ and $\lambda$ in the context of the MO-RTT are shown in Figures 2.4, 2.5 and 2.6 respectively, assuming $M = 8$. These PDFs were computed using Equations (2.30), (2.32), (2.35), (2.38), (2.39) and (2.40).

We can see from Figure 2.4 that when the SFH-MFSK system experiences Rayleigh fading, the values of $Y_1$ tend to be quite low, even when the detection is correct. We also notice in Figure 2.4 that, even when the jammer power is low, i.e. at $E_b/N_J = 20$dB for example, the PDF curves corresponding to $H_1$ and

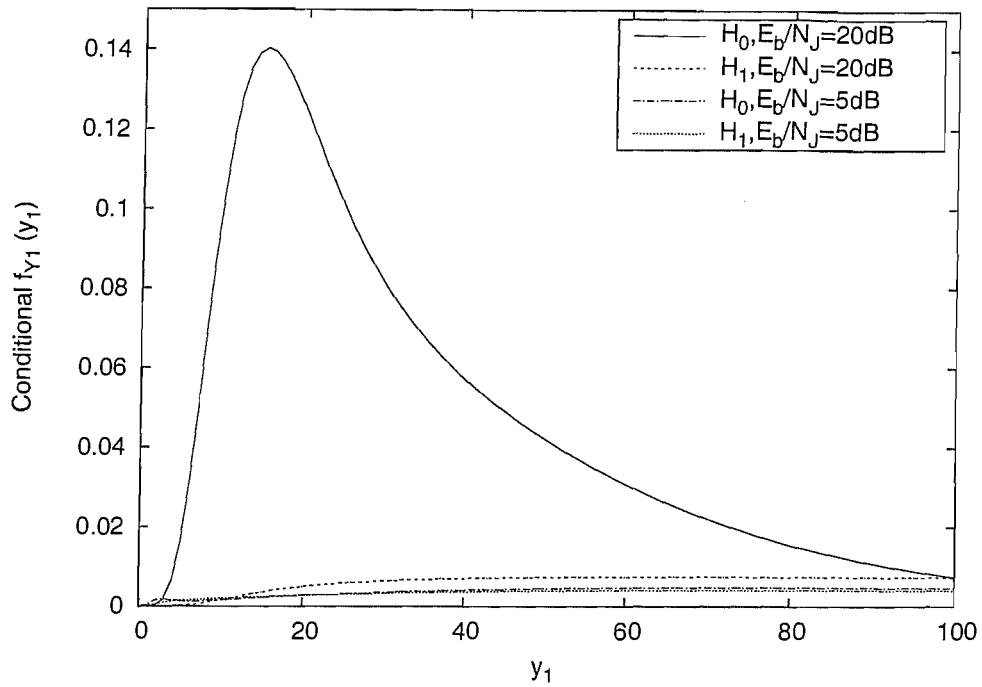


**Figure 2.4:** PDF of the largest square-law detector output $Y_1$ in the context of the OTT scheme under the hypothesis of $H_1$ and $H_0$ in Rayleigh fading channels in the presence of $n = 1$-band MTJ , when assuming an uncoded 8-ary non-coherent FSK system and $E_b/N_0 = 16$dB. The PDFs were computed using Equations (2.30) and (2.32).

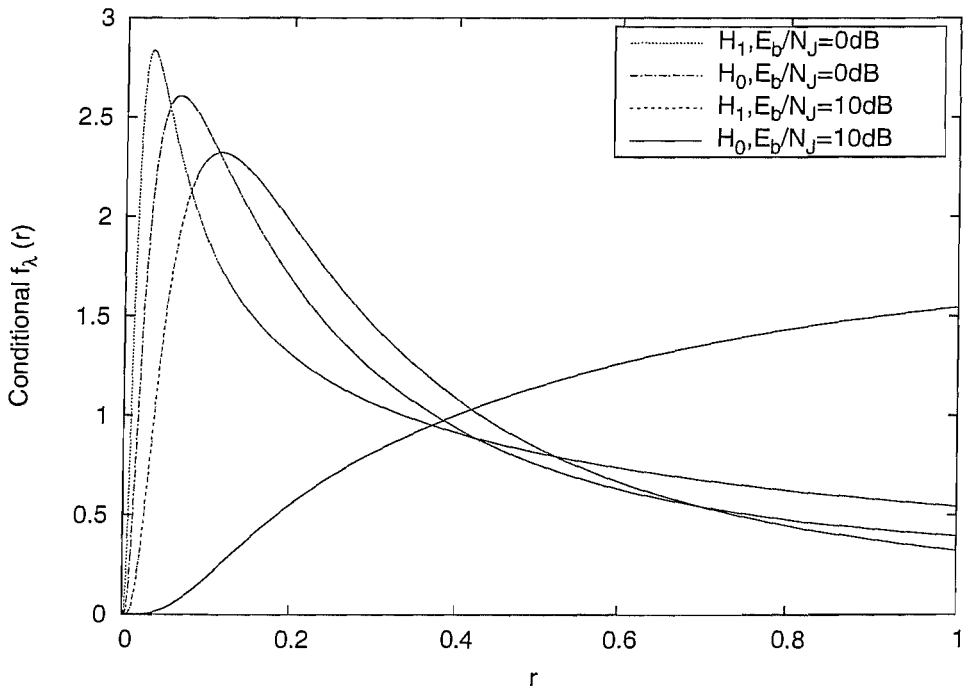


**Figure 2.5:** PDF of the ratio $Y_2/Y_1$ in the context of the RTT scheme under the hypothesis of $H_1$ and $H_0$ in Rayleigh fading channels in the presence of $n = 1$-band MTJ, when assuming an uncoded 8-ary non-coherent FSK system and $E_b/N_0 = 5$dB. The PDFs were computed using Equations (2.39) and (2.40).

$H_0$ overlap substantially, which implies that it is difficult to set a threshold of $Y_1$ for the OTT, in order to distinguish the correctly detected symbols from the incorrectly detected ones. The above observation is justified because the OTT is basically an EI scheme designed to combat fading, thus its ability to provide

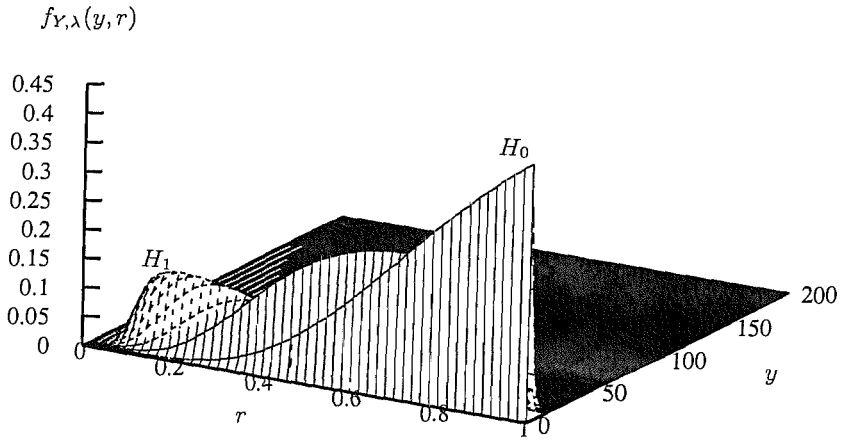


**Figure 2.6:** Joint PDF of the ratio $Y_2/Y_1$ and $Y_1$ in the context of the MO-RTT scheme under the hypothesis of $H_1$ and $H_0$ in Rayleigh fading channels in the presence of $n = 1$-band MTJ, when assuming an uncoded 8-ary non-coherent FSK system, at $E_b/N_J = 10$dB and $E_b/N_0 = 5$dB. The PDFs were computed using Equations (2.35), and (2.38).

useful erasures is severely hampered by the presence of interference. In contrast to the OTT of Figure 2.4, as shown in Figure 2.5 for the RTT, the PDF curves corresponding to $H_1$ and $H_0$ are mainly concentrated in the opposite ends of the horizontal axis, when $E_b/N_J = 10$dB. This observation suggests that if the jamming power is not too high, detection errors might occur mostly when $\lambda = Y_2/Y_1$ is high. Consequently, when the ratio $\lambda = Y_2/Y_1$ is low, we can have a high confidence that the corresponding symbols are correctly detected. However, when $E_b/N_J = 0$dB, as shown in Figure 2.5, the ability of the RTT based scheme to separate the correctly detected symbols from the incorrectly detected ones is severely degraded. In the context of the MO-RTT based scheme, Figure 2.6 shows that the PDFs corresponding to the hypothesis of $H_1$ and $H_0$, are explicitly distinct from each other, although there still exists some overlapping. Hence, when using the MO-RTT, a suitable set of thresholds might be employed for erasing the unreliable symbols.

In Figure 2.7, the probability of erasure corresponding to $\lambda_T = 0.4$ in the context of the RTT has been shown based on both analytical and simulation results, when SFH assisted MFSK system communicates in a Rayleigh fading channel and is interfered by $n = 1$-band MTJ. The results shown in Figure 2.7 are for $M = 2$, 4 and 8 and indicate that our analytical results of the probability of erasure tally with the corresponding simulations results.

In Figures 2.8 and 2.9, we evaluated the codeword error probability against a range of values of $Y_T$ and $\lambda_T$ respectively, for various values of $M$ and the corresponding RS code. The codeword error probability in these figures was computed using Equations (2.41) to (2.44) and Equation (2.47). The purpose of these plots is to find the optimum threshold in the context of the OTT and the RTT based schemes, required to achieve the lowest codeword error probability. Firstly, we can observe in both Figures 2.8 and 2.9 that the system corresponding to $M = 16$ achieves the lowest codeword error probability, while that corresponding

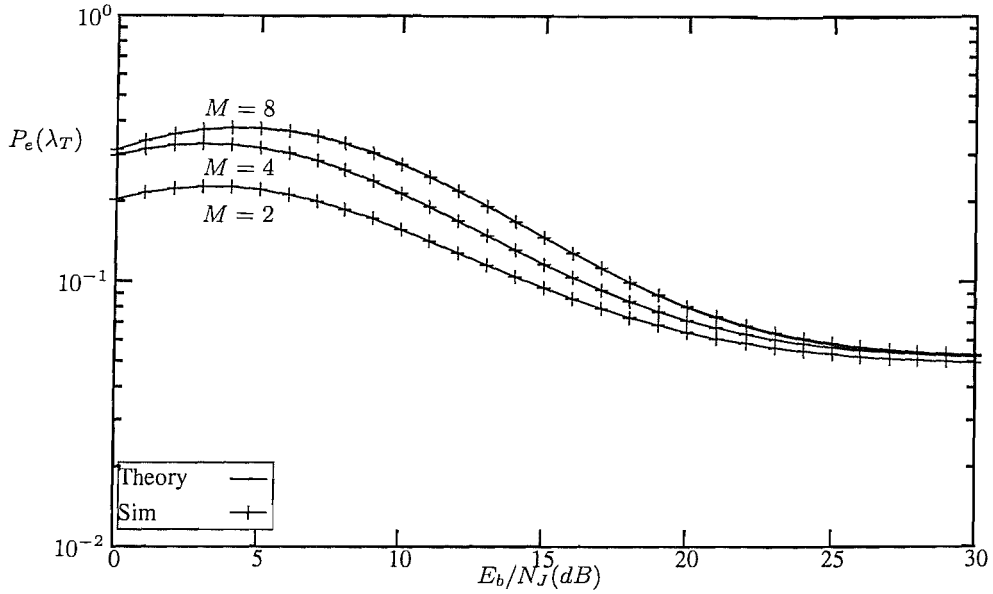


**Figure 2.7:** Comparison of the analytical and simulation results of the probability of erasure $P_e(\lambda_T)$ corresponding to the RTT for uncoded non-coherent MFSK in a Rayleigh fading channel in the presence of $n = 1$-band MTJ, when assuming a threshold of $\lambda_T$=0.4 and $E_b/N_0 = 16$dB. $P_e(\lambda_T)$ is computed using Equation (2.41).

to $M = 8$ achieves the second best. In Section 1.5 and in the context of Figure 2.3 we have shown that while symbol energy increases with increasing $M$, the degradation inflicted by single tone jamming on MFSK system also increases with increasing $M$. Thus, in the context of the system under consideration, increasing the value of $M$ results in conflicting affects on the BER performance. Consequently, in Figure 2.3 $M = 4$ is the best option for the MFSK system under single tone jamming and Rayleigh fading conditions at $E_b/N_J = 10$dB. In RS-coded system, there is another important factor, namely the error correction capability of the RS code given by $t = \frac{N-K}{2}$. In the context of the RS-coded system, using a higher value of $M$ implies a high error correcting capability, when the code rate $K/N$ is a constant [34]. Thus, for the codes chosen in Figure 2.8 and 2.9, we have $t = 1$ when $M = 8$, $t = 3$ when $M = 16$, $t = 5$ when $M = 32$ and $t = 11$ when $M = 64$. Consequently, the combined effects of interference, transmitted symbol energy and error correcting capability result in the observation that the system corresponding to $M = 16$ achieves the best performance, when using error-and-erasure aided RS-decoding.

It is noteworthy from Figures 2.8 and 2.9 that the value of optimum threshold, in the context of both the OTT and RTT, varies with the values of $E_b/N_J$, $E_b/N_0$ and $M$. Furthermore, in a similar fashion, it can be shown that, in the context of the MO-RTT, there exist optimum values of the thresholds of $\lambda_T$ and $Y_T$, which result in the best system performance employing error-and-erasure aided RS-decoding.

In Figure 2.10, we evaluated the BER of the RS-coded SFH assisted MFSK, when it employs OTT based EI and when assuming optimum values of the thresholds for each value of $E_b/N_J$ and $M$. For the sake of comparison, the corresponding BER when using ECO decoding has also been shown. The results of Figure 2.10 show that for all values of $M$, error-and-erasure RS-decoding outperforms the ECO decoding. However, the BER improvement of the error-and-erasures decoding is noteworthy only when the jammer

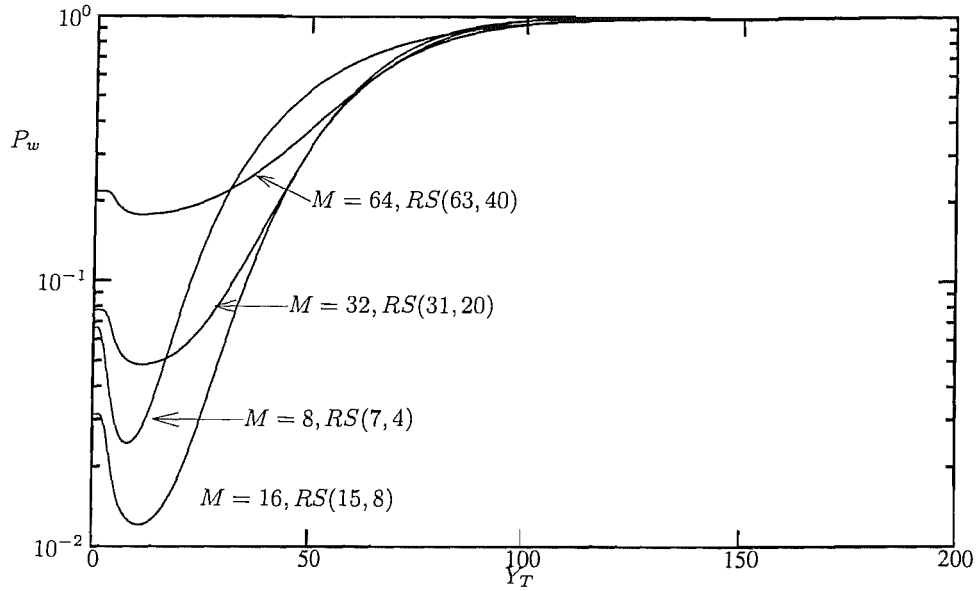


**Figure 2.8:** Codeword error probability $P_w$ versus OTT threshold $Y_T$ for RS-coded SFH assisted non-coherent MFSK using the OTT, when communicating over a Rayleigh fading channel in the presence of $n = 1$-band MTJ at $E_b/N_J = 20$dB, $E_b/N_0 = 16$dB and various values of $M$. $P_w$ is computed using Equation (2.47) in conjunction with Equations (2.43) and (2.44).

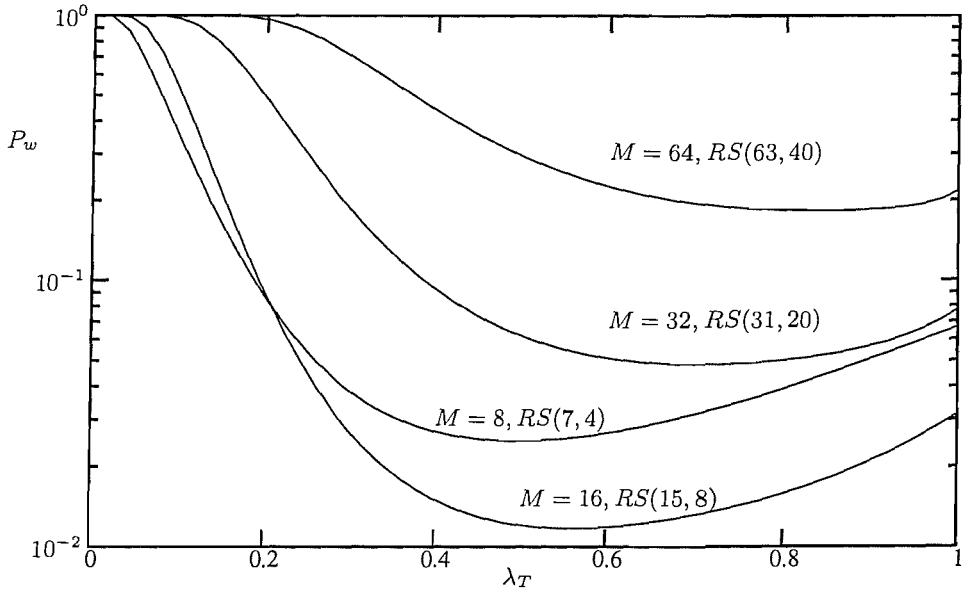


**Figure 2.9:** Codeword error probability $P_w$ versus RTT threshold $\lambda_T$ for RS-coded SFH assisted non-coherent MFSK using RTT, when communicating over a Rayleigh fading channel in the presence of $n = 1$-band MTJ at $E_b/N_J = 20$dB, $E_b/N_0 = 16$dB and various values of $M$. $P_w$ is computed using Equation (2.47) in conjunction with Equations (2.41) and (2.42).

power is sufficiently low. Specifically, as seen in Figure 2.10, EI assisted performance is noticeably better than that using no erasures only when $E_b/N_J$ exceeds approximately 12dB in case of $M = 8$, 14dB in case of $M = 16$ and 16dB in case of $M = 32$. Furthermore, when the signal to jamming power ratio is sufficiently high, i.e. for example when $E_b/N_J$ exceeds 20dB, a higher performance gain can be achieved, especially in the case of $M = 32$, owing to the higher error correcting capability of the RS(31,20) code used.

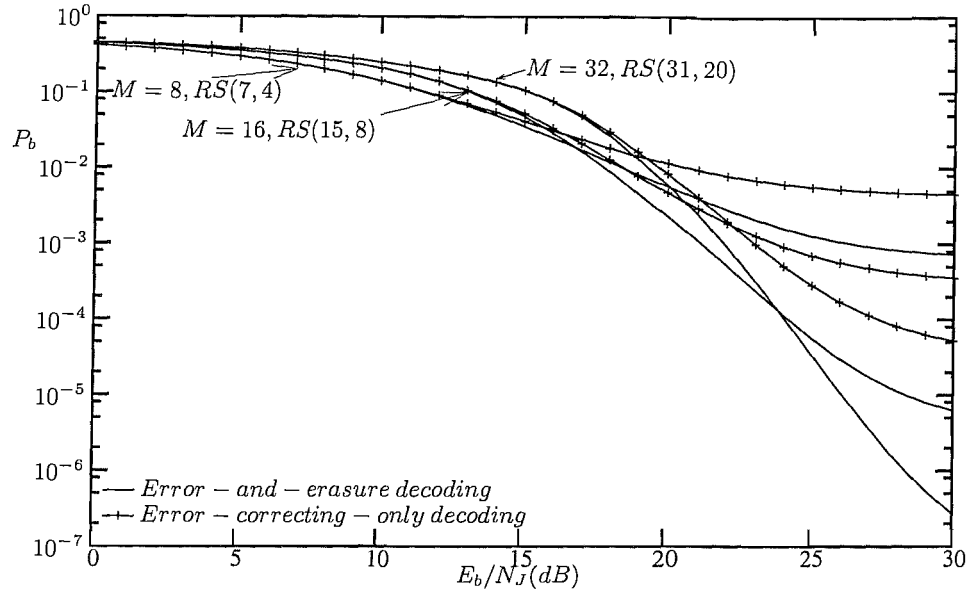


**Figure 2.10:** BER $P_b$ versus $E_b/N_J$ performance of RS-coded SFH assisted MFSK system using the OTT based EI for $E_b/N_0 = 16$dB, when communicating over Rayleigh fading channels in the presence of $n = 1$-band MTJ and when assuming optimum thresholds. $P_b$ is computed using Equations (2.48) and (2.25).

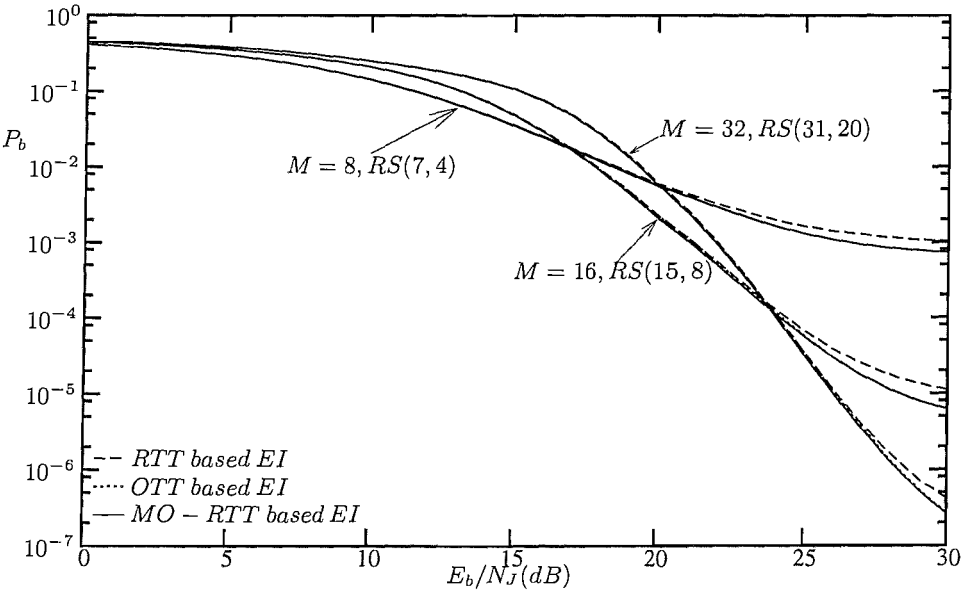


**Figure 2.11:** Comparison of the BER $P_b$ versus $E_b/N_J$ performance of the RS-coded SFH assisted MFSK system using OTT, RTT and MO-RTT based EI for $E_b/N_0 = 16$dB, when communicating over Rayleigh fading channels in the presence of $n = 1$-band MTJ and when assuming optimum thresholds. $P_b$ is computed using Equations (2.48) and (2.25).

Finally, in Figure 2.11 we show our BER performance comparison for the RS-coded SFH assisted MFSK system, when employing the three different types of EI schemes considered in this chapter. We can see from the results of Figure 2.11 that the BERs of the three types of EI schemes are hardly distinguishable from each other when $E_b/N_J$ is relatively low, i.e. for example when $E_b/N_J \leq 20$dB. By contrast, when $E_b/N_J$ is sufficiently high, i.e. for example when $E_b/N_J \geq 25$dB, both the OTT and MO-RTT based systems outperform the RTT based system. The reason for this observation can be explained as follows. For the system studied, we considered both Rayleigh fading as well as single tone jamming whose effect

is dependent upon the value of $E_b/N_J$. As we have discussed in Section 2.4, the OTT based EI erases any symbol that is deemed unreliable due to severe fading, while the RTT based EI aims to erase unreliable symbols owing to interference. Figure 2.11 shows that both these EI schemes result in a similar BER provided that the $E_b/N_J$ is less than a certain value, which is approximately 18dB in case of $M = 8$, 24dB in case of $M = 16$ and 27dB in case of $M = 32$. Beyond these values of $E_b/N_J$, the OTT based EI outperforms the RTT based EI, regardless of the choice of $M$. This is because when the jamming power is low, the effects of interference are reduced and, hence, most errors are imposed by the Rayleigh fading. Finally, the MO-RTT based EI is marginally better than both the OTT and RTT based EI, especially for $M = 32$, since it exploits the joint information provided by the OTT and the RTT. However, for the system under consideration, the BER performance resulting from the MO-RTT based EI is very close to that of the OTT.

In order to show the associated performance differences in detail, the minimum achievable BER values using 16-ary FSK have been summarised in Table 2.1, in the context of the RTT, OTT and MO-RTT based EI schemes. It is noteworthy from Table 2.1 that when $E_b/N_J$ is relatively low, i.e. 15 or 20 dB, and $E_b/N_0$ is relatively high, i.e. 20 or 25 dB, the RTT outperforms the OTT. For all other values of $E_b/N_J$ and $E_b/N_0$ shown in Table 2.1, the OTT performs better than the RTT based EI scheme. This observation implies that when thermal noise power is high, the OTT based scheme is more effective than the RTT based scheme.

## 2.6 Conclusion

In this chapter, we have for the first time mathematically analyzed the BER performance of the RS-coded SFH system using MFSK modulation, assuming that the SFH assisted MFSK signals are transmitted over Rayleigh fading channels in the presence of $n = 1$-band MTJ. Three different types of EI schemes have been investigated which are based on the OTT, the RTT and the MO-RTT. We have derived the PDFs of the variables invoked in these EI schemes which were given in Equations (2.30), (2.32), (2.35), (2.38), (2.39) and (2.40). Then, the probability of erasure and probability of random error after erasure have been derived as seen in Equations (2.49) to (2.54). Finally, we computed the codeword error probability and the BER of the RS-coded system, using Equations (2.47), (2.48) and (2.25), when employing any of these EI schemes. From our analysis and results we found that $n = 1$-band MTJ using a duty factor of unity severely degrades the BER performance of the SFH assisted MFSK receiver, especially when the transmitted signal experiences Rayleigh fading. However, with the aid of error-and erasure RS decoding assisted by one of the three EI schemes considered in this chapter, the system performance can be significantly improved, provided that the jamming power is not excessively high. Since Rayleigh fading is the most hostile type of fading and $n = 1$-band MTJ is the worst case of jamming, it can be expected that the performance of the SFH assisted MFSK system employing these EI schemes will be better in less severe conditions. It was demonstrated that the OTT based EI is efficient in terms of erasing erroneous symbols affected by fading and thermal noise, while the RTT based EI is effective from the point of view of erasing incorrect symbols inflicted by

**Table 2.1:** Comparison of BER achieved by RS-coded SFH 16-ary FSK using various EI schemes, when subjected to Rayleigh fading and $n = 1$-band MTJ. BER values are computed using Equations (2.48) and (2.25).

| $E_b/N_J$ (dB) | $E_b/N_0$ (dB) | Minimum BER | | |
|---|---|---|---|---|
| | | RTT | OTT | MO-RTT |
| 15 | 5 | 0.196845 | 0.19082 | 0.19082 |
| | 10 | 0.0794641 | 0.07266 | 0.07259 |
| | 15 | 0.0503719 | 0.048873 | 0.048778 |
| | 20 | 0.0444911 | 0.045427 | 0.04432 |
| | 25 | 0.043019 | 0.04448 | 0.043019 |
| 20 | 5 | 0.1682 | 0.16022 | 0.16005 |
| | 10 | 0.01828 | 0.014816 | 0.014718 |
| | 15 | 0.0028153 | 0.0026626 | 0.0025726 |
| | 20 | 0.0016041 | 0.0017065 | 0.0015004 |
| | 25 | 0.0013616 | 0.0014783 | 0.0012826 |
| 25 | 5 | 0.1618 | 0.15215 | 0.15193 |
| | 10 | 0.0089072 | 0.0064891 | 0.0064363 |
| | 15 | 0.00012875 | 0.00010024 | 9.8246e-5 |
| | 20 | 1.6447e-5 | 1.5894e-5 | 1.2825e-5 |
| | 25 | 1.1437e-5 | 9.2379e-6 | 7.3238e-6 |
| 30 | 5 | 0.16093 | 0.15022 | 0.14999 |
| | 10 | 0.00759135 | 0.0053956 | 0.0053506 |
| | 15 | 3.55648e-5 | 2.0125e-5 | 1.9863e-5 |
| | 20 | 2.11812e-7 | 1.7064e-7 | 1.6061e-7 |
| | 25 | 3.63849e-8 | 2.6517e-8 | 1.9652e-8 |

interference. Therefore, when the jamming power is low, the OTT usually outperforms RTT. By contrast, the RTT proves to be superior to the OTT when the jamming power is relatively high. Since the MO-RTT is constituted by the amalgam of the OTT and the RTT based EI schemes, it always outperforms both the OTT and the RTT, although the corresponding performance is typically very close to that of one of these two.

In terms of complexity, OTT and RTT are comparable, since both of these EI schemes require to compute one variable each, which is the maximum in case of the OTT-based scheme, while the ratio of the maximum and the second maximum of the $M$ decision variables is considered when RTT-based EI is involved. In order to achieve minimum possible BERs, optimum thresholds $Y_T$ and $\lambda_T$ corresponding to these variables will also have to be recorded for a wide range of system parameters such as SNR, $M$ and code configurations. Since MO-RTT involves erasure decisions based on both of the above variables, its complexity is twice that of the OTT and the RTT-based schemes. However, despite imposing increased complexity, the MO-RTT based scheme does not yield significant performance improvement compared to OTT and RTT as seen in Figure 2.11. Hence, the OTT and the RTT based schemes offer more attractive design alternatives.

The performance of the three schemes is summarised in Tables 2.2 and 2.3.

| | BER=$10^{-3}$ | | BER=$10^{-4}$ | |
|---|---|---|---|---|
| | ECO decoding | OTT-based EI | ECO decoding | OTT-based EI |
| $M = 16$, RS(15,8) | 24dB | 21.1dB | NA | 24.3dB |
| $M = 32$, RS(31,20) | 22.9dB | 21.8dB | 27.6dB | 24.1dB |

NA means "Not achieved".

**Table 2.2:** $E_b/N_J$ values required by the ECO and the OTT based EI decoding schemes to achieve BERs of $10^{-3}$ and $10^{-4}$ when employed in RS-coded SFH-MFSK receiver communicating over a Rayleigh fading channel in the presence of $n = 1$-band MTJ, assuming $E_b/N_0 = 16$dB. The values are extracted from Figure 2.10.

| | BER=$10^{-5}$ | | | BER=$10^{-4}$ | | |
|---|---|---|---|---|---|---|
| | RTT | OTT | MO-RTT | RTT | OTT | MO-RTT |
| $M = 16$, RS(15,8) | 30dB | 28.3dB | 28.2dB | 24.4dB | 24.3dB | 24.2dB |
| $M = 32$, RS(31,20) | 26.2dB | 26.2dB | 26.1dB | 24.1dB | 24.1dB | 24.1dB |

**Table 2.3:** $E_b/N_J$ values required by various EI schemes to achieve BERs of $10^{-4}$ and $10^{-5}$ when employed in RS-coded SFH-MFSK receiver communicating over a Rayleigh fading channel in the presence of $n = 1$-band MTJ, assuming $E_b/N_0 = 16$dB. The values are extracted from Figure 2.11.

## 2.A APPENDIX: Derivation of $P_e$ and $P_t$

In this appendix, we provide the final expressions for the probability $P_e$ of erasure and the probability $P_t$ of error after erasure, in the context of the three schemes considered.

**RTT-based EI** Using binomial expansion [1] and inserting relevant expressions for the PDFs from Equations (2.39) and (2.40) in Equations (2.41) and (2.42), we get

$$
\begin{aligned}
P_e(\lambda_T) &= \frac{M-1}{M}\Bigg[\sum_{n=0}^{M-2}(-1)^n\binom{M-2}{n}\Bigg\{\frac{1}{1+n}\Big[\frac{1}{1+\lambda_T(1+n)(1+\gamma_{cj})}-\frac{1}{1+(1+n)(1+\gamma_{cj})}\Big]\\
&+\frac{1+\gamma_j}{1+n(1+\gamma_j)}\Big[\frac{1}{1+\gamma_j+\lambda_T(1+\gamma_c)[1+n(1+\gamma_j)]}-\frac{1}{1+\gamma_j+(1+\gamma_c)[1+n(1+\gamma_j)]}\Big]\\
&+\frac{1+\gamma_c}{1+n(1+\gamma_c)}\Big[\frac{1}{1+\gamma_c+\lambda_T(1+\gamma_j)[1+n(1+\gamma_c)]}-\frac{1}{1+\gamma_c+(1+\gamma_j)[1+n(1+\gamma_c)]}\Big]\\
&+\frac{(1+\gamma_{cj})}{1+n(1+\gamma_{cj})}\Big[\frac{1}{1+\gamma_{cj}+\lambda_T[1+n(1+\gamma_{cj})]}-\frac{1}{2+\gamma_{cj}+n(1+\gamma_{cj})}\Big]\Bigg\}\\
&+(M-2)\sum_{n=0}^{M-3}(-1)^n\binom{M-3}{n}\Bigg\{\frac{1}{1+n}\Big[\frac{1}{1+\lambda_T(1+n)(1+\gamma_c)}-\frac{1}{1+(1+n)(1+\gamma_c)}\Big]\\
&-\frac{(1+\gamma_j)^2}{1+(1+n)(1+\gamma_j)}\Big[\frac{1}{1+\gamma_j+\lambda_T(1+\gamma_c)[1+(1+n)(1+\gamma_j)}\\
&-\frac{1}{1+\gamma_j+(1+\gamma_c)[1+(1+n)(1+\gamma_j)]}\Big]\\
&+\frac{1+\gamma_j}{1+n(1+\gamma_j)}\Big[\frac{1}{1+\gamma_j+\lambda_T[1+n(1+\gamma_j)]}-\frac{1}{2+\gamma_j+(1+n)(1+\gamma_j)}\Big]\\
&+\frac{1+\gamma_c}{1+n(1+\gamma_c)}\Big[\frac{1}{1+\gamma_c+\lambda_T[1+n(1+\gamma_c)]}-\frac{1}{2+\gamma_c+(1+n)(1+\gamma_c)}\Big]
\end{aligned}
$$

$$
\begin{aligned}
&+ \frac{1}{1+n}\left[\frac{1}{1+\lambda_T(1+n)(1+\gamma_j)} - \frac{1}{1+(1+n)(1+\gamma_j)}\right] \\
&- \frac{(1+\gamma_j)(1+\gamma_c)(2+\gamma_{cj})}{n(1+\gamma_j)(1+\gamma_c)+(2+\gamma_{cj})}\left[\frac{1}{(1+\gamma_j)(1+\gamma_c)+\lambda_T[2+\gamma_{cj}+n(1+\gamma_j)(1+\gamma_c)]}\right. \\
&\left.- \frac{1}{(1+\gamma_j)(1+\gamma_c)+2+\gamma_{cj}+n(1+\gamma_j)(1+\gamma_c)}\right] \\
&- \frac{(1+\gamma_c)^2}{1+(n+1)(1+\gamma_c)}\left[\frac{1}{1+\gamma_c+\lambda_T(1+\gamma_j)[1+(n+1)(1+\gamma_c)]}\right. \\
&\left.- \frac{1}{1+\gamma_c+(1+\gamma_j)[1+(n+1)(1+\gamma_c)]}\right] + \frac{1}{1+n}\left[\frac{1}{1+\lambda_T(1+n)} - \frac{1}{2+n}\right] \\
&- \frac{(1+\gamma_{cj})^2}{1+(1+\gamma_{cj})(1+n)}\left[\frac{1}{1+\gamma_{cj}+\lambda_T[(1+n)(1+\gamma_{cj})+1]} - \frac{1}{1+(2+n)(1+\gamma_{cj})}\right]\Bigg\} \\
&+ (M-2)(M-3)\sum_{n=0}^{M-4}(-1)^n\binom{M-4}{n}\left\{\frac{(1+\gamma_c)^2(1+\gamma_j)^2}{2+\gamma_{cj}+(1+n)(1+\gamma_c)(1+\gamma_j)}\right. \\
&\times \left[\frac{1}{(1+\gamma_c)(1+\gamma_j)+\lambda_T[2+\gamma_{cj}+(1+n)(1+\gamma_c)(1+\gamma_j)}\right. \\
&\left.- \frac{1}{(1+\gamma_c)(1+\gamma_j)+[2+\gamma_{cj}+(1+n)(1+\gamma_c)(1+\gamma_j)}\right] \\
&+ \frac{1}{1+n}\left[\frac{1}{1+\lambda_T(1+n)} - \frac{1}{2+n}\right] - \frac{(1+\gamma_c)^2}{1+(n+1)(1+\gamma_c)} \\
&\times \left[\frac{1}{1+\gamma_c+\lambda_T[1+(1+\gamma_c)(1+n)]} - \frac{1}{2+\gamma_c+(1+n)(1+\gamma_c)}\right] - \frac{(1+\gamma_j)^2}{1+(n+1)(1+\gamma_j)} \\
&\times \left.\left[\frac{1}{1+\gamma_j+\lambda_T[1+(1+\gamma_j)(1+n)]} - \frac{1}{2+\gamma_j+(1+n)(1+\gamma_j)}\right]\right\}\Bigg] \qquad (2.49)
\end{aligned}
$$

and

$$
\begin{aligned}
P_t(\lambda_T) &= \frac{M-1}{M}\left[\sum_{n=0}^{M-2}(-1)^n\binom{M-2}{n}\left\{\frac{1+\gamma_c}{1+n(1+\gamma_c)}\right.\right. \\
&\times \left[\frac{1}{1+\gamma_c} - \frac{1}{1+\gamma_c+\lambda_T(1+\gamma_j)[1+n(1+\gamma_c)]}\right] \\
&+ \left.\frac{(1+\gamma_{cj})}{1+n(1+\gamma_{cj})}\left[\frac{1}{1+\gamma_{cj}} - \frac{1}{1+\gamma_{cj}+\lambda_T[1+n(1+\gamma_{cj})]}\right]\right\} \\
&+ (M-2)\sum_{n=0}^{M-3}(-1)^n\binom{M-3}{n}\left\{\frac{1}{1+n}\left[1-\frac{1}{1+\lambda_T(1+n)(1+\gamma_j)}\right]\right. \\
&- \frac{(1+\gamma_j)}{1+n(1+\gamma_j)}\left[\frac{1}{1+\gamma_j} - \frac{1}{1+\gamma_j+\lambda_T[1+n(1+\gamma_j)]}\right] \\
&+ \frac{1+\gamma_c}{1+n(1+\gamma_c)}\left[\frac{1}{1+\gamma_c} - \frac{1}{1+\gamma_c+\lambda_T[1+n(1+\gamma_c)]}\right] + \frac{1}{1+n}\left[1-\frac{1}{1+\lambda_T(1+n)}\right] \\
&- \frac{(1+\gamma_j)(1+\gamma_c)(2+\gamma_{cj})}{n(1+\gamma_j)(1+\gamma_c)+(2+\gamma_{cj})}\left[\frac{1}{(1+\gamma_j)(1+\gamma_c)}\right. \\
&\left.- \frac{1}{(1+\gamma_j)(1+\gamma_c)+\lambda_T[2+\gamma_{cj}+n(1+\gamma_j)(1+\gamma_c)]}\right] \\
&- \frac{(1+\gamma_c)^2}{1+(n+1)(1+\gamma_c)}\left[\frac{1}{1+\gamma_c} - \frac{1}{1+\gamma_c+\lambda_T(1+\gamma_j)[1+(n+1)(1+\gamma_c)]}\right]
\end{aligned}
$$

$$
\begin{aligned}
&- \frac{(1+\gamma_{cj})^2}{1+(1+n)(1+\gamma_{cj})}\Big[\frac{1}{1+\gamma_{cj}} - \frac{1}{1+\gamma_{cj}+\lambda_T[1+(1+n)(1+\gamma_{cj})}\Big\} \\
&+ (M-2)(M-3)\sum_{n=0}^{M-4}(-1)^n\binom{M-4}{n}\Big\{\frac{(1+\gamma_c)^2(1+\gamma_j)^2}{2+\gamma_{cj}+(1+n)(1+\gamma_c)(1+\gamma_j)} \\
&\times \Big[\frac{1}{(1+\gamma_c)(1+\gamma_j)} - \frac{1}{(1+\gamma_c)(1+\gamma_j)+\lambda_T[2+\gamma_{cj}+(1+n)(1+\gamma_c)(1+\gamma_j)}\Big] \\
&- \frac{1}{1+n}\Big[1-\frac{1}{1+\lambda_T(1+n)}\Big] + \frac{(1+\gamma_c)^2}{1+(n+1)(1+\gamma_c)} \\
&\times \Big[\frac{1}{1+\gamma_c} - \frac{1}{1+\gamma_c+\lambda_T[1+(1+n)(1+\gamma_c)]}\Big] - \frac{(1+\gamma_j)^2}{1+(n+1)(1+\gamma_j)} \\
&\times \Big[\frac{1}{1+\gamma_j} - \frac{1}{1+\gamma_j+\lambda_T[1+(1+n)(1+\gamma_j)]}\Big]\Big\}\Big]. \qquad (2.50)
\end{aligned}
$$

**OTT-based EI** Likewise, by inserting relevant expressions for the PDFs from Equations (2.30) and (2.32) into Equations (2.43) and (2.44), we get

$$
\begin{aligned}
P_e(Y_T) &= \frac{1}{M}\Bigg[\sum_{n=0}^{M-1}(-1)^n\binom{M-1}{n}\frac{1}{1+n(1+\gamma_{cj})}\Big[1-\exp\Big(\frac{-Y_T[1+n(1+\gamma_{cj})]}{1+\gamma_{cj})}\Big)\Big] \\
&+ (M-1)\sum_{n=0}^{M-2}(-1)^n\binom{M-2}{n}\Big\{\frac{1}{1+n(1+\gamma_c)}\Big[1-\exp\Big(\frac{-Y_T[1+n(1+\gamma_c)]}{1+\gamma_c}\Big)\Big] \\
&- \frac{1+\gamma_j}{2+\gamma_{cj}+n(1+\gamma_c)(1+\gamma_j)}\Big[1-\exp\Big(\frac{-Y_T[2+\gamma_{cj}+n(1+\gamma_c)(1+\gamma_j)]}{(1+\gamma_c)(1+\gamma_j)}\Big)\Big] \\
&+ \frac{1}{n+1}\Big[1-\exp\Big(-Y_T(n+1)\Big)\Big] + \frac{1}{1+n(1+\gamma_j)}\Big[1-\exp\Big(\frac{-Y_T[1+n(1+\gamma_j)]}{1+\gamma_j}\Big)\Big] \\
&- \frac{1+\gamma_{cj}}{1+(1+n)(1+\gamma_{cj})}\Big[1-\exp\Big(\frac{-Y_T[1+(1+n)(1+\gamma_{cj})]}{1+\gamma_{cj})}\Big)\Big] \\
&- \frac{1+\gamma_c}{2+\gamma_{cj}+n(1+\gamma_c)(1+\gamma_j)}\Big[1-\exp\Big(\frac{-Y_T[2+\gamma_{cj}+n(1+\gamma_c)(1+\gamma_j)]}{(1+\gamma_c)(1+\gamma_j)}\Big)\Big]\Big\} \\
&+ (M-1)(M-2)\sum_{n=0}^{M-3}(-1)^n\binom{M-3}{n}\Big\{\frac{1}{n+1}\Big[1-\exp\Big(-Y_T(n+1)\Big)\Big] \\
&- \frac{1+\gamma_j}{1+(1+n)(1+\gamma_j)}\Big[1-\exp\Big(\frac{-Y_T[1+(1+n)(1+\gamma_j)]}{1+\gamma_j}\Big)\Big] \\
&- \frac{1+\gamma_c}{1+(1+n)(1+\gamma_c)}\Big[1-\exp\Big(\frac{-Y_T[1+(1+n)(1+\gamma_c)]}{1+\gamma_c}\Big)\Big] \\
&+ \frac{(1+\gamma_j)(1+\gamma_c)}{2+\gamma_{cj}+(n+1)(1+\gamma_c)(1+\gamma_j)} \\
&\times \Big[1-\exp\Big(\frac{-Y_T[2+\gamma_{cj}+(n+1)(1+\gamma_c)(1+\gamma_j)]}{(1+\gamma_c)(1+\gamma_j)}\Big)\Big]\Big\}\Bigg] \qquad (2.51)
\end{aligned}
$$

and

$$
P_t(Y_T) = P(H_0) - \frac{M-1}{M}\Bigg[\sum_{n=0}^{M-2}(-1)^n\binom{M-2}{n}\Big\{
$$

$$
\begin{aligned}
&\times \frac{1}{n+1}\Big[1-\exp\Big(-Y_T(n+1)\Big)\Big]+\frac{1}{1+n(1+\gamma_j)}\Big[1-\exp\Big(\frac{-Y_T[1+n(1+\gamma_j)]}{1+\gamma_j}\Big)\Big]\\
&- \frac{1+\gamma_{cj}}{1+(1+n)(1+\gamma_{cj})}\Big[1-\exp\Big(\frac{-Y_T[1+(1+n)(1+\gamma_{cj})]}{1+\gamma_{cj}}\Big)\Big]\\
&- \frac{1+\gamma_c}{2+\gamma_{cj}+n(1+\gamma_c)(1+\gamma_j)}\Big[1-\exp\Big(\frac{-Y_T[2+\gamma_{cj}+n(1+\gamma_c)(1+\gamma_j)]}{(1+\gamma_c)(1+\gamma_j)}\Big)\Big]\Bigg\}\\
&+ (M-2)\sum_{n=0}^{M-3}(-1)^n\binom{M-3}{n}\Bigg\{\frac{1}{n+1}\Big[1-\exp\Big(-Y_T(n+1)\Big)\Big]\\
&- \frac{1+\gamma_j}{1+(1+n)(1+\gamma_j)}\Big[1-\exp\Big(\frac{-Y_T[1+(1+n)(1+\gamma_j)]}{1+\gamma_j}\Big)\Big]\\
&- \frac{1+\gamma_c}{1+(1+n)(1+\gamma_c)}\Big[1-\exp\Big(\frac{-Y_T[1+(1+n)(1+\gamma_c)]}{1+\gamma_c}\Big)\Big]\\
&+ \frac{(1+\gamma_j)(1+\gamma_c)}{2+\gamma_{cj}+(n+1)(1+\gamma_c)(1+\gamma_j)}\\
&\times \Big[1-\exp\Big(\frac{-Y_T[2+\gamma_{cj}+(n+1)(1+\gamma_c)(1+\gamma_j)]}{(1+\gamma_c)(1+\gamma_j)}\Big)\Big]\Bigg\}\Bigg]. \qquad (2.52)
\end{aligned}
$$

**MO-RTT-based EI** Finally, by inserting relevant expressions for the PDFs from Equations (2.35) and (2.38) into Equations (2.45) and (2.46), we get

$$
\begin{aligned}
P_e(Y_T,\lambda_T) &= \frac{M-1}{M}\Bigg[\sum_{n=0}^{M-2}(-1)^n\binom{M-2}{n}\Bigg\{\frac{1+\gamma_c}{1+n(1+\gamma_c)}\\
&\times \Bigg[\frac{1-\exp\Big(\frac{-Y_T\left[\lambda_T(1+\gamma_j)[1+n(1+\gamma_c)]+1+\gamma_c\right]}{(1+\gamma_c)(1+\gamma_j)}\Big)}{\lambda_T(1+\gamma_j)[1+n(1+\gamma_c)]+1+\gamma_c}-\frac{1-\exp\Big(\frac{-Y_T\left[(1+\gamma_j)[1+n(1+\gamma_c)]+1+\gamma_c\right]}{(1+\gamma_c)(1+\gamma_j)}\Big)}{(1+\gamma_j)[1+n(1+\gamma_c)]+1+\gamma_c}\Bigg]\\
&+ \frac{1+\gamma_{cj}}{1+n(1+\gamma_{cj})}\Bigg[\frac{1-\exp\Big(\frac{-Y_T\left[\lambda_T[1+n(1+\gamma_{cj})]+1+\gamma_{cj}\right]}{1+\gamma_{cj}}\Big)}{\lambda_T[1+n(1+\gamma_{cj})]+1+\gamma_{cj}}-\frac{1-\exp\Big(\frac{-Y_T\left[2+n(1+\gamma_{cj})+\gamma_{cj}\right]}{1+\gamma_{cj}}\Big)}{2+n(1+\gamma_{cj})+\gamma_{cj}}\Bigg]\\
&+ \frac{1}{1+n}\Bigg[\frac{1-\exp\Big(\frac{-Y_T\left[1+\lambda_T(1+n)(1+\gamma_{cj})\right]}{(1+\gamma_{cj})}\Big)}{1+\lambda_T(n+1)(1+\gamma_{cj})}-\frac{1-\exp\Big(\frac{-Y_T\left[1+(1+n)(1+\gamma_{cj})\right]}{(1+\gamma_{cj})}\Big)}{1+(n+1)(1+\gamma_{cj})}\Bigg]\\
&+ \frac{1+\gamma_j}{1+n(1+\gamma_j)}\Bigg[\frac{1-\exp\Big(\frac{-Y_T\left[\lambda_T(1+\gamma_c)[1+n(1+\gamma_j)]+1+\gamma_j\right]}{(1+\gamma_j)(1+\gamma_c)}\Big)}{\lambda_T(1+\gamma_c)[1+n(1+\gamma_j)]+1+\gamma_j}\\
&- \frac{1-\exp\Big(\frac{-Y_T\left[(1+\gamma_c)[1+n(1+\gamma_j)]+1+\gamma_j\right]}{(1+\gamma_j)(1+\gamma_c)}\Big)}{(1+\gamma_c)[1+n(1+\gamma_j)]+1+\gamma_j}\Bigg]\Bigg\}\\
&+ (M-2)\sum_{n=0}^{M-3}(-1)^n\binom{M-3}{n}\Bigg\{\frac{1+\gamma_c}{1+n(1+\gamma_c)}\\
&\times \Bigg[\frac{1-\exp\Big(\frac{-Y_T\left[\lambda_T[1+n(1+\gamma_c)]+1+\gamma_c\right]}{1+\gamma_c}\Big)}{\lambda_T[1+n(1+\gamma_c)]+1+\gamma_c}-\frac{1-\exp\Big(\frac{-Y_T\left[2+n(1+\gamma_c)+\gamma_c\right]}{1+\gamma_c}\Big)}{2+n(1+\gamma_c)+\gamma_c}\Bigg]\\
&+ \frac{1+\gamma_j}{1+n(1+\gamma_j)}\Bigg[\frac{1-\exp\Big(\frac{-Y_T\left[\lambda_T[1+n(1+\gamma_j)]+1+\gamma_j\right]}{1+\gamma_j}\Big)}{\lambda_T[1+n(1+\gamma_j)]+1+\gamma_j}-\frac{1-\exp\Big(\frac{-Y_T\left[2+n(1+\gamma_j)+\gamma_j\right]}{1+\gamma_j}\Big)}{2+n(1+\gamma_j)+\gamma_j}\Bigg]
\end{aligned}
$$

$$
\begin{aligned}
&- \frac{(1+\gamma_j)^2(1+\gamma_c)}{1+\gamma_j+(1+\gamma_c)[1+n(1+\gamma_j)]}\left[\frac{1-\exp\left(\frac{-Y_T\left[\lambda_T[2+\gamma_{cj}+n(1+\gamma_c)(1+\gamma_j)]+(1+\gamma_c)(1+\gamma_j)\right]}{(1+\gamma_c)(1+\gamma_j)}\right)}{\lambda_T[2+\gamma_{cj}+n(1+\gamma_c)(1+\gamma_j)]+(1+\gamma_c)(1+\gamma_j)}\right.\\
&\left.- \frac{1-\exp\left(\frac{-Y_T\left[2+\gamma_{cj}+n(1+\gamma_c)(1+\gamma_j)+(1+\gamma_c)(1+\gamma_j)\right]}{(1+\gamma_c)(1+\gamma_j)}\right)}{[2+\gamma_{cj}+n(1+\gamma_c)(1+\gamma_j)]+(1+\gamma_c)(1+\gamma_j)}\right]\\
&- \frac{(1+\gamma_c)^2(1+\gamma_j)}{1+\gamma_c+(1+\gamma_j)[1+n(1+\gamma_c)]}\left[\frac{1-\exp\left(\frac{-Y_T\left[\lambda_T[2+\gamma_{cj}+n(1+\gamma_c)(1+\gamma_j)]+(1+\gamma_c)(1+\gamma_j)\right]}{(1+\gamma_c)(1+\gamma_j)}\right)}{\lambda_T[2+\gamma_{cj}+n(1+\gamma_c)(1+\gamma_j)]+(1+\gamma_c)(1+\gamma_j)}\right.\\
&\left.- \frac{1-\exp\left(\frac{-Y_T\left[2+\gamma_{cj}+n(1+\gamma_c)(1+\gamma_j)+(1+\gamma_c)(1+\gamma_j)\right]}{(1+\gamma_c)(1+\gamma_j)}\right)}{[2+\gamma_{cj}+n(1+\gamma_c)(1+\gamma_j)]+(1+\gamma_c)(1+\gamma_j)}\right]\\
&- \frac{(1+\gamma_c)^2}{1+n(1+\gamma_c)}\left[\frac{1-\exp\left(\frac{-Y_T\left[\lambda_T(1+\gamma_j)[1+(1+n)(1+\gamma_c)]+1+\gamma_c\right]}{(1+\gamma_c)(1+\gamma_j)}\right)}{\lambda_T(1+\gamma_j)[1+(1+n)(1+\gamma_c)]+1+\gamma_c}\right.\\
&\left.- \frac{1-\exp\left(\frac{-Y_T\left[(1+\gamma_j)[1+(1+n)(1+\gamma_c)]+1+\gamma_c\right]}{(1+\gamma_c)(1+\gamma_j)}\right)}{(1+\gamma_j)[1+(1+n)(1+\gamma_c)]+1+\gamma_c}\right]\\
&+ \frac{1}{n+1}\left[\frac{1-\exp\left(\frac{-Y_T\left[1+\lambda_T(n+1)(1+\gamma_j)\right]}{(1+\gamma_j)}\right)}{1+\lambda_T(n+1)(1+\gamma_j)}-\frac{1-\exp\left(\frac{-Y_T\left[1+(n+1)(1+\gamma_j)\right]}{(1+\gamma_j)}\right)}{1+(n+1)(1+\gamma_j)}\right]\\
&+ \frac{1}{n+1}\left[\frac{1-\exp\Big(-Y_T[1+\lambda_T(n+1)]\Big)}{1+\lambda_T(n+1)}-\frac{1-\exp\Big(-Y_T[2+n]\Big)}{2+n}\right]+\frac{(1+\gamma_{cj})^2}{1+n(1+\gamma_{cj})}\\
&\times \left[\frac{1-\exp\left(\frac{-Y_T\left[\lambda_T[1+(n+1)(1+\gamma_{cj})]+1+\gamma_{cj}\right]}{1+\gamma_{cj}}\right)}{\lambda_T[1+(n+1)(1+\gamma_{cj})]+1+\gamma_{cj}}-\frac{1-\exp\left(\frac{-Y_T\left[(n+1)(1+\gamma_{cj})+2+\gamma_{cj}\right]}{1+\gamma_{cj}}\right)}{(n+1)(1+\gamma_{cj})+2+\gamma_{cj}}\right]\\
&+ \frac{1}{1+n}\left[\frac{1-\exp\left(\frac{-Y_T\left[1+\lambda_T(1+n)(1+\gamma_c)\right]}{(1+\gamma_c)}\right)}{1+\lambda_T(n+1)(1+\gamma_c)}-\frac{1-\exp\left(\frac{-Y_T\left[1+(1+n)(1+\gamma_c)\right]}{(1+\gamma_c)}\right)}{1+(n+1)(1+\gamma_c)}\right]\\
&- \frac{(1+\gamma_j)^2}{1+(1+n)(1+\gamma_j)}\left[\frac{1-\exp\left(\frac{-Y_T\left[\lambda_T(1+\gamma_c)[1+(1+n)(1+\gamma_j)]+1+\gamma_j\right]}{(1+\gamma_c)(1+\gamma_j)}\right)}{\lambda_T(1+\gamma_c)[1+(1+n)(1+\gamma_j)]+1+\gamma_j}\right.\\
&\left.- \frac{1-\exp\left(\frac{-Y_T\left[(1+\gamma_c)[1+(1+n)(1+\gamma_j)]+1+\gamma_j\right]}{(1+\gamma_c)(1+\gamma_j)}\right)}{(1+\gamma_c)[1+(1+n)(1+\gamma_j)]+1+\gamma_j}\right]\Bigg\}\\
&+ (M-2)(M-3)\sum_{n=0}^{M-4}(-1)^n\binom{M-4}{n}\Bigg\{\\
&\times \frac{1}{n+1}\left[\frac{1-\exp\Big(-Y_T[1+\lambda_T(n+1)]\Big)}{1+\lambda_T(n+1)}-\frac{1-\exp\Big(-Y_T[2+n]\Big)}{2+n}\right]\\
&- \frac{(1+\gamma_c)^2}{1+n(1+\gamma_c)}\left[\frac{1-\exp\left(\frac{-Y_T\left[\lambda_T[1+(n+1)(1+\gamma_c)]+1+\gamma_c\right]}{1+\gamma_c}\right)}{\lambda_T[1+(n+1)(1+\gamma_c)]+1+\gamma_c}\right.\\
&\left.- \frac{1-\exp\left(\frac{-Y_T\left[(n+1)(1+\gamma_c)+2+\gamma_c\right]}{1+\gamma_c}\right)}{(n+1)(1+\gamma_c)+2+\gamma_c}\right]-\frac{(1+\gamma_j)^2}{1+n(1+\gamma_j)}\\
&\times \left[\frac{1-\exp\left(\frac{-Y_T\left[\lambda_T[1+(n+1)(1+\gamma_j)]+1+\gamma_j\right]}{1+\gamma_j}\right)}{\lambda_T[1+(n+1)(1+\gamma_j)]+1+\gamma_j}-\frac{1-\exp\left(\frac{-Y_T\left[(n+1)(1+\gamma_j)+2+\gamma_j\right]}{1+\gamma_j}\right)}{(n+1)(1+\gamma_j)+2+\gamma_j}\right]\\
&- \frac{(1+\gamma_c)^2(1+\gamma_j)^2}{2+\gamma_{cj}+(1+n)(1+\gamma_c)(1+\gamma_j)}
\end{aligned}
$$

$$\times \left[\frac{1-\exp\left(\frac{-Y_T\left[\lambda_T[2+\gamma_{cj}+(n+1)(1+\gamma_c)(1+\gamma_j)]+(1+\gamma_c)(1+\gamma_j)\right]}{(1+\gamma_c)(1+\gamma_j)}\right)}{\lambda_T[2+\gamma_{cj}+(n+1)(1+\gamma_c)(1+\gamma_j)]+(1+\gamma_c)(1+\gamma_j)]} - \frac{1-\exp\left(\frac{-Y_T\left[2+\gamma_{cj}+(n+1)(1+\gamma_c)(1+\gamma_j)+(1+\gamma_c)(1+\gamma_j)\right]}{(1+\gamma_c)(1+\gamma_j)}\right)}{2+\gamma_{cj}+(n+1)(1+\gamma_c)(1+\gamma_j)+(1+\gamma_c)(1+\gamma_j)}\right]\Bigg\}\Bigg] \tag{2.53}$$

and

$$\begin{aligned}
P_t(Y_T,\lambda_T) &= P(H_0) - \frac{M-1}{M}\Bigg[\sum_{n=0}^{M-2}(-1)^n\binom{M-2}{n}\Bigg\{\frac{1}{1+n(1+\gamma_c)} \\
&\times \left[\frac{1-\exp\left(\frac{-Y_T\left[\lambda_T(1+\gamma_j)[1+n(1+\gamma_c)]+1+\gamma_c\right]}{(1+\gamma_c)(1+\gamma_j)}\right)}{\lambda_T(1+\gamma_j)[1+n(1+\gamma_c)]+1+\gamma_c} - \frac{1-\exp\left(\frac{-Y_T\left[(1+\gamma_j)[1+n(1+\gamma_c)]+1+\gamma_c\right]}{(1+\gamma_c)(1+\gamma_j)}\right)}{(1+\gamma_j)[1+n(1+\gamma_c)]+1+\gamma_c}\right] \\
&+ \frac{1+\gamma_{cj}}{1+n(1+\gamma_{cj})}\left[\frac{1-\exp\left(\frac{-Y_T\left[\lambda_T[1+n(1+\gamma_{cj})]+1+\gamma_{cj}\right]}{1+\gamma_{cj}}\right)}{\lambda_T[1+n(1+\gamma_{cj})]+1+\gamma_{cj}} - \frac{1-\exp\left(\frac{-Y_T\left[2+n(1+\gamma_{cj})+\gamma_{cj}\right]}{1+\gamma_{cj}}\right)}{2+n(1+\gamma_{cj})+\gamma_{cj}}\right]\Bigg\} \\
&+ (M-2)\sum_{n=0}^{M-3}(-1)^n\binom{M-3}{n}\Bigg\{\frac{1+\gamma_c}{1+n(1+\gamma_c)} \\
&\times \left[\frac{1-\exp\left(\frac{-Y_T\left[\lambda_T[1+n(1+\gamma_c)]+1+\gamma_c\right]}{1+\gamma_c}\right)}{\lambda_T[1+n(1+\gamma_c)]+1+\gamma_c} - \frac{1-\exp\left(\frac{-Y_T\left[2+n(1+\gamma_c)+\gamma_c\right]}{1+\gamma_c}\right)}{2+n(1+\gamma_c)+\gamma_c}\right] \\
&+ \frac{1+\gamma_j}{1+n(1+\gamma_j)}\left[\frac{1-\exp\left(\frac{-Y_T\left[\lambda_T[1+n(1+\gamma_j)]+1+\gamma_j\right]}{1+\gamma_j}\right)}{\lambda_T[1+n(1+\gamma_j)]+1+\gamma_j} - \frac{1-\exp\left(\frac{-Y_T\left[2+n(1+\gamma_j)+\gamma_j\right]}{1+\gamma_j}\right)}{2+n(1+\gamma_j)+\gamma_j}\right] \\
&- \frac{(1+\gamma_j)^2(1+\gamma_c)}{1+\gamma_j+(1+\gamma_c)[1+n(1+\gamma_j)]}\left[\frac{1-\exp\left(\frac{-Y_T\left[\lambda_T[2+\gamma_{cj}+n(1+\gamma_c)(1+\gamma_j)]+(1+\gamma_c)(1+\gamma_j)\right]}{(1+\gamma_c)(1+\gamma_j)}\right)}{\lambda_T[2+\gamma_{cj}+n(1+\gamma_c)(1+\gamma_j)]+(1+\gamma_c)(1+\gamma_j)}\right. \\
&\left. - \frac{1-\exp\left(\frac{-Y_T\left[2+\gamma_{cj}+n(1+\gamma_c)(1+\gamma_j)+(1+\gamma_c)(1+\gamma_j)\right]}{(1+\gamma_c)(1+\gamma_j)}\right)}{[2+\gamma_{cj}+n(1+\gamma_c)(1+\gamma_j)]+(1+\gamma_c)(1+\gamma_j)}\right] \\
&- \frac{(1+\gamma_c)^2(1+\gamma_j)}{1+\gamma_c+(1+\gamma_j)[1+n(1+\gamma_c)]}\left[\frac{1-\exp\left(\frac{-Y_T\left[\lambda_T[2+\gamma_{cj}+n(1+\gamma_c)(1+\gamma_j)]+(1+\gamma_c)(1+\gamma_j)\right]}{(1+\gamma_c)(1+\gamma_j)}\right)}{\lambda_T[2+\gamma_{cj}+n(1+\gamma_c)(1+\gamma_j)]+(1+\gamma_c)(1+\gamma_j)}\right. \\
&\left. - \frac{1-\exp\left(\frac{-Y_T\left[2+\gamma_{cj}+n(1+\gamma_c)(1+\gamma_j)+(1+\gamma_c)(1+\gamma_j)\right]}{(1+\gamma_c)(1+\gamma_j)}\right)}{[2+\gamma_{cj}+n(1+\gamma_c)(1+\gamma_j)]+(1+\gamma_c)(1+\gamma_j)}\right] \\
&- \frac{(1+\gamma_c)^2}{1+n(1+\gamma_c)]}\left[\frac{1-\exp\left(\frac{-Y_T\left[\lambda_T(1+\gamma_j)[1+(1+n)(1+\gamma_c)]+1+\gamma_c\right]}{(1+\gamma_c)(1+\gamma_j)}\right)}{\lambda_T(1+\gamma_j)[1+(1+n)(1+\gamma_c)]+1+\gamma_c]}\right. \\
&\left. - \frac{1-\exp\left(\frac{-Y_T\left[(1+\gamma_j)[1+(1+n)(1+\gamma_c)]+1+\gamma_c\right]}{(1+\gamma_c)(1+\gamma_j)}\right)}{(1+\gamma_j)[1+(1+n)(1+\gamma_c)]+1+\gamma_c]}\right] \\
&+ \frac{1}{n+1}\left[\frac{1-\exp\left(\frac{-Y_T\left[1+\lambda_T(n+1)(1+\gamma_j)\right]}{(1+\gamma_j)}\right)}{1+\lambda_T(n+1)(1+\gamma_j)} - \frac{1-\exp\left(\frac{-Y_T\left[1+(n+1)(1+\gamma_j)\right]}{(1+\gamma_j)}\right)}{1+(n+1)(1+\gamma_j)}\right] \\
&+ \frac{1}{n+1}\left[\frac{1-\exp\left(-Y_T[1+\lambda_T(n+1)]\right)}{1+\lambda_T(n+1)} - \frac{1-\exp\left(-Y_T[2+n]\right)}{2+n}\right] + \frac{(1+\gamma_{cj})^2}{1+n(1+\gamma_{cj})}
\end{aligned}$$

$$
\begin{aligned}
&\times \left[\frac{1-\exp\left(\frac{-Y_T\left[\lambda_T[1+(n+1)(1+\gamma_{cj})]+1+\gamma_{cj}\right]}{1+\gamma_{cj}}\right)}{\lambda_T[1+(n+1)(1+\gamma_{cj})]+1+\gamma_{cj}} - \frac{1-\exp\left(\frac{-Y_T\left[(n+1)(1+\gamma_{cj})+2+\gamma_{cj}\right]}{1+\gamma_{cj}}\right)}{(n+1)(1+\gamma_{cj})+2+\gamma_{cj}}\right]\Bigg\} \\
&+ (M-2)(M-3)\sum_{n=0}^{M-4}(-1)^n\binom{M-4}{n}\Bigg\{ \\
&\times \frac{1}{n+1}\left[\frac{1-\exp\Big(-Y_T[1+\lambda_T(n+1)]\Big)}{1+\lambda_T(n+1)} - \frac{1-\exp\Big(-Y_T[2+n]\Big)}{2+n}\right] \\
&- \frac{(1+\gamma_c)^2}{1+n(1+\gamma_c)}\left[\frac{1-\exp\left(\frac{-Y_T\left[\lambda_T[1+(n+1)(1+\gamma_c)]+1+\gamma_c\right]}{1+\gamma_c}\right)}{\lambda_T[1+(n+1)(1+\gamma_c)]+1+\gamma_c}\right. \\
&\left. - \frac{1-\exp\left(\frac{-Y_T\left[(n+1)(1+\gamma_c)+2+\gamma_c\right]}{1+\gamma_c}\right)}{(n+1)(1+\gamma_c)+2+\gamma_c}\right] - \frac{(1+\gamma_j)^2}{1+n(1+\gamma_j)} \\
&\times \left[\frac{1-\exp\left(\frac{-Y_T\left[\lambda_T[1+(n+1)(1+\gamma_j)]+1+\gamma_j\right]}{1+\gamma_j}\right)}{\lambda_T[1+(n+1)(1+\gamma_j)]+1+\gamma_j} - \frac{1-\exp\left(\frac{-Y_T\left[(n+1)(1+\gamma_j)+2+\gamma_j\right]}{1+\gamma_j}\right)}{(n+1)(1+\gamma_j)+2+\gamma_j}\right] \\
&- \frac{(1+\gamma_c)^2(1+\gamma_j)^2}{2+\gamma_{cj}+(1+n)(1+\gamma_c)(1+\gamma_j)} \\
&\times \left[\frac{1-\exp\left(\frac{-Y_T\left[\lambda_T[2+\gamma_{cj}+(n+1)(1+\gamma_c)(1+\gamma_j)]+(1+\gamma_c)(1+\gamma_j)\right]}{(1+\gamma_c)(1+\gamma_j)}\right)}{\lambda_T[2+\gamma_{cj}+(n+1)(1+\gamma_c)(1+\gamma_j)]+(1+\gamma_c)(1+\gamma_j)]}\right. \\
&\left. - \frac{1-\exp\left(\frac{-Y_T\left[2+\gamma_{cj}+(n+1)(1+\gamma_c)(1+\gamma_j)+(1+\gamma_c)(1+\gamma_j)\right]}{(1+\gamma_c)(1+\gamma_j)}\right)}{2+\gamma_{cj}+(n+1)(1+\gamma_c)(1+\gamma_j)+(1+\gamma_c)(1+\gamma_j)}\right]\Bigg\}\Bigg]. \qquad (2.54)
\end{aligned}
$$

Chapter 3

# Mellin Transform Based Performance Analysis of a FFH-MFSK Receiver Using Product Combining in PBNJ

In this chapter, we continue our investigation of the FH systems combatting jamming. More precisely, we now analyze the bit error ratio (BER) performance of fast frequency hopping assisted (FFH) $M$-ary frequency shift keying (MFSK) using product combining (PC). PC scheme constitutes an efficient yet low-complexity diversity combining technique that can be employed in FFH-MFSK receivers to combat the detrimental effects of partial band noise jamming (PBNJ) or multitone jamming (MTJ). In Section 1.4, we discussed the basic principles of the PC in the context of FFH-MFSK system. In Section 1.5.2, we demonstrated using simulation results that the PC receiver is capable of attaining useful BER performance gain, when the system is operating in a channel contaminated by multitone jamming (MTJ). In this chapter, we propose a novel approach to the analysis of this receiver system, which is based on the Mellin transform [118]. More explicitly, using this approach, the probability density function (PDF) of the PC output is expressed in a closed form. Based on the resultant PDF, the BER of the FFH-MFSK PC receiver operating in Rayleigh fading channel is evaluated analytically. We consider both a jamming free channel and a scenario when the transmitted signal encounters partial band noise jamming (PBNJ). We will demonstrate that the Mellin transform considerably simplifies the analysis of the PC receiver, and for the first time allows the BER analysis of the FFH-MFSK PC receiver having $M > 2$.

## 3.1 Review of Previous Works

Owing to its useful anti-jamming properties, the PC receiver of Section 1.4 has attracted considerable research attention. The main challenge in the analysis of the PC receiver is that the PDF of a product of

random variables has to be derived, in order to compute the symbol error ratio. In [43,56,58,64,119,120], the authors have analyzed the product combining based FFH binary frequency shift keying (BFSK) receiver under various fading and jamming conditions, employing the characteristic function (CF) [34] of the energy detector outputs and using the natural logarithm to convert the product into summation, for the sake of deriving the PDF of the PC output. The technique used in [57] is similar to that employed in [43], although the operation of the system has been considered in Nakagami-$m$ fading channel. The problem associated with the natural logarithm based approach is that closed form expressions for the PDF of the PC output cannot be readily obtained. Consequently, the symbol error probability is expressed using a double integral, when BFSK is considered. For $M$-ary FSK, the corresponding expressions are expected to be more complicated, involving multiple integrals.

Let us elaborate on this point using the relevant expressions for the PDF of the PC output and for the symbol error probability. In the context of the CF and the natural logarithm based method employed in [43,56,58,64,119], if

$$Z_m = \prod_{l=0}^{L-1} U_{ml} \tag{3.1}$$

denotes the PC output, we have

$$\ln Z_m = \sum_{l=0}^{L-1} \ln U_{ml}, \tag{3.2}$$

where $U_{ml}$ denotes the energy detector output and $m = 0, 1, \ldots, M-1$. Hence, the PDF of $\ln Z_m$ is derived in terms of the PDFs of the $\ln U_{ml}$ using the CF method [34,56,57]. Thus, we have

$$\phi(\ln Z_m) = \prod_{l=0}^{L-1} \phi(\ln U_{ml}), \tag{3.3}$$

where $\phi(x)$ denotes the CF of $x$. The PDF of $\ln Z_m$ can then be obtained from its CF [34]. To determine the PDF of the PC output $Z_m$ from the PDF of $\ln Z_m$, further mathematical steps are involved. For the sake of BER calculation, the symbol error probability is derived in the context of MFSK based schemes using the relation [34]:

$$P_s = 1 - \int_0^{\infty} f_{Z_0}(y_0) \Big[ \int_0^{y_0} f_{Z_m}(y_m) dy_m \Big]^{M-1} dy_0, \tag{3.4}$$

given that $m = 0$ is the transmitted tone. For BFSK, i.e for $M = 2$, the relation given by Equation (3.4) is equivalent to finding the probability that $(Z_1 > Z_0)$. The natural logarithm based method of [56, 57] instead finds the probability that $(\ln Z_1 > \ln Z_0)$. Alternatively, some simpler technique may be invoked, such as finding the probability that $\ln(Z_1 - Z_0) > 0$ [57], thus obviating the need to find the PDF of the PC output $Z_m$. However, for modulation orders greater than 2, the analysis invloves $M > 2$ decision variables and no similar *short cut* may be applied. Thus, if $M > 2$ is considered, Equation (3.4) would consist of 4 integrals. This is the reason that the natural logarithm method [56,57] has not been applied to modulation

orders greater than 2.

In [59, 61], the employment of Fox's $H$-functions was proposed to derive the PDFs of the PC output and the BER of the FFH-BFSK PC receiver. $H$-functions [59] constitute a family of general functions incorporating numerous functions such as exponential, Bessel and hypergeometric functions, which may be expressed as special cases of the $H$-function. In their analysis, the authors of [59,61] have exploited the fact that a product of $H$-functions is also an $H$-function [121] and the BER is expressed in terms of Meijer's $G$-function [122], which has also been expressed in the form of a computationally convenient infinite series. This method has been applied to BFSK only, targetting the probability that $(Z_1/Z_0 > 1)$, since only two decision variables are involved. For such a simple case, an expression involving $H$-functions and Meijer's $G$-functions can be formulated. However, for $M > 2$, the relevant expressions become intractable and this method has not been extended to $M > 2$. Moreover, as reported by the authors of [59–61], the $H$-function may not be readily invoked for the sake of deriving the PDF of the PC output, when more generalized forms of fading, such as Rician and Nakagami model, are considered.

The authors [60,61] have also employed another technique which consists of generalized $F$-variates for the sake of deriving the corresponding BER expressions. However, this latter method is more computationally demanding.

In this chapter, we employ the Mellin transform [121,123] to analyze PC aided FFH-MFSK. The Mellin transform of a random variable is related to its PDF and, like Laplace and Fourier transform, it is an integral transform. It has been shown in [121,123] that the Mellin transform of a product of random variables is the product of the Mellin transforms of the individual random variables. This fact allows us to derive the PDF of the PC's output which can in turn be used to determine an expression characterising the symbol error probability of the system. It will be shown that the proposed Mellin transform based technique substantially simplifies the BER analysis of the PC FFH-MFSK system and hence facilitates for the first time the analysis of $M$-ary FSK based FFH PC receiver for $M > 2$. Furthermore, none of the above-mentioned methods [56, 57, 61] allows a convenient way of expressing the PDF of the PC output in a closed or semi-closed form. By contrast, the Mellin transform method does provide this convenience, thereby providing further insights into the system's behaviour.

The remainder of this chapter is structured as follows. In Section 3.2, the system under consideration is briefly described. In Section 3.3, the proposed Mellin transform based technique is discussed and both the relevant statistics as well as the corresponding BER expression are derived, when the FFH-MFSK receiver employs square-law detection and operates in a jamming-free, Rayleigh fading channel. In Section 3.4, the proposed technique is employed for the derivation of the relevant statistics, when the FFH-MFSK receiver employs envelope detection and the channel is additionally contaminated by PBNJ. Analytical results are discussed and compared with simulation results for both Sections 3.3 as well as Section 3.4 separately. Finally, in Section 3.5, our conclusions are presented. Furthermore, in Appendix 3.A, we provide a brief discussion on the Mellin transform, elaborating its definition, the inverse transform, its various applications

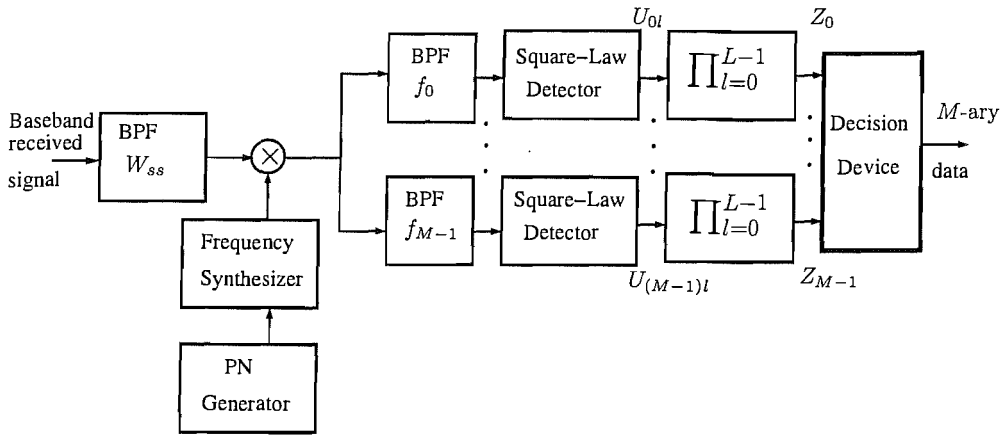


**Figure 3.1:** Receiver schematic of the FFH-MFSK system using square-law detection and PC

and its relationship to other integral transforms.

## 3.2 System Description

The system considered is similar to that in [56] and [61], except that in this chapter we consider an $M$-ary FSK system, where we have $M \geq 2$. The block diagram of the FFH-MFSK transmitter is shown in Figure 1.1, where the MFSK signal modulates a carrier generated by a frequency synthesizer, which is controlled by a pseudo-noise (PN) generator in order to implement frequency hopping. The transmitted frequency of the hopped signal may assume any one of a set of legitimate frequencies, which are determined by a random $L$-tuple address output by the PN generator, where $L$ is the number of frequency hops per symbol. Hence, the FH frequency is changed $L$ times within each symbol duration. Thus, the hop or chip interval $T_h$ is related to the symbol interval $T_s$ by the relation $T_h = T_s/L$. Correspondingly, the bandwidth occupied by the signal transmitted during each FFH chip interval is approximated by that of its main spectral lobe occupying $R_h = 1/T_h$. The frequency separation between adjacent frequency tones is assumed to be $R_h$. Thus, the orthogonality of the FFH frequencies is maintained.

The channel is modeled as flat Rayleigh fading channel for each of the transmitted frequencies. We assume that the frequency separation between adjacent signalling frequencies is higher than the coherence bandwidth of the channel. Therefore, all FH tones conveying the same symbol experience independent fading.

The block diagram of the FFH $M$-ary FSK receiver is shown in Figure 3.1 which is constituted by a bandpass filter, a frequency de-hopper, $M$ branches of the noncoherent MFSK demodulator and finally a decision device. The bandpass filter of Figure 3.1 removes any frequencies that fall outside the spread spectrum bandwidth $W_{ss}$. The de-hopper consists of a PN generator, which is identical to and aligned with the PN generator, as well as a frequency synthesizer and a multiplier. The de-hopper de-spreads the received signal by exploiting the knowledge of the transmitter's unique FFH address. Each of the $M$ demodulator

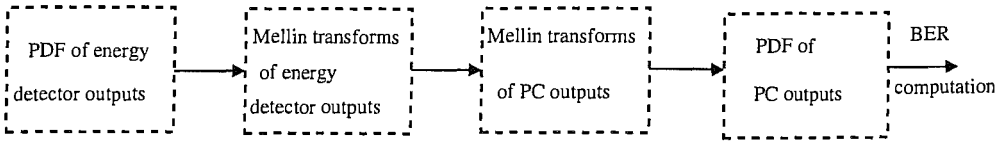


**Figure 3.2:** Schematic of the methodology employed for derivation of BER

branches corresponds to an MFSK tone and consists of a square-law detector, followed by a PC, as seen in Figure 3.1.

## 3.3 BER Analysis with Square-Law Detection

In this section, we employ the Mellin transform to derive the BER of the system shown in Figure 3.1. The transmitted signal experiences Rayleigh fading, but does not encounter any kind of jamming or interference. The methodology followed to derive the BER expression is outlined in Figure 3.2, where the energy detector may either be a square-law detector or an envelope detector. In this section, we assume the employment of square-law detector as seen in Figure 3.1. From the PDFs of the square-law detector outputs, we derive their Mellin transforms, which yield the Mellin transform of the PC output and consequently its inverse transform gives the PDF of the PC output. Finally, the PDFs of the PC outputs are employed to compute the symbol error ratio (SER) and the BER.

### 3.3.1 Derivation of PDF of PC Output

We assume witout loss of generality that the first of the $M$ tones is activated by the transmitter. It can be shown that the PDF of the square-law detector output corresponding to the signal tone normalized by the noise variance is given by [34,61]

$$f_{U_{0l}}(x) = \frac{1}{1+\gamma_h} \exp\left[-\frac{x}{1+\gamma_h}\right] = a\exp(-ax), \qquad x \geq 0, \tag{3.5}$$

where $\gamma_h = \gamma_s/L$ is the signal to noise power ratio (SNR) per hop, $\gamma_s = E_s/N_0$ is the SNR per symbol, $E_s$ is the transmitted symbol energy and $a = 1/(1+\gamma_h)$. Similarly, corresponding to all the undesired tones $m = 1, 2, \ldots, M-1$, the PDF of the square-law detector output, which is normalized by the noise variance, is given by

$$f_{U_{ml}}(x) = \exp(-x), \qquad x \geq 0, m > 1. \tag{3.6}$$

**Mellin transforms:** Next, we derive the Mellin transforms of the PDFs of the square-law detector outputs given by Equations (3.5) and (3.6). In Appendix 3.A, we provide a brief discussion on Mellin transform and discuss some of its properties that are relevant to our application. From the definition of the Mellin

transform given by Equation (3.76), the Mellin transforms of the PDFs given by Equations (3.5) and (3.6) characterising the variables $U_0$ and $U_m, m = 1, 2, \ldots, M-1$ respectively, may be expressed as

$$\begin{aligned} \mathcal{M}[f_{U_{0l}}(x), z] &= \int_0^\infty x^{z-1} f_{U_{0l}}(x) dx = a \int_0^\infty \exp(-ax) x^{z-1} dx \\ &= a a^{-z} \Gamma(z) = a^{1-z} \Gamma(z) \end{aligned} \tag{3.7}$$

and

$$\mathcal{M}[f_{U_{ml}}(y), z] = \Gamma(z), \quad m = 1, 2, \ldots, M-1, \tag{3.8}$$

where $\Gamma(.)$ denotes the Gamma function [1], and the results of Equations (3.7) and (3.8) have been obtained using the transform tables [124].

It has been shown that the Mellin transform of the product of random variables is equal to the product of the Mellin transforms of the individual random variables [121, 123]. In Appendix 3.A, we also demonstrate how this property of the Mellin transform can be intuitively derived from its relationship with the Fourier transform. Thus, if $Z_m$, $m = 0, 1, \ldots, M-1$, represents the output of the $m$th PC shown in Figure 3.1, which is given by

$$Z_m = \prod_{l=0}^{L-1} U_{ml}, \quad m = 0, 1, \ldots, M-1, \tag{3.9}$$

then, with the aid of [121], we arrive at

$$\mathcal{M}[f_{Z_m}(y), z] = \prod_{l=0}^{L-1} \mathcal{M}[f_{U_{ml}}(x), z], \quad m = 0, 1, \ldots, M-1. \tag{3.10}$$

Since the faded random variables in all hops are independent and identically distributed (*iid*), from Equation (3.10) we have

$$\mathcal{M}[f_{Z_m}(y), z] = \Big(\mathcal{M}[f_{U_{ml}}(x), z]\Big)^L, \quad m = 0, 1, \ldots, M-1. \tag{3.11}$$

Consequently, with the aid of Equation (3.7), for the desired signal tone we have

$$\mathcal{M}[f_{Z_0}(y), z] = \Big(\mathcal{M}[f_{U_{0l}}(x), z]\Big)^L = a^{L(1-z)} \Gamma^L(z), \tag{3.12}$$

while, from Equation (3.8) for the non-signal tones, we have

$$\mathcal{M}[f_{Z_m}(y), z] = \Big(\mathcal{M}[f_{U_{ml}}(x), z]\Big)^L = \Gamma^L(z), \quad m = 1, 2, \ldots, M-1. \tag{3.13}$$

**Inverse Mellin transforms:** Having derived the Mellin transforms of the decision variables, which are the PC outputs as seen in Figure 3.1, let us now investigate the inverse Mellin transform, which is introduced in

Appendix 3.A.

The PDF of $Z_m, m = 0, 1, \ldots, M-1$ can be obtained as the inverse Mellin transform of the expressions given in Equation (3.12) and (3.13). Thus, from the definition of the inverse Mellin transform given in Equations (3.80) and from Equations (3.12) and (3.13), we have

$$f_{Z_0}(y) = \frac{1}{2\pi i} \int_{c-i\infty}^{c+i\infty} y^{-z} a^{L(1-z)} \Gamma^L(z) dz \tag{3.14}$$

and

$$f_{Z_m}(y) = \frac{1}{2\pi i} \int_{c-i\infty}^{c+i\infty} y^{-z} \Gamma^L(z) dz, \qquad m = 1, 2, \ldots, M-1. \tag{3.15}$$

From the Residue theorem [118, 121, 125], we know that the complex integral at the right-hand side of the above equations can be computed by summing the residues of the integrand associated with all its poles. Thus, we have

$$f_{Z_0}(y) = \sum_j \mathcal{R}\left[a^{L(1-z)} y^{-z} \Gamma^L(z)\right]_{(z=-j)}, \tag{3.16}$$

and

$$f_{Z_m}(y) = \sum_j \mathcal{R}\left[y^{-z} \Gamma^L(z)\right]_{(z=-j)}, \tag{3.17}$$

where $\mathcal{R}[.]_j$ represents the residue at the $j$th pole of the integrand and the summation is carried out over all possible values of $j$. The PDF of $Z_0$ and $Z_m$, $m = 1, 2, \ldots, M-1$, can be determined numerically from Equations (3.16) and (3.17) by using a symbolic mathematics based software, such as Maple or Mathematica, invoking the appropriate function for finding residues of any integrable expression. However, it is more insightful to derive analytical expressions for Equations (3.16) and (3.17), which we do now with special emphasis on Equation (3.16).

For the sake of computing Equation (3.16), we have to investigate the poles and residues of the integrand seen in Equation (3.14). It can be readily seen that there are no poles contributed by the terms $y^{-z}$ and $a^{L(1-z)}$, and all poles are contributed by $\Gamma^L(z)$. Furthermore, it can be shown with the aid of [1, 122, 125] that the function $\Gamma(z)$ has an infinite number of poles at $z = -j$ for $j = 0, 1, 2, \ldots$. The residue of $\Gamma(z)$ at $z = -j$ can be obtained by evaluating $[\Gamma(z)(z+j)]$ at $z = -j$. Now, it transpires from [1, 125] that

$$\Gamma(z)\Gamma(1-z) = \frac{\pi}{\sin(\pi z)}. \tag{3.18}$$

Thus, we can write

$$\Gamma(z)(z+j) = \frac{\pi(z+j)}{\sin(\pi z)} \frac{1}{\Gamma(1-z)}$$

$$= \frac{\pi(z+j)}{\sin(\pi(z+j))}\frac{(-1)^j}{\Gamma(1-z)} \tag{3.19}$$

and

$$\Gamma(z)(z+j)|_{(z=-j)} = \frac{(-1)^j}{j!}, \tag{3.20}$$

which, by definition, gives us the residue of $\Gamma(z)$ at $z=-j$.

Now, $\Gamma^L(z)$ has an $L$th-order pole at each integer value of $z=-j$. We know from [1, 121, 125] that if a function $M(z)$ has $L$-order poles at $z=-j$, then its residue at this value of $z$ is given by

$$\mathcal{R}_{(z=-j)} = \frac{1}{(L-1)!}\frac{d^{L-1}}{dz^{L-1}}\Big[M(z)(z+j)^L\Big]. \tag{3.21}$$

Consequently, the PDF of $Z_0$ can be expressed from Equation (3.16) as

$$\begin{aligned} f_{Z_0}(y) &= \sum_{j=0}^{\infty}\frac{1}{(L-1)!}\frac{d^{L-1}}{dz^{L-1}}\Big[y^{-z}a^{L(1-z)}\Gamma^L(z)(z+j)^L\Big]_{(z=-j)} \\ &= \frac{a^L}{(L-1)!}\sum_{j=0}^{\infty}\frac{d^{L-1}}{dz^{L-1}}\Big[(a^Ly)^{-z}\Gamma^L(z)(z+j)^L\Big]_{(z=-j)}. \end{aligned} \tag{3.22}$$

If we let $\mathcal{U}(z) = (a^Ly)^{-z}$ and $\mathcal{V}(z) = \Gamma^L(z)(z+j)^L$, then by using Leibnitz' rule [1] for higher order derivatives of a product of functions, we get

$$f_{Z_0}(y) = \frac{a^L}{(L-1)!}\sum_{j=0}^{\infty}\sum_{r=0}^{L-1}\binom{L-1}{r}\Big[\mathcal{U}^{(r)}(z)\mathcal{V}^{(L-1-r)}(z)\Big]_{(z=-j)}, \tag{3.23}$$

where $\mathcal{U}^{(r)}(z)$ and $\mathcal{V}^{(r)}(z)$ denote the $r$th derivatives of $\mathcal{U}(z)$ and $\mathcal{V}(z)$, respectively.

The $r$th derivative of $\mathcal{U}$ can be readily found by writing

$$\mathcal{U}(z) = (a^Ly)^{-z} = \exp[-z\ln(a^Ly)], \tag{3.24}$$

yielding

$$\mathcal{U}^{(r)}(z) = [-\ln(a^Ly)]^r(a^Ly)^{-z}. \tag{3.25}$$

Hence, the $r$th derivative of $\mathcal{U}(z)$, when evaluate at $z=-j$, can be expressed as

$$\mathcal{U}^{(r)}(z)|_{(z=-j)} = [-\ln(a^Ly)]^r(a^Ly)^j. \tag{3.26}$$

In order to derive an expression for the $r$th derivative of $\mathcal{V}(z) = \Gamma^L(z)(z+j)^L$, we first express $\mathcal{V}(z)$ as [61]

$$\begin{aligned}\mathcal{V}(z) &= \frac{\Gamma^L(z+j+1)(z+j)^L}{(z+j)^L(z+j-1)^L \ldots z^L} \\ &= \frac{\Gamma^L(z+j+1)}{\prod_{k=1}^{j}(z+j-k)^L},\end{aligned} \tag{3.27}$$

where we have used the relation [122]

$$\Gamma(z+j+1) = (z+j)! = (z+j).(z+j-1)\ldots z.\Gamma(z). \tag{3.28}$$

When evaluated at $z = -j$, $\mathcal{V}(z)$ can be readily expressed as

$$\mathcal{V}(z)|_{(z=-j)} = \frac{1}{[(-1)^j(j!)]^L} = \frac{(-1)^{jL}}{(j!)^L}. \tag{3.29}$$

Note that we can also arrive at the same expression by raising Equation (3.20) to the $L$th power.

Next, we note that we have [61]

$$\frac{d\mathcal{V}(z)}{dz} = \mathcal{V}(z)\frac{d[\ln \mathcal{V}(z)]}{dz}. \tag{3.30}$$

Moreover, $d[\ln \Gamma(z)]/dz = \psi(z)$ holds, where $\psi(.)$ is the Psi function [1]. Thus, inserting Equation (3.27) in Equation (3.30), it can be shown that

$$\frac{d\mathcal{V}(z)}{dz} = \mathcal{V}^{(1)}(z) = L\mathcal{V}(z)\left[\psi(z+j+1) - \sum_{k=1}^{j}\frac{1}{(z+j-k)}\right]. \tag{3.31}$$

Consequently, we have

$$\mathcal{V}^{(1)}(z)|_{(z=-j)} = L\frac{(-1)^{jL}}{(j!)^L}\left[\psi(1) - \sum_{k=1}^{j}\frac{1}{(-k)}\right], \tag{3.32}$$

where $\psi(1) \approx -0.5772156649$, which equals the negative of the Euler's constant [1].

The higher order derivatives of $\mathcal{V}(z)$ can be derived from Equation (3.31). Thus, we have

$$\mathcal{V}^{(r)}(z) = \frac{d^{r-1}}{dz^{r-1}}[\mathcal{V}^{(1)}(z)]. \tag{3.33}$$

Using Leibnitz' rule [1] in the context of Equation (3.31), we arrive at

$$\begin{aligned}\mathcal{V}^{(r)}(z) &= L\Bigg\{\sum_{t=0}^{r-1}\binom{r-1}{t}\mathcal{V}^{(t)}(z)\psi^{(r-1-t)}(z+j+1) \\ &- \sum_{t=0}^{r-1}\binom{r-1}{t}\mathcal{V}^{(t)}(z)\sum_{k=1}^{j}\frac{d^{r-1-t}}{dz^{r-1-t}}\left[\frac{1}{(z+j-k)}\right]\Bigg\}\end{aligned}$$

$$= L\Bigg\{\sum_{t=0}^{r-1}\binom{r-1}{t}\mathcal{V}^{(t)}(z)(-1)^{r-t}(r-1-t)!\sum_{k=0}^{\infty}\Big[\frac{1}{(z+j+1+k)^{r-t}}\Big]$$
$$- \sum_{t=0}^{r-1}\binom{r-1}{t}\mathcal{V}^{(t)}(z)\sum_{k=1}^{j}\frac{(-1)^{r-t-1}}{(z+j-k)^{r-t}}\Bigg\}, \tag{3.34}$$

where we have used the $r$th derivative of $\psi(x)$ given by [1]

$$\psi^{(r)}(x) = (-1)^{r+1}r!\sum_{k=0}^{\infty}\Big[\frac{1}{(x+k)^{r+1}}\Big]. \tag{3.35}$$

When $\mathcal{V}^{(r)}(z)$ is evaluated at $z=-j$, we have

$$\mathcal{V}^{(r)}(z)|_{(z=-j)} = L\Bigg\{\sum_{t=0}^{r-1}\binom{r-1}{t}\mathcal{V}^{(t)}(z)|_{(z=-j)}(-1)^{r-t}(r-1-t)!\sum_{k=0}^{\infty}\Big[\frac{1}{(1+k)^{r-t}}\Big]$$
$$+ \sum_{t=0}^{r-1}\binom{r-1}{t}\mathcal{V}^{(t)}(z)|_{(z=-j)}\sum_{k=1}^{j}\frac{1}{(k)^{r-t}}\Bigg\}. \tag{3.36}$$

As can be seen in Equation (3.36), all derivatives of $\mathcal{V}(z)$ at $z=-j$ can be evaluated recursively from previous, i.e. lower order, derivatives. Moreover, we note that $\mathcal{V}^{(0)}(z) = \mathcal{V}(z)$, which is given by Equation (3.27) and by Equation (3.29), when evaluated at $z=-j$.

Having derived the expressions for all the derivatives of $\mathcal{V}(z)$ given by Equation (3.36) as well as those of $\mathcal{U}(z)$ given by Equation (3.26), the PDF of $Z_0$ can be determined from Equation (3.23). The PDF of $Z_m$, $m>0$ can also be determined from the same equation, by letting $a=1$ in Equation (3.26).

### 3.3.2 SER Expressions

Finally, having derived the PDFs of the PC outputs, the probability of symbol error can be evaluated as [34]

$$P_s = 1 - \int_0^{\infty} f_{Z_0(y_0)}\Big[\int_0^{y_0} f_{Z_m(y_m)}dy_m\Big]^{M-1}dy_0. \tag{3.37}$$

Correspondingly, the BER can be determined using the relation [34]

$$P_b = \frac{M/2}{M-1}P_s \tag{3.38}$$

Alternatively, we can express the probability of symbol error as [34]

$$P_s = 1 - \int_0^{\infty} f_{Z_0(y_0)}\Big[F_{Z_m}(y_0)\Big]^{M-1}dy_0, \tag{3.39}$$

where $F_{Z_m}(y_0)$ is the cumulative distribution function (CDF) of $Z_m$, $m > 0$, which is given by

$$F_{Z_m}(y_0) = \int_0^{y_0} f_{Z_m(y_m)} dy_m. \tag{3.40}$$

**CDF of $Z_m$:** From [118, 124], we know that the Mellin transform of the integral of a function can be evaluated using the relation

$$\mathcal{M}\left[\int_0^u f(x)dx, z\right] = -\frac{1}{z}\mathcal{M}[f(x), z+1]. \tag{3.41}$$

Hence, from Equation (3.13) we have

$$\mathcal{M}[F_{Z_m}(y_0), z] = -\frac{1}{z}\Gamma^L(z+1). \tag{3.42}$$

Upon taking the inverse Mellin transform according to Equation (3.80), Equation (3.42) yields

$$\begin{aligned} F_{Z_m}(y_0) &= -\int_{c-i\infty}^{c+i\infty} \frac{1}{z} y_0^{-z} \Gamma^L(z+1) dz \\ &= -\sum_j \mathcal{R}\left[\frac{1}{z} y_0^{-z} \Gamma^L(z+1)\right]_{(z=-j)} \\ &= -\frac{1}{(L-1)!} \sum_{j=1}^{\infty} \frac{d^{L-1}}{dz^{L-1}} \left[\frac{1}{z}(y_0)^{-z} \Gamma^L(z+1)(z+j)^L\right]_{(z=-j)}. \end{aligned} \tag{3.43}$$

In Appendix 3.B, we employ the method used in this section to derive a convenient expression for Equation (3.43). Therefore, symbol error probability can also be computed using Equation (3.39), which involves only one integration rather than two integrations, as seen in Equation (3.37).

### 3.3.3 Analytical Results and Discussion on Performance in Jamming-free Channel

In this section, we present the analytical results of the PDF and BER expressions derived in Sections 3.3.1 and 3.3.2, when the FFH-MFSK PC receiver invokes square-law detection while communicating in a Rayleigh fading channel. The PDFs and CDF given by Equations (3.23) and (3.93) respectively have to be evaluated numerically. Note that the infinite series seen in Equations (3.23) and (3.93) should be convergent in order to allow the computation of the PDF from a finite number of terms. It has been found that residues for $j \leq 25$ are sufficient for computing the PDF and the BER sufficiently accurately. Furthermore, it is evident that the infinite series seen in Equation (3.36) converge and hence the upper limit can be replaced by a finite computationally manageable integer.

In order to perform the infinite integration seen in Equations (3.37) or (3.39), plotting the PDFs $f_{Z_0}(y)$ can assist us in finding the value of $Z_0$ at which the PDF converges. In Figure 3.3, we have plotted the PDF of the PC output corresponding to the desired signal tone for FFH-4FSK, assuming $E_b/N_0 = 10$dB and various values of the diversity order. Note that the case when we have $L = 1$ implies no diversity and is

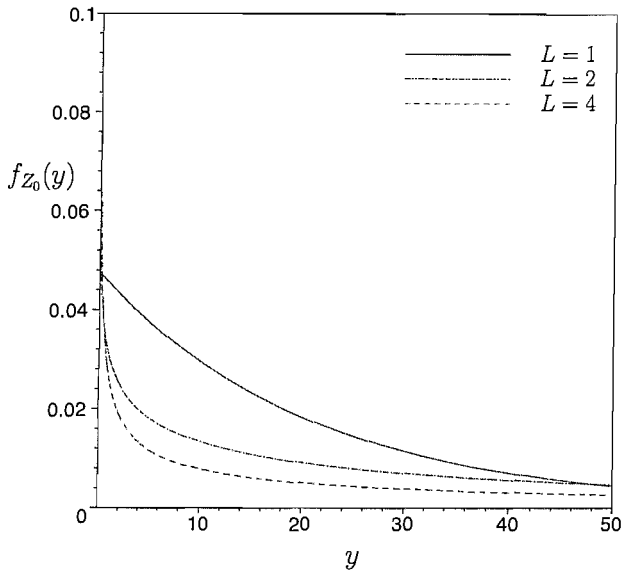


**Figure 3.3:** The PDF of the PC output, corresponding to the desired signal tone for FFH 4-ary FSK communicating in Rayleigh fading channel, assuming $E_b/N_0 = 10$dB and various values of $L$. The PDF is computed using Equation (3.23).

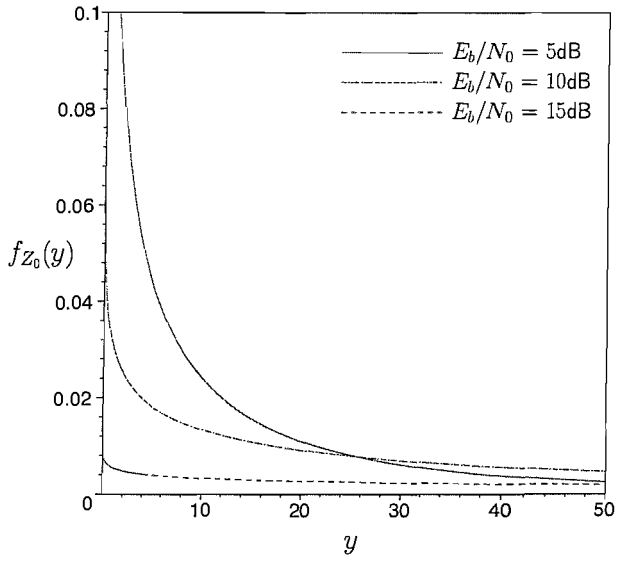


**Figure 3.4:** The PDF of the PC output, corresponding to the desired signal tone, for FFH 4-ary FSK communicating over a Rayleigh fading channel, assuming $L = 2$ and various values of $E_b/N_0$. The PDF is computed using Equation (3.23).

equivalent to the PDF of the square-law detector output. It can be seen from Figure 3.3 that the PDF curve becomes flatter and its tail gets longer upon increasing the values of $L$. This is expected, because owing to the multiplication invoked in the combiner, there is a non-zero probability of $Z_0$ attaining high values, if $L$ is high. Thus for high values of $L$, the PDF converges slowly.

The effects of both the SNR and the modulation order $M$ on the PDF of the product combiner output corresponding to the desired signal tone are shown in Figures 3.4 and 3.5, respectively. As expected, the results of Figures 3.4 and 3.5 show that the convergence of the PDF is slow, when either SNR or $M$ is

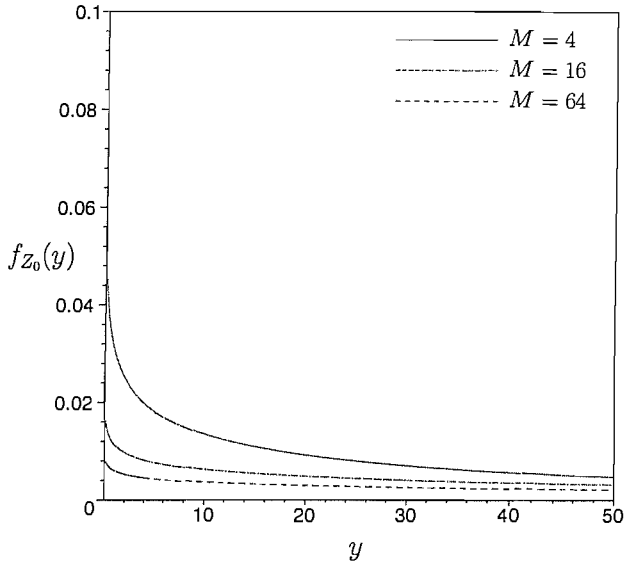


**Figure 3.5:** The PDF of the PC output, corresponding to the desired signal tone, for FFH $M$-ary FSK communicating over a Rayleigh fading channel, assuming $L = 2$, $E_b/N_0 = 10$dB and various $M$ values. The PDF is computed using Equation (3.23).

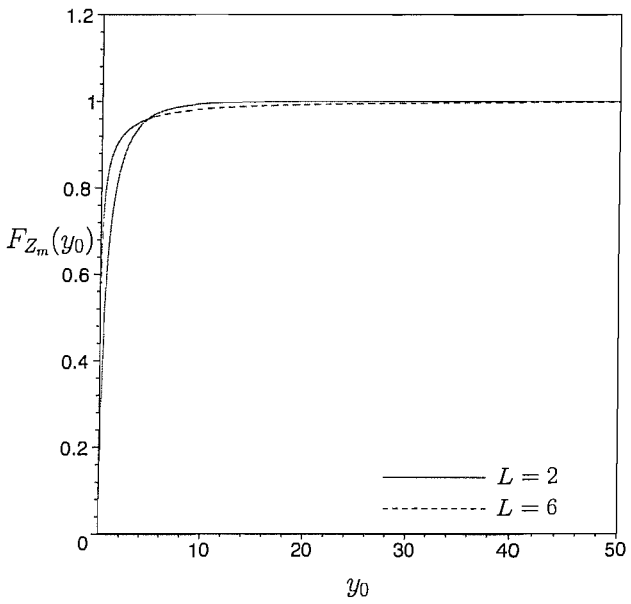


**Figure 3.6:** The CDF of the PC output, corresponding to the non-signal tone, for FFH 4-ary FSK communicating over a Rayleigh fading channel, assuming $E_b/N_0 = 10$dB and $L = 2$ and 6. The CDF is computed using Equation (3.93).

high, because both parameters may result in high symbol energy and, consequently, high expected combiner output value. Note in Figures 3.4 and 3.5, however, that the effect of increasing the modulation order on the shape of the PDF is not as significant as that of the SNR.

Thus, the evaluation of the PDF from Equation (3.23) is computationally cumbersome for large values of $M$, $L$ and SNR. An influential factor that facilitates the numerical evaluation of the BER is the fact that the CDF of the combiner output for non-signal tones rapidly approaches unity, as seen in Figure 3.6, which is valid for all values of $L$. Thus, while using Equation (3.39), $F_{Z_m}(y_0)$ can be replaced by 1 beyond a

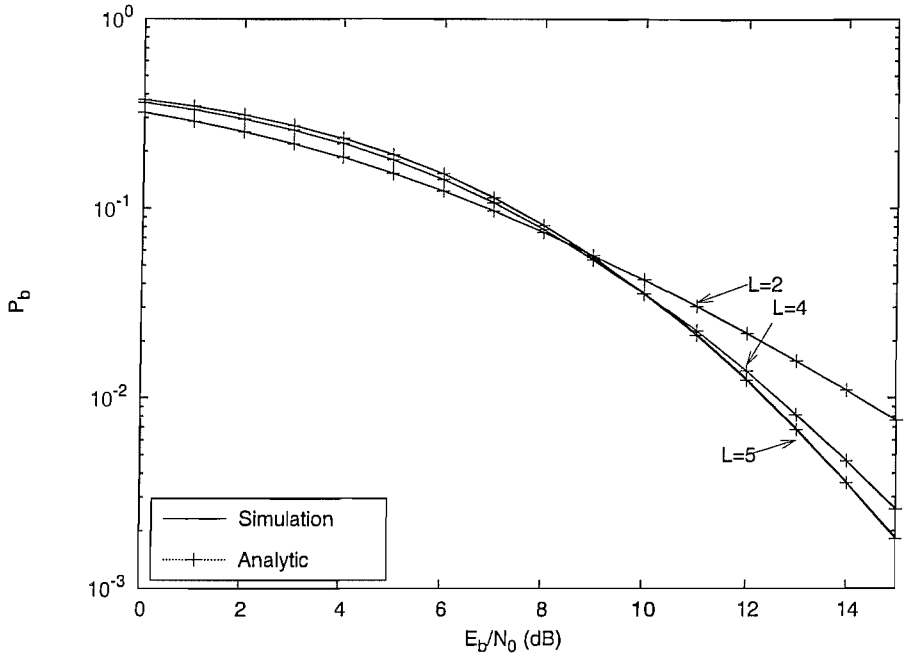


**Figure 3.7:** Comparison of the analytical and simulation results of the BER $P_b$ versus $E_b/N_0$ performance of FFH 4-ary FSK PC receiver communicating over a Rayleigh fading channel, assuming various values of $L$.

certain value of $y_0$ for the sake of approximate computation of the symbol error rate. In other words, we may modify Equation (3.39) as

$$P_s \approx 1 - \left[ \int_0^{Z_{0i}} f_{Z_0}(y_0) \left[ F_{Z_m}(y_0) \right]^{M-1} dy_0 + \int_{Z_{0i}}^{Z_{0t}} f_{Z_0}(y_0) dy_0 \right], \tag{3.44}$$

where $Z_{0i}$ and $Z_{0t}$ are arbitrarily chosen values of $Z_0$, such that $\left[ F_{Z_m}(y_0) \right]^{M-1} \approx 1$ at $Z_0 > Z_{0i}$ and $Z_{0t}$ is an appropriate substitute for $+\infty$.

Using the approximation seen in Equation (3.44), in conjunction with Equations (3.38), (3.93) and (3.23), we have evaluated the SER and the BER and plotted it in Figure 3.7 for $M = 4$ and in Figure 3.8 for $M = 32$, assuming various values of $L$. It can be seen from these figures that our analytic technique is fairly accurate and the results obtained match the simulation results for most values of the SNR in the range below 15 dB. For $M = 32$ and $L = 4$ in Figure 3.8, the BER value at $E_b/N_0 = 15$dB obtained analytically slightly differs from the corresponding simulation result. This inaccuracy accrues from the approximation invoked in Equation (3.44), as explained above. Another reason for the inaccuracy of these results is that the computation of the SER at high values of $L$ incurs higher-order differentials, which result in round-off errors involved in the computation of Equations (3.23) and (3.93). In Figure 3.9, both analytical and simulation results are provided for the BER of the system assuming $L = 4$ and various values of $M$. We observe that except for a slight difference for $M = 64$ at $E_b/N_0 = 15$dB, all analytical results tally with the corresponding simulation results. In general, for $E_b/N_0 \geq 20$dB, accurate computation of BER is difficult and some precision has to be sacrificed. Some values of the BER at $E_b/N_0 = 20$dB, assuming various

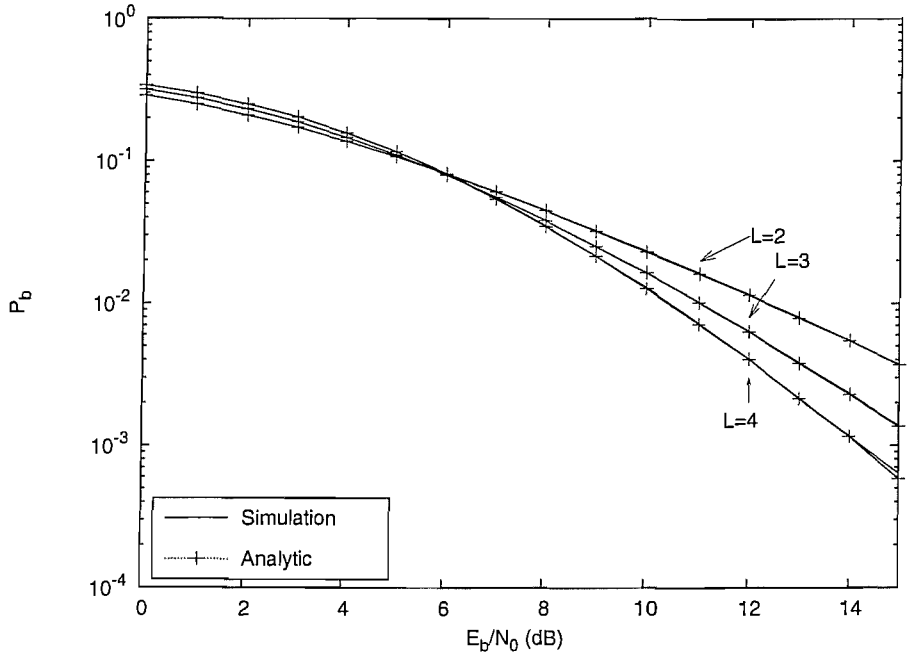


**Figure 3.8:** Comparison of the analytical and simulation results of the BER $P_b$ versus $E_b/N_0$ performance of FFH 32-ary FSK PC receiver communicating over a Rayleigh fading channel, assuming various values of $L$.

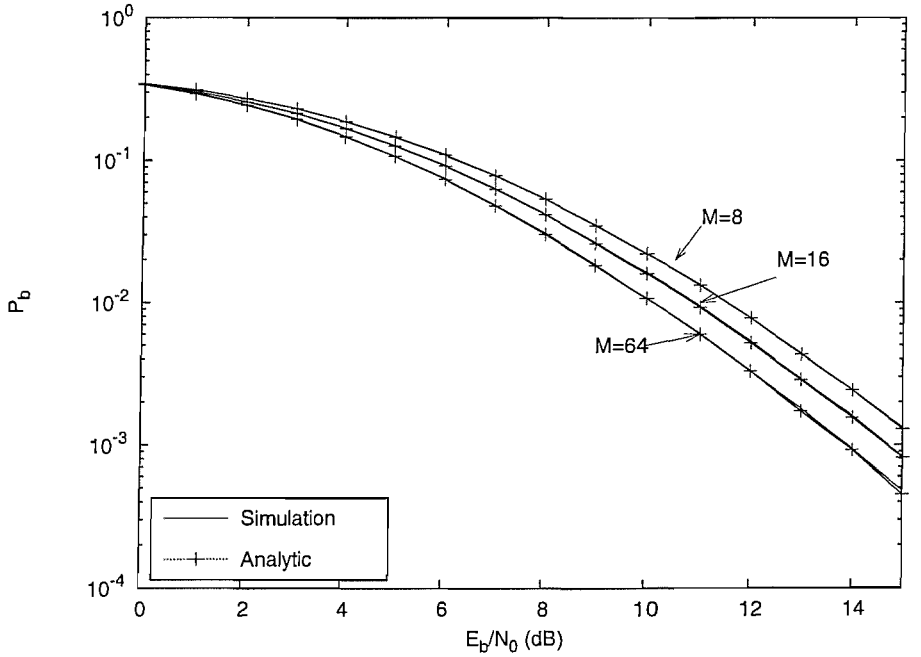


**Figure 3.9:** Comparison of the analytical and simulation results of the BER $P_b$ versus $E_b/N_0$ performance of FFH $M$-ary FSK PC receiver communicating over a Rayleigh fading channel, assuming $L = 4$ and for various values of $M$.

modulation and diversity orders are listed in Table 3.1. As the results suggest, the BER values obtained analytically differ from the simulation results, for high $M$ and $L$ values, for example, when we have $M = 2$ and $L = 5$ or $M = 4$ and $L = 4$.

**Table 3.1:** Comparison of the analytical and simulation based BER results for the FFH-MFSK PC receiver communicating over a Rayleigh fading channel, assuming $E_b/N_0 = 20$dB and various values of $M$ and $L$.

| $M$ | $L$ | BER | |
|---|---|---|---|
| | | Analytic | Simulation |
| 2 | 2 | 0.00266 | 0.00266 |
| 2 | 3 | 0.001018 | 0.001013 |
| 2 | 4 | 0.0004747 | 0.004628 |
| 2 | 5 | 0.000331 | 0.000259 |
| 4 | 2 | 0.001121 | 0.0010895 |
| 4 | 3 | 0.0003013 | 0.00028983 |
| 4 | 4 | 0.0001042 | 9.5066e-5 |

## 3.4 BER Analysis with Envelope Detection in PBNJ

In Section 3.3, we derived expressions for the PDFs of the PC outputs, when the FFH-MFSK receiver employs square-law detection. In Section 3.3.3, we observed that the tail of the PDF of the PC becomes very long, prohibiting numerical integration of the PDF when high diversity orders or high SNR values are involved. Since envelope detection [34] may also be employed in noncoherent MFSK demodulator with no change in the system's BER performance and since the square-root operation is likely to result in a narrower range of the detector output as compared to when square-law detection is employed, we now opt for envelope detector in FFH-MFSK PC receiver. Therefore, in this section, we derive all the metrics of Section 3.3 considering envelope detection of the FFH-MFSK signal instead of square-law detection in the PC receiver. Hence, the receiver schematic is given by Figure 3.10, while the envelope detector is elaborated with a schematic in Figure 3.11 [34].

Furthermore, since our ultimate objective of employing PC is to combat some form of jamming or inter-

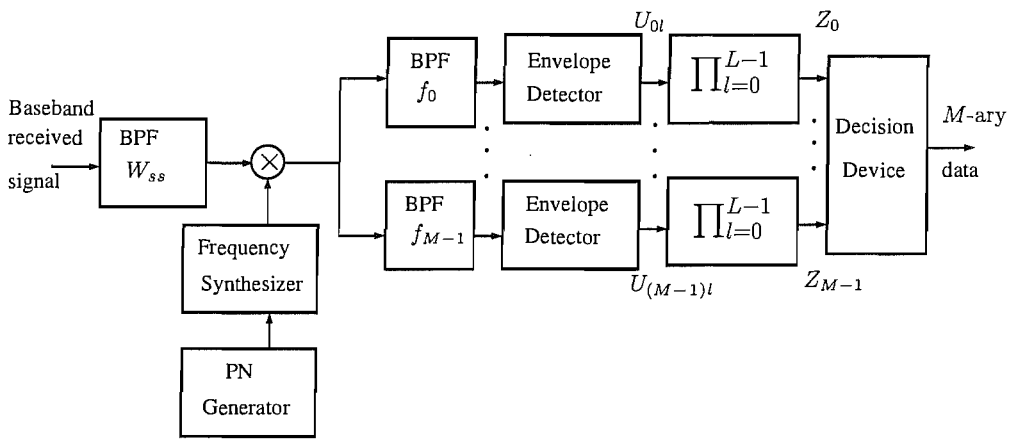


**Figure 3.10:** Receiver schematic of the FFH-MFSK system using envelope detection and PC

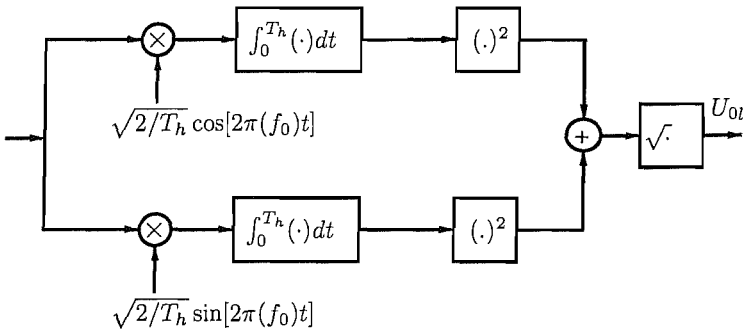


**Figure 3.11:** The schematic an envelope detector tuned to frequency $f_0$.

ference, we consider a channel contaminated by PBNJ. Hence, we assume that in addition to the AWGN, the transmitted signal encounters a PBNJ signal having single-sided power spectral density of $N_J$. We assume that the PBNJ signal jams a fraction $0 \leq \rho \leq 1$ of the total spread spectrum bandwidth $W_{ss}$. We also assume that the PBNJ signal is contiguous and hence all $M$ FSK tones of a particular band are jammed, if the jamming signal is present in that band. Thus, the probability that a band or a tone is jammed is given by $\rho$, while the probability that the band is not jammed is $(1-\rho)$. Our analysis method remains the same as that outlined in Figure 3.2. We outline the PDFs of the envelope detector outputs and employ the Mellin transform for deriving the PDFs and CDFs of the PC's outputs. Finally, these PDFs and CDFs will assist us in computing the BER [34, 56].

### 3.4.1 Derivation of PDF of PC Output

When the signal suffers from Rayleigh fading, the output of the noncoherent envelope detector is also Rayleigh distributed [34]. Therefore, assuming that the first of the $M$ tones is activated by the transmitter, it can be shown that the PDF of the envelope detector's output signal $U_{ml}, m = 0, 1, \ldots, M-1, l = 0, 1, \ldots, L-1$, corresponding to the desired signal tone, when the transmitted signal is jammed by PBNJ is given by [34, 61]

$$f_{U_{0l(j)}}(x) = \frac{x}{2(\sigma_0^2+\sigma_J^2)(1+\gamma_{ht})} \exp\left(\frac{-x^2}{2[\sigma_0^2+\sigma_J^2][1+\gamma_{ht}]}\right), \quad x \geq 0, \tag{3.45}$$

where $\gamma_{ht} = bE_b/(N_T L)$ is the signal to interference plus noise ratio (SINR) per hop, $N_T = N_0 + N_J/\rho$, $E_b$ is the transmitted energy per bit and $b$ is the number of bits per symbol. Furthermore, in Equation (3.45) the $(j)$ in the subscript explicitly indicates that the tone suffers from PBNJ and $\sigma_0^2 = R_h N_0$ and $\sigma_J^2 = R_h N_J/\rho$ represent the variance of the AWGN and the PBNJ, respectively. By contrast, when the signal is not jammed, the corresponding PDF can be expressed as [34, 61]

$$f_{U_{0l}}(x) = \frac{x}{2\sigma_0^2(1+\gamma_h)} \exp\left(\frac{-x^2}{2\sigma_0^2[1+\gamma_h]}\right), \quad x \geq 0, \tag{3.46}$$

where $\gamma_h = bE_b/(N_0L)$ is the signal to noise ratio (SNR) per hop. Similarly, the corresponding expressions for the PDFs of the undesired tones of $m = 1, 2, \ldots, M-1$, are given by [34, 61]

$$f_{U_{ml(j)}}(x) = \frac{x}{2(\sigma_0^2 + \sigma_J^2)} \exp\left(\frac{-x^2}{2[\sigma_0^2 + \sigma_J^2]}\right), \quad x \geq 0, m > 0 \tag{3.47}$$

and

$$f_{U_{ml}}(x) = \frac{x}{2\sigma_0^2} \exp\left(\frac{-x}{2\sigma_0^2}\right), \qquad x \geq 0, m > 0. \tag{3.48}$$

Therefore, the Mellin transforms of the PDFs given by Equations (3.45) to (3.48) may be expressed using Equation (3.76) as [121, 124, 126, 127]

$$\mathcal{M}[f_{U_{0l(j)}}(x), z] = \alpha_J^{(1-z)/2}\Gamma(z/2 + 1/2), \tag{3.49}$$

$$\mathcal{M}[f_{U_{0l}}(x), z] = \alpha^{(1-z)/2}\Gamma(z/2 + 1/2), \tag{3.50}$$

$$\mathcal{M}[f_{U_{ml(j)}}(x), z] = \beta_J^{(1-z)/2}\Gamma(z/2 + 1/2), \quad m > 0 \tag{3.51}$$

and

$$\mathcal{M}[f_{U_{ml}}(x), z] = \beta^{(1-z)/2}\Gamma(z/2 + 1/2), \quad m > 0, \tag{3.52}$$

where we have $\alpha_J = 1/[2(\sigma_0^2 + \sigma_J^2)(1 + \gamma_{ht})]$, $\alpha = 1/[2\sigma_0^2(1 + \gamma_h)]$, $\beta_J = 1/[2(\sigma_0^2 + \sigma_J^2)]$ and $\beta = 1/2\sigma_0^2$. Assuming that $p$ out of the $L$ hops of a symbol are jammed, the output of the $m$th PC, $m = 0, 1, \ldots, M-1$, seen in Figure 3.1 may be expressed as

$$Z_m = \prod_{l=0}^{p-1} U_{ml(j)} \prod_{l=0}^{L-p-1} U_{ml}. \tag{3.53}$$

Since signals in all hops are independent, the Mellin transform of the $m$th PC's output, given that $p$ out of the $L$ hops are jammed, may be expressed as

$$\mathcal{M}[f_{Z_m}(y_m|p), z] = \left[\mathcal{M}[f_{U_{ml(j)}}(x), z]\right]^p \left[\mathcal{M}[f_{U_{ml}}(x), z]\right]^{L-p}, \tag{3.54}$$

where $f_{Z_m}(y_m|p)$ represents the PDF of the $m$th PC output, $m = 0, 1, \ldots, M-1$. Consequently, from Equations (3.49), (3.50) and (3.54), we have for the desired signal tone

$$\mathcal{M}[f_{Z_0}(y_0|p), z] = \alpha_J^{p(1-z)/2}\alpha^{(L-p)(1-z)/2}\Gamma^L(z/2 + 1/2), \tag{3.55}$$

while from (3.51) and (3.52) for the undesired (nonsignal) tones, corresponding to $m > 0$, we have

$$\mathcal{M}[f_{Z_m}(y_m|p), z] = \beta_J^{p(1-z)/2}\beta^{(L-p)(1-z)/2}\Gamma^L(z/2 + 1/2). \tag{3.56}$$

Then, using Equation (3.80), the PDF of $Z_0$ can be generated as the inverse Mellin transform of Equation (3.55), yielding

$$f_{Z_0}(y_0|p) = \frac{1}{2\pi i}\int_{c-i\infty}^{c+i\infty} y_0^{-z}\alpha_J^{p(1-z)/2}\alpha^{(L-p)(1-z)/2}\Gamma^L[(z+1)/2]dz. \tag{3.57}$$

We now invoke the change of variable technique and replace $(z + 1)/2$ by $z$ in the above equation, since this does not affect the path of integration [121]. Hence, after further simplification, we have

$$f_{Z_0}(y_0|p) = \frac{2}{2\pi i}\int_{c-i\infty}^{c+i\infty} y_0^{1-2z}\alpha_J^{p(1-z)}\alpha^{(L-p)(1-z)}\Gamma^L(z)dz. \tag{3.58}$$

Upon applying the residue theorem [118, 121, 125, 126, 128] to Equation (3.58), we have

$$f_{Z_0}(y_0|p) = \sum_j \mathcal{R}\left[2y_0^{1-2z}\alpha_J^{p(1-z)}\alpha^{(L-p)(1-z)}\Gamma^L(z)\right]_{(z=-j)}. \tag{3.59}$$

Next, following the method employed in Section 3.3, we have

$$f_{Z_0}(y_0|p) = \frac{2\alpha_J^p\alpha^{L-p}y_0}{(L-1)!}\sum_{j=0}^{\infty}\frac{d^{L-1}}{dz^{L-1}}\left[(\alpha_J^p\alpha^{L-p}y_0^2)^{-z}\Gamma^L(z)(z+j)^L\right]_{(z=-j)}. \tag{3.60}$$

Letting $\mathcal{U}(z) = (\alpha_J^p\alpha^{L-p}y_0^2)^{-z}$ and $\mathcal{V}(z) = \Gamma^L(z)(z+j)^L$ and using Leibnitz' rule [1,126], Equation (3.60) may be expressed as

$$f_{Z_0}(y_0|p) = \frac{2\alpha_J^p\alpha^{L-p}y_0}{(L-1)!}\sum_{j=0}^{\infty}\sum_{r=0}^{L-1}\binom{L-1}{r}\left[\mathcal{U}^{(r)}(z)\mathcal{V}^{(L-1-r)}(z)\right]_{(z=-j)}, \tag{3.61}$$

where $\mathcal{U}^{(r)}(z)$ and $\mathcal{V}^{(r)}(z)$ denote the $r$th derivatives of $\mathcal{U}(z)$ and $\mathcal{V}(z)$, respectively. Then, it can be readily shown that we have

$$\mathcal{U}(z)|_{(z=-j)} = (\alpha_J^p\alpha^{L-p}y_0^2)^j \tag{3.62}$$

and

$$\mathcal{U}^{(r)}(z)|_{(z=-j)} = [-\ln(\alpha_J^p\alpha^{L-p}y_0^2)]^r(\alpha_J^p\alpha^{L-p}y_0^2)^j, \tag{3.63}$$

while, following the same method used in Section 3.3, we arrive at

$$\mathcal{V}(z)|_{(z=-j)} = \frac{(-1)^{jL}}{(j!)^L}. \tag{3.64}$$

and

$$\begin{aligned}\mathcal{V}^{(r)}(z)|_{(z=-j)} &= L\Bigg\{\sum_{t=0}^{r-1}\binom{r-1}{t}\mathcal{V}^{(t)}(z)|_{(z=-j)}(-1)^{r-t}(r-1-t)!\sum_{k=0}^{\infty}\Big[\frac{1}{(1+k)^{r-t}}\Big] \\ &+ \sum_{t=0}^{r-1}\binom{r-1}{t}\mathcal{V}^{(t)}(z)|_{(z=-j)}\sum_{k=1}^{j}\frac{1}{(k)^{r-t}}\Bigg\}.\end{aligned} \tag{3.65}$$

Hence, the PDF of $Z_0$, conditioned on the assumption that $p$ out of the $L$ hops are jammed, can be determined from Equation (3.61), while the PDF of $Z_m$, $m > 0$ can be similarly expressed as [1, 121, 125, 126, 128]

$$f_{Z_m}(y_m|p) = \frac{2\beta_J^p\beta^{L-p}y_m}{(L-1)!}\sum_{j=0}^{\infty}\sum_{r=0}^{L-1}\binom{L-1}{r}\Big[\mathcal{U}_m^{(r)}(z)\mathcal{V}^{(L-1-r)}(z)\Big]_{(z=-j)}, \tag{3.66}$$

where

$$\mathcal{U}_m(z)|_{(z=-j)} = (\beta_J^p\beta^{L-p}y_m^2)^j \tag{3.67}$$

and

$$\mathcal{U}_m^{(r)}(z)|_{(z=-j)} = [-\ln(\beta_J^p\alpha^{L-p}y_m^2)]^r(\beta_J^p\beta^{L-p}y_m^2)^j. \tag{3.68}$$

### 3.4.2 SER Expressions

Given the PDFs $f_{Z_0}(y_0|p)$ and $f_{Z_m}(y_m|p)$, the SER, conditioned on the assumption that $p$ out of the $L$ hops are jammed by PBNJ, is given by [34]

$$P_s(p) = 1 - \int_0^{\infty} f_{Z_0}(y_0|p)\Big[\int_0^{y_0} f_{Z_m}(y_m|p)dy_m\Big]^{M-1}dy_0. \tag{3.69}$$

Using the conditional SER, the overall average SER may be computed using [56]

$$P_s = \sum_{p=0}^{L}\binom{L}{p}\rho^p(1-\rho)^{L-p}P_s(p). \tag{3.70}$$

Given the SER, the corresponding BER can be determined using Equation (3.38).

Alternatively, we can express the conditional symbol error probability as [34]

$$P_s(p) = 1 - \int_0^{\infty} f_{Z_0}(y_0|p)\Big[F_{Z_m}(y_0|p)\Big]^{M-1}dy_0, \tag{3.71}$$

where $F_{Z_m}(y_0|p)$ is the CDF of $Z_m$, $m > 0$, conditioned on $p$ out of the $L$ hops being jammed. An analytical expression, similar to that derived in Appendix 3.A for square-law detected signal, can also be derived for $F_{Z_m}(y_0|p)$ which in this case is given by

$$F_{Z_m}(y_0|p) = -\frac{\beta_J^p \beta^{L-p} y_0}{(L-1)!} \sum_{j=0}^{\infty} \sum_{r=0}^{L-1} \binom{L-1}{r} \left[ \mathcal{U}_{m0}^{(r)}(z) \mathcal{V}_m^{(L-1-r)}(z) \right]_{(z=-j)}, \tag{3.72}$$

where

$$\mathcal{U}_{m0}(z) = (\beta_J^p \beta^{L-p} y_0^2)^{-z} \tag{3.73}$$

and

$$\mathcal{U}_{m0}^{(r)}(z)|_{(z=-j)} = [-\ln(\beta_J^p \alpha^{L-p} y_0^2)]^r (\beta_J^p \beta^{L-p} y_0^2)^j. \tag{3.74}$$

Furthermore, in (3.72) we have $\mathcal{V}_m(z) = \mathcal{V}(z)/(z-1)$, while its $r$th order differential may be expressed, using Leibnitz' rule [1], as

$$\mathcal{V}_m^{(r)}(z)|_{(z=-j)} = -\sum_{t=0}^{r} \binom{r}{t} \mathcal{V}^{(t)}(z)|_{(z=-j)} \frac{(r-t)!}{(1+j)^{r-t+1}}, \tag{3.75}$$

where $\mathcal{V}^{(t)}(z)|_{(z=-j)}$ is given by Equation (3.65). Given $F_{Z_m}(y_0|p)$, $P_s(p)$ can also be computed using Equation (3.71).

### 3.4.3 Analytical Results and Discussion on Performance against PBNJ

In this section, we validate our analysis detailed in Sections 3.4.1 and 3.4.2 using analytical results and discuss the achievable performance of the FFH-MFSK PC receiver invoking envelope detection while communicating in a Rayleigh fading channel. As discussed in the context of Section 3.3.3, the integrations seen in Equations (3.69) and (3.71) are performed numerically. Moreover, the technique of truncating the PDF or CDF discussed in the context of Equation (3.39) may also be applied. Using Equation (3.61), we portray the PDF of the PC's output corresponding to the FFH-MFSK signal tone in Figure 3.12, assuming $M = 4$, $L = 3$ and 5 and $E_b/N_0 = 10$dB in the absence of jamming. The PDF of the PC's output assuming square-law detection has also been shown using results from Section 3.3.1. It can be seen in Figure 3.12 that beyond a certain value of PC's output, envelope detection of the received signal leads to smaller area under the tail of its PDF compared to square-law detection. The high probability of encountering high PC output values for square-law detection are due to its squaring operation. By contrast, as observed in Figure 3.12, the PDF has a more limited dynamic range, when envelope detection is employed. Since accurate numerical integration in Equation (3.69) and (3.71) requires the truncation of the PDF at a point where it becomes negligible, the employment of envelope detection facilitates the numerical computation of the BER.

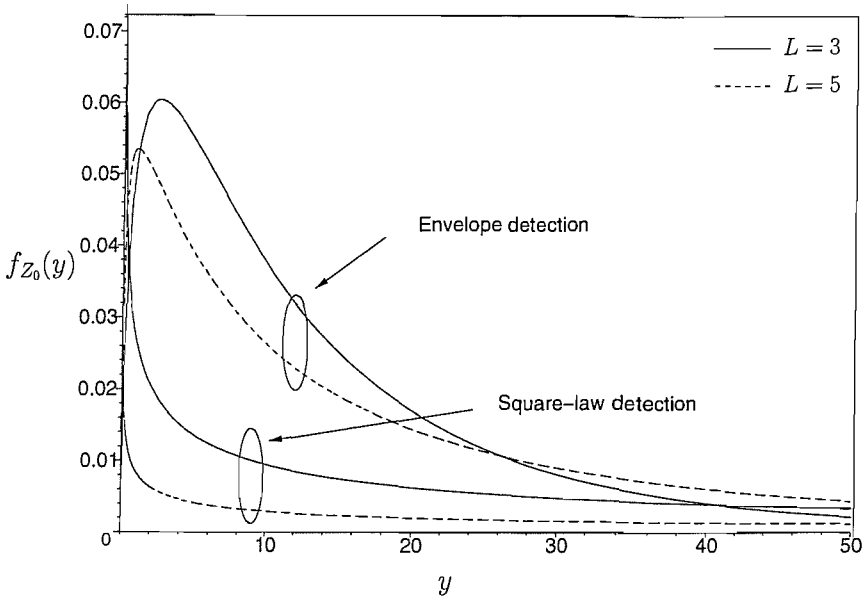


**Figure 3.12:** The PDF of PC output for both square-law and envelope detection of desired tone, for a FFH aided 4-ary FSK PC receiver, communicating over an interference-free Rayleigh fading channel, assuming $L = 3$ and 5 and $E_b/N_0 = 10$dB. The PDFs have been computed using Equations (3.23) and (3.61).

Using Equations (3.38), (3.70) and (3.71), in conjunction with Equations (3.61) and (3.72), the effects of increasing the diversity order on the system BER $P_b$ has been characterised in Figure 3.13. In this figure, the parameters of $M = 8$, $\rho = 0.1$ and $E_b/N_0 = 20$dB have been assumed. This figure demonstrates that increasing the value of $L$ enhances the achievable diversity gain, which results in an improved BER. Figure 3.13 also demonstrates that our analytical results match the simulation results, although we note in Figure 3.13 that at $L = 5$, the analytical results slightly deviate from the simulation results, especially when $E_b/N_J$ approaches 20dB. The reason for this inaccuracy is that having a high diversity order prevents the accurate computation of Equation (3.61), (3.66) and (3.71), as explained in Section 3.3.3.

In Figure 3.14, we have plotted the BER for $M = 32$, $L = 3$, $E_b/N_0 = 20$dB and for various values of the PBNJ duty factor $\rho$. We note from this figure that the BER performance of the system using $M$-ary FSK follows similar trends to those reported in the context of BFSK in [61]. Specifically, as seen in Figure 3.14, $\rho = 1$ results in the worst BER performance, and hence for $\rho < 1$ a better BER performance is recorded. This observation demonstrates that PBNJ associated with a duty factor of unity constitutes the worst-case jamming scenario in Rayleigh fading. This result is in agreement with previous results on FFH-BFSK PC systems designed for combatting PBNJ [56, 57, 61]. However, note that under less severe fading conditions or in AWGN, the value of worst case duty factor may be less than unity, as reported in numerous contributions, including [35–37, 39, 40, 78]. Note also in Figure 3.14 that as the signal power increases in comparison to the jammer power, the performance of the system becomes less sensitive to $\rho$.

We also note in Figure 3.14 that the analytical results pertaining to $\rho = 0.01$ slightly deviate from the corresponding simulation results. The reason for this difference is that at a low PBNJ duty factor, the effective jammer power encountered in a jammed hop increases, contributing to the increased magnitude of

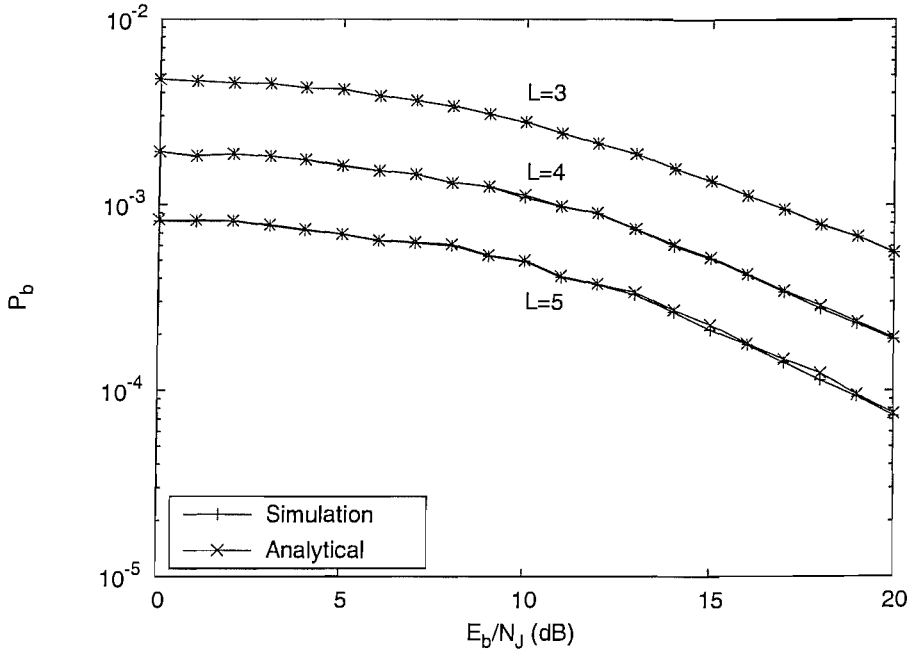


**Figure 3.13:** Comparison of the analytical results of (3.70) and the simulation results of the BER $P_b$ versus the $E_b/N_J$ performance of a FFH aided 8-ary FSK PC receiver communicating over a Rayleigh fading channel, assuming $E_b/N_0 = 20$dB, $\rho = 0.1$ and various $L$ values.

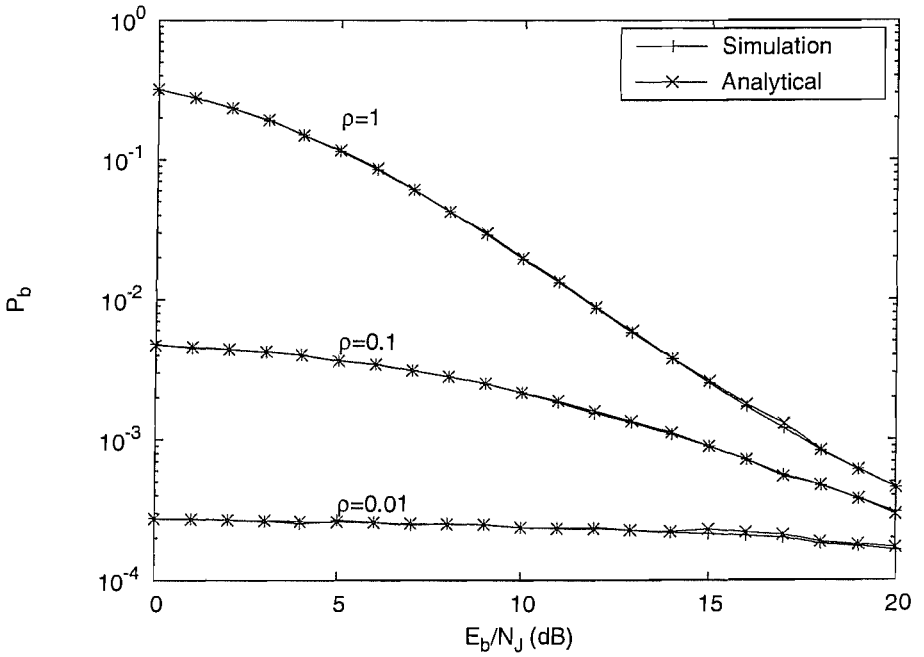


**Figure 3.14:** Comparison of the analytical results of (3.70) and the simulation results of the BER $P_b$ versus the $E_b/N_J$ performance of a FFH aided 32-ary FSK PC receiver communicating over a Rayleigh fading channel, assuming $L = 3$, $E_b/N_0 = 20$dB and various values of the PBNJ duty factor $\rho$.

the received signal. Thus, in this scenario the resultant PC output may become high and the area under the tail of its PDF may increase. Consequently, under these conditions, the computation of the PDFs and the BER using Equations (3.61), (3.66) and (3.71) may be less accurate.

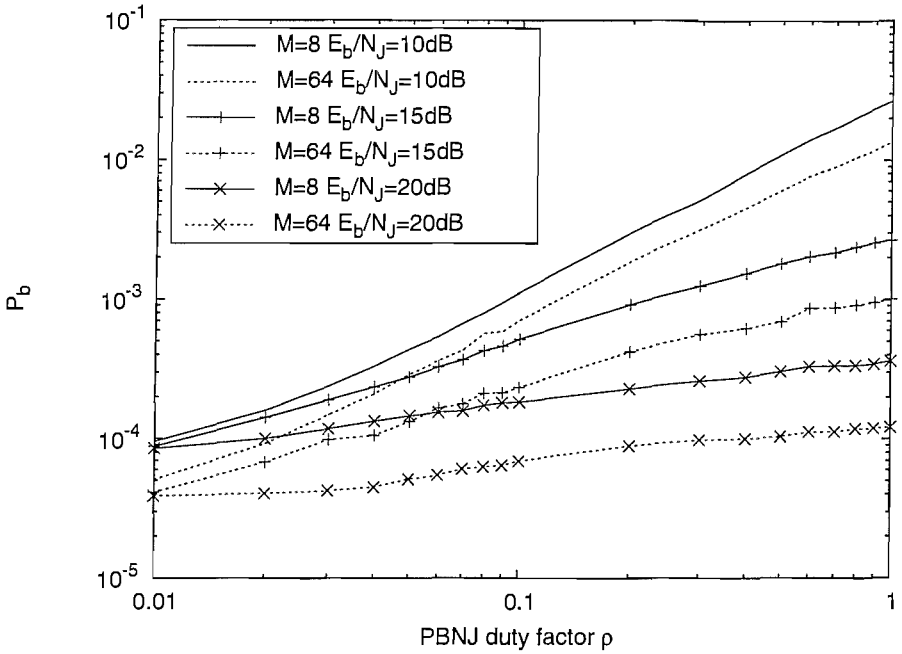


**Figure 3.15:** BER $P_b$ versus PBNJ duty factor performance of a FFH aided MFSK PC receiver communicating over a Rayleigh fading channel, assuming $L = 4$, $E_b/N_0 = 20$dB and various values of the $M$ and $E_b/N_J$.

In a nutshell, it has been observed in our investigations that the computation of the BER becomes challenging for $L > 5$, for low values of the jamming duty factor as well as for $E_b/N_J$ and $E_b/N_0 > 20$dB in conjunction with high $M$, and hence some numerical precision may have to be sacrificed.

Having validated our analysis using Figures 3.13 and 3.14, we further illustrate the effects of the PBNJ duty factor on the achievable system performance by plotting the BER against $\rho$ in Figure 3.15 for $M = 8$ and 64 as well as for $E_b/N_J = 10, 15$ and 20dB. This figure confirms that $\rho = 1$ constitutes the worst-case PBNJ. Furthermore, we note in Figure 3.15 that for the relatively high value of $E_b/N_J = 20$dB the effect of the jammer duty factor is not as significant as it is when $E_b/N_J = 10$dB is used. Thus the BER curves corresponding to $E_b/N_J = 20$dB are significantly flatter than those for $E_b/N_J = 10$dB. This is understandable because when jammer power is low in comparison to the signal power, the duty factor has little influence on the communication system's performance. Another important observation inferred from Figure 3.15 is that the lower the duty factor value, the less dramatic the effect of the jammer power on the BER. More specifically, observe in Figure 3.15 that at low values of the PBNJ duty factor, for instance at $\rho \approx 0.01$, the BER values recorded are limited to a narrower range, almost regardless of the SJR value considered. This is because since $\rho = 1$ is the worst-case duty factor, at lower $\rho$ values, the jammer power becomes less effective.

Let us now portray our BER results for various values of the modulation order in Figure 3.16, where the parameter values of $L = 3$, $\rho = 0.1$ and $E_b/N_0 = 20$dB have been assumed. The results of this figure demonstrate that the performance of the system improves, as the modulation order is increased. This result is in agreement with our prior knowledge in the context of $M$-ary systems [34]. However, only a

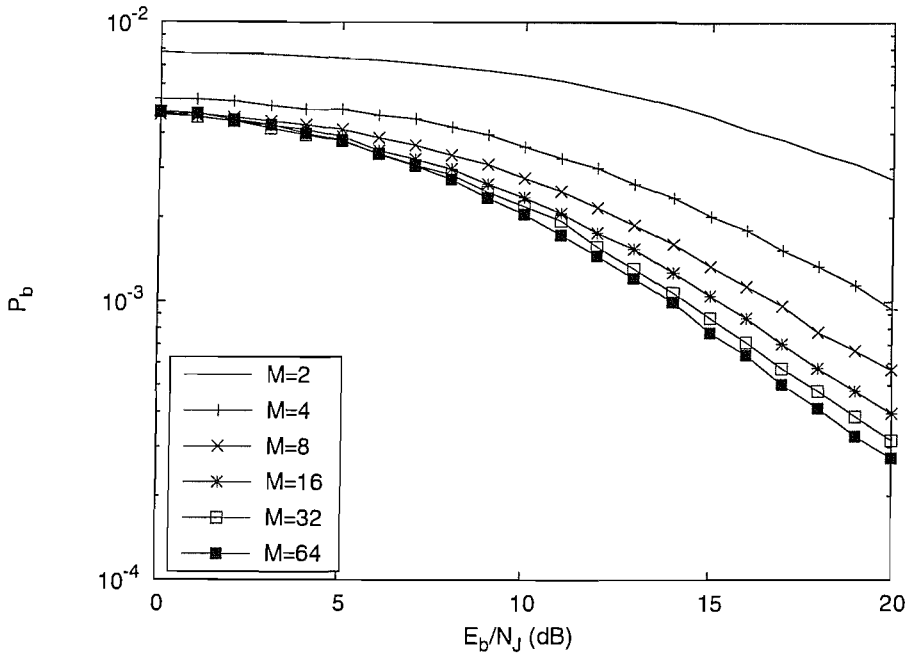


**Figure 3.16:** BER $P_b$ versus $E_b/N_J$ performance of a FFH aided MFSK PC receiver communicating over a Rayleigh fading channel, assuming $L = 3$, $E_b/N_0 = 20$dB, $\rho = 0.1$ and various $M$ values.

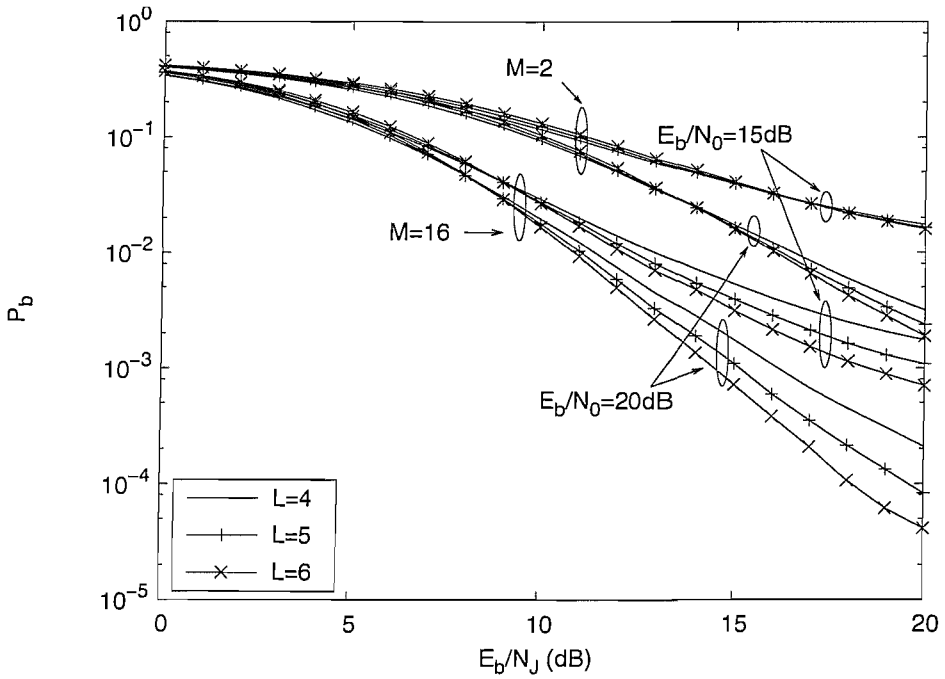


**Figure 3.17:** BER $P_b$ versus $E_b/N_J$ performance of a FFH aided MFSK PC receiver communicating over a Rayleigh fading channel, assuming $\rho = 1$, $M = 2$ and 16, $E_b/N_0 = 15$ and 20dB, and various $L$ values.

modest performance improvement is observed in Figure 3.16 upon increasing $M$ beyond $M = 16$. Thus, for the sake of striking a good balance between the achievable performance improvement and the bandwidth expansion imposed, $M = 8$ or 16 constitutes a beneficial trade-off in the context of the system considered.

Next, we quantify the system performance against worst case PBNJ, which corresponds to $\rho = 1$, as

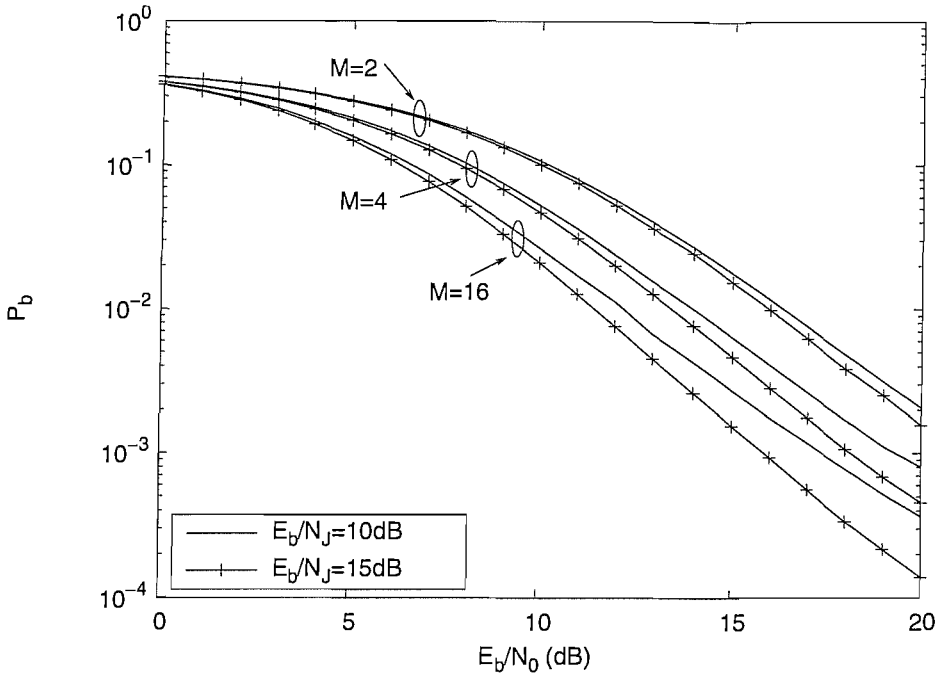


**Figure 3.18:** BER $P_b$ versus $E_b/N_0$ performance of a FFH aided MFSK PC receiver communicating over a Rayleigh fading channel, assuming $L = 5$, $\rho = 0.1$, $E_b/N_J = 10$ and 15dB, and various $M$ values.

mentioned above in the context of Figures 3.14 and 3.15. In Figure 3.17, we plot the BER against $E_b/N_J$ for $\rho = 1$ and for both $M = 2$ and $M = 16$, as well as for various SNR values. Our first observation in Figure 3.17 is that the attainable diversity gain is low, when worst-case jamming is encountered, especially when $E_b/N_0$ is also low. This observation becomes more explicit upon comparing Figure 3.17 and Figure 3.13, where $\rho < 1$ is assumed and consequently increasing the value of $L$ results in a significant BER improvement. By contrast, we observe in Figure 3.17 that initially no diversity gain is attained, but it becomes more apparent beyond $E_b/N_J \approx 10$dB. For instance, for $M = 2$ and $E_b/N_0 = 20$dB, the system using $L = 6$ outperforms $L = 4$ and $L = 5$, when $E_b/N_J$ exceeds 15dB. This trend has been reported in the context of all FFH-MFSK diversity combining receivers [35–37, 39, 40, 56], and it may be attributed to the noncoherent combining losses, which limit the diversity gain at a low signal power. We also observe in Figure 3.17 that the achievable diversity gain is significant in case of $M = 16$, while corresponding to BFSK there is hardly any benefit in using higher values of $L$, especially at $E_b/N_0 = 15$dB. This observation demonstrates that, as expected, having an increased modulation order $M$ typically yields a higher diversity gain. Another observation that we make from Figure 3.17 is that the SNR has a significant effect on the attainable BER performance of the system.

In order to further characterise the effect of the SNR on the achievable system performance, we plot the system's BER against $E_b/N_0$ for $L = 5$ as well as for various $M$ and SJR values in Figure 3.18. Comparing Figure 3.18 with Figures 3.13 and 3.17, our earlier observation that the SNR has a substantial impact on system's BER is confirmed. More specifically, we note that while in Figure 3.13 the BER corresponding to a particular value of $L$ is limited to a narrower range of SJR values spanning from 0 to 20dB, in Figure 3.18

the BER varies with the SNR over a significantly wider range. The reason for the more substantial impact of the SNR on the system's BER is that the detrimental effect of jammer power is limited by another factor, namely by the PBNJ duty factor, as discussed in the context of our discussion on Figure 3.15 above. By contrast, the AWGN is imposed on the transmitted signal under all conditions and thus imposes a more substantial effect on the BER.

## 3.5 Conclusion

We have used the Mellin transform to analyze the PC receiver used in a FFH-MFSK system, operating in a Rayleigh fading channel, assuming both an interference-free scenario as well as a channel contaminated by PBNJ. Employing the proposed Mellin transform based technique, the PDF and CDF of the PC output was determined in semi-closed forms, given in Equations (3.23) and (3.93) for the jamming-free channel and in Equations (3.61), (3.66) and (3.72) for the PBNJ-contaminated channel. With the aid of the PDFs and CDFs, the SER and the BER of the system was evaluated analytically using Equations (3.37), (3.39), (3.69), (3.70) and (3.71), thus enabling for the first time the analysis of this receiver for $M > 2$. The proposed technique has been shown to be accurate and the analytical results obtained match the simulation results for most practical values of the modulation order, for diversity order $L \leq 5$, for PBNJ duty factor and for $E_b/N_0 \leq 20$dB. For large values of $M$, $L$, $E_b/N_0$ and $E_b/N_J$, the PDF of the combiner output corresponding to the desired signal tone becomes flatter and converges slowly, resulting in less accurate computation of the BER. We also observed that in contrast to the square-law detection, envelope detection in the MFSK demodulator leads to a narrower dynamic range of the PC outputs, thus facilitating the numerical integration of the PDF of the PC outputs, which is needed for the SER computation. Hence, for the scenario where the signal encounters PBNJ, we opted for envelope detector based demodulator.

Our analytical results demonstrate that effect of the PBNJ is greatly governed by its duty factor and that the PBNJ having a jamming duty factor of unity results in the worst-case jamming scenario for the FFH-MFSK system communicating over Rayleigh fading channels. Moreover, the BER performance of the system improves, as either the modulation order or the diversity order is increased. An important observation made through our results is that significantly greater diversity gain can be achieved from FFH if higher modulation order is employed. In Tables 3.2 and 3.3, we have summarised the performance of the PC receiver in PBNJ by listing the $E_b/N_J$ values required to maintain a BER=$10^{-3}$, when assuming various system parameters.

The proposed method can readily be applied to a scenario, where the channel is interfered by MTJ. Furthermore, the channel that we assumed in our analysis was modeled on Rayleigh fading channel. In general, the Nakagami-$m$ and the Rician models present more generalized and versatile models than the Rayleigh channel. Fortunately, the Mellin transforms of the PDF of the energy detector output also exist [124], when the transmitted signal experiences Rician or Nakagami-$m$ fading. This observation suggests that the analysis

of the FFH-MFSK receiver using PC in more generalized fading conditions may also be possible.

Having investigated the anti-jamming capabilities of FH systems in this and the previous two chapters, we now focus our attention on the multiple access capabilities of FFH in the next chapter.

| | $E_b/N_0 = 20$dB | | | $E_b/N_0 = 15$dB | | |
|---|---|---|---|---|---|---|
| $L$ | 4 | 5 | 6 | 4 | 5 | 6 |
| $E_b/N_J$ | 16.1 | 15.1 | 14.4 | NA | 20 | 18.2 |

NA means "Not achieved".

**Table 3.2:** Summary of the $E_b/N_J$ values in dBs required for FFH-MFSK PC receiver to achieve a BER of $10^{-3}$, when communicating over a Rayleigh fading channel, assuming $M = 16$, $\rho = 1$, $E_b/N_0 = 20$ and 15 dB and various $L$ values. The results were extracted from Figure 3.17.

| $M$ | 4 | 8 | 16 | 32 | 64 |
|---|---|---|---|---|---|
| $E_b/N_J$ | 19.6 | 16.8 | 15.5 | 14.3 | 13.9 |

**Table 3.3:** Summary of the $E_b/N_J$ values in dBs required for FFH-MFSK PC receiver to achieve a BER of $10^{-3}$, when communicating over a Rayleigh fading channel, assuming $L = 3$, $\rho = 0.1$, $E_b/N_0 = 20$dB and various $M$ values. The results were extracted from Figure 3.16.

## 3.A APPENDIX: A Brief Discussion on Mellin Transform

In this appendix, we discuss the Mellin transform and its various properties. The Mellin transform of a function $f(x)$ is defined as [118, 121]

$$\mathcal{M}[f(x), z] = \int_0^\infty x^{z-1} f(x) dx \tag{3.76}$$

In terms of probability theory, the Mellin transform of a random variable uniquely determines its PDF and is defined based on its PDF. Specifically, if the function $f(x)$ represents the PDF of a random variable, then the Mellin transform of the random variable, or alternatively that of its PDF, is given by Equation (3.76).

Mellin transform has been employed in the solution of boundary value problems [123], summation of harmonic sums [123, 129, 130], searching and sorting algorithms [123, 130], analysis of asymptotes [129], besides a myriad of other analyses. It is especially suited to the solution of functional equations involving scaling functions such as [129, 131]:

$$f(x) = a(x) + \alpha f(px) + \beta f(qx), \tag{3.77}$$

where $\alpha$, $\beta$, $p$ and $q$ are constants and $a(x)$ is a known function. Such equations are often encountered in search algorithms [123, 130]. Mellin transform allows us to convert such equations into algebraic form and thus recover $f(x)$. Due to these reasons, Mellin transform has found a number of applications in classical mathematics [130, 132], physics [123, 130], communication protocols [130, 133], signal analysis [134–136],

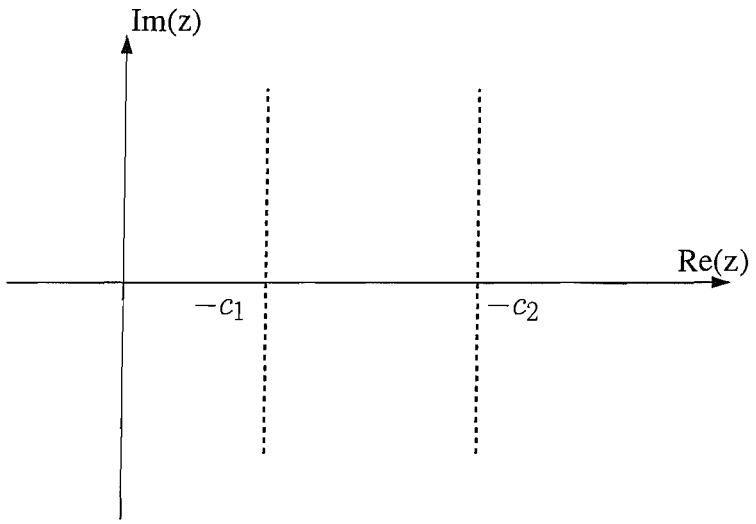


**Figure 3.19:** The strip of analyticity of Mellin transform lies between $-c_1$ and $-c_2$

image processing and pattern recognition [131, 137, 138], voice coding [139, 140] etc.

**Existence of the Mellin transform:** It is relevant here to discuss the existence of the Mellin transform of a function, as given by Equation (3.76). Let $f(x)$ be a continuous function from 0 to $\infty$ such that

$$f(x) = \begin{cases} O(x^{c_1}) & x \to 0 \\ O(x^{c_2}) & x \to \infty, \end{cases} \tag{3.78}$$

where $O(.)$ is *Landau symbol* [129] denoting asymptotic[1] value. The Mellin transform exists for any complex number $z$ in the the region $-c_1 < Re(z) < -c_2$, which is referred to as the *strip of analyticity* of the Mellin transform of $f(x)$ and denoted by $(-c_1, -c_2)$ [118, 129].

Examples: Let $f(x) = \frac{1}{1+x}$. Then, from Equation (3.78), the asymptotic values of $f(x)$ are:

$$\begin{aligned} \frac{1}{1+x} &= O(x^0), x \to 0, \\ \frac{1}{1+x} &= O(x^{-1}), x \to \infty. \end{aligned} \tag{3.79}$$

Thus, the strip of analyticity of the Mellin transform of $f(x)$ is $(0, 1)$. Similarly, for the function $e^{-x}$, the strip of analyticity is (0,$\infty$). A simpler way of perceiving the concept is that the strip of analyticity corresponds to the range of values of $z$ for which the Mellin transform of the function exists. For example, the Mellin transform of $f(x) = \frac{1}{1+x}$ is $\frac{\pi}{\sin \pi z}$ [124], which is valid in the range $(0, 1)$. Similarly, the Mellin transform of $f(x) = e^{-x}$ is $\Gamma(z)$, which is valid in the range $(0, \infty)$. The concept of strip of analyticity is depicted in Figure 3.19.

**Inverse Mellin transform:** Having expressed the condition of existence of the Mellin transform, let us

[1]We say that $f(x) = O\big(g(x)\big)$ as $x \to x_0$, if there is a constant C such that $|f(x)| \leq C|g(x)|$ for $x$ very close to $x_0$ [129]. The value of the constant C depends upon how close to $x_0$ we wish the bound to hold.

discuss how a function can be recovered from its Mellin transform. If the Mellin transform exists and is continuous in the strip of analyticity discussed above, then the inverse Mellin transform is defined as [118, 121]

$$f(x) = \frac{1}{2\pi i}\int_{c-i\infty}^{c+i\infty} x^{-z}\mathcal{M}[f(x), z]dz, \tag{3.80}$$

where $i = \sqrt{-1}$ and the integration is along any line parallel to the imaginary axis and lying within the strip of analyticity [121].

**Relationship with other Integral Transforms:** It is readily evident that Mellin transform is related to the two other more popular types of integral transforms, namely the Laplace and the Fourier transforms. For example, if we replace $x = e^t$ in Equation (3.76), we get

$$\begin{aligned}\mathcal{M}[f(x = e^t), z] &= \int_0^{\infty} e^{t(z-1)} f(e^t) d(e^t) \\ &= \int_{-\infty}^{\infty} e^{tz} f(t) dt,\end{aligned} \tag{3.81}$$

which is evidently the double-sided Laplace transform of the $f(t)$. We conclude that the Mellin transform of $f(e^x)$ can be viewed as the Laplace transform of the $x$. Similarly, by making a replacement $x = e^{jw}$ in Equation (3.76), it can be shown that a similar relationship exists between the Mellin transform and the Fourier transform, i.e. the Mellin transform of $f(e^x)$ is the Fourier transform of the $x$. Note that the Fourier transform is a special case of Laplace transform. Conversely, the Fourier transform of $f(\ln x)$ is in fact the Mellin transform of $x$.

Note that in [43, 56, 64], in order to derive the PDF of the PC output, the researchers have employed the CFs and used natural logarithm to convert the product into sum of random variables. Now since, the CF is akin to the Fourier transform of a random variable, we emphasize that the Mellin transform allows us to use the same approach as that employed in [43, 56, 64], but in a more convenient manner. We elaborate this point further by supposing that $C$ is a random variable that is a product of two random variables $A$ and $B$. We can transform the operation of multiplication into addition by taking the natural logarithm. Thus, we have

$$\ln(C) = \ln(A) + \ln(B). \tag{3.82}$$

We know that the CF of the sum of two variables is the product of the CFs of the two variables [34]. Thus,

$$E[\ln(C)] = E[\ln(A)]E[\ln(B)] \tag{3.83}$$

where $E[.]$ denotes the CF. Using the results of Equation (3.81), we may express Equation (3.83) in terms of the Mellin transforms as

$$\mathcal{M}[C] = \mathcal{M}[A]\mathcal{M}[B], \tag{3.84}$$

which means that the Mellin transform of the product of the random variables equals the product of their Mellin transforms. The same principle can be extended to a product of any number of random variables.

In [121], it has been shown that the PDF of product of random gamma, beta and gaussian variables can be expressed in the form of Fox's $H$-function, or in the form of Meijer's $G$-function which is a special case of $H$ function. In [59,61], the PDF of the PC output is also expressed both in terms of Fox's $H$-function and Meijer's $G$-function. This observation and the fact that the Mellin transform of the product of independent random variables is equal to the product of the Mellin transform of the random variables suggests that Mellin transform is also closely related to $H$ and $G$ functions. In fact, our approach in this chapter demonstrates that, for the sake of determining the PDF of the PC output, use of the Mellin transform is a much simpler technique than that involving $H$ and $G$ functions [59, 61].

## 3.B APPENDIX: Derivation of CDF of $Z_m$

In this appendix, we derive the CDF of $Z_m$ outlined in Equation (3.43). Based on our analysis considered in Section 3.3.1, we note that $\Gamma^L(z+1)$ in Equation (3.43) has poles at $z=-j$, for $j=1,2,\ldots$. Moreover, the single pole at $z=0$ contributed by the term $1/z$ falls outside the path of the integration as seen in Figure 3.19. Let $\mathcal{V}_{m1}(z)=\Gamma^L(z+1)(z+j)^L=z^L\Gamma^L(z)(z+j)^L$. Then, following the procedure used to derive Equation (3.27), we have

$$\mathcal{V}_{m1}(z)=\frac{\Gamma^L(z+j+1)}{\prod_{k=1}^{j-1}(z+j-k)^L}. \tag{3.85}$$

and from Equation (3.29), we have

$$\begin{aligned}\mathcal{V}_{m1}(z)|_{(z=-j)} &= z^L\Gamma^L(z)(z+j)^L|_{(z=-j)}\\ &= (-j)^L\frac{(-1)^{jL}}{(j!)^L}=\frac{(-1)^{L(j+1)}}{[(j-1)!]^L}.\end{aligned} \tag{3.86}$$

Furthermore, let

$$\mathcal{V}_m(z)=\frac{1}{z}\Gamma^L(z+1)(z+j)^L=\frac{\mathcal{V}_{m1}(z)}{z}. \tag{3.87}$$

By using Leibnitz' rule [1] in the context of Equation (3.87), the $r$th derivative of $\mathcal{V}_m(z)$ can be expressed as

$$\begin{aligned}\mathcal{V}_m^{(r)}(z) &= \sum_{t=0}^{r}\binom{r}{t}\mathcal{V}_{m1}^{(t)}(z)\frac{d^{r-t}}{dz^{r-t}}\left[\frac{1}{z}\right]\\ &= \sum_{t=0}^{r}\binom{r}{t}\mathcal{V}_{m1}^{(t)}(z)\frac{(-1)^{r-t}(r-t)!}{(z)^{r-t+1}},\end{aligned} \tag{3.88}$$

which, when evaluated at $z = -j$, yields

$$\mathcal{V}_m^{(r)}(z)|_{(z=-j)} = -\sum_{t=0}^{r} \binom{r}{t} \mathcal{V}_{m1}^{(t)}(z)|_{(z=-j)} \frac{(r-t)!}{(j)^{r-t+1}}. \tag{3.89}$$

In Equation (3.88), the $t$th derivative of $\mathcal{V}_{m1}(z)$ can be expressed from Equation (3.85), using Leibnitz' rule and the technique employed in deriving Equation (3.34), as

$$\begin{aligned} \mathcal{V}_{m1}^{(t)}(z) &= L\Bigg\{ \sum_{u=0}^{t-1} \binom{t-1}{u} \mathcal{V}_{m1}^{(u)}(z)(-1)^{t-u}(t-1-u)! \sum_{k=0}^{\infty} \Big[ \frac{1}{(z+j+1+k)^{t-u}} \Big] \\ &- \sum_{u=0}^{t-1} \binom{t-1}{u} \mathcal{V}_{m1}^{(u)}(z) \sum_{k=1}^{j-1} \frac{(-1)^{t-u-1}}{(z+j-k)^{t-u}} \Bigg\}, \end{aligned} \tag{3.90}$$

which yields

$$\begin{aligned} \mathcal{V}_{m1}^{(t)}(z)|_{(z=-j)} &= L\Bigg\{ \sum_{u=0}^{t-1} \binom{t-1}{u} \mathcal{V}_{m1}^{(u)}(z)|_{(z=-j)}(-1)^{t-u}(t-1-u)! \sum_{k=0}^{\infty} \Big[ \frac{1}{(1+k)^{t-u}} \Big] \\ &+ \sum_{u=0}^{t-1} \binom{t-1}{u} \mathcal{V}_{m1}^{(u)}(z)|_{(z=-j)} \sum_{k=1}^{j-1} \frac{1}{(k)^{t-u}} \Bigg\}. \end{aligned} \tag{3.91}$$

Finally, if we write $\mathcal{U}_m(z) = y_0^{-z}$, we have

$$\mathcal{U}_m^{(r)}(z)|_{(z=-j)} = [-\ln(y_0)]^r y_0^j. \tag{3.92}$$

Hence, we can express Equation (3.43) as

$$F_{Z_m}(y_0) = -\frac{1}{(L-1)!} \sum_{j=1}^{\infty} \sum_{r=0}^{L-1} \binom{L-1}{r} \mathcal{U}_m^{(r)}(z)|_{(z=-j)} \mathcal{V}_m^{(L-1-r)}(z)|_{(z=-j)}, \tag{3.93}$$

where $\mathcal{V}_m^{(r)}(z)|_{(z=-j)}$ can be obtained from Equation (3.89) and $\mathcal{U}_m^{(r)}(z)|_{(z=-j)}$ can be obtained from Equation (3.92).

Chapter 4

# Single User- and Multi-User Detection in FFH Systems

Having investigated the performance of FFH-MFSK under various jamming conditions in Chapters 1 to 3, we now turn our attention to its ability to support multiple users. Specifically, we investigate its performance when employed in cellular applications. FFH based code division multiple access (CDMA) offers an attractive alternative to the direct sequence (DS) CDMA philosophy [18, 21, 22, 49, 91, 141]. Various researchers have shown that FFH aided CDMA exhibits advantages over DS-CDMA in terms of the relative immunity to near-far problem and ease of chip level synchronization [29, 91, 141]. The BER performance of a single user in a multiple access (MA) system is dependent upon the system's capability to suppress the interference imposed by other users [91, 141]. The better this interference suppression capability, the larger the number of users the system is capable of supporting. From the perspective of interference suppression, the choice of an appropriate diversity combining scheme is an important consideration in the design of a noncoherent FFH assisted MFSK receiver [98, 142]. In this chapter, we investigate a number of diversity combining schemes discussed in Chapter 1 and some interference-suppression techniques for employment in FFH-MA systems.

## 4.1 Introduction

The system under consideration is a land mobile communication system that supports multiple users through a base-station (BS). We study the use of the considered combining schemes in the uplink only, i.e. the mobile user to the BS scenario. In the uplink scenario, from the viewpoint of one particular user's reception, the signals transmitted by all other users are treated as narrowband interferences. Narrowband interference imposed by other users is the main source of performance degradation in FFH-MA systems [143], because as we have discussed in Section 1.3.3.2, an interference tone is likely to cause detection error whenever its frequency coincides with any of the non-signal tones. If all users share the same number $M$ of FH tones, the

probability of an interference tone hitting one of the non-signal tones is $(M - 1/M)$, which is quite high. Additionally, owing to the mobility of the users and multipath effects which are characteristics of an urban cellular communication scenario, the signals transmitted by the transmitters experience fading [34]. For the uplink, the signals transmitted by various users follow independent paths and the channel can be modelled in a way that all users' signals can be assumed to undergo independent fading.

The receiver in the BS consists of a bank of conventional FFH noncoherent MFSK receivers, one receiver for each mobile user. Two strategies of detection can be adopted in the BS receiver. One strategy assumes that each receiver acts in a stand-alone fashion and makes independent detection. This type of detection scheme is referred to as *Single User Detection* (SUD) [91, 142]. However, the BS receiver has knowledge of the frequency hopping addresses of all users. When this knowledge is exploited and all receivers make joint detection, the process is often referred to as *Joint Detection* or *Multi-user Detection* (MUD) [93, 143, 144]. The SUD is applicable to ad hoc networks as well, besides cellular applications, whereas the MUD may only be applied in cellular systems or in networks supported by BSs. We will consider both types of detection separately in this chapter.

This chapter is structured as follows. The FFH-MA system employing hard-limiting majority vote combining (HLMV), which is the conventional combining scheme [93], will be discussed in detail in Section 4.2. The employment of various combining schemes for SUD will be treated in Section 4.3. Specifically, linear [35], self-normalization [37], HLMV [93, 94], soft limiter [142], product and order statistics-normalized envelope detection based diversity combining schemes [44] are considered. A brief discussion on each of these combining schemes has been included in Section 1.4. The comparison of various diversity combining schemes is based on the achievable BER versus the number of simultaneous users supported. It is shown in Section 4.3.1 using simulation results that although some of the combining schemes considered result in an inferior performance compared to the optimum soft limiting combiner, they offer the advantage of achieving an acceptable interference suppression performance without requiring side information. In Section 4.4, we consider various methods of MUD that may be employed by the BS receiver. After briefly reviewing the more popular MUD schemes proposed in the published literature, in Section 4.4.1 we propose two new MUD schemes which are based on successive interference cancellation and employ both the clipped and product combining schemes of Section 1.4. The performance of the proposed MUD scheme is discussed using a comparison with Fiebig's scheme [141] with the aid of simulation results in Section 4.4.3. Finally, we present our conclusions in Section 4.5.

## 4.2 System Description

In this section we briefly describe a MA system employing FFH-MFSK. The system under consideration is a land mobile communication system consisting of a single cell serving multiple mobile users with the aid of a single BS, as considered in [48]. All the users communicate with each other through the BS, with the

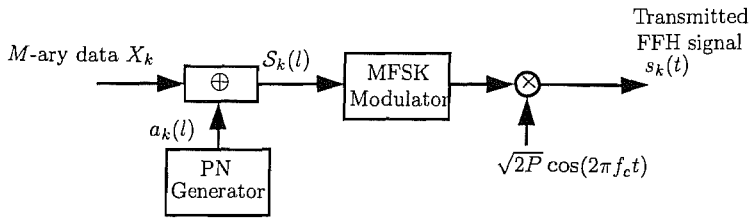


**Figure 4.1:** Transmitter schematic of the FFH-MA system using MFSK modulation

aid of FFH-MFSK signals.

The schematic of a FFH-MFSK transmitter is shown in Figure 4.1. As discussed in Section 1.3, in an FFH system, each symbol is transmitted using $L$ chips or hops, where $L > 1$. The hop or chip interval $T_h$ is related to the symbol interval $T_s$ by the relation $T_h = T_s/L$. Hence, if the data is transmitted at a rate of $R_b$ bits per second and $R_s$ is the symbol rate, then the hop rate is given by $R_h = R_s L = R_b L/b$, where $b = \log_2 M$ is the number of bits per symbol. In a FFH-MA system, the $k$th user, $k = 1, 2, \ldots, N_U$, $N_U$ being the total number of users sharing the system bandwidth, is assigned a unique and random $L$-tuple address denoted by $\mathbf{a_k} = [a_k(0), a_k(1), \ldots, a_k(L-1)]$ output by the PN generator, where $a_k(l) \in$ GF(M), $l = 0, 1, \ldots, L-1$, and GF(M) represents a Galois field of $M$ number of elements. The frequency $f_k(l)$ of the hopped signal for the $k$th user in the $l$th hop may assume any one of the $M$ legitimate values and is chosen by output of the operation given by [91]

$$\mathcal{S}_k = [\mathcal{S}_k(0), \mathcal{S}_k(1), \ldots, \mathcal{S}_k(L-1)] = X_k.\mathbf{1} \oplus \mathbf{a_k}, \tag{4.1}$$

where $\mathbf{1}$ denotes a unit vector of length $L$, $X_k$ is the $M$-ary symbol to be transmitted by the $k$th user and $\oplus$ denotes addition in the GF. Note that we have $X_k, a_k(l), \mathcal{S}_k(l) \in GF(M)$. The components of $\mathcal{S}_k$ are passed to an MFSK modulator, where an MFSK tone is chosen for transmission determined by the value of $\mathcal{S}_k(l)$ during the $l$th hop of duration $T_h$. The MFSK modulated signal is transmitted after modulating a carrier of frequency $f_c$. The transmitted signal for the $k$th user during the $l$th hop can be expressed as

$$s_k(t) = \sqrt{2P}\cos\left\{2\pi\left[f_c + f_k(l)\right]t + \theta_k(t)\right\}, \quad (l-1)T_h \leq t \leq lT_h, \tag{4.2}$$

where $P$ is the transmitted power and $\theta_k(t)$ is the phase introduced by the MFSK modulation and frequency hopping.

We assume that the bandwidth occupied by the signal transmitted during each FFH chip interval is approximated by that of its main spectral lobe occupying $R_h = 1/T_h$. The frequency separation between adjacent frequency hopping tones is also assumed to be $R_h$. Thus, the orthogonality of the FFH frequencies is maintained. Hence, if $W_{ss}$ is the spread spectrum bandwidth which consists of $M$ tones of $R_h$ bandwidth each, we have

$$M = \frac{W_{ss}}{R_h} = \frac{W_{ss} b}{R_b L}. \tag{4.3}$$

Furthermore the spectral efficiency, which is a measure of the bit rate supported by the MA system per unit bandwidth, of the system under consideration is given by [141]

$$\eta = \frac{N_U R_b}{W_{ss}} = \frac{N_U b R_h / L}{M R_h} = \frac{N_U b}{ML}, \tag{4.4}$$

where $R_b$ is the transmission rate in bits/second supported by the FFH-MA system for each user.

Note that the transmitter depicted in Figure 4.1 is different from that shown in Figure 1.1. The transmitter shown in Figure 4.1 is characterised by a spread spectrum bandwidth $W_{ss}$ consisting of $M$ tones only which are shared by all the users. By contrast, the system shown in Figure 1.1 would result in up to $L$ separate bands of $M$ FSK tones each, since as seen in Equation (1.2), the transmitted FFH signal corresponding to the system of Figure 1.1 has a frequency given by $f_m + f_l, m = 0, 1, \ldots, M-1, l = 0, 1, \ldots, L-1$. Since, bandwidth efficiency is of prime importance in MA systems, the system of Figure 4.1, which was proposed in [91, 93] for MA applications, is preferred over the one shown in Figure 1.1.

Note that the user addresses generated by Equation (4.1) may either be random or optimum [93, 143], where the latter implies that during $L$ hops, a specific user's signalling tone coincides with that of another user in only one FSK frequency. This results in less interference than that inflicted when random address scheme is used. Fiebig [141] has shown that there is negligible difference between the performance achievable using random and optimum address schemes, provided that sufficiently large values of $M$ and $N_U$ are used. In this chapter, we assume having random address schemes, and also replace additions in the GF with modulo-$M$ addition for ease of analysis.

The channel may be modeled by any of the classic fading models such as Rayleigh, Rician or Nakagami-$m$ for each of the transmitted frequencies. We opt for Nakagami-$m$ model since it fits a wide range of practical channel conditions. We assume that the frequency separation between the adjacent signalling frequencies is higher than the coherence bandwidth of the channel and thus, each signalling tone experiences independent fading. Moreover, the fading envelopes experienced by the various users are also independent of each other.

When a particular user transmits a signal to the BS, the signals transmitted by all the other $(N_U - 1)$ users can be modeled as continuous-wave interfering tones. We assume a chip-synchronous system, where the chip transitions of all users are aligned. This may be achieved by the transmissions of periodic clock alignment signals from the BS to all users [97]. Furthermore, perfect power control is assumed such that the power of all the signals received by the BS from all users is equal. Thus, the signal $r_k(t)$ for the $k$th user received at the BS can be modeled as

$$r_k(t) = h_s s_k(t - \tau) + \sum_{j=1}^{N'_U} h_j I_j(t) + n(t), \tag{4.5}$$

where $s_k(t)$ is the transmitted signal as expressed in Equation (4.2), $\tau$ is the propagation delay, $I_j(t)$ denotes

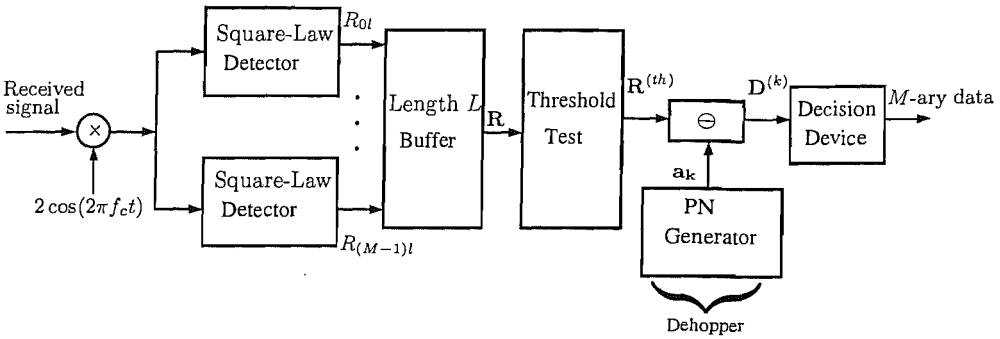


**Figure 4.2:** Receiver schematic of the FFH-MFSK system using HLMV combining, for the $k$th user, $k = 1, 2, \ldots, N_U$. Bandpass filters (BPFs) have not been shown.

the interference signal transmitted by the $j$th interferer and $N'_U \leq N_U - 1$ is the number of active interferers. Furthermore, $h_s = \alpha_s e^{i\theta_s}$ and $h_j = \alpha_j e^{i\theta_j}$ are the channel gains, $\alpha_s$ and $\alpha_j$ are the fading envelopes and $\theta_s$ and $\theta_j$ are the corresponding phases. Finally, in Equation (4.5), $n(t)$ is the AWGN of one-sided power spectral density $N_0$. Note that for our subsequent investigations, we assume that all the users are simultaneously active and thus we have $N'_U = N_U - 1$.

**HLMV Combining:** Next we discuss the conventional FFH-MFSK receiver employing HLMV combining which has been traditionally employed in FFH-MFSK receivers operating in MA channels [91, 93, 94]. The schematic of the receiver corresponding to the transmitter of Figure 4.1 is shown in Figure 4.2, which is slightly different form that shown in Figure 1.2, since in Figure 4.2 the dehopping process follows the noncoherent MFSK detection. In the recever, the carrier frequency is removed, and the signal is detected by a conventional non-coherent MFSK demodulator consisting of a bank of $M$ square-law detectors, which was detailed in Section 1.3.3. The output of the square-law detector in Figure 4.2 is the energy present in the corresponding tone during the particular hop of duration $T_h$. At the end of a symbol period of duration $T_s$, the outputs of the $M$ square-law detectors can be represented by a time-frequency (T-F) matrix $\mathbf{R}$ of $(M \times L)$ number of statistics, as seen in Figure 4.2. More explicitly, the element $R_{ml}$ of this matrix represents the output of the $m$th detector during the $l$th hop.

In a conventional HLMV combining based FFH receiver [93], each element of the matrix $\mathbf{R}$ is compared with a preset threshold. If the energy detector output exceeds that threshold, a logical 1 is assigned to the corresponding element; else, a logical 0 is assigned. Thus, as seen in Figure 4.2, we create another matrix $\mathbf{R}^{(th)}$ of logical 1s and 0s, whose elements are defined by

$$R_{ml}^{(th)} = \begin{cases} 1 & R_{ml} \geq \delta \\ 0 & \text{otherwise,} \end{cases} \qquad m = 0, 1, \ldots M-1; l = 0, 1, \ldots L-1, \tag{4.6}$$

where $\delta$ is a pre-set detection threshold. We have used the superscript *(th)* in the term $\mathbf{R}^{(th)}$ to indicate that this matrix is obtained by threshold test of $\mathbf{R}$, as indicated in Figure 4.2.

Next, dehopping is performed using Modulo-$M$ subtraction, as shown in Figure 4.2, such that we have

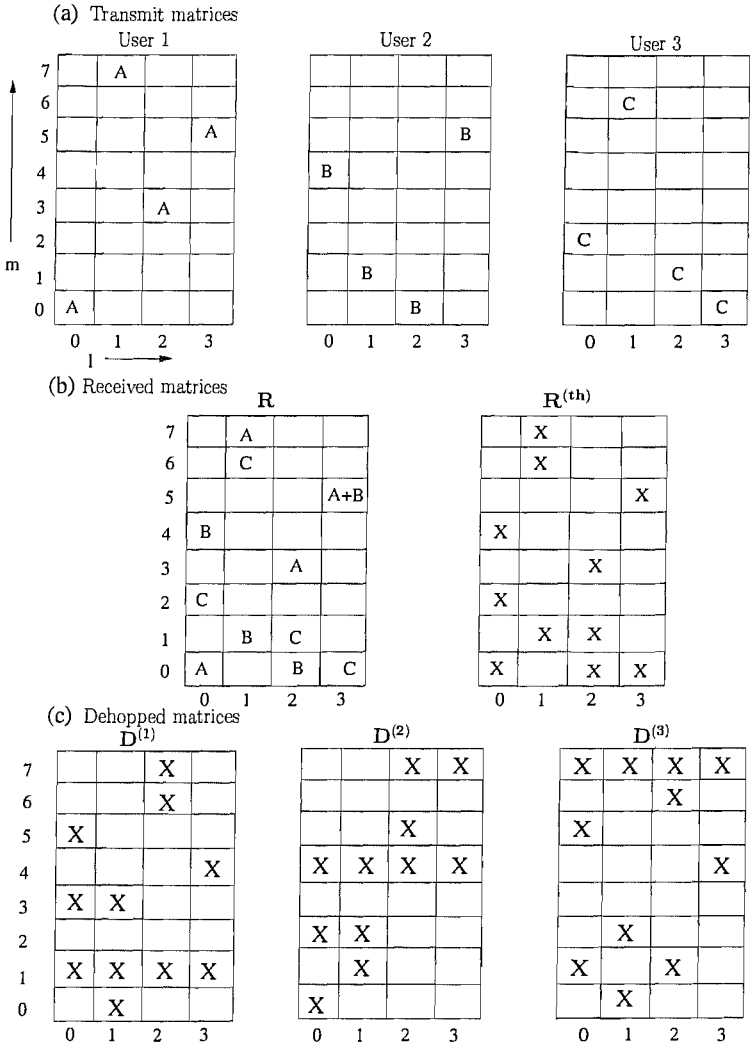


**Figure 4.3:** An example of FFH-MFSK detection using HLMV combining. (a) Transmit T-F matrices of the three users. The 8-ary symbols transmitted by the three users are denoted by the letters A, B and C, respectively. (b) Received matrix $\mathbf{R}$ at the energy detectors' output and the thresholded matrix $\mathbf{R}^{(th)}$. In $\mathbf{R}^{(th)}$, a logical 1 inserted as a result of the threshold test defined in Equation (4.6) is denoted by an X. (c) Dehopped T-F matrices $\mathbf{D}^{(k)}, k = 1, 2, 3$ of the three users.

a de-hopped matrix $\mathbf{D}^{(k)}$ for the $k$th user, whose elements are given by

$$D_{nl}^{(k)} = R_{ml}^{(th)}, \text{given } n = m \ominus a_k(l), \qquad m, n = 0, 1, \ldots, M-1; l = 0, 1, \ldots, L-1. \tag{4.7}$$

The decision device shown in Figure 4.2 selects the specific row having the highest number of entries of logical 1 in $\mathbf{D}^{(k)}$. The corresponding symbol, i.e. the index of the row with the highest number of non-zero entries is deemed to be the transmitted symbol. The scheme above described is often termed as *majority vote* combining, which was also discussed in Section 1.4. Furthermore, since we applied a threshold test as expressed in Equation (4.6), we refer to this combining scheme as the *hard limiting majority vote* (HLMV) combining. In the event when more than one rows have the largest number of non-zero entries, a decision ambiguity results and one of the candidate rows has to be chosen at random [91].

The demodulation operation described above can be understood with the aid of Figure 4.3, which shows

an 8-ary FFH-MFSK system, associated with $L = 4$ and $N_U = 3$. In this figure, we consider an example in the context of which the three users, denoted by A, B and C, are assumed to transmit symbols 1, 4 and 7 respectively and have the user addresses of [7,6,2,4], [0,5,4,1] and [3,7,1,2], respectively. Thus the hopping pattern of the first user A can be determined by using Equation (4.1) and is given by

$$\begin{aligned} \mathcal{S}_1 &= X_1.\mathbf{1} \oplus \mathbf{a_1} \\ &= [1,1,1,1] \oplus [7,6,2,4] = [0,7,3,5]. \end{aligned} \tag{4.8}$$

Similarly, the hopping patterns for the users B and C are given by $[4,4,4,4] \oplus [0,5,4,1] = [4,1,0,5]$ and $[7,7,7,7] \oplus [3,7,1,2] = [2,6,1,0]$, respectively. As explained above, the hopping patterns of the three users are mapped to frequency tones given by $f_m, m = 0,1,\ldots,M-1$. The resulting transmit matrices for the three users are shown in Figure 4.3(a), where a tone transmitted by each user is indicated by the corresponding alphabet. As shown in Figure 4.3(a), the hopping pattern [0,7,3,5] of user A translates into the tones $[f_0, f_7, f_3, f_5]$ to be transmitted in the four hops. Similarly, the frequency patterns for the users B and C during the current symbol interval are $[f_4, f_1, f_0, f_5]$ and $[f_2, f_6, f_1, f_0]$, respectively.

Figure 4.3(b) shows the corresponding received matrix $\mathbf{R}$, which represents the outputs of the energy detector, and the thresholded matrix $\mathbf{R}^{(th)}$ of Figure 4.2. In the absence of noise and fading, as seen in Figure 4.3(b), the received matrix $\mathbf{R}$ is seen to be merely a superposition of the transmit matrices of Figure 4.3(a). In such a idealistic channel, $\delta = 0$ may be chosen as the detection threshold seen in Equation (4.6). Consequently, in the matrix $\mathbf{R}^{(th)}$ of Figure 4.3, an X in the $(m,l)$-th element indicates the presence of a logical 1 corresponding to that tone, while a blank element indicates a logical 0.

The three matrices $\mathbf{D}^{(k)}, k = 1,2,3$ obtained by dehopping the $\mathbf{R}^{(th)}$ of Figure 4.3(b), using each user's address, as expressed in Equation (4.7), are shown in Figure 4.3(c). We can see in Figure 4.3(c) that in each user's dehopped matrix, a complete row appears corresponding to the transmitted symbol. Thus, since user A transmitted symbol 1, row 1 has an X in each element in $\mathbf{D}^{(1)}$. Similarly, row number 4 in $\mathbf{D}^{(2)}$ and row number 7 in $\mathbf{D}^{(3)}$ are complete. By contrast, where an X appears in other elements of all the dehopped matrices, as seen in Figure 4.3(c), they can be identified as induced by interferences because they do not constitute a full row. Hence, the decision device seen in Figure 4.2 can readily select the correct symbols in the considered example by selecting the indices of the complete rows of the dehopped matrices.

In such idealistic channels as considered above, the only source of error is the interference imposed by other users. When the number of simultaneous users is high, spurious entries may arise and they might contribute towards creation of a full row. In case of communication through both fading- and noise-contaminated channels, suitable value of $\delta$ has to be chosen that minimizes the probability of both false alarm (an incorrect detection when no signal is present) and deletions (missed detections). In such cases, there is non-zero probability that none of the rows becomes complete. We explain the phenomena of false alarms and deletions using Figure 4.4, in which the same example as considered in Figure 4.3 is assumed but now with the additional assumption that the channel is contaminated by noise and fading. In Figure 4.4 (a),

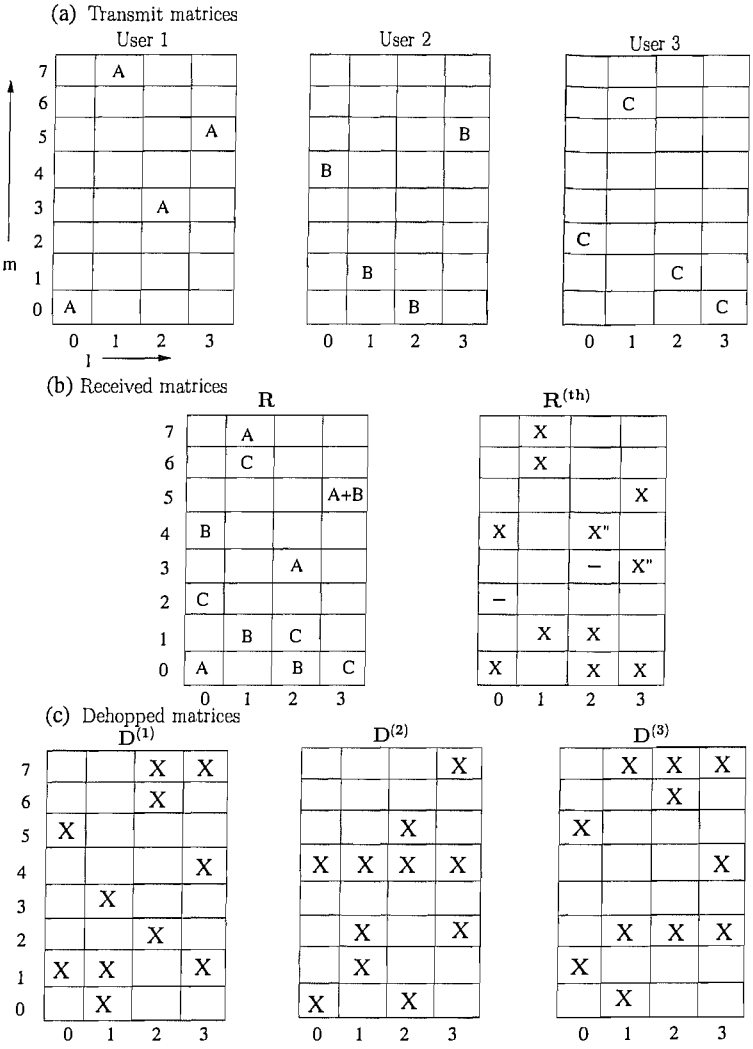


**Figure 4.4:** An example of FFH-MFSK detection using HLMV combining operating in noise-contaminated and fading conditions. The same system is assumed as in Figure 4.3, apart from two deletions, denoted by '-' and two false alarms, denoted by X", in the thresholded matrix $\mathbf{R}^{(th)}$ as seen in (b). Consequently, the dehopped matrices in sub-figure (c) are different from those in Figure 4.3(c).

the transmit matrices and the received matrix $\mathbf{R}$ are same as in Figure 4.3 (a). However, the elements of $\mathbf{R}$ in Figure 4.4 represent the outputs of the energy detector which may consist of AWGN in addition to the energy transmitted by various users. Additionally, AWGN is present in all tones represented by the empty elements of $\mathbf{R}$ of Figure 4.4(b). Moreover, note that $\mathbf{R}^{(th)}$ seen in Figure 4.4(b) is different from the corresponding matrix in Figure 4.3(b). Let us assume that, for the threshold test to be performed on $\mathbf{R}$, as defined in Equation (4.6), we choose a specific value of the threshold such that two deletions occur, one corresponding to the element $m = 2, l = 0$ and the other corresponding to $m = 3, l = 2$ of $\mathbf{R}^{(th)}$. In Figure 4.4(b), the deletions are represented by the symbol '-'. To elaborate on this point further, we have assumed that the signals transmitted corresponding to the elements of $m = 2, l = 0$ and $m = 3, l = 2$ suffered so much fading that they do not exceed the preset threshold and are consequently discarded, as governed by Equation (4.6). Similarly, we also assume that two false alarms occur in the tones corresponding to the elements $m = 4, l = 2$ and $m = 3, l = 3$ in $\mathbf{R}^{(th)}$ of Figure 4.4(b), where the symbol X" indicates a logical 1 resulting from a false alarm. Evidently, a false alarm may be a result of the noise level exceeding

the preset threshold. Now, when the matrix $\mathbf{R}^{(th)}$ of Figure 4.4(b) is dehopped by the three users we obtain the matrices $\mathbf{D}^{(k)}, k = 1, 2, 3$ shown in Figure 4.4(c). We can see that these matrices are different from the corresponding dehopped matrices shown in Figure 4.3(c), as a consequence of the assumed false alarms and deletions. However, as seen in Figure 4.4(c), the row corresponding to the symbol transmitted by user B is unaffected. By contrast, the row corresponding to the symbol transmitted by user A, i.e. the row indexed 1 in $\mathbf{D}^{(1)}$ of Figure 4.4(c), is not complete but still has the largest number of entries in $\mathbf{D}^{(1)}$. Thus, despite the presence of noise and fading, the receiver corresponding to user A will be able to make the correct decision. This is an advantage offered by the diversity, since the probability that all hops of a symbol experience false allarms or deletions is typically low. However, we observe that in $\mathbf{D}^{(3)}$ of Figure 4.4(c), two rows, i.e. rows number 2 and 7, have three entries each, whereas the actual transmitted symbol is 7. Thus, the decision device in the receiver corresponding to user C is faced with an ambiguity, which may result in an error with a probability of 0.5 for the current symbol, since two rows have the highest number of entries. Therefore, we have shown using the example depicted in Figure 4.4 that noise and fading may result in incorrect detection in the FFH-MA HLMV receiver in MA channel.

The problem with HLMV combining is that it discards useful information by mapping the received signal to logical 1s and 0s, as seen in Equation (4.6). In Section 4.3.1, we will analyze the BER performance of this scheme along with that of some other diversity combining schemes, and we will show how AWGN, fading and MA interference adversely affect the attainable system performance. We will also show that the product combining, order statistics-normalized envelope detection and the soft limiting combining schemes constitute better options than the HLMV system described above, when communication in channels corrupted by the above contaminations is considered.

## 4.3 SUD Using Various Diversity Combining Schemes

In the previous section, we have described the principles of the FFH-MA system using conventional HLMV based detection [91]. In this section, we investigate the performance of the FFH-MA system employing a range of diversity combining schemes. In the open literature, only a few combining schemes have been considered for use in FFH-MA systems. Specifically, based on the maximum likelihood criterion, Yue [48] has derived an optimum combining scheme and approximated it with a soft limiting combiner (SLC) . This combiner operates on the principle of clipping the outputs of the energy detectors, if they exceed a preset threshold, before performing linear combining. This clipped combining scheme is the same as that discussed in the context of a single user scenario in Section 1.4. In [48, 142] Yue showed that the SLC outperforms both the HLMV and the linear combining schemes. However, adapting the clipping thresholds at the energy detectors' output according to the SNR is required for the sake of clipping at the most suitable level and thus transmission of side information is required in the FFH-MFSK receiver employing a SLC. In [97, 145], the optimum SLC derived in [48] has been analyzed under Rician fading conditions and it has been shown that even without setting accurate clipping thresholds, the achievable performance gain is substantial.

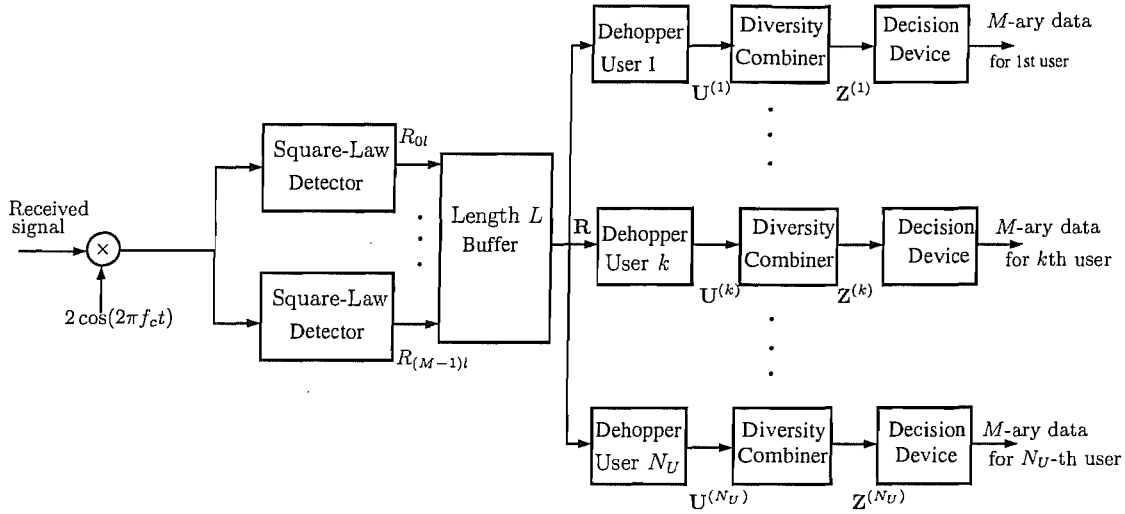


**Figure 4.5:** Schematic of the BS receiver employing single user FFH-MFSK detection for $N_U$ users. BPFs have not been shown.

In [98], the employment of various diversity combining schemes that do not require side information has been considered in a MA scenario. However, an explicit comparison of the schemes considered with the classic hard limiting [91] or the bench-mark SLC [48] was not included in their contribution. In this section, the achievable performance of various diversity combining schemes that may be used in FFH-MFSK systems for combatting the MA interference is investigated based on simulation results. Specifically, the HLMV [91], the SLC [48], the self-normalization (also known as NED) [98], the product combining receiver (PCR) [44] and the order statistics-normalized envelope detection (OS-NED) [98] based diversity combining schemes are considered. All these schemes were discussed in Section 1.4 in terms of their anti-jamming capability. Now we investigate their ability to combat MA interference.

One of the most important performance parameters in the analysis of MA systems is the number of simultaneous users supported, since this determines the achievable spectral efficiency of the system as defined in Equation (4.4). Thus, our metric for the comparison of the diversity combiners is the BER achieved, when a given number of users is supported. A Nakagami-$m$ fading channel is assumed, which is a realistic and flexible model of the mobile radio channel.

Before discussing the proposed schemes, we briefly explain the principle of SUD using Figure 4.5, where a schematic of the FFH-MFSK MUD receiver employed in the BS is shown. As seen in Figure 4.5, the energy detection stage is common for all users. After this stage, the received signal, captured in the form of a matrix $\mathbf{R}$, is passed in parallel to a bank of $N_U$ receivers each comprising of a de-hopper, a diversity combiner and a decision device. The dehopper consists of a PN sequence and a modulo-$M$ subtractor, as shown in detail in Figure 4.6. Note that all receivers differ from each other in only the PN addresses, which is unique for each user. Moreover the final detection decision is made separately by each receiver without exchange of any information among them.

Now, consider the receiver schematic shown in Figure 4.6 for the noncoherent FFH-MFSK system em-

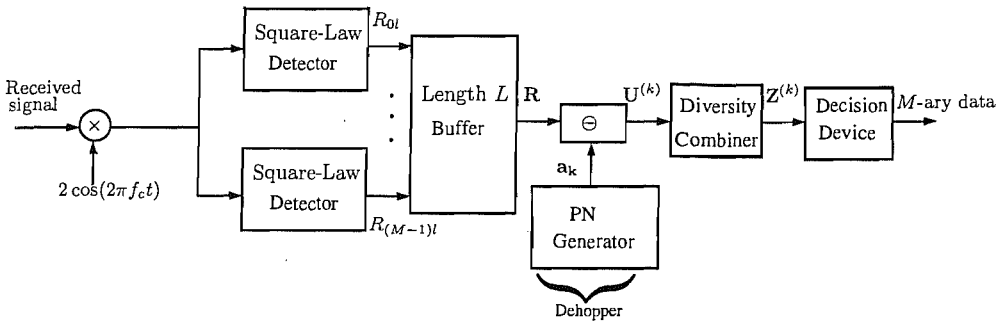


**Figure 4.6:** Receiver schematic of the FFH-MFSK system, using one of the many possible diversity combining schemes, for the $k$th user, $k = 1, 2, \ldots, N_U$. BPFs have not been shown.

ploying any of the diversity combining schemes considered, other than the HLMV. Comparing this system with that shown in Figure 4.2, we observe that in Figure 4.6 the threshold test is not applied to the received matrix $\mathbf{R}$. Thus, in the context of HLMV, as shown in Figure 4.2, the dehopping is performed on the matrix $\mathbf{R}^{(th)}$ and the decision is made on the matrix $\mathbf{D}^{(k)}$, where the elements of both these matrices are logical 1 or 0. By contrast, as shown in Figure. 4.6, the dehopping is performed on the matrix $\mathbf{R}$ whose elements consist of the energy detected by the square-law detectors. Additionally, we have a diversity combiner before the decision device seen in Figure 4.6. Thus the HLMV combining is now replaced by one of the diversity combining schemes that we consider in this section. In the context of the diversity combining schemes that we consider, the de-hopped matrix $\mathbf{U}^{(k)}$ is related to the received matrix $\mathbf{R}$ by

$$U_{nl}^{(k)} = R_{ml}, \text{given } n = m \ominus a_k(l), \qquad m, n = 0, 1, \ldots, M-1; l = 0, 1, \ldots, L-1. \tag{4.9}$$

Furthermore, in the context of the diversity combining schemes considered, at the output of the diversity combiner of Figure. 4.6, we have a vector $\mathbf{Z}^{(k)} = [Z_0, Z_1, \ldots, Z_{M-1}]$ of length $M$ for the $k$th user. The element $Z_m^{(k)}$ of this vector represents the output of the diversity combiner and the decision statistic corresponding to the $m$th tone, where $m = 0, 1, \ldots, M-1$. The decision device in Figure. 4.6 chooses the largest of the $\mathbf{Z}^{(k)}$ and maps it to a corresponding value in $0, \ldots, M-1$, which represents the estimate of the $M$-ary symbol transmitted by user $k$. The decision variable $Z_m$, generated in the context of single user scenario, when various diversity combining schemes are employed has already been discussed in Section 1.4. The same methodology applies in the present MA scenario.

### 4.3.1 Simulation Results of Various Diversity Combining Schemes

In this section we discuss the achievable performance of various diversity combining schemes, when the FFH-MFSK system operates in a MA scenario and is subjected to Nakagami-$m$ fading. It is customary to fix the hopping bandwidth $W_{ss}$ to the data rate $R_b$ ratio $W_{ss}/R_b$ and optimize the remaining parameters, i.e. $M$ and $L$, in order to achieve the best possible BER and $\eta$ [98, 141]. We assume having $W_{ss}/R_b = 128$ for all subsequent investigations, unless otherwise stated. As an example, for a single user, the corresponding

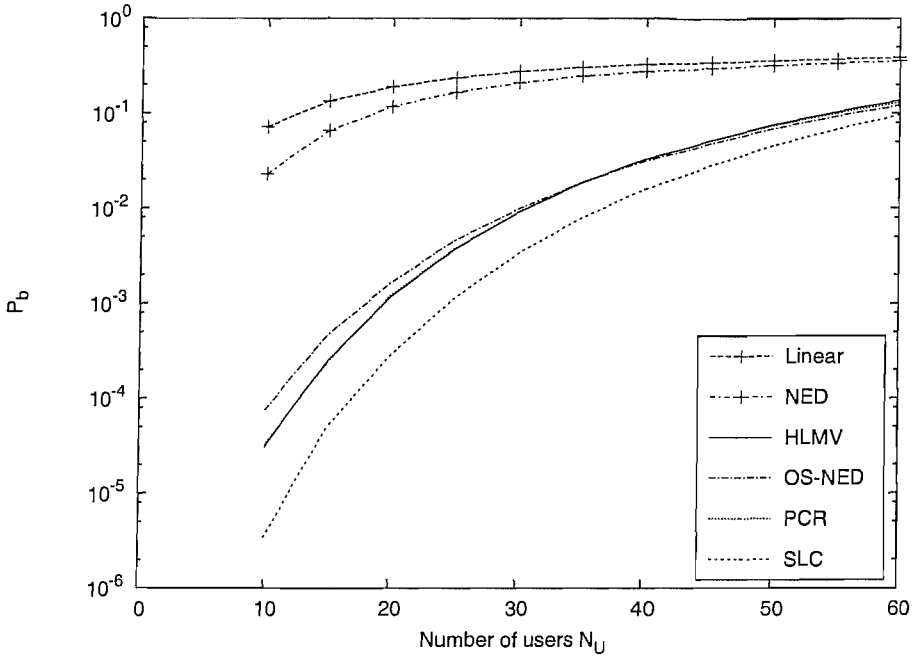


**Figure 4.7:** The BER $P_b$ versus number of users performance for various diversity combining schemes when employed in a FFH-MFSK system communicating over a Nakagami-$m$ fading MA channel, assuming $E_b/N_0 = 20$dB, $L = 12$, $M = 64$ and $m = 1$.

bandwidth efficiency given by Equation (4.4) is 1/128 bit/s/Hz, while for 128 users, $\eta = 1$bit/s/Hz would be achieved. Thus, for a fixed $W_{ss}/R_b$, the spectral efficiency of the system depends only on the number of users supported. From Equation (4.3), we have

$$L = \frac{W_{ss}}{R_b}\frac{b}{M}. \tag{4.10}$$

Since, the objective of this treatise is to compare the performance of various diversity combining schemes, we arbitrarily opt for having $M = 64$, which gives $L = 12$ for $W_{ss}/R_b = 128$.

In Figure 4.7, we have plotted the BER or the probability of bit error $P_b$ against the total number of users for the linear, the HLMV, the SLC , the NED, the PCR and the OS-NED based diversity combining schemes of Section 1.4. The results portrayed in this figure correspond to $m = 1$, which is equivalent to a Rayleigh fading channel, and $E_b/N_0 = 20$dB, where $E_b$ is the transmitted energy per bit. The results of Figure 4.7 show that the achievable performance of the linear combining scheme and the NED of Section 1.4 is poor, although when the number of users is low, for example when we have $N_U = 10$, their BER curves drop relatively sharply. Moreover, Figure 4.7 shows that the performance of the SLC is the best among the ones investigated, while the BER performance of the HLMV, the PCR and the OS-NED is similar to each other and inferior to that of the SLC.

In Figure 4.8, the BER performance of the SLC, the HLMV, the PCR and the OS-NED based combining schemes is shown for two more $E_b/N_0$ values, namely for 10 and 15 dB. It can be deduced from the results of Figures 4.7 and 4.8 that the HLMV scheme is more sensitive to the SNR than the other schemes considered.

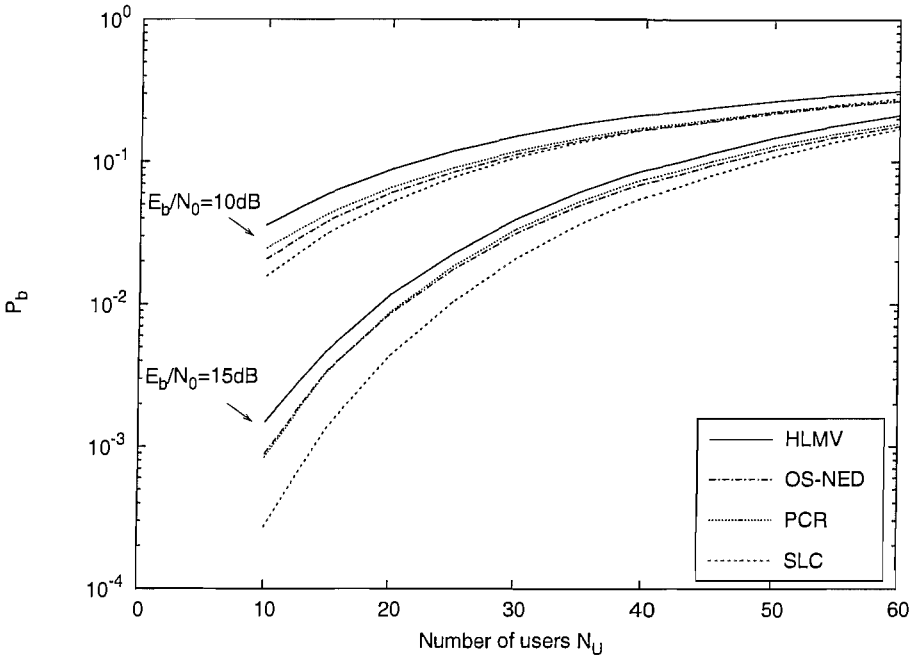


**Figure 4.8:** The BER $P_b$ versus number of users performance for various diversity combining schemes when employed in a FFH-MFSK system communicating over a Nakagami-$m$ fading MA channel, assuming $L = 12$, $M = 64$, $m = 1$ and $E_b/N_0$ as a parameter.

Thus, as seen in Figure 4.8, for $E_b/N_0 = 10$ and 15dB the performance of the HLMV is inferior to that of the PCR and the OS-NED, which is in contrast to the case when $E_b/N_0 = 20$ was assumed in Figure 4.7.

The results of Figure 4.9 show the effects of having different Nakagami fading parameters $m$ on the performance of the diversity combining schemes which were considered in Figure 4.8. As expected, the performance of all the schemes is inferior when $m = 1.5$ is assumed compared to that corresponding to $m = 10$. Furthermore, Figure 4.9 shows that the performance of the SLC is superior to those of the other schemes for both the $m$ values, while that of the OS-NED is the next best.

In Figure 4.10, the effects of increasing the diversity order on the performance of the SLC, the PCR and the OS-NED schemes are shown. With $M$ fixed at 64, an increase in $L$ results in a corresponding increase in the $W_{ss}/R_b$ ratio. Thus, we have $W_{ss}/R_b = 192$ and 256 for $L = 18$ and 24, respectively. As seen in Figure 4.10 for increasing values of $L$, the performance of all the schemes improves and, for all $L$ values, the SLC results in the best performance among the schemes shown.

In Figure 4.11, the effects of increased modulation order, which implies an increase in the number of hopping tones, on the performance of three schemes is shown. In conjunction with $L = 12$, an increase in $M$ results in a corresponding increase in the $W_{ss}/R_b$ ratio. Thus, we have $W_{ss}/R_b \approx 219$ and 384 for $M = 128$ and 256, respectively. As seen in Figure 4.11, for increasing values of $M$, the performance of all the schemes improves. This is primarily a benefit of a reduction in the probability of interference, when a high number of signalling tones is available. Note in Figure 4.11 that the SLC significantly benefits from having an increased $M$ value and its BER curve drops well below those of the other two schemes shown for

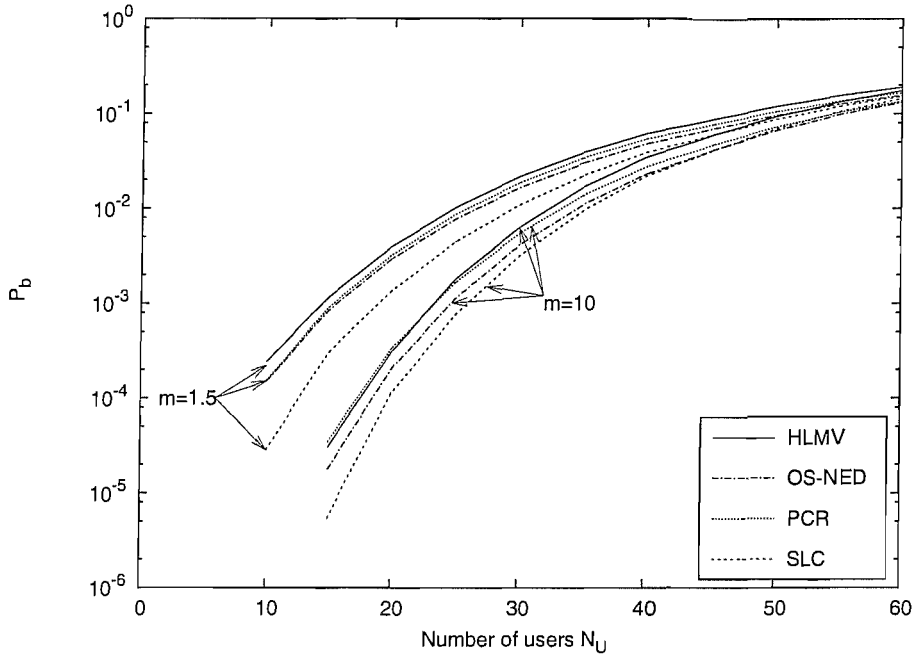


**Figure 4.9:** The BER $P_b$ versus number of users performance for various diversity combining schemes when employed in a FFH-MFSK system communicating over a Nakagami-$m$ fading MA channel, assuming $E_b/N_0 = 15$dB, $L = 12$, $M = 64$ and $m$ as a parameter.

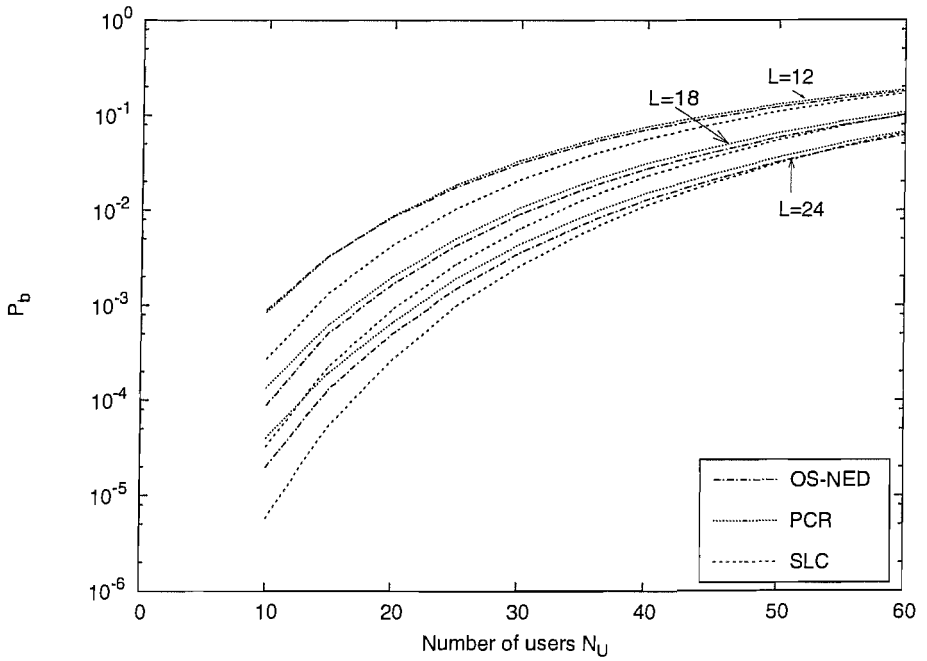


**Figure 4.10:** The BER $P_b$ versus number of users performance for various diversity combining schemes when employed in a FFH-MFSK system communicating over a Nakagami-$m$ fading MA channel, assuming $E_b/N_0 = 15$dB, $m = 1$, $M = 64$ and $L$ as a parameter.

a high number of users, for example when we have $N_U = 50$ and 60.

In Figure 4.12, the achievable BER corresponding to three different diversity combiners is plotted against the SNR for $N_U = 30$ users. The results of Figure 4.12 indicate the significance of using opti-

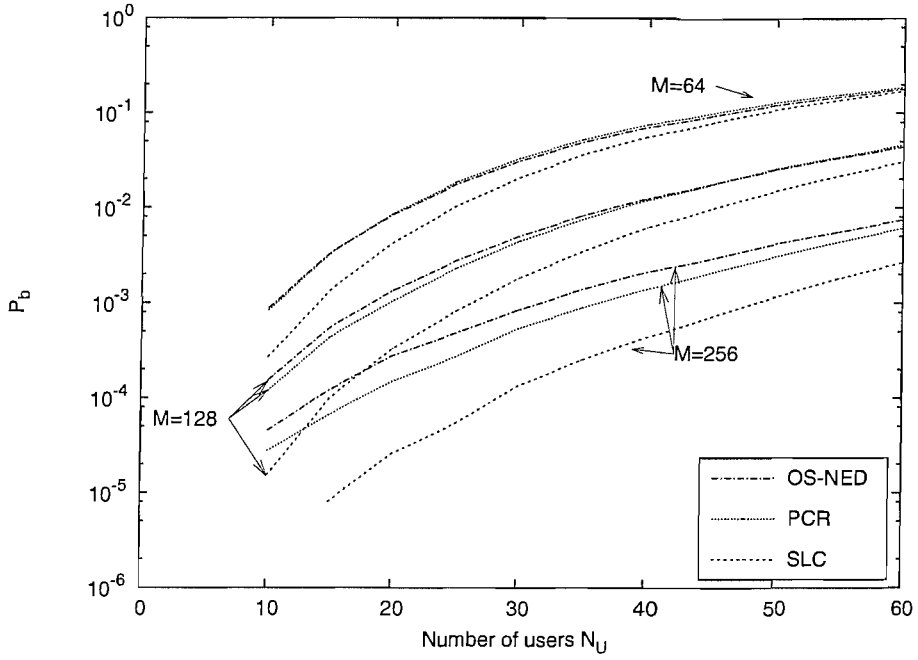


**Figure 4.11:** The BER $P_b$ versus number of users performance for various diversity combining schemes when employed in a FFH-MFSK system communicating over a Nakagami-$m$ fading MA channel, assuming $E_b/N_0 = 15$dB, $L = 12$, $m = 1$ and $M$ as a parameter.

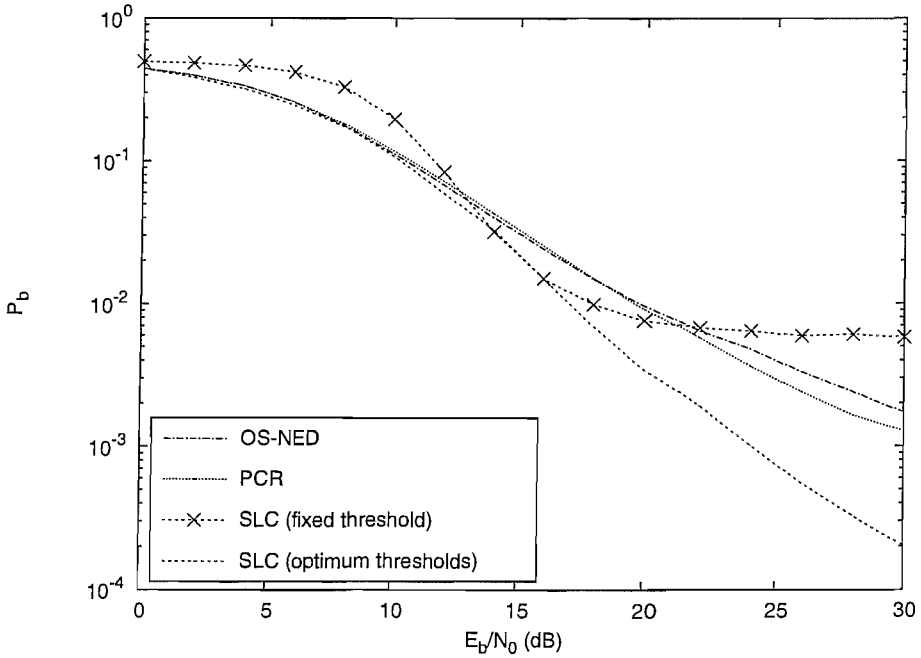


**Figure 4.12:** The BER $P_b$ versus $E_b/N_0$ performance for various diversity combining schemes when employed in a FFH-MFSK system communicating over a Nakagami-$m$ fading MA channel, assuming $N_U = 30$, $L = 12$, $M = 64$ and $m = 1$.

mum clipping thresholds in the context of the SLC. When a fixed threshold is employed in conjunction with the SLC for all SNR values, as seen in Figure 4.12, the performance of the SLC degrades so much that even the PCR and the OS-NED outperform it for $E_b/N_0$ values in excess of 22dB or less than 13dB.

## 4.4 MUD Employing Various Diversity Combining schemes

Having investigated a number of diversity combining schemes in the context of SUD in Section 4.3, in this section we focus our attention on joint detection or MUD techniques employed in the up-link of FFH-MA systems, i.e. in a mobile to the BS scenario. The conventional BS receiver system employs a separate receiver corresponding to each user, where each receiver is the same as that used in SUD, typically employing HLMV combining discussed in Section 4.2, although any other combining schemes, such as those discussed in Section 1.4 and Section 4.3, may be employed. By virtue of possessing the knowledge of all users' addresses, the BS receiver can be designed to carry out detection in multiple stages, cancelling the symbols detected in one stage from the detection process in the subsequent stages, thereby reducing the interference constituted by already detected symbols. This process of iterative interference cancellation is referred to as *successive interference cancellation* (SIC) [143].

Quite a few SIC techniques applicable to FFH-MA system employing HLMV based combining have been proposed in the published literature. Some of the more important ones of these contributions have been summarised in Table 4.1. Most of the SIC techniques proposed for FFH-MFSK employ HLMV combining. Therefore, the concepts discussed in Section 4.2 are relevant in the following discussion.

Timor [146, 147] proposed MUD methods based on interference cancellation exploiting the algebraic properties of the users' optimal addresses in a noise-free channel. Mabuchi *et. al* [148] proposed a BS receiver that may be termed as a maximum likelihood receiver. In the context of their proposed method, candidate received matrices are created from all symbols which, based on the number of entries in the corresponding row, can potentially be the correct symbols. All the candidate matrices are compared to the original received matrix and the specific candidate matrix that matches the original matrix in most number of entries is chosen as the correct one. This scheme, although promising in terms of its achievable performance, can be computationally demanding if either the number of users or the modulation order is high. Fiebig [143] proposed a more practical method of interference cancellation. This method consists of multiple SIC stages during each of which only the symbols having full unambiguous rows are selected for detection. In the following stages, the interference resulting from symbols that are thus successfully detected are erased. This scheme yields useful performance gains, although a specific drawback of this scheme is that the cancellation of interferences may result in erasures of undetected symbols also, if a cancelled symbol and an undetected symbol happen to invoke the same FSK tone. To circumvent this problem, Halford and Pearce [144] proposed a scheme that improved upon Fiebig's method [143]. They suggested exploiting the knowledge of the symbol energy to avoid cancelling those signals that resulted from *collisions* - a term describing the event in which two users transmit the same tone. This scheme results in a performance improvement over Fiebig's method [143]. However, the proposed scheme [144] was investigated in a non-fading channel only. Evidently, this scheme's efficacy is limited in fading channels, because under fading conditions, the received symbol energy cannot be determined sufficiently accurately. Fiebig [149] proposed another interference cancellation method which the author referred to as the *reduction*

*of candidate matrices* (REC) algorithm and which identifies interference signals from the desired signal by exploiting the knowledge of the addresses of all users. Fiebig [149] applied the REC method in an idealistic noise-and fading-free scenario (interference-only channel) and showed that, under these conditions, the method is near-optimum. Kozick and Sadler [150] modified the REC method and applied it to a Rayleigh fading channel for attaining useful performance gains.

A neural network based solution to this problem has also been proposed in [151], while Iltis *et. al.* proposed a least squares estimation based technique for interference rejection in FFH systems. However, the schemes proposed in these contributions [151,152] are basically SUD methods since they do not perform joint detection of all users. Some more contributions have been made in the area of MUD for FFH in [153–156], which are, however, variations of the schemes proposed in [143, 148, 149].

As mentioned above, most of the abovementioned MUD methods using SIC have been applied to HLMV based systems [143, 144, 146–150]. Motivated by the promising performance gains that some of the combining schemes yield compared to the HLMV combining, as seen in Section 4.3, here we propose two novel MUD methods, which employ clipped and product diversity combining schemes. These SIC schemes are based on the principle proposed by Fiebig's method [143], with appropriate adaptation according to the clipped and product diversity combining schemes.

### 4.4.1 Proposed SIC Schemes

In this section, we propose two MUD schemes employing product combining and clipped combining as well as SIC. Note that a MUD based receiver may also be represented by the schematic of Figure 4.5, although in the context of MUD there is information exchange between various receiver branches, as we will demonstrate in the proposed SIC-based MUD schemes.

In the context of the proposed SIC schemes, the detection process consists of multiple stages. In each stage, not all but the more reliable symbols are detected, as seen in Figure 4.13. To determine the reliability, we propose a test which is based on Viterbi's ratio threshold test (RTT) [106] and which will be explained in the forthcoming sections. After the more reliable symbols have been successfully demodulated at the

| Contribution | | | Researcher(s) | Year | References |
|---|---|---|---|---|---|
| Algorithm | Combining scheme | Channel | | | |
| Multistage decoding of FFH addresses | HLMV | Nonfading | Timor | 1980-81 | [146,147] |
| Maximum likelihood | HLMV | Nonfading | Mabuchi *et. al.* | 1995 | [148] |
| Multistage SIC | HLMV | Rayleigh | Fiebig | 1996 | [143] |
| REC scheme | HLMV | Nonfading | Fiebig | 1996 | [149] |
| Improvement of Fiebig's SIC scheme [143] | HLMV | Nonfading | Halford and Pearce | 2000 | [144] |
| Improvement of Fiebig's REC scheme [149] | HLMV | Rayleigh | Kozick and Sadler | 2000 | [150] |

**Table 4.1:** Summary of important contributions of various researchers towards investigation of MUD in FFH-MFSK systems

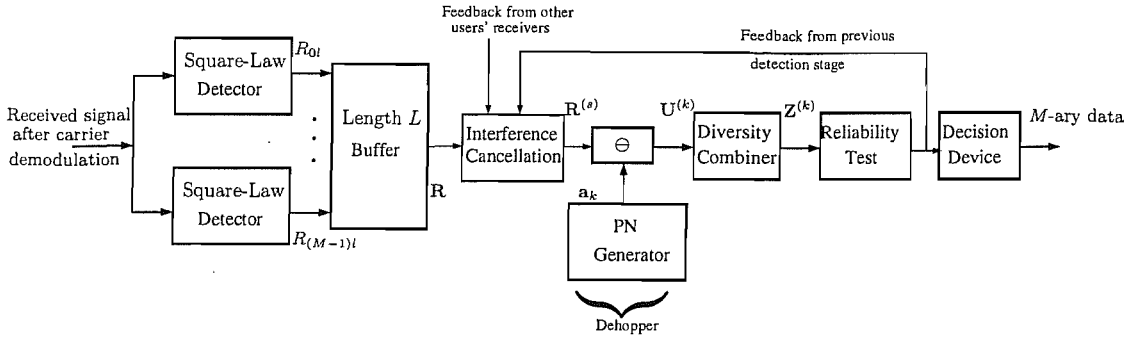


**Figure 4.13:** Schematic of the FFH-MFSK receiver of the $k$th user $k = 1, 2, \ldots, N_U$, employing SIC in the context of MUD in a BS receiver. BPFs have not been shown.

end of one stage, the received time frequency matrix $\mathbf{R}$, shown in Figure 4.13, is modified by erasing the signal contributions of the already detected symbols. Therefore, due to these erasures, in the next stage of detection, number of interferences are reduced, allowing more confident demodulation of the hitherto undetected symbols. Although, the proposed SIC schemes may lead to potential cancellation of undetected symbols, we will show that they result in useful performance gains and outperform the HLMV based system employing Fiebig's method [143], which we will refer to in the foregoing discussions as the Fiebig's scheme. Moreover, in Section 4.4.2, we propose a method of modifying the proposed SIC schemes in order to circumvent the problem of inadvertent cancellations.

In the subsequent sections, we highlight the methods employed in the proposed schemes and then analyze their performance with the aid of simulation results. Each method consists of a conventional detection (CD) stage and multiple SIC stages. It has been assumed in our subsequent discussions that all transmitted signals experience independent frequency-flat Nakagami-$m$ fading. All the other assumptions made in Sections 4.2 and 4.3 hold in the subsequent analysis.

#### 4.4.1.1 Clipped Combining Aided SIC

The first proposed scheme, which we refer to as the SLC-SIC arrangement, employs clipped diversity combining or SLC and is discussed below with the aid of Figures 4.13 and 4.14, where an example of interference cancellation is shown. The values assumed in this example are the same as those assumed in Figure 4.3. The basic algorithm used in the SLC-SIC scheme is also depicted in the form of a flowchart in Figure 4.15.

1) In the received $(M \times L)$-dimensional matrix $\mathbf{R}$ at the output of the energy detectors, seen in Figure 4.13, the element $R_{ml}$, $m = 0, 1, \ldots, M-1, L = 0, 1, \ldots, L-1$ represents superposition of the signal energy transmitted by up to $N_U$ users and the AWGN received in the $m$th tone during the $l$th hop. The received signals are separately dehopped by each receiver using the corresponding unique address, as defined in Equation (4.9), resulting in the matrix $\mathbf{U}^{(k)}$ for the $k$th user. The dehopped matrices are shown in Figure 4.14(b).

2) Clipped combining is performed on the dehopped signals, resulting in $M$ decision variables, for each

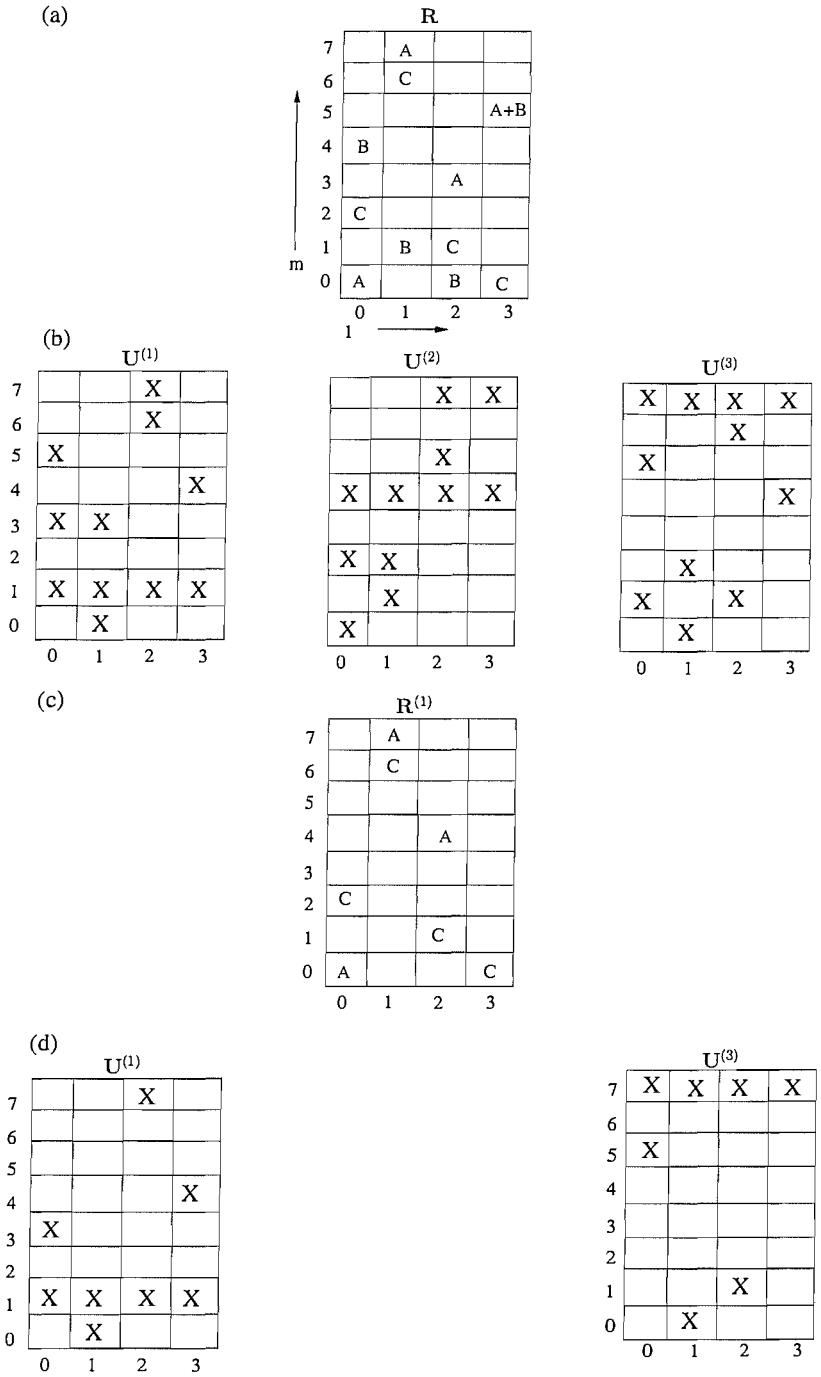


**Figure 4.14:** An example of interference cancellation in the proposed SIC schemes. The same system is assumed as in Figure 4.3. Blank elements of all the matrices indicate the presence of AWGN only. (a) Received $M \times L$ matrix $\mathbf{R}$. The symbols transmitted by the three users, generated using Equation (4.1), are denoted by the letters A, B and C, respectively. (b) Three de-hopped matrices $\mathbf{U}^{(k)}$ $k = 1, 2, 3$ corresponding to the three users, generated using Equation (4.9). An X in an element denotes the presence of transmitted signal in the corresponding tone and hop. (c) Modified received matrix $\mathbf{R}^{(1)}$, generated using Equation (4.18), after cancellation of all entries owing to symbol 4 of user B, which is assumed to have been successfully detected after diversity combining and RTT. (d) Dehopped matrices of users A and C generated by invoking Equation (4.9) on $\mathbf{R}^{(1)}$.

of the user. The process of clipping can be expressed as a function $f()$ performed on $\mathbf{U}^{(k)}$ such

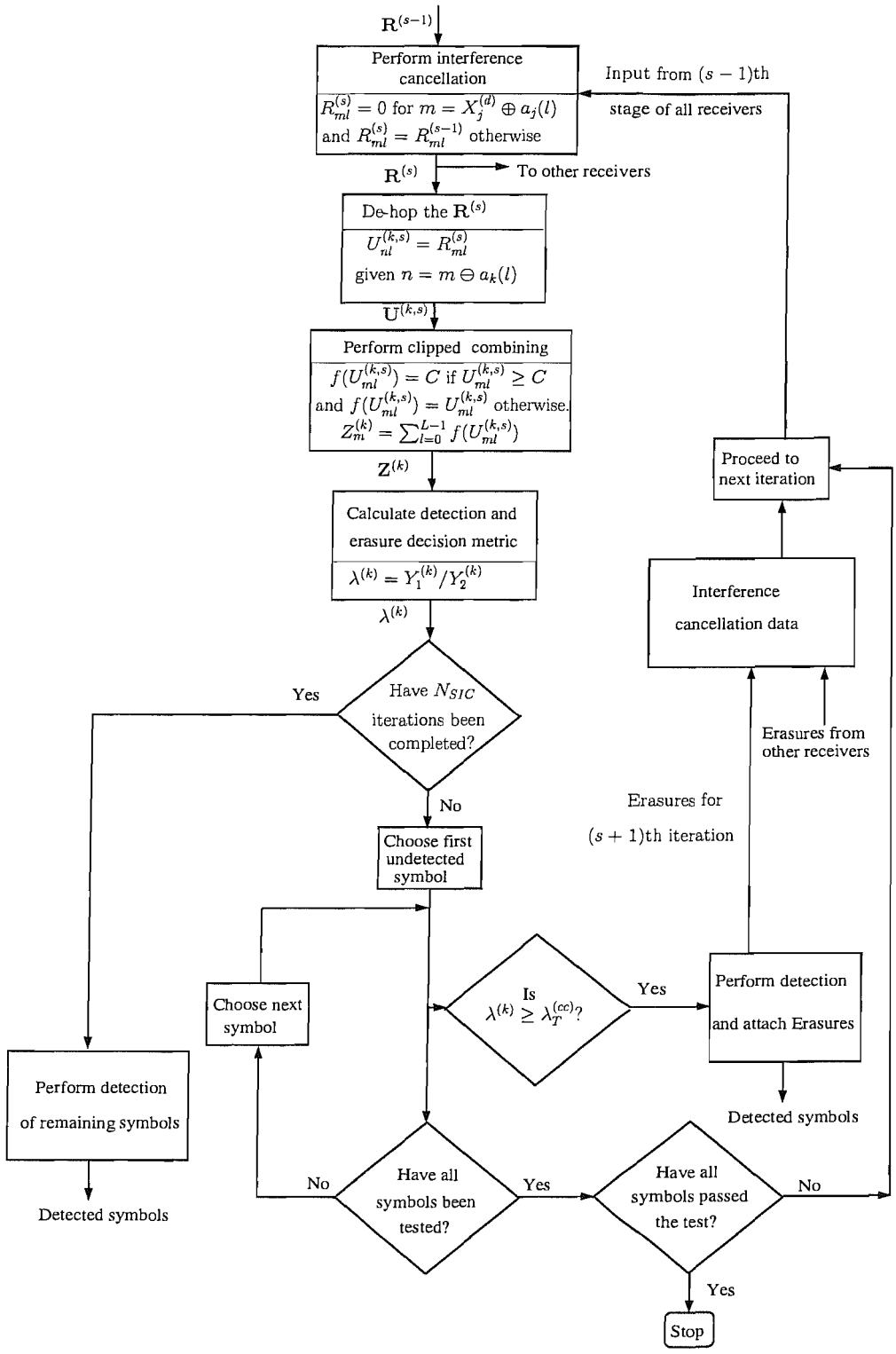


**Figure 4.15:** Flowchart of the algorithm invoked in the SLC-SIC scheme, proposed in Section 4.4.1.1 in the context of the $k$th receiver

that [48]

$$f(U_{ml}^{(k)}) = \begin{cases} C & \text{for } U_{ml}^{(k)} \geq C \\ U_{ml}^{(k)} & \text{otherwise,} \end{cases} \qquad m = 0, 1, ...M-1, l = 0, 1, ...L-1 \tag{4.11}$$

where $C$ represents an appropriately chosen clipping threshold. The decision variable for the $k$th user is given by

$$Z_m^{(k)} = \sum_{l=0}^{L-1} f(U_{ml}^{(k)}), \qquad m = 0, 1, ...M-1. \tag{4.12}$$

3) To determine the reliability of the detected symbols, the following test is performed for each of the users. Let $Y_1^{(k)}$ be the largest and $Y_2^{(k)}$ be the second largest of all the $M$ decision variables $\mathbf{Z}^{(k)}$ corresponding to the $k$th user. Thus, if we use $\max[.]$ to denote the largest and $\max 2[.]$ to denote the second largest, we have

$$Y_1^{(k)} = \max[Z_0^{(k)}, Z_1^{(k)}, \ldots, Z_{M-1}^{(k)}] \tag{4.13}$$

and

$$Y_2^{(k)} = \max 2[Z_0^{(k)}, Z_1^{(k)}, \ldots, Z_{M-1}^{(k)}]. \tag{4.14}$$

Next, we define the ratio of the largest to the second largest of the $M$ decision variables as

$$\lambda^{(k)} = \frac{Y_1^{(k)}}{Y_2^{(k)}}, \tag{4.15}$$

which should be as high as possible for the sake of reliable decision. Now, if we have

$$\lambda^{(k)} \geq \lambda_T^{(cc)}, \tag{4.16}$$

where $\lambda_T^{(cc)}$ is an appropriately chosen threshold in the context of the clipped combining, then we establish that the symbol is reliable. This statistic is based on the RTT [106] which is a reasonable measure of whether a symbol is reliable or not. The reliable symbols are demodulated using the conventional maximum likelihood principle. That is, if the $j$th user's symbol, $j = 1, 2, \ldots, N_U$ satisfies the above mentioned RTT, then $X_j^{(d)}$ is the estimate of the $j$th user's symbol, where $X_j^{(d)}$ is the index of $\max[\mathbf{Z}^{(j)}]$, and $m, X_j^{(d)} = 0, 1, \ldots, M-1$. If a user's symbol fails to meet the RTT, we assume that it has been corrupted by fading, interference or both and hence cannot be reliably detected. Therefore its detection is deferred till later stages. If all users' symbols pass the test, the detection process for the considered symbol is complete. On the other hand, if no user passes the test, we choose only the $p$th user's symbol for demodulation and subsequent erasure, such that

$$\lambda^{(p)} = \max[\lambda^{(1)}, \lambda^{(2)}, \ldots, \lambda^{(N_U)}], \qquad p = 1, 2, ...N_U. \tag{4.17}$$

4) If some but not all symbols are reliably detected, proceed with the $s$th stage of SIC, where $s = 1, 2, \ldots$ and we use $s = 0$ to indicate the CD stage. We also define $\mathbf{R}^{(s)}$ as the modified form of $\mathbf{R}$ at the $s$th stage. By this definition, we have $\mathbf{R} = \mathbf{R}^{(0)}$. The $s$th stage, $s \geq 1$, consists of the following steps:

(a) In the $s$th stage, the matrix $\mathbf{R}^{(s-1)}$ is modified by cancelling the signals which correspond to all

the symbols that were reliably detected in Step 3. Specifically, if $X_{k(d)}$ is the detected symbol of the $k$th user, then, after the interference cancellation operation, we have

$$R_{ml}^{(s)} = \begin{cases} 0 & \text{for } m = X_{k(d)} \oplus a_k(l) \\ R_{ml}^{(s-1)} & \text{otherwise,} \qquad m = 0,1,...M-1, l = 0,1,...L-1. \end{cases} \tag{4.18}$$

(b) Repeat step 1 for the $\mathbf{R}^{(s)}$ matrix for all users whose symbols have not been detected so far. Specifically, the dehopped matrices in the $s$th SIC stage, which we denote by $\mathbf{U}^{(k,s)}$, are obtained using $\mathbf{R}^{(s)}$ and can be expressed for the $k$th user as

$$\begin{aligned} U_{nl}^{(k,s)} &= R_{ml}^{(s)}, \text{given } n = m \ominus a_k(l), \qquad m,n = 0,1,\ldots,M-1; \\ &\quad l = 0,1,\ldots,L-1; k = 1,2,\ldots,N_U - N_U^{(d)}, \end{aligned} \tag{4.19}$$

where $N_U^{(d)}$ denotes the number of users whose symbols have already been detected in the previous stages.

(c) Repeat step 2 for $\mathbf{U}^{(k,s)}$, where $k = 1,2,\ldots,N_U - N_U^{(d)}$. Specifically, perform clipped diversity combining defined by the following equations:

$$\begin{aligned} f(U_{ml}^{(k,s)}) &= \begin{cases} C & \text{for } U_{ml}^{(k,s)} \geq C \\ U_{ml}^{(k,s)} & \text{otherwise,} \end{cases} \\ &\quad m = 0,1,...M-1; l = 0,1,...L-1; \\ &\quad k = 1,2,\ldots,N_U - N_U^{(d)}. \end{aligned} \tag{4.20}$$

The decision variable of the $k$th user is given by

$$Z_m^{(k)} = \sum_{l=0}^{L-1} f(U_{ml}^{(k,s)}), \qquad m = 0,1,...M-1, k = 1,2,\ldots,N_U - N_U^{(d)}. \tag{4.21}$$

Note that the values of the decision variable vector $\mathbf{Z}^{(k)}$ of $k$th user in the $s$th SIC stage replace its values in the $(s-1)$th stage.

(d) Repeat step 3 for $\mathbf{Z}^{(k)}$, where $k = 1,2,\ldots,N_U - N_U^{(d)}$ by computing $\lambda^{(k)}$ as defined in Equation (4.15) and performing the RTT given by Equation (4.16). Thus, for the $s$th SIC stage, the symbols to be demodulated and erased for subsequent stages are decided, as outlined in step 3 above.

The SIC operations, consisting of Steps 4(a) to (d), can be continued until all users' symbols meet the RTT condition or, until a pre-defined number of stages $N_{SIC}$ have been completed. In the latter case, all remaining symbols in the last stage are detected in the conventional manner, without carrying out the RTT. In Figure 4.14, we assume that symbol 4 of user B satisfies the RTT and is hence demodulated and erased from the matrix $\mathbf{R}$ to obtain a modified matrix $\mathbf{R}^{(1)}$ shown in Figure 4.14(c).

Note in Figure 4.14(a) and (c) that by erasure of symbol B, one of the entries of user A is also erased in $\mathbf{R}^{(1)}$.

In summary, the idea behind this scheme is to demodulate only those symbols, which are considered reliable, and then erase the transmissions resulting from the demodulated symbols for subsequent stages of detection. The advantage of this scheme is that erasures of reliable symbols lead to reduced interference for those symbols that are detected in subsequent SIC stages. However, a disadvantage of this scheme is that erasures may also result in removal of undetected symbols, if they happen to coincide with the detected symbols, as seen in Figure 4.14(a) and (c). Consequently, such inadvertent erasures can result in propagation of decision error. As will be shown in Section 4.4.3, the overall benefit of using this SIC scheme is improved BER. Moreover, in Section 4.4.2, we will illustrate a method of circumventing this problem to a considerable extent, which aids in further improving the BER performance.

#### 4.4.1.2 Product and Clipped Combining Aided SIC

The second SIC scheme that we propose employs both the product combining and clipped diversity combining schemes discussed in Section 1.4. Specifically, in the CD stage, product combining is employed, while in the subsequent stages of SIC, clipped diversity combining is used. Except for the product combining invoked in the CD stage, this scheme is identical to the SLC-SIC scheme proposed in Section 4.4.1.1. This difference between the two SIC schemes can be observed by comparing the flowcharts in the Figure 4.15 for the SLC-SIC scheme and Figure 4.16 for this scheme, which we refer to as the PC-SLC-SIC arrangement. Note that Figure 4.14 also applies to this scheme. The detection process invoked in the context of the PC-SLC-SIC scheme consists of the following steps:

1) Again, the detection process commences by setting up the received time-frequency ($M \times L$) matrix $\mathbf{R}$ shown in Figure 4.13. The received signals represented by $\mathbf{R}$ are dehopped by each receiver separately using the unique address corresponding to a particular user, resulting in the matrix $\mathbf{U}^{(k)}$ for the $k$th user, which is defined in Equation (4.9).

2) Product combining is performed on the dehopped signals of each user, resulting in the vector $\mathbf{Z}^{(k)}$ of $M$ decision variables for the $k$th user during a symbol duration. Specifically, the decision variable generated in the context of product combining for the $k$th user is given by [44]

$$Z_m^{(k)} = \prod_{l=0}^{L-1} U_{ml}^{(k)}, \qquad m = 0, 1, \ldots, M-1. \tag{4.22}$$

3) Next, the RTT is performed on the $M$ decision variables $\mathbf{Z}^{(k)}$ by computing $\lambda^{(k)}$ for the $k$th user as outlined in Equation (4.15). Then, if the condition of

$$\lambda^{(k)} \geq \lambda_T^{(pc)} \tag{4.23}$$

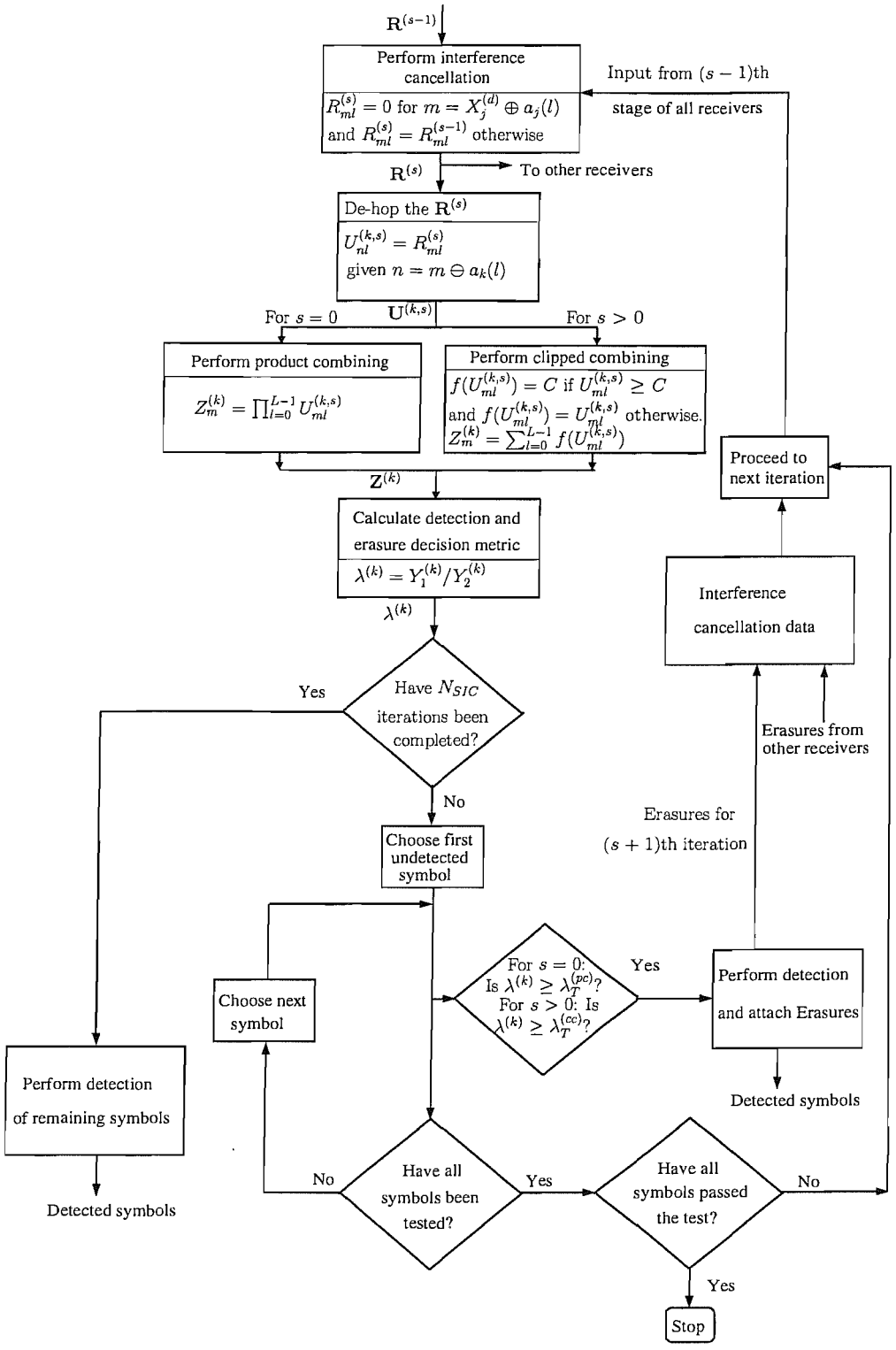


**Figure 4.16:** Flowchart of the algorithm invoked in the PC-SLC-SIC scheme, proposed in Section 4.4.1.2, in the context of the $k$th receiver

is satisfied, where $\lambda_T^{(pc)}$ is an appropriately chosen threshold for the product combining scheme, then it is concluded that the user's symbol is reliable, which is demodulated in the conventional maximum likelihood rule discussed in Section 4.4.1.1. If all users pass the RTT, the detection process for that symbol is complete. If a user's symbol fails the RTT, its detection is delayed until later SIC stages. If

no user passes the RTT, we choose only that particular user's symbol for demodulation which has the maximum value of $\lambda^{(k)}$ for all $k = 1, 2, \ldots, N_U$, as shown in Equation (4.17).

4) If some but not all symbols are reliably detected, proceed with the $s$th stage of SIC, where $s = 1, 2, \ldots$ and $s = 0$ refers to the CD stage. Moreover, we define $\mathbf{R}^{(s)}$ as the modified form of $\mathbf{R}$ in the $s$th stage. Therefore, we have $\mathbf{R} = \mathbf{R}^{(0)}$. The $s$th SIC stage, $s \geq 1$, consists of the following steps:

   (a) The matrix $\mathbf{R}^{(s-1)}$ is modified by cancelling the signals that correspond to all the symbols that were reliably detected in the previous stage. Specifically, if $X_{k(d)}$ is a detected symbol at the end of the $(s-1)$th SIC stage, then the interference contributed by $X_{k(d)}$ is removed by using the scheme described by Equation (4.18) to obtain $\mathbf{R}^{(s)}$.

   (b) The matrix $\mathbf{R}^{(s)}$ is dehopped as defined in Equation (4.19) to obtain $\mathbf{U}^{(k,s)}$, where $k = 1, 2, \ldots, N_U - N_U^{(d)}$ matrices, and $N_U^{(d)}$ is the number of users whose symbols have already been detected.

   (c) Clipped combining is performed on $\mathbf{U}^{(k,s)}$, $k = 1, 2, \ldots, N_U - N_U^{(d)}$, as defined by Equations (4.20) and (4.21).

   (d) RTT is carried out on the decision variables $Z_m^{(k)}$, $m = 0, 1, \ldots, M-1$ obtained in the $s$th SIC stage for all the $(N_U - N_U^{(d)})$ users, by computing $\lambda^{(k)}$ as explained in step 3 above. Specifically, if $\lambda^{(k)} \geq \lambda_T^{(cc)}$, where $\lambda_T^{(cc)}$ is an appropriately chosen threshold for the clipped combining scheme, then it is decided that the user's symbol is reliable and is demodulated in the conventional manner, as explained in step 3 above. If a user's symbol fails to meet the RTT, its detection is deferred until later SIC stages. If all users pass the test, the detection process for that symbol is complete. If no user passes the RTT, we choose only that user's symbol, which has the maximum value of $\lambda^{(k)}$ for all $k = 1, 2, \ldots, N_U - N_U^{(d)}$ for demodulation and subsequent erasure, as defined in Equation (4.17).

   As in the case of SLC-SIC, the SIC stages can be extended until all symbols are reliably detected or until we have $s = N_{SIC}$.

The advantage of using product combining in the CD stage is that due to the multiplicative operation, difference between the correct and incorrect decision variables is quite large. This factor allows a convenient demarcation of the maximum and the second maximum in terms of setting threshold for RTT as given in Equation (4.23).

**Fiebig's scheme:** Here, for the sake of comparison, we briefly describe the proposed method as applied to the HLMV combining scheme of Section 4.2. We refer to this scheme as Fiebig's scheme since it is identical to the method proposed by Fiebig in [143]. This scheme can be described by the following steps:

1) The matrix $\mathbf{R}^{(th)}$ is dehopped by each receiver separately using its own unique address as defined in Equation (4.7). This process results in the $\mathbf{D}^{(k)}$ matrices, where $k = 1, 2, \ldots, N_U$.

2) For each user, a single row with the highest number of entries in $\mathbf{D}^{(k)}$ is chosen in order to estimate the transmitted symbol as explained in Section 4.2. If there are more than one rows with the same value of the highest number of entries (i.e. an ambiguity exists) for a particular user, the decision for that particular user's symbol is delayed until subsequent SIC stages. Moreover, in case of ambiguity about a specific user's symbol, the rows having the maximum number of non-zero entries in that particular user's $\mathbf{D}^{(k)}$ matrix are identified and labelled them as *ambiguity rows*. If all users's symbols contain ambiguities, the detection process is completed by randomly choosing one row from all ambiguous or candidate rows for each user. If no ambiguity exists in any user's symbol, the detection process is successful and complete.

3) Steps 1 and 2 constitute the CD stage first introduced in Section 4.2. If some but not all user's symbols are successfully detected, we proceed with the $s$th SIC stage, $s = 0, 1, 2, \ldots$. We define $\mathbf{R}^{(th,s)}$ as the modified form of $\mathbf{R}^{(th)}$ in the $s$th stage. By this definition, we have $\mathbf{R}^{(th)} = \mathbf{R}^{(th,0)}$. The $s$th SIC stage consists of the following steps:

   (a) In the $s$th SIC stage, the matrix $\mathbf{R}^{(th,s-1)}$ is modified by cancelling the signals, which correspond to all the symbols that were reliably detected in the previous stage (step 2). Specifically, if $X_{k(d)}$ is the detected symbol, then, after the interference cancellation operation, we have

$$R_{ml}^{(th,s)} = \begin{cases} 0 & \text{for } m = X_{k(d)} \oplus a_k(l) \\ R_{ml}^{(th,s-1)} & \text{otherwise,} \quad m = 0, 1, \ldots M-1, l = 0, 1, \ldots L-1. \end{cases} \tag{4.24}$$

   (b) Step 1 is repeated on the matrix $\mathbf{R}^{(th,s)}$ for each user whose symbol has yet not been detected, resulting in $\mathbf{D}^{(k,s)}$ for the $k$th user.

   (c) From amongst the rows which were identified as ambiguity rows in the matrix $\mathbf{D}^{(k)}$ during the CD stage (Step 2), an unambiguous row in $\mathbf{D}^{(k,s)}$ having the maximum number of non-zero entries is chosen to estimate the transmitted symbol, as explained in Section 4.2. In case an ambiguity about a particular user's symbol still remains, its detection is deferred till later SIC stages.

The process can be repeated till all symbols are reliably detected or closed when $s = N_{SIC}$.

Note that in the context of Fiebig's scheme [143], during each stage, choice of the maximum entries row is made from amongst those rows which were decided as candidate rows in the CD stage. Thus knowledge of the decisions made in CD stage is retained. This knowledge is useful because erasure of detected symbols may result in erasing of undetected symbols also, if there are collisions.

Here, based on the foregoing discussions, we underline some key differences between the proposed SIC schemes and Fiebig's SIC scheme [143]. Firstly, in the context of Fiebig's scheme described above and introduced in [143], a user's symbol is chosen for detection if it results in one unambiguous row with the

largest number of non-zero entries. By contrast, the reliability test in the proposed SLC-SIC and PC-SLC-SIC schemes is the RTT. Secondly, in Fiebig's method [143], if all users's symbols lead to ambiguities, the detection process is stopped by choosing at random one row corresponding to each user's dehopped matrix $\mathbf{D}^{(k)}$. By contrast, in the proposed SLC-SIC and PC-SLC-SIC schemes, if all users' symbols fail the RTT, the one user with the highest value of $\lambda^{(k)}$ is selected for detection and interference cancellation, as shown in Equation (4.17).

We observe that the achievable performance of the proposed SIC schemes is dependent upon the specific choice of the RTT threshold values determining which symbols are reliable. Too low a threshold would allow relatively unreliable symbols to be passed. By contrast, too high a threshold will result in a larger number of SIC iterations, thereby increasing the complexity of the detection process; an unnecessarily high threshold may also lead to rejection of some symbols that are sufficiently reliable. Since, the SLC of Section 1.4 is invoked in both schemes, appropriate clipping threshold values also have to be determined. Consequently, for the SLC-SIC scheme, two thresholds, while for the PC-SLC-SIC, three thresholds are required. The value of the RTT threshold depends upon all factors that govern the magnitude of the energy received in a tone. These factors include the modulation order, the diversity order, the received SNR, the number of users, transmitted symbol energy and the fading conditions. For the purpose of determining the optimum thresholds, the SNR may be estimated to a reasonable degree of accuracy by computing a running average of the received AWGN power over a large number of received samples, while all of the remaining parameters are known at the receiver. Thus a look-up table may be maintained at the receiver, which stores the optimum values of $C$ and RTT thresholds for various settings of the system parameters. We assume in this contribution that the received SNR is accurately known at the receiver.

### 4.4.2 Partial Cancellation Based SIC Schemes

The interference cancellation method in the proposed SIC schemes may be modified to circumvent the problem of inadvertent cancellations of undetected symbols. According to the modified SIC scheme, Equation (4.18) in the context of both the SLC-SIC scheme and the PC-SLC-SIC scheme may be modified to yield

$$R_{ml}^{(s)} = \begin{cases} \delta_c R_{ml}^{(s)} & \text{for } m = X_{k(d)} \oplus a_k(l) \\ R_{ml}^{(s-1)} & \text{otherwise,} \qquad m = 0, 1, ...M-1, l = 0, 1, ...L-1, \end{cases} \tag{4.25}$$

where $\delta_c$, $0 < \delta_c < 1$, is referred to as the cancellation coefficient. The reason for employing a cancellation coefficient $\delta_c$ in Equation (4.25) is as follows. Suppose that we have $\delta_c = 0$ in Equation (4.25), which reduces it to Equation (4.18), implying a scenario where the signals corresponding to the reliable symbols are completely cancelled. It can be observed from our discussion of the SIC schemes that complete cancellation of the symbols which were declared reliable in a specific stage may lead to inadvertent cancellation of the hitherto undetected desired symbols, if two users happen to transmit the same FFH tone, that is when we have $X_{k(d)} \oplus a_k(l) = X_j \oplus a_j(l), j, k = 1, 2, \ldots, N_U, j \neq k$. This unintentional cancellation might lead to

erroneous decisions and to subsequent propagation of decision errors, especially in the PC receiver where multiplication of the signals is employed. In order to avoid the resultant propagation of errors, we assume having a nonzero value of $\delta_c$, i.e. we have $0 < \delta_c < 1$, so that the signal is only partially cancelled in the next SIC stage and hence the potentially unwanted cancellations are avoided. Note also that $\delta_c = 1$ implies no cancellation which corresponds to conventional detection. It has been demonstrated through our simulation results that choosing $\delta_c = 0.2$ for $E_b/N_0$ values below 10dB and $\delta_c = 0.1$ for $E_b/N_0$ values above 10dB yields the best compromise in terms of BER results for most values of system parameters and fading conditions. In [154] a similar technique of partial cancellation was proposed, which employed a cancellation coefficient that was adapted based on the value of the fading parameter corresponding to a specific hop and MFSK tone. This technique would require the pilot-assisted estimation of the fading envelope [154] and therefore may become overly complicated for practical implementation. Hence, we modify the partial cancellation mechanism of [154] by employing a near-fixed cancellation coefficient seen in Equation (4.25), thus creating a low-complexity SIC scheme.

We will refer to the proposed SIC schemes as 'Modified SLC-SIC' and the 'Modified PC-SLC-SIC' schemes, when they invoke partial cancellation as expressed by Equation (4.25) as opposed to the full cancellation of Equation (4.18).

### 4.4.3 Simulation Results of Various SIC Schemes

In this section we present simulation results of the BER performance of the SIC schemes proposed and discussed in Section 4.4.1, when the FFH-MFSK system operates in a frequency-flat Nakagami-$m$ fading MA channel. We provide comparison of the proposed schemes with Fiebig's scheme [143]. For each SIC scheme under consideration, following the CD stage, a maximum of three SIC stages per symbol have been allowed, after which the detection process is concluded, i.e. we have $N_{SIC} = 3$. Additionally, optimum detection thresholds $\delta$, clipping thresholds $C$ and the RTT thresholds $\lambda_T^{(cc)}$ and $\lambda_T^{(pc)}$, as defined in Equations (4.6) and (4.11) and discussed in Section 4.4.1 respectively, have been employed in all simulations.

In Figure 4.17, we have plotted the BER achievable by the SIC schemes under consideration, i.e. by the SLC-SIC, the PC-SLC-SIC schemes and Fiebig's scheme [143], against the number of active users $N_U$. The corresponding BER results achievable using HLMV and SLC in conventional detection (CD) mode, i.e. without SIC, have also been shown. In Figure 4.17, the $E_b/N_0$ value was set to 25dB, the fading parameter $m = 1$ implying Rayleigh fading and $M = 128$ and $L = 7$ have been assumed . We can see from Figure 4.17 that as expected all SIC schemes outperform the CD schemes. Moreover, the SLC-SIC and the PC-SLC-SIC schemes outperform Fiebig's scheme when we have $N_U < 45$. For a high number of users, Fiebig's scheme performs slightly better than the other two SIC schemes, although for $N_U \geq 60$ the BER achieved by all three SIC schemes considered in Figure 4.17 is excessive for practical use. We also observe from Figure 4.17 that the performance of the PC-SLC-SIC scheme is poorer than those of the other two SIC schemes when $N_U$ is high. However, when we have $N_U < 45$, the PC-SLC-SIC scheme performs better

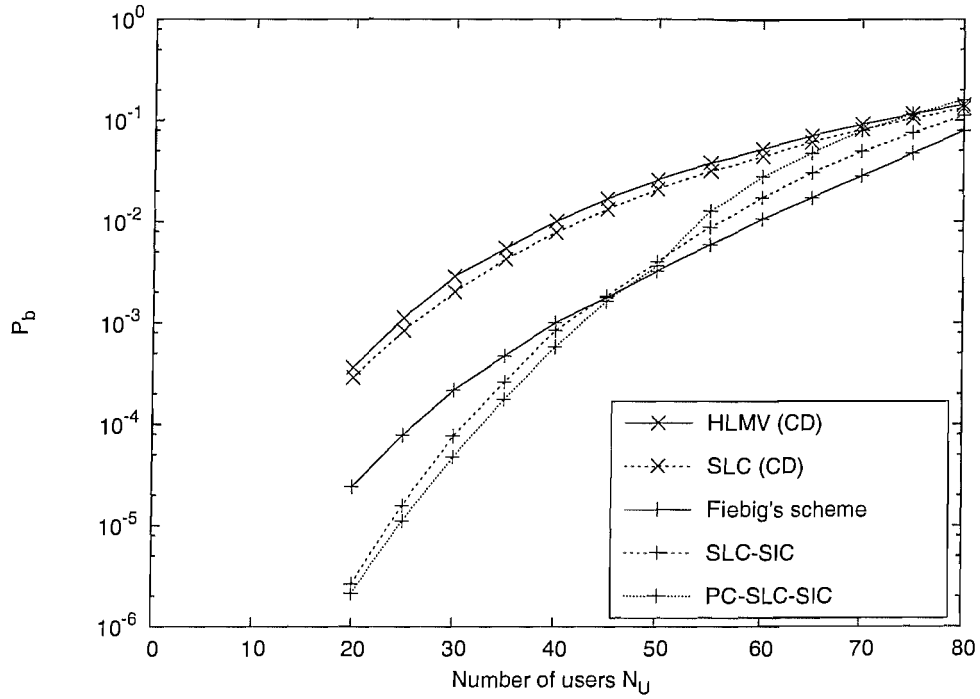


**Figure 4.17:** BER $P_b$ versus number of users performance for various conventional detection (CD) and SIC schemes employed in a FFH-MFSK system communicating over a Nakagami-$m$ fading MA channel, assuming $L = 7, M = 128, m = 1$ and $E_b/N_0 = 25$dB.

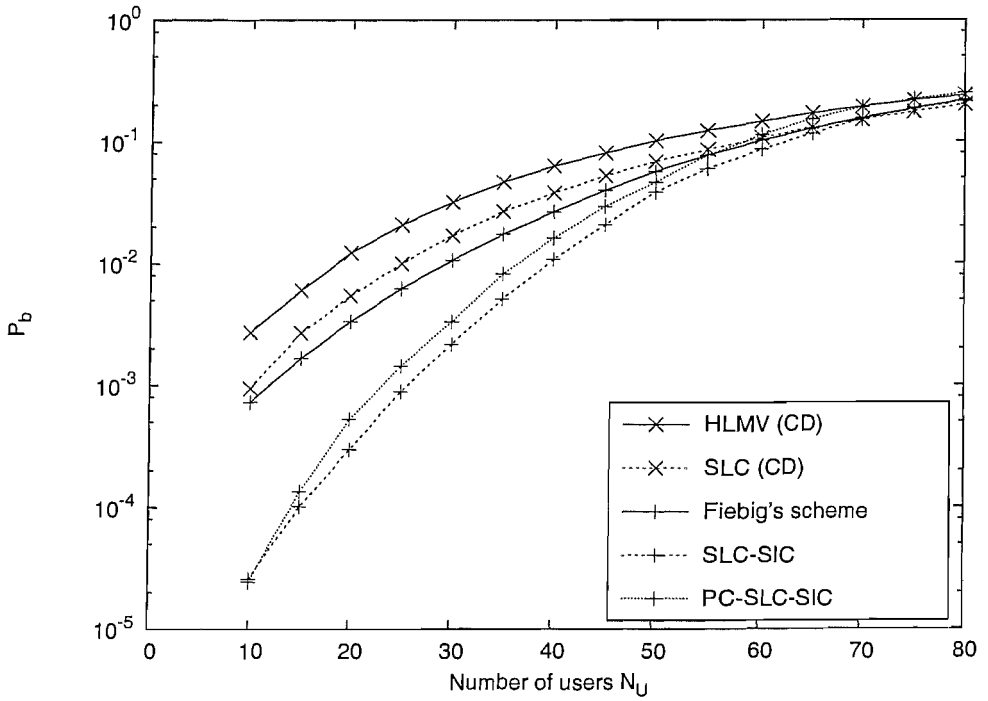


**Figure 4.18:** BER $P_b$ versus number of users performance for various conventional detection (CD) and SIC schemes, employed in a FFH-MFSK system communicating over a Nakagami-$m$ fading MA channel, assuming $L = 7, M = 128, m = 1$ and $E_b/N_0 = 15$dB.

than the other two schemes.

In Figure 4.18, the same comparisons have been carried out as those shown in Figure 4.17, but assum-

ing $E_b/N_0 = 15$dB. We can observe in Figure 4.18 that when the SNR is relatively low, the performance of Fiebig's scheme degrades more dramatically compared to those of the other two SIC schemes. Consequently, it can be observed from Figure 4.18 that the performance of the Fiebig's is no longer better than that of the SLC-SIC scheme at high values of $N_U$, which is in contrast to the scenario of Figure 4.17, when the SNR was high. We have already demonstrated in Section 4.3.1 that the HLMV based diversity combining scheme is more sensitive to noise and yields a good performance only when the SNR is sufficiently high. This observation has been endorsed by comparing the results shown in Figures 4.17 and 4.18, since Fiebig's scheme employs HLMV combining. Furthermore, in Figure 4.17, we observed that the PC-SLC-SIC scheme performs better than the SLC-SIC scheme for a wide range of $N_U$ values. In Figure 4.18, we can observe that the PC-SLC-SIC scheme yields poorer performance results than the SLC-SIC, apart from when we have $N_U = 10$. Comparison of the results plotted in Figures 4.17 and 4.18 thus show that the PC-SLC-SIC scheme is more sensitive to the SNR encountered than the SLC-SIC scheme.

In Figures 4.19 and 4.20, the BER performance for the systems under consideration has been portrayed for two more values of the Nakagami fading parameter $m$. Specifically, in Figure 4.19 $m = 1.5$ and in Figure 4.20 $m = 10$ was assumed. In both these figures, $E_b/N_0 = 15$dB has been assumed and the remaining parameters are the same as those assumed in Figure 4.17. Since, increased values of $m$ imply less severe fading in the context of the Nakagami model, as expected the performance of all the SIC and CD schemes improved, as seen by comparing Figures 4.19 and 4.20 with Figures 4.17 and 4.18. We also observe from these two figures that PC-SLC-SIC significantly benefits from reduced fading intensity. Thus, if we compare the results of Figures 4.19 and 4.20 to those shown in Figure 4.18, where the same SNR value is assumed, we observe that when $m = 1.5$ is assumed in Figure 4.19, the PC-SLC-SIC scheme outperforms the SLC-SIC scheme for low values of $N_U$. Furthermore, when we have $m = 10$ in Figure 4.20, the PC-SLC-SIC scheme yields better BER performance than the other two SIC methods considered almost regardless of the value of $N_U$. The significantly improved performance of the PC-SLC-SIC scheme recorded under mild fading conditions indicates that this scheme is sensitive to fading. This observation can be explained by considering the multiplication operation involved in product combining; under severe fading conditions, the product of energy detector outputs may acquire very low values, thus resulting in increased probability of detection error. By contrast, under less severe conditions, more accurate demarcation of reliable and unreliable symbols is facilitated in the product combining receiver with the aid of the RTT.

For the sake of characterizing the effect of the SNR on the performance of the considered SIC schemes, we have plotted their achievable BER against the SNR in Figure 4.21, when we have $M = 64$, $L = 6$, $N_U = 15$ and Nakagami parameter of $m = 3$ has been assumed. Also shown are the performance of the SIC schemes employing partial cancellations, which are labelled as the 'Modified SLC-SIC' and the 'Modified PC-SLC-SIC' schemes. We observe from Figure 4.21 that the difference between the performance of the Fiebig's scheme and the proposed SIC schemes is reduced at high $E_b/N_0$ values, indicating that the Fiebig's scheme performs better in the high-SNR region. We also observe the amongst the unmodified SIC schemes, PC-SLC-SIC scheme yields the best performance. This is because Nakagami parameter of $m = 3$ implies

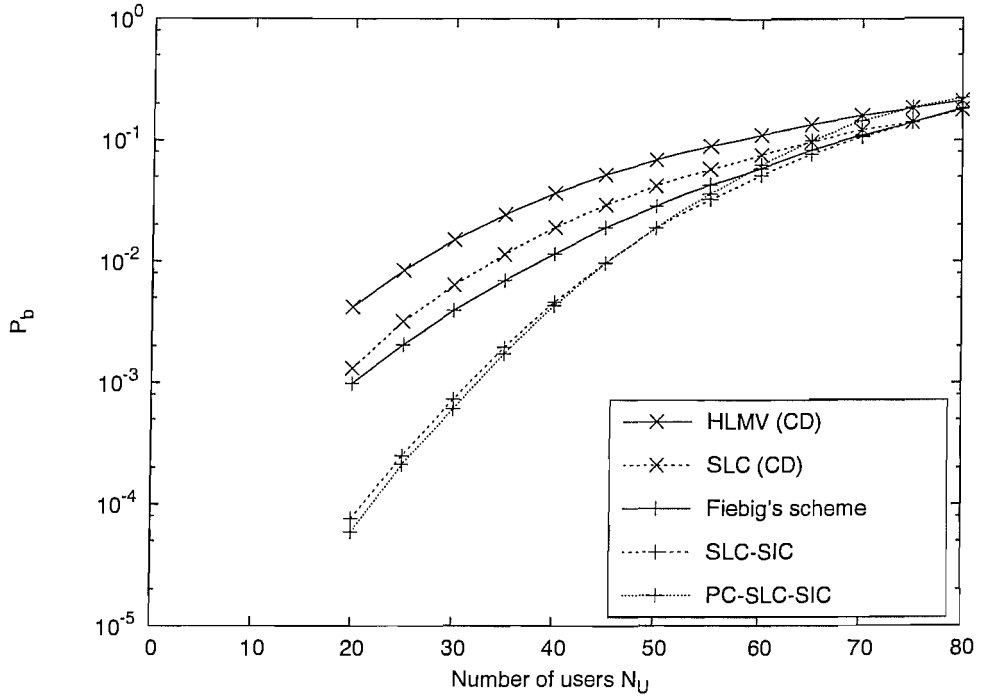


**Figure 4.19:** BER $P_b$ versus number of users performance for various conventional detection (CD) and SIC schemes employed in a FFH-MFSK system communicating over a Nakagami-$m$ fading MA channel, assuming $L = 7$, $M = 128$, $m = 1.5$ and $E_b/N_0 = 15$dB.

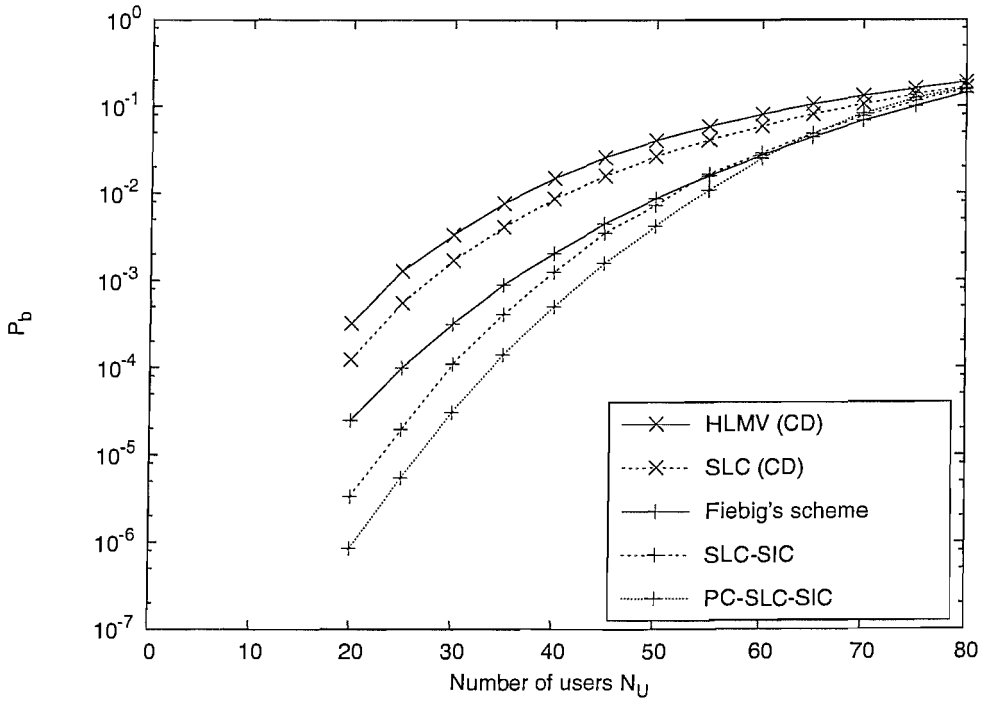


**Figure 4.20:** BER $P_b$ versus number of users performance for various conventional detection (CD) and SIC schemes employed in a FFH-MFSK system communicating over a Nakagami-$m$ fading MA channel, assuming $L = 7$, $M = 128$, $m = 10$ and $E_b/N_0 = 15$dB.

less severe fading which favours the PC-SLC-SIC scheme as we observed in Figure 4.20 as well. Finally we observe in Figure 4.21 that modified SIC schemes yield further improvement in performance, which

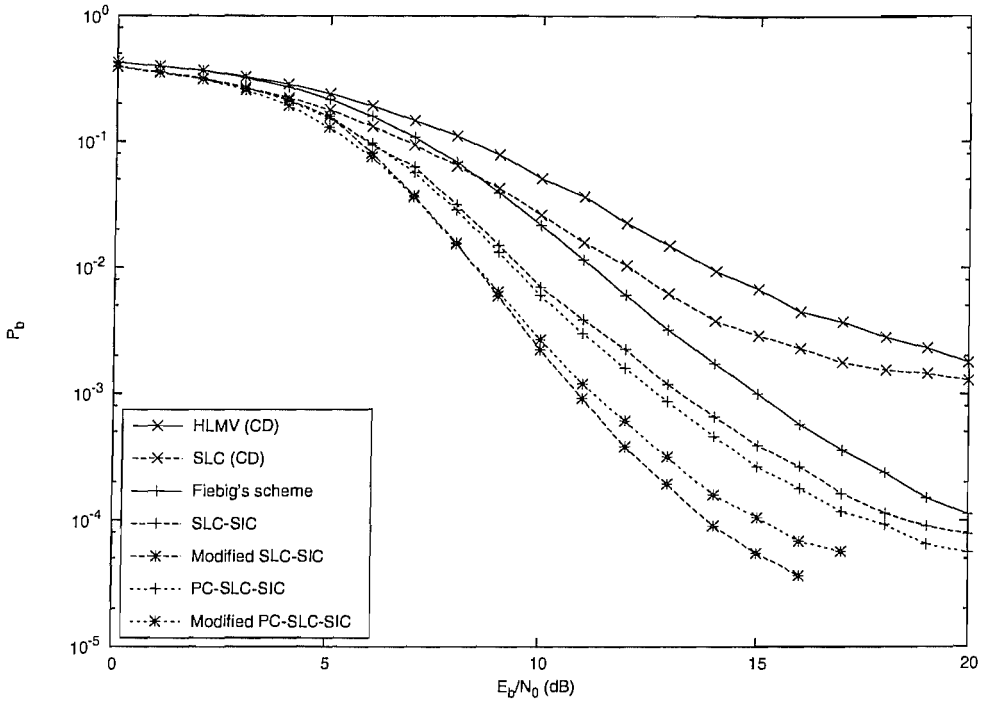


**Figure 4.21:** BER $P_b$ versus $E_b/N_0$ performance for various conventional detection (CD), SIC and the modified SIC schemes, employed in a FFH-MFSK system communicating over a Nakagami-$m$ fading MA channel, assuming $L = 6$, $M = 64$, $m = 3$ and $N_U = 15$.

is more significant in case of the SLC-SIC scheme whose modified version yields a further 4dB of gain at BER=$10^{-4}$. Thus, at this BER value, the modified SLC-SIC scheme is superior to the Fiebig's scheme by more than 7dB. We also observe that the performance of the modified PC-SLC-SIC scheme is not as significantly improved over the unmodified PC-SLC-SIC scheme as that of the modified SLC-SIC scheme is in comparison to its unmodified counterpart. The reason for this is that the fixed cancellation threshold $\delta_c$ does not suit the PC-SLC-SIC scheme which involves product combining in the first stage and SLC in the subsequent stages of detection.

Another factor that governs the performance of the SIC schemes is the number of SIC stages required to achieve the lowest possible BER at a given set of $M$, $L$, $N_U$ and $E_b/N_0$ values. In Table 4.2, we have listed some values of the lowest possible BER achievable using the considered SIC schemes along with the number of SIC iterations required. In Table 4.2, the parameter $N_{SIC,av}$ denotes the average number of SIC stages needed to achieve the lowest possible BER. Note that although a maximum of three SIC stages are allowed, for low values of $N_U$, the lowest possible BER is achieved at a significantly lower value of $N_{SIC,av}$, for all the schemes considered. This observation is readily understandable, because when there is less interference or noise, more symbols are likely to pass the RTT discussed in Section 4.4.1, resulting in fewer SIC stages. We also note from the results seen in Table 4.2 that at low SNR and high value of $N_U$, a larger number of stages are necessitated to achieve the minimum BER. The results listed in Table 4.2 demonstrate that the SLC-SIC scheme is also attractive from the perspective of reduced complexity, since it achieves the lowest possible BER at a low value of $N_{SIC,av}$, especially when the SNR is high. From the

same viewpoint, the performance of the PC-SLC-SIC scheme is inferior to that of the SLC-SIC scheme but better than that of Fiebig's scheme.

| $N_U$ | $E_b/N_0$ | Fiebig's scheme [143] | | SLC-SIC | | PC-SLC-SIC | |
|---|---|---|---|---|---|---|---|
| | (dB) | BER | $N_{SIC,av}$ | BER | $N_{SIC,av}$ | BER | $N_{SIC,av}$ |
| 20 | 25 | 2.40882e-5 | 1.656 | 2.63559e-6 | 0.5946 | 2.12913e-6 | 1.0342 |
| 20 | 15 | 0.00332699 | 2.947 | 0.000296844 | 1.941 | 0.000523414 | 1.936 |
| 40 | 25 | 0.001005 | 2.70 | 0.000841 | 1.064 | 0.00057852 | 2.334 |
| 40 | 15 | 0.0265562 | 2.955 | 0.0107515 | 2.635 | 0.0161537 | 2.716 |
| 60 | 25 | 0.010733 | 2.9856 | 0.0174295 | 1.989 | 0.0280861 | 2.94 |
| 60 | 15 | 0.102039 | 2.831 | 0.0862992 | 2.607 | 0.113554 | 2.954 |

**Table 4.2:** Comparison of the achievable BER and the average number of SIC stages required by the FFH-MFSK MA arrangement using various SIC schemes for communicating over a Rayleigh fading channel, assuming $L = 7, M = 128$

| Detection Scheme | Spectral efficiency $\eta$ (Bits/s/Hz) | | | |
|---|---|---|---|---|
| | $m = 1$ | | $m = 10$ | |
| | BER=$10^{-3}$ | BER=$10^{-4}$ | BER=$10^{-3}$ | BER=$10^{-4}$ |
| **SUD** | | | | |
| HLMV | 0.0625 | 0.014 | 0.1875 | 0.133 |
| OS-NED | 0.094 | 0.014 | 0.195 | 0.14 |
| PCR | 0.094 | 0.014 | 0.1875 | 0.13 |
| SLC | 0.109 | 0.028 | 0.203 | 0.152 |
| **MUD** | | | | |
| Fiebig's scheme [143] | 0.12 | 0.016 | 0.27 | 0.195 |
| SLC-SIC | 0.195 | 0.117 | 0.297 | 0.23 |
| PC-SLC-SIC | 0.18 | 0.109 | 0.336 | 0.266 |

**Table 4.3:** Comparison of the spectral efficiencies, in bits/sec/Hz, achieved by various SUD and MUD schemes corresponding to BERs of $10^{-3}$ and $10^{-4}$ when employed in FFH-MFSK communicating over Nakagami-$m$ fading MA channels, assuming $E_b/N_0 = 15$dB. The spectral efficiencies are computed using Equation (4.4), and the various parameter values are extracted from Figures 4.7 to 4.12 and Figures 4.17 to 4.20.

## 4.5 Conclusion

We have comparatively studied the performance of a range of diversity combining schemes in terms of their ability to combat MA interference, when they are used in a FFH-MFSK system communicating over

| SIC Scheme | $E_b/N_0$ (dB) | |
|---|---|---|
| | BER=$10^{-3}$ | BER=$10^{-4}$ |
| Fiebig's scheme [143] | 15 | 21.2 |
| SLC-SIC | 13.3 | 18.5 |
| PC-SLC-SIC | 12.8 | 17.4 |
| Modified SLC-SIC | 11 | 13.8 |
| Modified PC-SLC-SIC | 11.4 | 15.1 |

**Table 4.4:** Comparison of the $E_b/N_0$ values in dBs required by the various SIC schemes in order to achieve BERs of $10^{-3}$ and $10^{-4}$ when employed in FFH-MFSK communicating over Nakagami-$m$ fading MA channels, assuming $M = 64, L = 6, N_U = 15$ and $m = 3$. The $E_b/N_0$ values are extracted from Figure 4.21.

Nakagami-$m$ fading channels. Both SUD and MUD employing the considered combining schemes in the uplink were analyzed.

In the context of SUD, the various diversity combining schemes discussed in Section 1.4 were considered in a MA scenario. Our simulation results shown in Figures 4.7 to 4.12 demonstrate that the optimum SLC proposed in [48] and outlined in Section 1.4, outperforms all the other schemes highlighted in Section 4.3. The linear and the NED based combining schemes of Section 1.4 offer little advantage in terms of suppressing the MA interference. Two other schemes, namely the OS-NED and the PCR, offer useful performance gains in comparison to the conventional HLMV scheme introduced in Section 1.4.1 and, although their performance remains inferior to that of the optimum SLC, they constitute attractive design options. This is because, unlike the SLC and the HLMV, they do not require the assistance of side information. Furthermore, in the absence of a reliable noise power estimate, the OS-NED and the PCR outperform the SLC.

For MUD, in Section 4.4.1 two novel interference cancellation schemes were proposed that were derived from Fiebig's SIC scheme for the HLMV based systems [143]. One of the proposed schemes invokes the SLC, while the other uses product combining in the CD stage and the SLC in the SIC stages. Our simulation results given in Figures 4.17 to 4.21 and listed in Table 4.2 show that the SLC-SIC and the PC-SLC-SIC schemes yield better performance than Fiebig's scheme, for most values of the system parameters. By contrast, Fiebig's scheme constitutes the better design option when the number of active users is high as seen in Figures 4.17 and 4.18. However, under conditions of high number of simultaneous users, the achieved BER is too high, rendering the system unsuitable for any practical application. Moreover, as seen in Figures 4.17 to 4.21, Fiebig's scheme is more sensitive to the received SNR than the other two SIC schemes considered and its BER performance is more adversely affected, when the SNR is low. When SNR is not high, the SLC-SIC yields a better performance than the other two schemes. The PC-SLC-SIC scheme is the better design option, when the number of active users is low - less than about half of the modulation order - provided that the SNR value is high enough, as is evident from the Figures 4.17 to 4.21. Moreover, the PC-SLC-SIC scheme yields the best performance when the fading is less severe, as can be observed

in Figures 4.19 and 4.20. The SLC-SIC scheme is also attractive in terms of attaining the lowest possible BER using the least number of SIC stages. From this viewpoint, the PC-SLC-SIC scheme is also better than Fiebig's scheme. Finally, we also proposed a method of partial cancellation instead of full cancellation in the context of the SLC-SIC and the PC-SLC-SIC schemes in Section 4.4.2. The proposed SIC schemes employing partial cancellations yield a further performance improvement without any complexity overhead.

A specific drawback of the PC-SLC-SIC is that for achieving its best possible BER performance, three different values of thresholds have to be set. By contrast, the SLC-SIC scheme requires setting of two threshold values while Fiebig's scheme requires just one detection threshold to be set to optimum value. In summary for most values of system parameters that are of practical interest, our proposed SIC schemes proposed in Section 4.4.1 constitute better design options than the SIC scheme based on the conventional HLMV combining, which is the most prominent SIC scheme proposed in the open literature [148] to [150] for operation under fading conditions. The SLC-SIC and the PC-SLC-SIC schemes are capable of supporting higher number of users for a given BER. Alternatively, for a given number of users, the proposed schemes yield a lower BER than Fiebig's scheme [143]. Furthermore, for ease of analysis, in our investigation we have assumed a synchronous communication system exercising perfect power control. However, the proposed SIC schemes are readily applicable to asynchronous systems as well as to those dispensing with power control.

The spectral efficiencies achieved by the various diversity combining scheme as well as by the MUD schemes considered in this chapter have been listed in Table 4.3. Similarly, the SNR values required by various SIC schemes discussed in Section 4.4 to achieve BERs of $10^{-3}$ and $10^{-4}$ are given in Table 4.4. We note in Table 4.4 that the modified SLC-SIC scheme yields a $E_b/N_0$ gain of 7.4 dB over Fiebig's scheme [143].

Having investigated the achievable performance of uncoded FFH in MA channels, we will consider its performance in similar channels when assisted by soft decision decoding in Chapter 5.

Chapter 5

# Iterative Decoding and Soft Information Aided Interference Cancellation in FFH Multiuser System

It has been widely reported that soft decision decoding (SDD) has the potential of significantly enhancing a communication system's BER performance. In this chapter, we investigate various means of employing a FFH-MFSK system in conjunction with a soft-input-soft-output (SISO) channel decoder, in order to determine how much performance improvements may be achieved using SDD in FFH-MFSK scheme. More explicitly, we analyze a FFH-MFSK system employing SDD and iterative decoding (ID) both in an interference-free as well as in an MA channel. We derive soft information to be passed from the FFH-MFSK demodulator to the SISO decoder, assuming Rayleigh as well as Nakagami-$m$ fading channels. Employing EXtrinsic Information Transfer (EXIT) charts [157, 158], we analyze the extrinsic information exchange between a FFH-MFSK demodulator and a SISO decoder and investigate techniques of achieving arbitrarily low BERs at low SNRs.

Furthermore, we propose a method of invoking SDD assisted interference cancellation in a FFH-MFSK scheme operating in MA channels. In Chapter 4, we proposed two successive interference cancellation (SIC) schemes which operated on the principle of multistage detection. The basic principle employed in these SIC schemes was that during each stage, the most reliable symbols are selected so that in subsequent stages, the interference contributed by them may be removed. In the context of these schemes, the reliability of a symbol was assessed using Viterbi's ratio threshold test (RTT) [106]. More specifically, a particular symbol was declared reliable if the ratio of the maximum to the second maximum of its $M$ decision variables exceeded a preset threshold. It is well-known that SISO channel decoders are capable of generating *a posteriori* information about reliability of the channel encoded symbols. In this chapter, we look at means of exploiting the soft *a posteriori* output of the SISO decoder operating in conjunction with the FFH-MFSK

demodulator, in order to test the reliability of symbols and then to perform SIC of the reliable symbols.

## 5.1 Introduction

In Table 5.1, the key contributions dedicated towards investigation of turbo or SDD-aided MFSK, SFH-MFSK and FFH-MFSK based schemes have been summarised. The concept of iterative soft information exchange between an $M$-ary orthogonal demodulator and a SISO decoder was initially proposed in [159]. Valenti *et. al* [160, 161] used the term bit interleaved coded modulation (BICM), while employing binary channel coding in conjunction with $M$-ary noncoherent orthogonal modulation and also employed EXIT charts to gain insights into the ID process. EXIT charts constitute useful semi-analytical tools which were proposed by ten Brink [158] for the analysis of the convergence behaviour of iteratively decoded schemes. This analytical tool, however, has not been applied to FH-assisted schemes.

A plethora of work has been contributed towards the research of joint MUD and SISO decoding designed for direct sequence code division multiple access (DS-CDMA) [162, 163]. The basic idea behind soft-cancellation assisted iterative MUD, also referred to as *turbo MUD* [163] is to carry out demodulation/decoding in multiple stages. More specifically, in coherently detected DS-CDMA, estimates of the dispersive channel are generated, which facilitate the cancellation of the interference imposed by the reliably decoded symbols on the composite multiuser signal. This remodulated signal estimate can then be subtracted from the received signal. By contrast, FH systems are typically employed in conjunction with noncoherently detected MFSK. Thus, in the context of FH-MFSK the lack of knowledge concerning the channel conditions prohibits the employment of classic SIC based MUD schemes typically employed in DS-CDMA [164]. Consequently, the idea of joint decoding and MUD has attracted limited attention as far as FFH-MFSK systems are concerned. However, the concept of iterations between the demodulator and the SISO decoder in order to improve channel estimation and anti-jam performance in coherent slow-FH have been considered [102–104]. The reasons for this trend might be the difficulty of deriving soft information from the received signal in the context of noncoherent FFH-MFSK as well as the challenge of the subsequent exploitation of the soft information forwarded by the SISO decoder to the demodulator. Some diverse sub-optimum soft metrics, however, have been proposed in [115, 165, 166] for employment in noncoherent slow- and fast-FH.

In the context of combatting multi-user interference, Fiebig and Robertson [171] employed soft decision decoded convolutional, turbo and RS codes, although no attempt was made to exploit the decoder's soft output. Park and Lee [175] extended the work reported in [171] employing conventional ID. In the context of SFH-MFSK, Sharma *et al.* [114, 115] introduced the idea of iterations between the demodulator and the decoder in MA channels, employing erasures as well as hard and soft decision decoding with RS codes. A simplifying assumption stipulated in the above contributions [114, 115] is that the receiver has the knowledge of exactly which FH band involves a *hit*, a term implying the event when two users transmit in the same FH

| Contribution | | | Researcher(s) | Year | References |
|---|---|---|---|---|---|
| Channel encoder/decoder | Modulation | Channel | | | |
| Turbo coding | MFSK | Rayleigh | Chayat | 1996 | [167] |
| Concatenation of RS code and TCM | SFH-MFSK | MA, PBNJ | Rahman and Elhakeem | 1990 | [168] |
| RS and convolutional codes | SFH-MFSK | AWGN, PBNJ | Frank and Pursley | 1996 | [169] |
| Convolutional codes | FFH-MFSK | Rician, PBNJ | Theodoss and Robertson | 1996 | [170] |
| RS, convolutional and turbo codes | FFH-MFSK | Rayleigh, MA | Fiebig and Robertson | 1999 | [171] |
| Convolutional, TCM and Turbo codes | MFSK | AWGN | Durand *et al.* | 2000 | [172] |
| Joint MUD and channel decoding | | | | | |
| HDD of RS codes | SFH-MFSK | Rayleigh, MA | Sharma *et al.* | 2001 | [114] |
| SDD of RS Turbo codes | SFH-MFSK | Rayleigh, MA | Sharma *et al.* | 2003 | [115] |
| Sub-optimum soft metrics | | | | | |
| Convolutional codes | SFH-MFSK | AWGN, PBNJ | Pouttu | 1996 | [173] |
| Convolutional codes | FFH-MFSK | AWGN, PBNJ | Su and Chang | 1994 | [165] |
| Convolutional code | SFH-BFSK | Rayleigh, MA | Kim and Cheun | 2003 | [174] |
| Turbo codes | SFH-MFSK | MA | Peric *et al.* | 2005 | [166] |
| SISO concatenation of demodulator and channel decoder | | | | | |
| Turbo codes | MFSK | Rayleigh | Liang and Stark | 2000 | [159] |
| As above with EXIT chart analysis | MFSK | Rayleigh | Valenti and Cheng | 2005 | [161] |
| Convolutional and turbo codes | FFH-MFSK | Rayleigh, MA | Park and Lee | 2001 | [175] |

**Table 5.1:** Summary of important contributions of various researchers towards analysis of soft decoded noncoherent MFSK/SFH-MFSK/FFH-MFSK systems

band of MFSK tones. This assumption may not be valid in the context of FFH based MA systems.

In this chapter, we employ EXIT charts for analysis of a FFH-MFSK system employing ID both in an interference-free as well as in an MA channel. We characterise the proposed ID scheme using binary convolutional code. Soft information to be passed from the FFH-MFSK demodulator to the SISO decoder has been derived, assuming both Rayleigh as well as Nakagami-$m$ fading channels. The EXIT chart based analysis will aid us in determining the specific factors that influence the achievable iterative gain. Moreover, it assists us in suggesting specific methods of improving the BER performance of ID assisted FFH-MFSK. In this chapter, we also propose a novel MUD scheme designed for FFH-MFSK that invokes joint SIC and SISO decoding for mitigating the effects of multiuser interference. In the receiver, we employ clipped or soft limiter combining as well as interference cancellation based on the *a posteriori* information fedback from the SISO decoder to the FFH-MFSK demodulator.

The rest of this chapter is structured as follows. In Section 5.2, the system under consideration is briefly described. In Section 5.3, the conventional ID process between the FFH-MFSK demodulator and a binary convolutional channel decoder is considered. Furthermore, soft metrics appropriate for both Rayleigh as

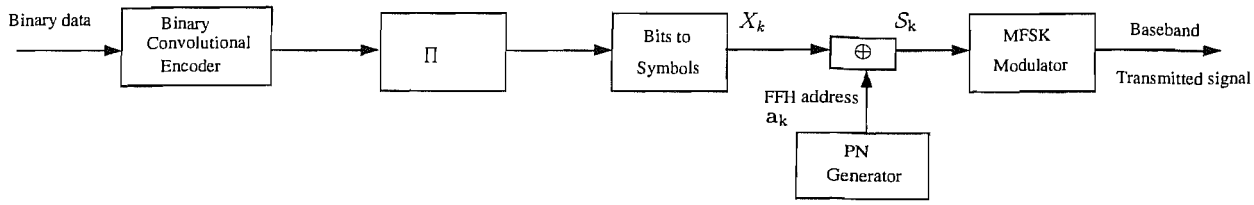


**Figure 5.1:** Block diagram of the convolutional encoded FFH-MFSK transmitter, for the $k$th user, $k = 1, 2, \ldots, N_U$.

well as Nakagami-$m$ fading channels are derived and the ID process is investigated using EXIT charts. In Section 5.4, some techniques for improving the achievable ID gain are discussed using EXIT charts. The SIC scheme using SISO decoding has been discussed in Section 5.5. Finally, in Section 5.6, we present our conclusions.

## 5.2 System Description

The FFH-MFSK system considered consists of a single cell serving multiple users with the aid of a BS and utilising a spread spectrum bandwidth $W_{ss}$. The transmitter schematic of the proposed system is depicted in Figure 5.1. All users' binary data are encoded by a binary convolutional code before bit interleaving. We will consider both the Recursive, Systematic Convolutional (RSC) as well as the non-recursive, Non-Systematic Convolutional (NSC) codes in this chapter. Following bit interleaving, the encoded bits are converted to $M$-ary symbols as shown in Figure 5.1.The $k$th user, $k = 1, 2, \ldots, N_U$, is assigned a unique and random $L$-tuple FH address denoted by $\mathbf{a_k} = [a_k(0), a_k(1), \ldots, a_k(L-1)]$, which is output by the PN generator, where $a_k(l) \in \text{GF}(M)$, $l = 0, 1, \ldots, L-1$, $L$ is the number of frequency hops per symbol and GF($M$) represents a Galois field having $M$ elements. The frequency of the the $k$th user's hopped signal in the $l$th hop may assume any of the $M$ legitimate values and is chosen according to

$$\mathcal{S}_\mathbf{k} = [\mathcal{S}_k(0), \mathcal{S}_k(1), \ldots, \mathcal{S}_k(L-1)] = X_k.\mathbf{1} \oplus \mathbf{a_k}, \tag{5.1}$$

where $\mathbf{1}$ denotes a unit vector of length $L$, $X_k$ is the symbol to be transmitted by the $k$th user and $\oplus$ denotes addition in the Galois field. The components of $\mathcal{S}_\mathbf{k}$ are passed to a MFSK modulator, where a MFSK tone is chosen for transmission which is determined by the value of $\mathcal{S}_k(l)$ during the $l$th hop of duration $T_h$.

The channel is modeled by either uncorrelated Rayleigh or uncorrelated Nakagami-$m$ frequency-flat fading for each of the transmitted frequencies. We assume that each signalling tone can be assumed to experience independent fading. Moreover, the fading envelopes experienced by the various users are also independent of each other. Furthermore, the transmitted signals are corrupted by AWGN having a single-sided power spectral density of $N_0$. Furthermore, all assumptions pertaining to MA channels stipulated in Section 4.2 also apply in the system considered.

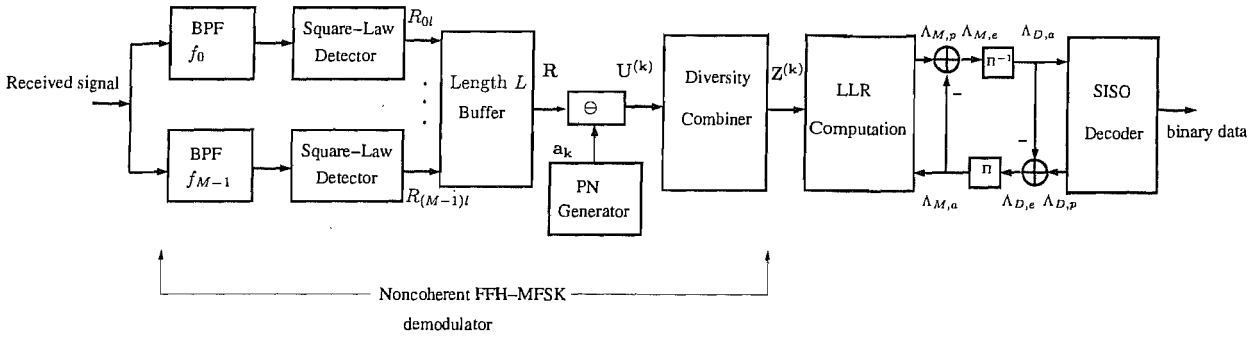


**Figure 5.2:** Block diagram of the FFH-MFSK receiver for the $k$th user, employing iterative decoding

The BS employs a bank of FFH-MFSK receivers, each of which is synchronised to one user. If single user detection (SUD) is employed, each receiver works in isolation and independent of other receivers. Alternatively, multiuser detection (MUD) may be employed, in the context of which all receivers exchange information about reliable symbols. In Section 5.5, we propose and investigate one such MUD scheme that is based on SIC in conjunction with SISO decoding. The schematic of one user's receiver is shown in Figure 5.2, where we assume that the FFH demodulator is in synchronism with the FFH modulator of the transmitter. After carrier demodulation, a bank of $M$ square-law detectors detect the energy received in each MFSK tone. The outputs of the detectors are dehopped and combined over $L$ hops using SLC [48]. The set of $M$ diversity combiner outputs constitutes the demodulator output, which is exploited to derive the soft information to be passed to the SISO decoder. The block labelled 'LLR Computation' in Figure 5.2 computes symbol probabilities from the received signal, converts them to Log-Likelihood Ratios (LLRs) and performs the inverse operations. Next, either the conventional extrinsic information exchange between the FFH-MFSK and outer SISO decoder is invoked, or the ID assisted SIC scheme is employed for cancelling the multiuser interference (MUI). The conventional ID scheme is discussed in Section 5.3, while the proposed SIC scheme is detailed in Section 5.5.

**Notations**: Note that in our discussions we use the notations $P_{M,a}$, $P_{M,p}$ and $P_{M,e}$ for the *a priori*, *a posteriori* and the extrinsic symbol probabilities of the demodulator, respectively. The corresponding notations for the channel decoder are $P_{D,a}$, $P_{D,p}$ and $P_{D,e}$. By contrast $P_{M,a}(X_k = n|\mathbf{Z})$ represents the *a priori* probability of the $n$th symbol only, $n = 0, 1, \ldots, M-1$. Moreover, a bold symbol denotes a set of $M$ variables, for example $\mathbf{Z} = [Z_0, Z_1, \ldots, Z_{M-1}]$ denotes a set of $M$ diversity combiner outputs, while $\mathbf{P}_{M,a}$ represents the set of $M$ *a priori* symbol probabilities at the demodulator output. Likewise, $\Lambda_{M,a}$, $\Lambda_{M,p}$ and $\Lambda_{M,e}$ denote the *a priori*, *a posteriori* and extrinsic LLRs of the demodulator, while $I_{M,a}$, $I_{M,p}$ and $I_{M,e}$ represent the associated mutual informations. The corresponding metrics for the outer decoder are denoted by $\Lambda_{D,a}$, $\Lambda_{D,p}$ and $\Lambda_{D,e}$ and $I_{D,a}$, $I_{D,p}$ and $I_{D,e}$. When the LLR of a particular bit is involved, we use a notation such as $\Lambda_{M,a}(i)$ for the $i$th bit. Finally, the superscript $(k)$ of a symbol signifies that the particular variable pertains to the $k$th user, $k = 1, 2, \ldots, N_U$.

## 5.3 Conventional Iterative Decoding for FFH-MFSK

The iterative soft information exchange between an $M$-ary orthogonal demodulator and a SISO binary decoder has been considered in [159,160,176]. We apply this concept in the context of the proposed FFH-MFSK receiver and refer to it as the SUD-ID scheme, where the term SUD implies that no attempt has been made to detect jointly all users' symbols. We will derive in Section 5.3.1 the soft information passed by the FFH-MFSK demodulator to the SISO decoder, assuming both Rayleigh as well as Nakagami-$m$ fading channels. In Section 5.3.2 we will investigate the extrinsic information exchange between the demodulator and the decoder with the aid of EXIT charts. In Section 5.3.3, we will present our simulation results of the SUD-ID scheme and verify the EXIT chart predictions made in Section 5.3.2.

### 5.3.1 Derivation of Soft Information

In the conventional SISO decoding scheme seen in Figure 5.2, the demodulator inputs the LLRs [177] of the received signal to the decoder. The LLR corresponding to the $i$th received bit $b_i$ of the $k$th user, $k = 1, 2, \ldots, N_U$ is given by [177]

$$\Lambda_{M,p}^{(k)}(i) = \log\left[\frac{P(b_i = 1)}{P(b_i = 0)}\right], \tag{5.2}$$

where $P(.)$ denotes the probability of an event. Since $M$-ary modulation scheme is employed, the LLRs have to be derived from the received $M$-ary symbol probabilities. More specifically, we need the probability that symbol $n = 0, \ldots, M-1$ was transmitted, given that signal vector of $\mathbf{Z}^{(k)}$, seen in Figure 5.2, is received at the outputs of the $M$ diversity combiners. This probability is given by

$$P_{M,p}^{(k)}(X_k = n|\mathbf{Z}^{(k)}) = \frac{p^{(k)}(\mathbf{Z}^{(k)}|X_k = n)P^{(k)}(X_k = n)}{P^{(k)}(\mathbf{Z}^{(k)})}, \tag{5.3}$$

where $p^{(k)}(\mathbf{Z}^{(k)}|X_k = n)$ is the PDF of the received signal $\mathbf{Z}^{(k)}$ given that the $nth$ symbol $X_k = n$ is transmitted, $P^{(k)}(X_k = n)$ is the *a priori* probability of the symbol $X_k = n$, while $P^{(k)}(\mathbf{Z}^{(k)})$ is the probability of receiving signal $\mathbf{Z}^{(k)}$ which is given by

$$P^{(k)}(\mathbf{Z}^{(k)}) = \sum_{n=0}^{M-1} p^{(k)}(\mathbf{Z}^{(k)}|X_k = n)P^{(k)}(X_k = n). \tag{5.4}$$

The probability given by Equation (5.4) is a constant for a given signal $\mathbf{Z}^{(k)}$. Moreover, for equiprobable symbols, $P^{(k)}(X_k = n) = 1/M$. Hence, the PDF $p^{(k)}(\mathbf{Z}^{(k)}|X_k = n)$ constitutes sufficient statistics for estimating the probability $P^{(k)}(X_k = n|\mathbf{Z}^{(k)})$.

In the context of the system considered, the signal $\mathbf{Z}^{(k)}$ represents the set of $M$ outputs of the diversity combiners seen in Figure 5.2. For independent fading of the received signals in $M$ branches, the PDF

$p(\mathbf{Z}^{(k)}|X_k = n)$ is given by [160]

$$p(\mathbf{Z}^{(k)}|X_k = n) = f_{Z_n}(x_n|X_k = n) \prod_{j=0, j\neq n}^{M-1} f_{Z_j}(x_j|X_k = n), \tag{5.5}$$

where $f_{Z_n}(x_n)$ represents the PDF of the $n$th diversity combiner output, $n = 0, 1, \ldots, M-1$.

In order to derive the PDFs of the diversity combiner outputs, we first consider the PDFs of the square-law detector outputs after dehopping, as seen in Figure 5.2. Although the signal transmitted by one user is interfered by other active users' signals, it is technically challenging to derive the PDF of the square-law detector output considering all possible combinations of the interfering tones. Hence, we assume a simplistic interference-free channel and attempt to extract the soft information from the channel observations based on idealistic conditions. Furthermore, it can be argued that if the interference imposed by a large number of other users is considered, the received signal becomes so random that no useful information about the expected value of the received signal can be provided by the demodulator for the decoder. By contrast, the PDF based on an interference-free channel is likely to provide more useful information about the expected values of the symbols. Moreover, although clipped combining is employed in the receiver, we perform the forthcoming analysis assuming linear combining, i.e. without clipping. This assumption has been stipulated to further simplify our analysis and is supported by the observation that clipping is merely an operation performed for the sake of reducing effects of interference. Hence, our analysis may result in sub-optimal soft information but, as we will show in Section 5.3.3, appreciable performance can be achieved using this approach.

#### 5.3.1.1 Soft Information in Rayleigh Fading Channel

In this section, we derive the soft information passed by the FFH-MFSK demodulator to the SISO decoder, assuming that the transmitted signal experiences Rayleigh fading. Assuming that the $n$th FSK tone is transmitted, it can be readily shown that, for independent Rayleigh fading of the FSK tones, the PDF of the noise-normalized square-law detector output $U_{nl}$ corresponding to the $k$th user, if $X_k = n$ is the transmitted symbol in the $l$th hop, is given by [34]

$$f_{U_{nl}}(y_n|X_k = n) = \frac{1}{(1+\gamma_h)} e^{\frac{-y_n}{1+\gamma_h}}, \qquad y_n \geq 0, \tag{5.6}$$

where $\gamma_h = bR_cE_b/(LN_0)$ is the SNR per hop, $R_c$ is the code rate, $E_b$ is the transmitted energy per bit and $b$ is the number of bits per symbol.

Similarly, for all the non-signal tones, $j = 0, 1, \ldots, M-1, j \neq n$, the corresponding PDF is given by

$$f_{U_{jl}}(y_j|X_k = n) = e^{-y_j}, \qquad 0 \leq y_j \leq \infty. \tag{5.7}$$

In order to derive the PDF of the diversity combiner output, we employ the characteristic function (CF) approach [34]. The CF of the PDF given in Equation (5.6) is readily shown to be [34]

$$\phi_{U_{nl}}(\omega|X_k = n) = \int_0^\infty f_{U_{nl}}(x)e^{\mathcal{J}\omega y_n}dy_n = \frac{1}{1-\mathcal{J}\omega(1+\gamma_h)}, \tag{5.8}$$

where $\mathcal{J} = \sqrt{-1}$. Since the signals in all hops are *i.i.d.*, the CF of the linear combiner output is given by [34]

$$\phi_{Z_n}(\omega|X_k = n) = [\phi_{U_{nl}}(\omega|X_k = n)]^L = \left[\frac{1}{1-\mathcal{J}\omega(1+\gamma_h)}\right]^L. \tag{5.9}$$

Next, the PDF of $Z_n$ can be derived from the CF, yielding

$$\begin{aligned} f_{Z_n}(x_n|X_k = n) &= \frac{1}{2\pi}\int_{-\infty}^{\infty}\phi_{Z_n}(\omega|X_k = n)e^{-\mathcal{J}\omega x_n}d\omega \\ &= \frac{x_n^{L-1}}{(1+\gamma_h)^L\Gamma(L)}e^{-x_n/(1+\gamma_h)} \end{aligned} \tag{5.10}$$

Similarly, for all the non-signal tones, we have

$$f_{Z_j}(x_j|X_k = n) = \frac{x_j^{L-1}}{\Gamma(L)}e^{-x_j}, \qquad j = 0, 1, ..., M-1, j \neq n. \tag{5.11}$$

Inserting Equations (5.10) and (5.11) in Equation (5.5), we have

$$\begin{aligned} p^{(k)}(\mathbf{Z}^{(k)}|X_k = n) &= \frac{x_n^{L-1}}{(1+\gamma_h)^L\Gamma(L)}e^{-x_n/(1+\gamma_h)}\prod_{j=1,j\neq n}^{M-1}\frac{x_j^{L-1}}{\Gamma(L)}e^{-x_j} \\ &= \frac{x_n^{L-1}}{(1+\gamma_h)^L\Gamma(L)}e^{-x_n}e^{\frac{x_n\gamma_h}{(1+\gamma_h)}}\prod_{j=1,j\neq n}^{M-1}\frac{x_j^{L-1}}{\Gamma(L)}e^{-x_j} \\ &= \frac{1}{(1+\gamma_h)^L}\left[\prod_{j=0}^{M-1}\frac{x_j^{L-1}}{\Gamma(L)}e^{-x_j}\frac{1}{\Gamma(L)}\right][e^{\frac{x_n\gamma_h}{(1+\gamma_h)}}]. \end{aligned} \tag{5.12}$$

We can see in Equation (5.12) that for any of the $n$th symbol, $n = 0, 1, ..., M-1$, all the terms except the last exponential are common. Since, the computation of LLRs in Equation (5.2) requires logarithm of the bit probabilities, we ignore the common terms as a normalization factor and express the normalized probability $p^{(k)}(\mathbf{Z}^{(k)}|X_k = n)$ as

$$p^{(k)}(\mathbf{Z}^{(k)}|X_k = n) = \exp\left[\frac{x_n\gamma_h}{1+\gamma_h}\right]. \tag{5.13}$$

We note that the soft metric given by Equation (5.13) bears similarity to that derived in [160, 161]. The only differences are that the one derived in [160, 161] is for envelope detection of MFSK signals while we assumed square-law detection in this analysis and also, in Equation (5.13) $\gamma_h$ signifies SNR per hop.

Inserting Equation (5.13) in Equation (5.3), we can derive normalized symbol probabilities. The bit

probabilities can be derived from the symbol probabilities using the following relation [159, 171]:

$$P_{M,p}(b_i = 0|\mathbf{Z}^{(k)}) = \sum_{t=0}^{M/2-1} P_{M,p}(X_k = n|\mathbf{Z}^{(k)}), \qquad n = t + \lfloor \frac{t}{2^i} \rfloor 2^i, \quad i = 0, 1, \ldots, \log_2 M - 1, \tag{5.14}$$

where $\lfloor x \rfloor$ denotes the largest integer less than or equal to $x$. The corresponding probability of $(b_i = 1)$ is given by $P_{M,p}(b_i = 1|\mathbf{Z}^{(k)}) = 1 - P_{M,p}(b_i = 0|\mathbf{Z}^{(k)})$. Finally, the LLRs for the $k$th user are computed using Equation (5.2).

#### 5.3.1.2 Soft Information in Nakagami-$m$ Fading Channel

Next, we characterise the soft demodulator output, assuming that the transmitted signal experiences Nakagami- $m$ fading. Assuming that the $n$th tone, $n = 0, 1, \ldots, M-1$, is transmitted, the linear combiner's output conditioned on the received SNR is then non-central Chi-square distributed with $2L$ degrees of freedom [34]. Consequently, the PDF of the noise-normalized combiner output, may be expressed as

$$f_{Z_n}(x_n|\gamma, X_k = n) = \left(\frac{x_n}{\gamma}\right)^{(L-1)/2} e^{-(x_n+\gamma)} I_{L-1}(2\sqrt{x\gamma}), \tag{5.15}$$

where $\gamma = \gamma_h \sum_{l=0}^{L-1} \alpha_l^2$, $\alpha_l$ is the Nakagami-$m$ distributed attenuation factor during the $l$th hop and $I_{L-1}(.)$ is the modified Bessel function of the first kind of $(L-1)$th order. For the $j$th non-signal tone, $j = 0, 1, \ldots, M-1, j \neq n$, the linear combiner output is central Chi-squared distributed with $2L$ degrees of freedom [34], and the corresponding PDF is given by

$$f_{Z_j}(x_j|X_k = n) = \frac{x_j^{L-1}}{\Gamma(L)} e^{-x_j}. \tag{5.16}$$

In order to derive the unconditional PDF of $Z_n$, the expression given by Equation (5.15) has to be averaged over the PDF of $\gamma$, which can be derived from the PDF of $\alpha_l$. Since $\alpha_l$ is Nakagami-$m$ distributed, its PDF is given by [34]

$$f_{\alpha_l}(t) = \frac{2t^{2m-1}}{\Gamma(m)} \left(\frac{m}{\Omega}\right)^m e^{-mt^2/\Omega}, \tag{5.17}$$

where $m$ is the Nakagami fading parameter, and $\Omega = E[\alpha_l^2]$. Consequently, it can be shown that $\gamma_l = \gamma_h \alpha_l^2$ is Gamma distributed and its PDF can be readily derived, with the aid of [34], yielding

$$f_{\gamma_l}(r) = \frac{r^{m-1}}{\Gamma(m)} \left(\frac{m}{\gamma_h}\right)^m e^{-mr/\gamma_h}. \tag{5.18}$$

The CF of the PDF in Equation (5.18) may be readily expressed as [34]

$$\phi_{\gamma_l}(\omega) = \frac{1}{(1 - \jmath\omega\gamma_h/m)^m}. \tag{5.19}$$

Since the signals in all hops are *i.i.d.* the CF of the $\gamma$ is given by [34]

$$\phi_\gamma(\omega) = \frac{1}{(1 - \jmath\omega\gamma_h/m)^{mL}}. \tag{5.20}$$

From the above CF, we can derive the PDF of the random variable $\gamma$ which is given by

$$f_\gamma(\gamma) = \frac{\gamma^{mL-1}}{\Gamma(mL)}\left(\frac{m}{\gamma_h}\right)^{mL} e^{-m\gamma/\gamma_h}. \tag{5.21}$$

Now, the unconditional PDF $f_{Z_n}(x_n|X_k = n)$ may be derived by averaging Equation (5.15) over $[0, \infty]$ using the PDF of $\gamma$ given by Equation (5.21). Consequently, we have

$$\begin{aligned} f_{Z_n}(x_n|X_k = n) &= \int_0^\infty f_{Z_n}(x_n|\gamma, X_k = n) f_\gamma(\gamma) d\gamma \\ &= \int_0^\infty \left(\frac{x_n}{\gamma}\right)^{(L-1)/2} e^{-(x_n+\gamma)} I_{L-1}(2\sqrt{x\gamma}) \\ &\times \frac{\gamma^{mL-1}}{\Gamma(mL)}\left(\frac{m}{\gamma_h}\right)^{mL} e^{-m\gamma/\gamma_h} d\gamma. \end{aligned} \tag{5.22}$$

Upon applying a suitable change of variable, the above equation may be expressed with the aid of [122] as

$$f_{Z_n}(x_n|X_k = n) = x_n^{L-1} e^{-x_n} \frac{1}{\Gamma(L)}\left(\frac{m}{m+\gamma_h}\right)^{mL} \Phi\left(mL, L, \frac{\gamma_h x_n}{m+\gamma_h}\right), \tag{5.23}$$

where $\Phi(a, b, c)$ is the hypergeometric function [1, 122]. Note that for $m = 1$, it can be shown with the aid of the relation [1]

$$\Phi\left(L, L, \frac{\gamma_h x_n}{1+\gamma_h}\right) = \exp\left(\frac{\gamma_h x_n}{1+\gamma_h}\right) \tag{5.24}$$

that Equation (5.23) reduces to the corresponding expression derived for Rayleigh fading channels in Equation (5.10).

Inserting Equations (5.23) and (5.16) into Equation (5.5), and after minor simplifications, we arrive at:

$$p^{(k)}(\mathbf{Z}^{(k)}|X_k = n) = \left[\prod_{j=0}^{M-1}\left[\frac{x_j^{L-1} e^{-x_j}}{\Gamma(L)}\right]\left(\frac{m}{m+\gamma_h}\right)^{mL}\right] \Phi\left(mL, L, \frac{\gamma_h x_n}{m+\gamma_h}\right). \tag{5.25}$$

Again, we can see in Equation (5.25) that for any of the $n$th symbol, $n = 0, 1, ..., M-1$, all the terms except for the hypergeometric function term are common. Consequently, the normalized probability $p(\mathbf{Z}^{(k)}|X_k = n)$ may be expressed as

$$p^{(k)}(\mathbf{Z}^{(k)}|X_k = n) = \Phi\left(mL, L, \frac{\gamma_h x_n}{m+\gamma_h}\right), \tag{5.26}$$

which can also be expressed as [122]

$$p^{(k)}(\mathbf{Z}^{(k)}|X_k = n) = \exp\left(\frac{\gamma_h x_n}{m+\gamma_h}\right)\Phi\left(L(1-m), L, \frac{-\gamma_h x_n}{m+\gamma_h}\right). \tag{5.27}$$

Inserting Equation (5.27) into Equation (5.3), we can derive the normalized symbol probabilities.

For ease of computation, the hypergeometric function may be written in the form of an infinite series given by [122]

$$\Phi\left(L(1-m), L, \frac{-\gamma_h x_n}{m+\gamma_h}\right) = \sum_{i=0}^{\infty} \frac{\Big(L(1-m)\Big)_i}{(L)_i i!}\left[\frac{-\gamma_h x_n}{m+\gamma_h}\right]^i, \tag{5.28}$$

where $(a)_i = a(a+1)\ldots(a+k-1) = (a+i-1)!/(a-1)!$ is the Pochammer function [122]. For negative integers, we have $(-a)_i = (-1)^i(a)!/(a-i)!$. Note in Equation (5.28) that for $m > 1$, the infinite series is reduced to a finite one, consisting of $L(m-1)$ terms.

In the foregoing analysis, we noted that the knowledge of the received SNR is required to compute symbol probabilities from Equations (5.13) and (5.27). In noncoherent systems, especially FFH-MFSK, accurate estimation of the channel during a hop interval which is typically a fraction of the symbol interval may not be practicable. However, the SNR may be estimated to a reasonable degree of accuracy by computing a running average of the received AWGN power over a sufficiently large number, say 20, of received samples. We assume in this foregoing discussions that the received SNR is accurately known at the receiver.

### 5.3.2 EXIT Chart Based Analysis

Having derived the soft information generated by the FFH-MFSK demodulator, we can now investigate the convergence behaviour of the SUD-ID scheme and determine the factors that influence its iterative gain. In this section, we employ EXIT charts for the analysis of the convergence behaviour of the iteratively decoded FFH-MFSK receiver. EXIT charts were proposed by ten Brink [157,158] as a semi-analytical tool for predicting the convergence behaviour of iterative decoding by examining the evolution of the input/output mutual information (MI) between the inner and outer decoders of a concatenated scheme in successive iterations. We will employ this tool for analyzing the convergence behaviour of the iterative demodulation/decoding scheme discussed in Section 5.2.

The application of the EXIT charts is conditioned on the validity of two assumptions:

1) the *a priori* LLR values are fairly uncorrelated.

2) the PDF of the *a priori* LLR values is Gaussian.

The first assumption can be satisfied by using sufficiently large interleaver lengths. The second assumption is verified by plotting the histogram of the outer convolutional decoder's extrinsic LLR output which was

indeed found to be Gaussian.

We now examine the MI transfer characteristics of the FFH-MFSK in the following section.

#### 5.3.2.1 Transfer Characteristics of the FFH-MFSK Demodulator

As discussed in Section 5.3.1, using the channel's output observations, the demodulator generates the *a posteriori* information $\Lambda_{M,p}$ and subtracts the *a priori* information $\Lambda_{M,a}$ from it to produce the extrinsic information $\Lambda_{M,e}$. During the first ID iteration, $\Lambda_{M,a} = 0$ since SISO decoder's output is not available. Based on the above assumptions, the *a priori* information $\Lambda_{M,a}$ can be modelled as an independent Gaussian variable $n_A$ having a variance of $\sigma_A^2$. Thus the *a priori* information $\Lambda_{M,a}$ may be written as [158]

$$\Lambda_{M,a} = \mu_A x + n_A, \tag{5.29}$$

where x $\in \{+1,-1\}$ represents the interleaved bits and $\mu_A = \sigma_A^2/2$, since $\Lambda_{M,a}$ is Gaussian distributed. Consequently, its conditional PDF is given by

$$p_A(\varsigma|X = x) = \frac{1}{\sqrt{2\pi}\sigma_A} \exp\Big(-\frac{(\varsigma - \sigma_A^2 x/2)^2}{2\sigma_A^2}\Big). \tag{5.30}$$

The MI $I_{M,a} = I(X; \Lambda_{M,a})$, $0 < I_{A_M} < 1$, between the outer decoded and interleaved bits $x$ and the LLR values $\Lambda_{M,a}$ is given by [158]

$$I_{M,a} = \frac{1}{2} \sum_{x=0,1} \int_{-\infty}^{\infty} p_A(\varsigma)|X = x) \log_2 \frac{2p_A(\varsigma)|X = x)}{p_A(\varsigma)|X = 0) + p_A(\varsigma)|X = 1)} d\varsigma. \tag{5.31}$$

Inserting Equation (5.30) into Equation (5.31), we have

$$I_{M,a} = 1 - \frac{1}{\sqrt{2\pi}\sigma_A} \int_{-\infty}^{\infty} \exp\Big(-\frac{(\varsigma - \sigma_A^2 x/2)^2}{2\sigma_A^2}\Big) \log_2[1 + e^{-\varsigma}] d\varsigma. \tag{5.32}$$

In order to highlight the dependence of $I_{M,a}$ on $\sigma_A^2$, we introduce the following abbreviation [158]:

$$\begin{aligned} J(\sigma) &\triangleq I_{M,a}(\sigma_A = \sigma) \\ \lim_{\sigma \to 0} J(\sigma) &= 0, \lim_{\sigma \to \infty} J(\sigma) = 1, \quad \sigma > 0. \end{aligned} \tag{5.33}$$

Figure 5.3 shows a plot of $J(\sigma)$ as a function of $\sigma$. Since $J(\sigma)$ is monotonically increasing, its inverse exists and is given by

$$\sigma_A = J^{-1}(I_{M,a}). \tag{5.34}$$

The extrinsic MI at the demodulator's output is a function of both the *a priori* input and the channel

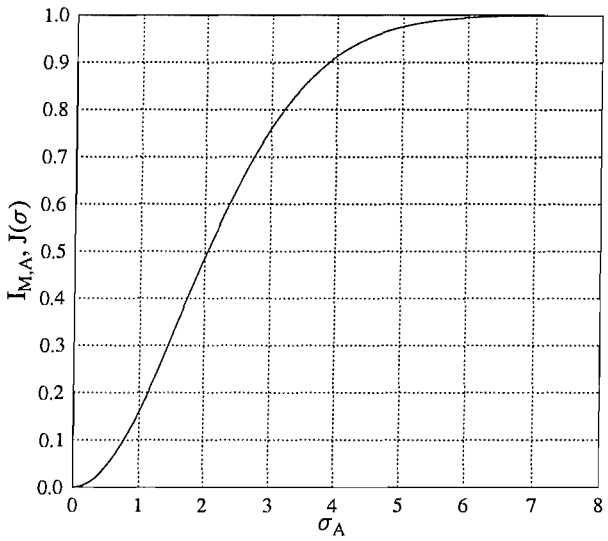


**Figure 5.3:** Mutual information $I_{M,a}$ or $J(\sigma)$ as a function of $\sigma_A$, evaluated using Equation (5.32)

SNR. Thus we define the demodulator's transfer characteristics as [158]

$$I_{M,e} = T(I_{M,a}, E_b/N_0). \tag{5.35}$$

Similar to Equation (5.32), we have

$$I_{M,e} = \frac{1}{2} \sum_{x=0,1} \int_{-\infty}^{\infty} p_E(\varsigma)|X = x) \log_2 \frac{2p_E(\varsigma)|X = x)}{p_E(\varsigma)|X = 0) + p_E(\varsigma)|X = 1)} d\varsigma, \tag{5.36}$$

where $p_E$ represents the PDF of the extrinsic output. Note that no restrictions are imposed on $p_E$ [158].

Next, we outline the method used to evaluate the transfer characteristics of the FFH-MFSK demodulator.

1) Using Equation (5.34), $\sigma_A$ is evaluated as the inverse of the particular value of $I_{M,a}$ where the extrinsic transfer characteristics are to be evaluated.

2) The resultant value of $\sigma_A$ is used for generating LLR value $\Lambda_{M,a}$ with the aid of Equation (5.29), which is applied as the *a priori* input to the FFH-MFSK demodulator.

3) The extrinsic LLR value $\Lambda_{M,e}$ of the demodulator is evaluated by subtracting the *a priori* input from the demodulator's *a posteriori* output $\Lambda_{M,p}$, yielding

$$\Lambda_{M,e} = \Lambda_{M,p} - \Lambda_{M,a}. \tag{5.37}$$

4) Finally, the MI $I_{M,e} = I(X; \Lambda_{M,e})$ between the outer encoded and interleaved bits $x$ and the LLR

values $\Lambda_{M,e}$ is evaluated using Equation (5.36), employing the PDF $p_E$ of the extrinsic output. This requires the determination of the distribution $p_E$ using a histogram-based approximation obtained through Monte Carlo simulation. Alternatively, we can employ a simpler method discussed below. It was shown in [178] that the MI between equiprobable bits $X$ and their respective LLR values $\Lambda$ for symmetric and consistent LLR values [1] simplifies to

$$\begin{aligned} I(X;\Lambda) &= 1 - \int_{-\infty}^{+\infty} p(\Lambda|X=1)\log_2[1+e^{-\Lambda}]d\Lambda \\ &= 1 - E_{X=1}\{\log_2[1+e^{-\Lambda}]\}, \end{aligned} \tag{5.38}$$

where $p(.)$ represents the PDF of the LLR values and $E$ represents the expected value. By invoking the ergodicity theorem in Equation (5.38), namely by replacing the expected value by the corresponding time average, the MI can be evaluated for a sufficiently large number of samples $N$ using the following relation:

$$I(X;\Lambda_{M,e}) = 1 - E_{X=1}\{\log_2[1+e^{-\Lambda_{M,e}}]\} \approx 1 - \frac{1}{N}\sum_{n=1}^{N}\log_2\left[1+e^{-x(n)\Lambda_{M,e}(n)}\right], \tag{5.39}$$

where $N$ denotes the number of coded bits in one block.

The MI transfer characteristics of the FFH-MFSK demodulator recorded for transmission over a interference-free Nakagami-$m$ fading channel characterised by fading parameter of $m = 3$ is shown in Figure 5.4 for various $M$ values, assuming $L = 1$ and $E_b/N_0 = 6$dB. This figure demonstrates that for $M = 2$, i.e. for BFSK, the EXIT curve is a horizontal line, indicating that the BFSK based demodulator will yield no improvement in its output extrinsic MI, upon increasing the *a priori* MI. Thus, no iterative gain is expected from the BFSK demodulator if it is employed as depicted in Figure 5.2. By contrast, as shown in Figure 5.4, for higher $M$ values not only do the EXIT curves emerge from a higher point on the $Y$-axis, but they are also steeper. This observation indicates that a relatively higher iterative gain is expected from MFSK demodulator, using higher $M$ value.

In Figure 5.5, the MI transfer characteristics of the FFH-MFSK demodulator communicating in a Nakagami-$m$ MA channel, characterised by fading parameter of $m = 1$, are shown for $M = 16$, $E_b/N_0 = 15$dB, $N_U = 4$ and assuming various $L$ values. This figure demonstrates that the extrinsic MI of the FFH-MFSK demodulator improves as $L$ is increased, indicating the benefits of diversity. However, we also observe in Figure 5.5 that the EXIT curves lose their slope upon increasing $L$, which implies that the attainable iterative gain is expected to be low at higher $L$ values. Moreover, plotting the MI transfer characteristics yields further insights into the system's expected BER performance. For example, Figure 5.5 demonstrates that very little additional diversity gain is expected by increasing $L$ beyond 4 for the system using the set of parameters considered. Thus, the EXIT chart aids us in predicting the achievable BER

[1] The LLR values are symmetric if their PDF is symmetric, i.e. $p(-\varsigma|X=1) = p(\varsigma|X=0)$. Furthermore, all LLR values with symmetric distributions satisfy the consistency condition [178]: $p(-\varsigma|X=x) = e^{-\Lambda x\varsigma}p(\varsigma|X=x)$.

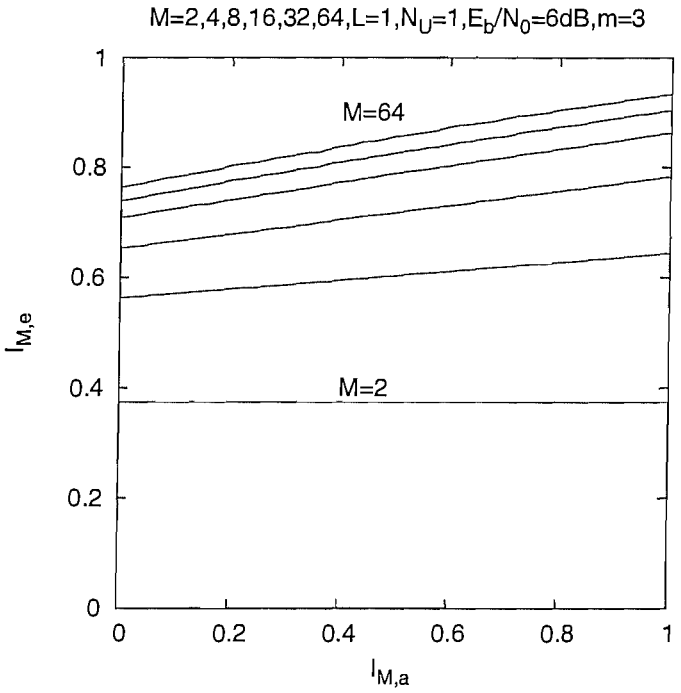


**Figure 5.4:** Extrinsic information transfer characteristics of a FFH-MFSK demodulator in uncorrelated Nakagami-$m$ fading channel, assuming various $M$ values.

performance without performing the bit-by-bit Monte-Carlo simulations.

#### 5.3.2.2 Transfer Characteristics of the Convolutional Decoder

Let us now investigate the EXIT characteristics of the outer channel decoder seen in Figure 5.2. The FFH-MFSK demodulator's extrinsic output $\Lambda_{M,e}$ becomes the *a priori* input $\Lambda_{D,a}$ for the convolutional decoder. The extrinsic information transfer characteristics of the convolutional decoder, being independent of the $E_b/N_0$ value, depend only on its *a priori* input and hence may be written as

$$I_{D,e} = T_D(I_{D,a}), \tag{5.40}$$

where $I_{D,a} = I(C; \Lambda_{D,a})$ denotes the MI between the outer channel coded bits $c$ and the LLR values $\Lambda_{D,a}$. Similarly, $I_{D,e} = I(C; \Lambda_{D,e})$ denotes the MI between the outer channel coded bits $c$ and the extrinsic LLR values $\Lambda_{D,e}$ at the decoder's output.

The procedure of evaluating the transfer characteristics of the convolutional decoder is similar to that used for the demodulator and is summarised below:

1) Using Equation (5.34), $\sigma_A$ is evaluated as the inverse of the particular value of $I_{D,a}$, where the transfer characteristics are to be evaluated.

2) With the aid of Equation (5.29), the value of $\sigma_A$ is used for generating the LLR value $\Lambda_{D,a}$, which is

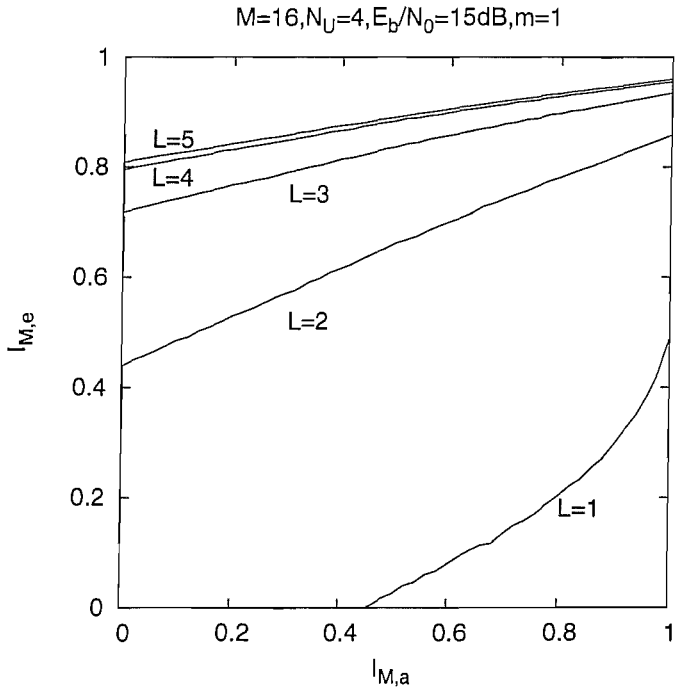


**Figure 5.5:** Extrinsic information transfer characteristics of a FFH-MFSK demodulator in uncorrelated Rayleigh fading channel, assuming various $L$ values.

applied as the *a priori* input $\Lambda_{D,a}$ to the decoder.

3) The extrinsic LLR value $\Lambda_{D,e}$ of the demodulator is evaluated by subtracting the *a priori* input from the decoder's *a posteriori* output $\Lambda_{D,p}$, yielding

$$\Lambda_{D,e} = \Lambda_{D,p} - \Lambda_{D,a}. \tag{5.41}$$

4) Finally, the mutual information of $I_{D,e} = I(C; \Lambda_{D,e})$ between the outer encoded bits $c$ and the LLR values $\Lambda_{D,e}$ is evaluated using the following relation:

$$I(C; \Lambda_{D,e}) = 1 - E\{\log_2[1 + e^{-\Lambda_{D,e}}]\} \approx 1 - \frac{1}{N}\sum_{n=1}^{N} \log_2 [1 + e^{-c(n)\Lambda_{D,e}(n)}]. \tag{5.42}$$

Figure 5.6 shows the extrinsic information transfer characteristics of various half-rate outer RSC codes, characterised by different constraint lengths $v$ and octal generator polynomials $(G, G_r)$. This figure demonstrates that for $I_{D,a} > 0.5$, RSC codes having higher constraint lengths converge faster upon increasing $I_{D,a}$. This is because RSC codes having higher constraint lengths exhibit a better minimum free distance than those associated with shorter constraint lengths [177].

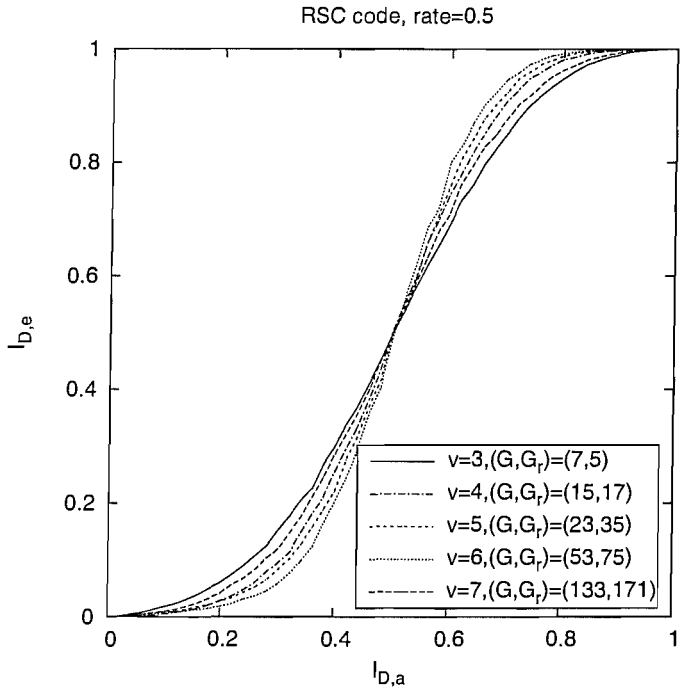


**Figure 5.6:** Extrinsic information transfer characteristics of various RSC codes, having different constraint length ($v$) and generator polynomials ($G, G_r$).

### 5.3.2.3 EXIT Charts of the System

Let us now exploit the EXIT characteristics of the FFH-MFSK demodulator and the SISO convolutional decoder to analyze the exchange of MI across the entire schematic of Figure 5.2. This is carried out by plotting the transfer characteristics of the two components of Figure 5.2 in the same plot in order to generate the EXIT chart. The channel decoder's extrinsic information $I_{D,e}$ becomes the *a priori* input $I_{M,a}$ to the demodulator, while the demodulator's extrinsic information $I_{M,e}$ becomes the channel decoder's *a priori* input $I_{D,a}$. Accordingly the axes of the Figure 5.6 are swapped in order to obtain the EXIT chart shown in Figure 5.7, where we have $M = 64$, $L = 3$ and various $E_b/N_0$ values. Furthermore, in Figure 5.7, the EXIT curves of both the NSC and of the RSC codes characterised by the octal generator polynomial of (7,5) are also shown. The system communicates over an interference-free, Rayleigh fading channel, characterised by Nakagami parameter of $m = 1$. Based on the lessons of [158], in order for the exchange of MI between the demodulator and decoder to converge successfully at a specific $E_b/N_0$ value, their EXIT curves at that $E_b/N_0$ value must intersect only at the $(1, 1)$ point. If this condition is satisfied, then a so called open *convergence tunnel* [158] appears between the demodulator's and decoder's extrinsic MI curves. By contrast, if they intersect at any point before the $(1, 1)$ point in the EXIT chart, this implies that no further evolution of extrinsic MI is possible and hence the channel decoder may not be able to decode the encoded bits. If, however, the demodulator EXIT curve intersects the decoder curve at a point infinitesimally close to $I_{D,e} = 1.0$, an arbitrarily low BER might still be achieved. Consequently, the EXIT chart of Figure 5.7 suggests that at $E_b/N_0 \approx 9$dB, an arbitrarily low BER might be attained.

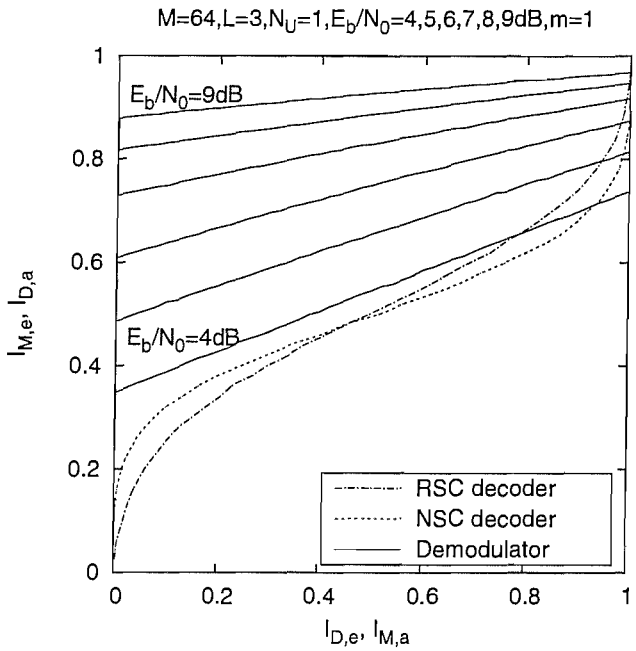


**Figure 5.7:** EXIT chart of convolutionally coded FFH-MFSK demodulator, when communicating over uncorrelated Rayleigh fading channel, assuming various $E_b/N_0$ values. EXIT curves of both the RSC and the NSC codes are shown.

It was stated in [179, 180] that to achieve near-zero BER at an SNR close to the system capacity, the convergence tunnel should be as narrow as possible. This is because the area of the tunnel is characteristic of the SNR discrepancy from the binary erasure channel (BEC) capacity. There is experimental evidence of similar conclusions for Rayleigh channels as well. Hence, an important observation that can be inferred from the EXIT chart of Figure 5.7 is that at $E_b/N_0 \approx 9$dB, a large area appears between the EXIT curves of the demodulator and the channel decoder, which implies that this performance is far from capacity.

We also observe in Figure 5.7 that for the same constraint length of $v = 3$ the EXIT curve of the RSC decoder is steeper than that of the NSC decoder in the range of 0.2 to 0.8. Hence, the demodulator's EXIT curve intersects the RSC decoder's curve at lower MI value, indicating that due to the low-gradient nature of the FFH-MFSK demodulator's EXIT curves, this modulation scheme may be more beneficially concatenated with the NSC code than with the RSC code. We will verify this conclusion using the corresponding BER results in Section 5.3.3.

The effects of increasing MUI on the evolution of the FFH-MFSK demodulator's MI are depicted in Figure 5.8, where we assume various values of number of users $N_U$. As expected, with increased MUI, resulting from high number of users, the demodulator MI degrades and the corresponding MI curves originate from lower points on the $Y$-axis. However, the slope of the curves increases as $N_U$ increases suggesting more degradation of the BER performance but better achievable iterative gain at high $N_U$ values. The validity of our EXIT chart analysis, corresponding to the scenario supporting $N_U = 6$ users, is also confirmed by recording the actual MI points at the output of the demodulator and the outer decoder during each decoding iteration and then plotting them in Figure 5.8. We observe that the iterative trajectory more or less follows

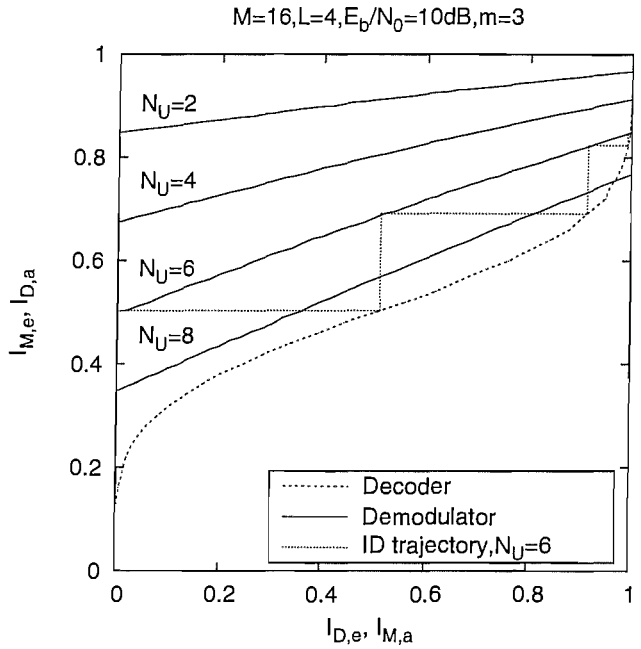


**Figure 5.8:** EXIT chart and ID trajectroy of NSC coded FFH-MFSK demodulator, when communicating over uncorrelated Nakagami-$m$ fading channel, assuming various number of users $N_U$.

the EXIT curves. The slight mismatch observed is owing to having finite interleaver length employed in the actual iterative operation, in contrast to the infinite interleaver length inherently assumed in the theoretical EXIT chart analysis.

### 5.3.3 Simulations Results and Discussion on the ID Scheme

In this section we present our BER performance results for the SUD-ID assisted FFH-MFSK scheme seen in Figure 5.2. The performance of the scheme will be evaluated, when it is operating in a frequency-flat Nakagami-$m$ fading MA channel. In our simulations, unless otherwise stated, we employ the system parameter values listed in Table 5.2.

We commence our investigations by considering the SUD-ID scheme's performance in an interference-free channel, characterised by $N_U = 1$. In Figure 5.9, the BER versus SNR performance of the SUD-

| Channel code | NSC |
|---|---|
| Generator polynomial (octal) | (7,5) |
| Code rate $R_c$ | 0.5 |
| Constraint length $v$ | 3 |
| Interleaver type | Random |
| Interleaver size | 24000 bits |

**Table 5.2:** List of parameters values used in the simulation results of Figures 5.9 to 5.24.

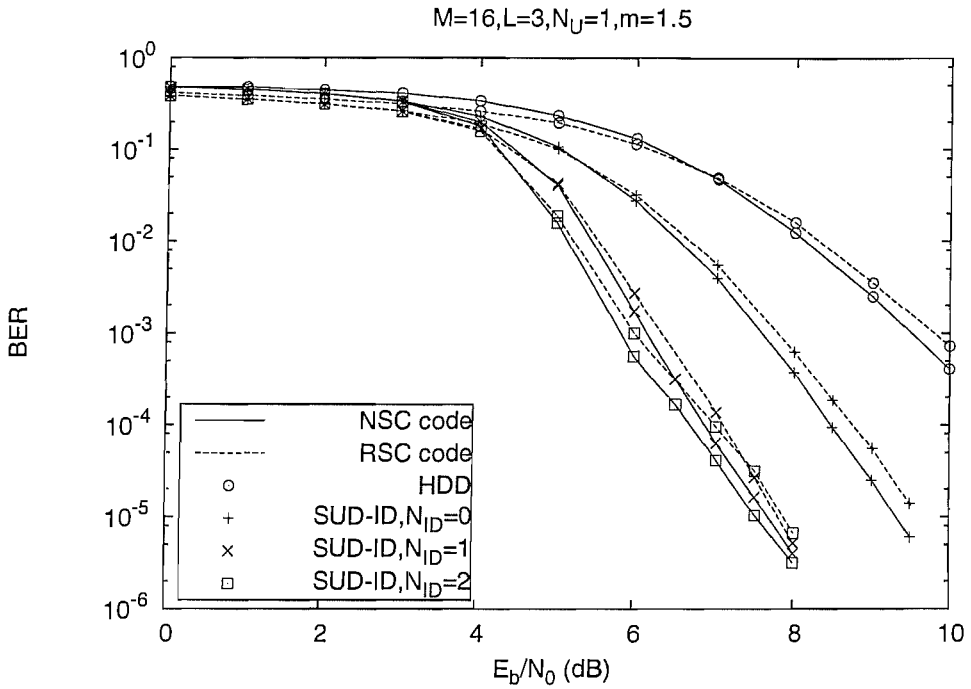


**Figure 5.9:** BER versus $E_b/N_0$ performance of the HDD and ID based schemes employed in FFH-MFSK SLC receiver communicating over a Nakagami-$m$ fading interference-free channel.

ID scheme invoking various number of ID iterations has been shown, assuming $L = 3$, $M = 16$ and a Nakagami fading parameter of $m = 1.5$. The performance of FFH-MFSK using hard decision decoding (HDD) has also been shown. The results of Figure 5.9 demonstrate that the SDD scheme, labelled as SUD-ID with $N_{ID} = 0$ in the figure, outperforms the HDD by about 2dB at BER= $10^{-3}$, validating the soft information derived in Section 5.3.1 and demonstrating the benefits of exploiting SDD. Hence, in case of the SDD-based schemes, when the MI becomes sufficiently reliable at high enough SNR, the BER drops relatively rapidly as compared to the HDD case. The results of this figure also demonstrate that an overall gain of about 1.7dB is obtained at BER= $10^{-5}$ by invoking $N_{ID} = 2$ iterations, although only a modest iterative gain is achieved after the 2nd iteration. Moreover, we observe that the NSC code remains superior to its RSC counterpart, regardless of the number of iterations invoked, thus confirming the accuracy of our EXIT chart analysis of Figure 5.7. Therefore, in our subsequent results, we opt for using the NSC code.

Let us now evaluate the SUD-ID scheme, when the system encounters MA interference. In Figure 5.10, the BER versus $E_b/N_0$ performance of the SUD-ID scheme invoking various number of iterations in an MA channel has been shown, where we assume $M = 16$, $L = 7$, the Nakagami fading parameter of $m = 2.5$ and $N_U = 8$. The results of Figure 5.10 demonstrate that the SUD-ID scheme with $N_{ID} = 0$ outperforms the HDD based scheme by about 2dB at BER= $10^{-2}$. Hence, even in an MA channel the soft information derived in Section 5.3.1 yields a useful SNR gain over the HDD based scheme, although it was derived based on simplifying assumptions. The results of this figure also demonstrate that an additional gain of about 4.5dB over the scheme characterised by $N_{ID} = 0$ iterations is obtained at BER= $10^{-3}$ by invoking $N_{ID} = 4$ iterations, but there is modest iterative gain after the 4th iteration. Therefore, in the subsequent

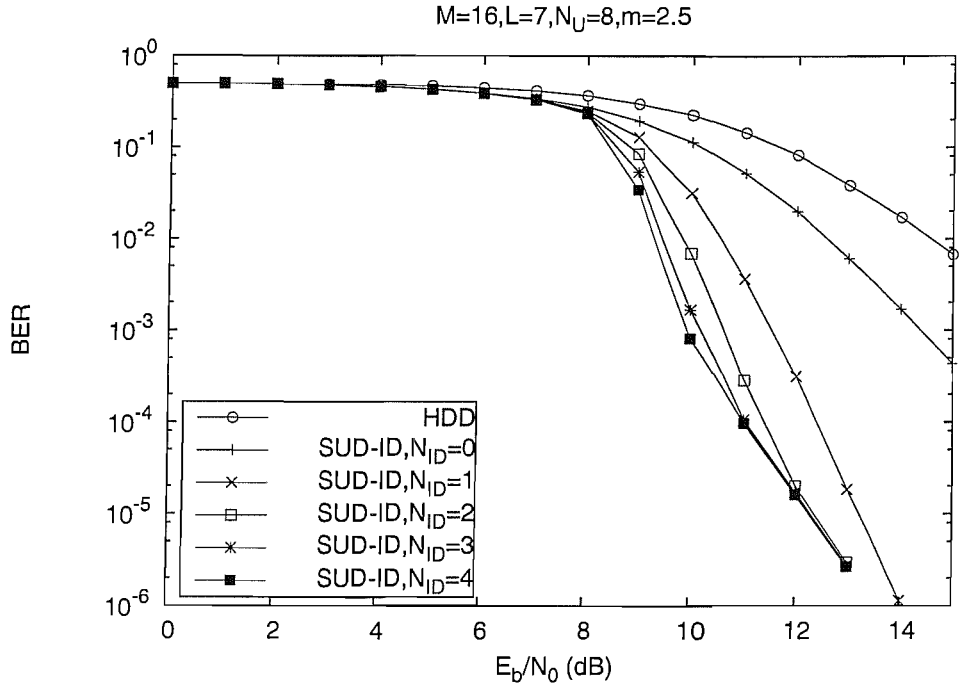


**Figure 5.10:** BER versus $E_b/N_0$ performance of the HDD and ID based schemes employed in FFH-MFSK SLC receiver communicating over a Nakagami-$m$ fading MA channel.

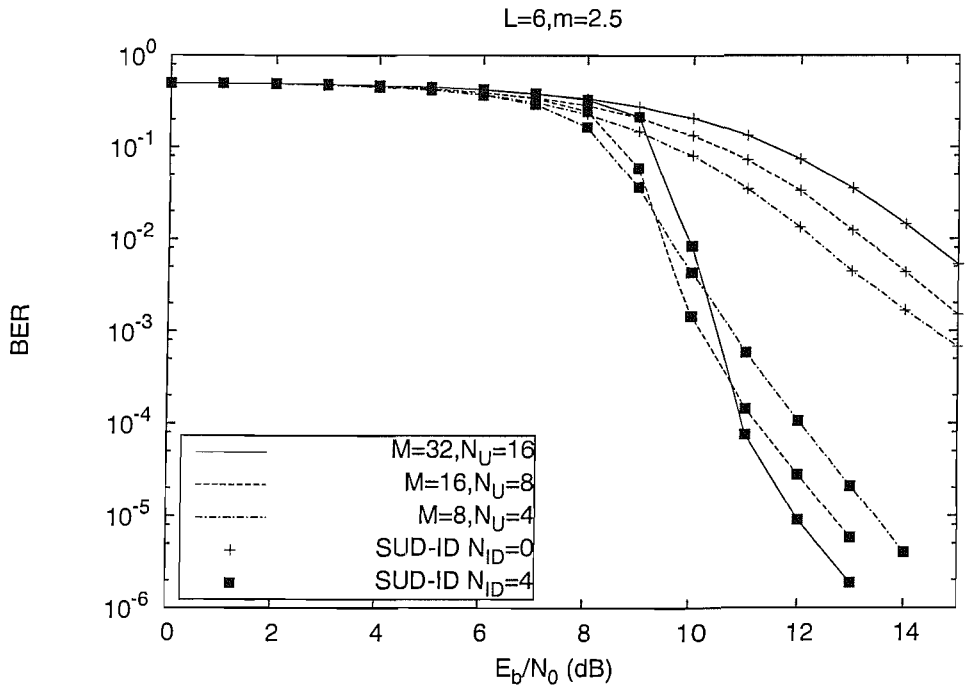


**Figure 5.11:** BER versus $E_b/N_0$ performance of the SUD-ID scheme employed in FFH-MFSK SLC receiver communicating over a Nakagami-$m$ fading MA channel, assuming various $M$ and $N_U$ values.

results we will employ $N_{ID} = 4$ iterations. More importantly, we observe that at SNR values in excess of 12dB, the achievable iterative gain becomes negligible after the second iteration, resulting in an *error floor* in the high-SNR region. This observation is consistent with our EXIT chart results of Figure 5.7, which

predicted that the attainable iterative gain is reduced at high SNRs. Another important observation made from Figure 5.10 is that as compared to the interference-free scenario discussed with the aid of Figure 5.9, the iterative gain becomes higher when MA interference is imposed. This observation verifies the prediction of Figure 5.8, in which we observed that increased MUI leads to improved iterative gain.

In Figure 5.11 the BER versus SNR performance of the SUD-ID scheme is shown for various values of $M$. Since the number of users supported by a FFH-MFSK scheme is a function of the available number of MFSK tones and, hence, of the modulation order $M$, we assume $N_U = M/2$ for the sake of ensuring approximately similar BER performance for each of the $M$ values considered. We observe in Figure 5.11 that, beyond a certain value of SNR, greater iterative gain is attained when using a higher modulation order. Hence, although the system using $M = 32$ is inferior to those using $M = 8$ and 16 when $N_{ID} = 0$ is assumed, the iterative gain yielded by $N_{ID} = 4$ iterations more than compensates for this difference of performance, at SNR values characterised by $E_b/N_0 > 10$dB. Similarly, the system using $M = 16$ yields inferior performance compared to that using $M = 8$ at $N_{ID} = 0$, but the former outperforms the latter when $N_{ID} = 4$ iterations are invoked. This result supports our EXIT chart results of Figure 5.4 which predicted a higher iterative gain for higher $M$ values.

## 5.4 Precoder Aided FFH-MFSK

The EXIT chart analysis conducted in Section 5.3 has demonstrated that only modest iterative gain is possible using MFSK based schemes, because the demodulator's MI transfer curve has low gradient and consequently it intersects the channel decoder's MI transfer curve before reaching the $(1, 1)$ point in the EXIT chart. With the introduction of diversity the performance is expected to improve but the problem of residual BER persists. In this section we investigate one effective means of circumventing this problem. It is well known that the channel may be rendered recursive by incorporating a unity-rate precoder between the channel encoder and the modulator of Figure 5.1 [181–184]. The precoder imposes memory upon the channel, thus rendering it recursive[2].

In Figure 5.12, the schematic of a unity-rate precoder assisted FFH-MFSK transmitter and a possible implementation of the corresponding receiver is shown. The rate-1 encoder's generator polynomial may be expressed as $1/(1 + D)$. In the receiver, the demodulator generates soft information, as discussed in Section 5.3.1, and passes it to the rate-1 decoder which carries out the ID process in conjunction with the outer convolutional decoder. Hence, in Figure 5.12 the *a priori*, *a posteriori* and the extrinsic information of the rate-1 decoder are labelled as $\Lambda_{P,a}$, $\Lambda_{P,p}$ and $\Lambda_{P,e}$, respectively. The corresponding mutual information will be denoted by $I_{P,a}$ $I_{P,p}$ and $I_{P,e}$ respectively, in the forthcoming EXIT chart analysis of the precoded system.

[2]Recursivity in this context implies that the channel has an infinite impulse response.

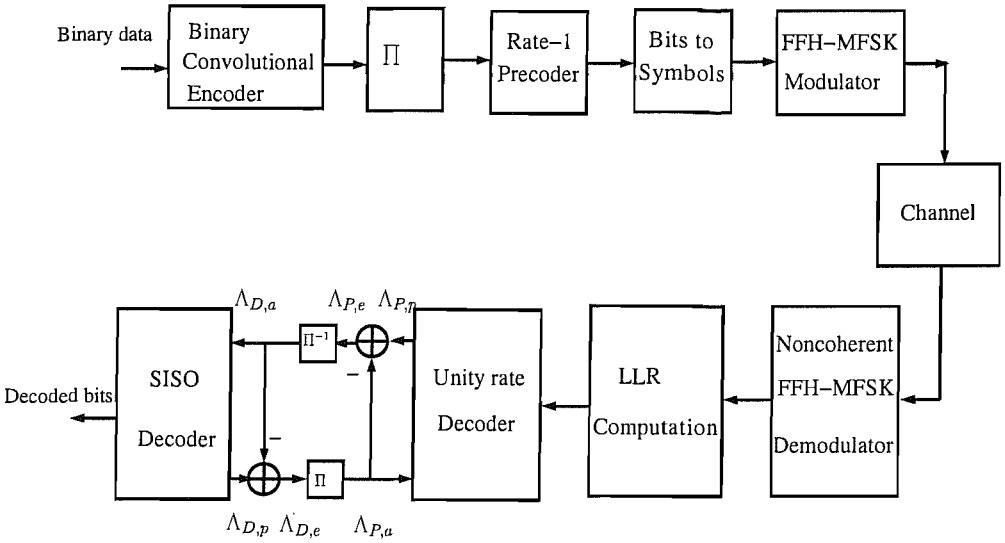


**Figure 5.12:** Block diagram of the precoder assisted convolutional encoded FFH-MFSK system, where the FFH-MFSK demodulator is as shown in Figure 5.2.

### 5.4.1 EXIT Charts of Precoder Aided System

The EXIT chart of the precoder assisted system seen in Figure 5.12 is shown in Figure 5.13. For comparison, the MI transfer characteristics of the FFH-MFSK demodulator, when used in the configuration of Figures 5.1 and 5.2 is also shown. We can observe in Figure 5.13 that corresponding to the *a priori* input value of 0, the $I_{P,e}$ of the rate-1 decoder emerges from a lower value than $I_{M,e}$ of the demodulator, as seen on the $Y$-axis on the left of the chart. However, at higher values of the *a priori* input, the extrinsic MI of the rate-1 decoder starts to rise more rapidly, as evidenced by the dramatic change in the gradient of its curve. Hence, observe that for $M = 16$, while the EXIT curve of the demodulator intersects the outer decoder's curve, that of the rate-1 decoder runs almost parallel to it. This property of the precoder assisted system stems from its ability to impose recursivity on the channel. Furthermore, it indicates that while the precoder assisted system might exhibit inferior BER performance as compared to the one operating without the precoder during the initial ID iterations, after a certain number of iterations, the former becomes capable of outperforming the latter. Furthermore, the rate-1 decoder's EXIT curves do indeed reach the $(I_E, I_A) = (1, 1)$ point.

Let us now investigate the influence of MUI on the precoded system. In Figure 5.14, a comparison has been made between the effect of precoding on a system communicating in interference-free channel and one encountering MUI. For the sake of a fair comparison we keep the area between the demodulator/rate-1 decoder and the outer decoder's EXIT curves approximately the same. Thus, for an interference-free channel, we opted for the system parameters of $L = 3$ and $E_b/N_0 = 8$dB while when a total of $N_U = 6$ users are communicating, we chose $L = 7$ and $E_b/N_0 = 13$dB. The first observation that we make about the EXIT chart of Figure 5.14 is that for the system operating without precoder the demodulator's EXIT curve has a higher slope when MUI is present than when there is no interference. We have already seen in the context of Figure 5.8 that increased MUI leads to steeper MI curve. Hence, as the *a priori* input

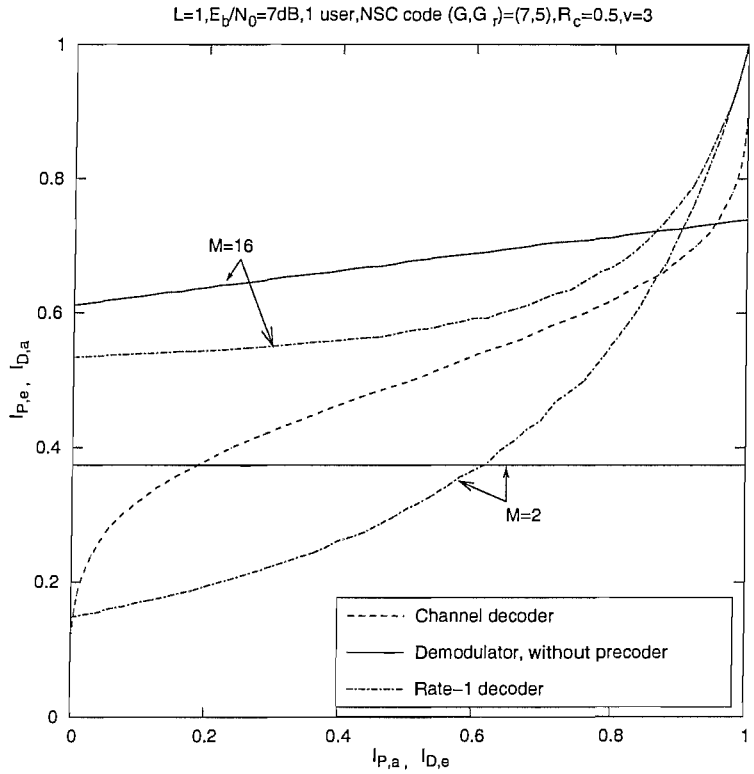


**Figure 5.13:** EXIT chart of NSC coded and precoder assisted FFH-MFSK system, when communicating over uncorrelated Rayleigh fading channel, assuming precoder of memory 1 and $M = 2$ and 16.

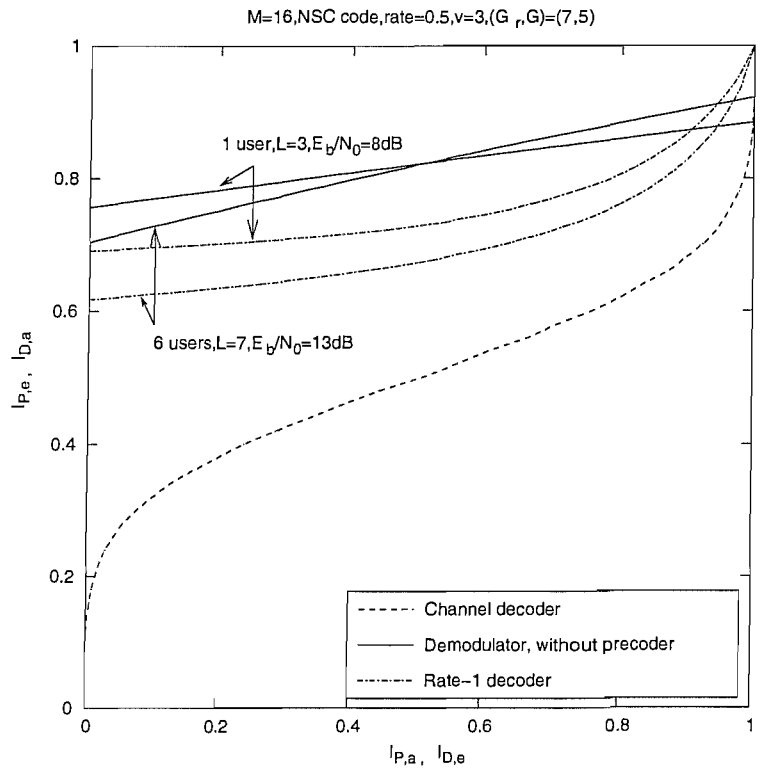


**Figure 5.14:** EXIT chart of NSC coded and precoder assisted FFH-MFSK system, when communicating over uncorrelated Rayleigh fading channel, assuming precoder of memory 1 and $N_U = 1$ and 6.

value improves, the demodulator's EXIT curve corresponding to the system contaminated by MUI crosses over the one for the interference-free system. By contrast, when the system is precoded, the EXIT curve recorded for the system encountering MUI remains inferior to the one operating in an interference-free channel. A possible solution to this problem is to include the FFH-MFSK demodulator in the ID process, thereby allowing extrinsic information exchange amongst the demodulator, the unity-rate decoder and the outer decoder. Investigation of this 3-stage concatenation scheme constitutes our future work.

### 5.4.2 Iteratively Decoded Irregular Variable Length Coding and Precoder Aided FFH-MFSK

In order to demonstrate how the inner rate-1 decoder and an outer decoder may be beneficially concatenated for attaining a high performance, we now investigate the serial concatenation of precoder-aided FFH-MFSK with an outer irregular variable length coding (IrVLC) scheme[3].

EXIT chart analysis [158] has opened avenues towards the investigation and performance improvement of iteratively decoded communication systems. A significant contribution made in the field of ID with the aid of EXIT charts is the introduction of irregular convolutional coding (IrCC) [185–187]. An IrCC consists of multiple sub-codes, each having a different code rate, which are used to encode specific fractions of the source block. By optimally choosing the code rates of the IrCC component codes and the associated fractions of the input block, the convergence of the ID process may be achieved at low SNRs. In analogy to IrCC (IrCC) [185], the family of so-called IrVLCs [188] employs a number of component VLC codebooks having different coding rates [189–192] for encoding particular fractions of the input source symbol stream. We will investigate the proposed scheme in a Rayleigh fading channel contaminated by partial band noise jamming (PBNJ). With the aid of EXIT charts [158], the appropriate lengths of these fractions may be chosen in order to shape the inverted EXIT curve of the IrVLC codec, so that it does not cross the EXIT curve of the inner channel codec. In this way, an open EXIT chart tunnel may be created even at low values of SNR.

**Joint source and channel coding** We consider $K_s = 16$-ary source symbol values that have the probabilities of occurrence that result from the Lloyd-Max (LM) quantization [193] of independent Laplacian distributed source samples. More explicitly, we consider the 4-bit LM quantization of a Gaussian source. Note that these occurrence probabilities vary by more than an order of magnitude between 0.0023 and 0.1616. These probabilities correspond to entropy or average information values between 2.63 bits and 8.74 bits, motivating the application of VLC and giving an overall source entropy of $E = 3.47$bits/VLC symbol.

In the transmitter shown in Figure 5.15, the source symbol frame $\mathbf{s}$ comprises of $J$ 4-bit source symbols having $K_s = 16$-ary values $\{s_j\}_{j=1}^{J} \in [1 \dots K]$. These source symbols are decomposed into $N_v$ number of components $\{\mathbf{s}^n\}_{n=1}^{N_v}$, where we opted for $N_v = 16$ in the case of the IrVLC-FFH-MFSK scheme and

[3]This work is based on collaboration with the coauthors of the publication no. 10 in the Section titled 'List of Publications' of this thesis; this collaboration project provided me access to the required VLC codes.

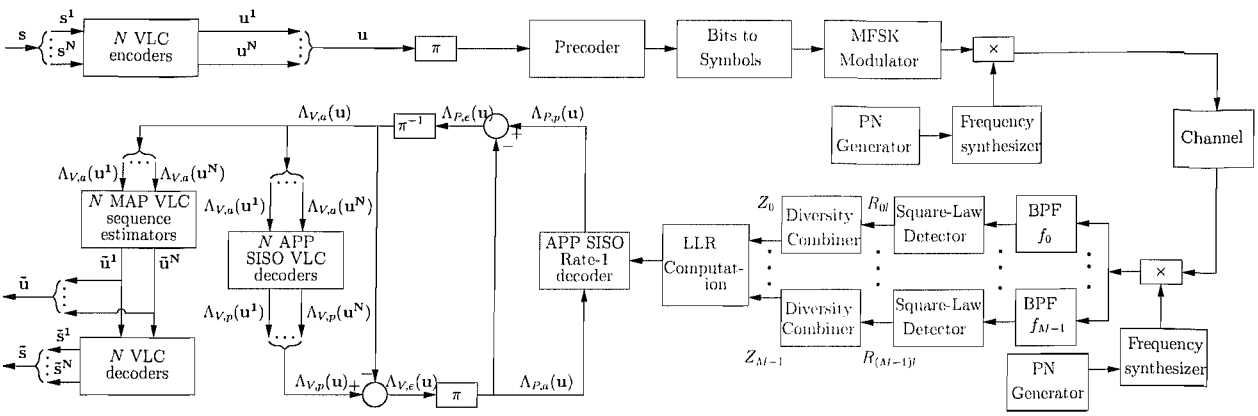


**Figure 5.15:** Schematic of the IrVLC- and VLC-based schemes employed in conjunction with FFH-MFSK. In the IrVLC coded scheme $N = 16$, whilst $N = 1$ in the VLC-coded scheme.

$N_v = 1$ in the case of the VLC-based scheme. The number of symbols in the source symbol frame $\mathbf{s}$ that are decomposed into the source symbol frame component $\mathbf{s^n}$ is specified as $J^n$, where we have $J^1 = J$ in the case of the VLC-based scheme. By contrast, in the case of the IrVLC-based scheme, the specific values of $\{J^n\}_{n=1}^{N_v}$ may be chosen in order to shape the inverted EXIT curve of the IrVLC codec so that it does not cross the EXIT curve of the precoder, as will be detailed below.

Each of the $N_v$ number of source symbol frame components $\{\mathbf{s^n}\}_{n=1}^{N_v}$ is VLC-encoded using the corresponding codebook from the set of $N_v$ number of VLC codebooks $\{\mathbf{VLC}^n\}_{n=1}^{N_v}$, having a range of coding rates $\{R^n\}_{n=1}^{N_v} \in [0, 1]$, satisfying

$$\sum_{n=1}^{N} \alpha_n R^n = R, \tag{5.43}$$

where $\alpha_n = J^n/J$ is the particular fraction of the source symbol frame coded by the $n$th sub-code and $R$ is the average code rate of the VLC or the IrVLC scheme. The specific source symbols having the value of $k \in [1 \ldots K_s]$ and encoded by the specific VLC codebook $\mathbf{VLC}^n$ are represented by the codeword $\mathbf{VLC}^{n,k}$, which has a length of $\mathcal{I}^{n,k}$ bits. The $J^n$ number of VLC codewords that represent the $J^n$ number of source symbols in the source symbol frame component $\mathbf{s^n}$ are concatenated to provide the transmission frame component $\mathbf{u^n} = \{\mathbf{VLC}^{n,s^n_{jn}}\}_{jn=1}^{J^n}$.

Owing to the variable length of the VLC codewords, the number of bits comprised by each transmission frame component $\mathbf{u^n}$ will typically vary from frame to frame. In order to facilitate the VLC decoding of each transmission frame component $\mathbf{u^n}$, it is necessary to explicitly convey its length $\mathcal{I}^n = \sum_{jn=1}^{J^n} \mathcal{I}^{n,s^n_{jn}}$ to the receiver with the aid of side information. Furthermore, this highly error-sensitive side information must be reliably protected against transmission errors. This may be achieved using a low rate block code or repetition code, for example. For the sake of avoiding obfuscating details, this is not shown in Figure 5.15.

**FFH-MFSK modulation:** The $N_v$ number of transmission frame components $\{\mathbf{u^n}\}_{n=1}^{N_v}$ are concatenated at the transmitter, as shown in Figure 5.15. The resultant transmission frame $\mathbf{u}$ has a length of $\sum_{n=1}^{N_v} \mathcal{I}^n$ bits. Following the interleaver, the transmission frame $\mathbf{u}$ is precoded and the precoded bits are converted to $M$-ary symbols [171], which are transmitted by the FFH-MFSK modulator of Figure 5.15, as

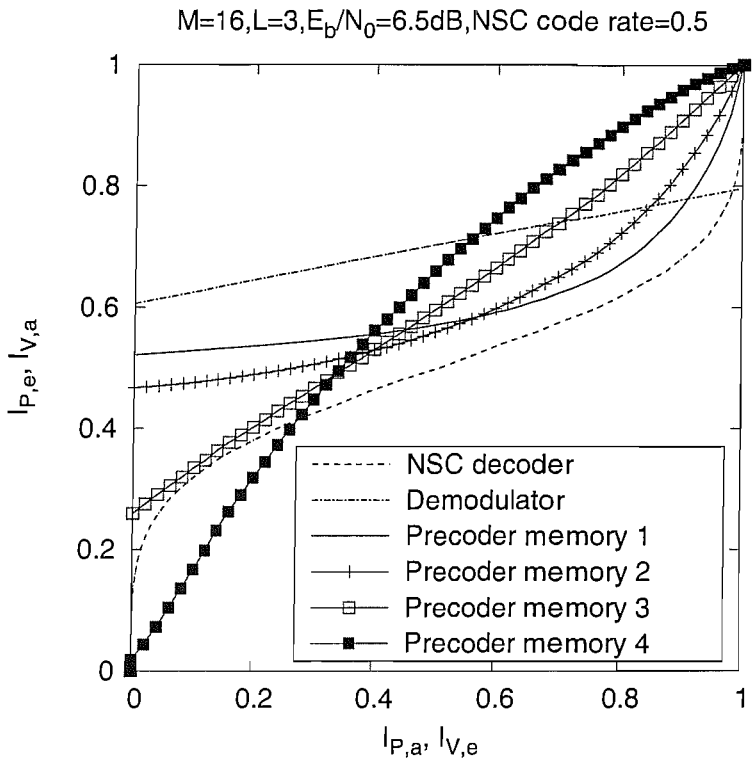


**Figure 5.16:** Extrinsic information transfer characteristics of the rate-1 decoder in Rayleigh fading channel, assuming various values of the precoder memory.

discussed in Section 1.3.1.

**The Channel:** The channel is assumed to be a frequency-flat Rayleigh fading medium for each of the transmitted frequencies. The transmitted signal is also corrupted by AWGN and a PBNJ signal having single-sided power spectral densities of $N_0$ and $N_J$, respectively. We assume that the PBNJ signal jams a fraction $0 \leq \rho \leq 1$ of the total spread spectrum bandwidth $W_{ss}$. We also assume that the PBNJ signal is contiguous and hence all the $M$ FSK tones of a particular band are jammed, if the jamming signal is present in that band. Thus, the probability that a band or a tone is jammed is given by $\rho$, while the probability that the band is not jammed is $(1-\rho)$.

**FFH-MFSK demodulation:** The receiver schematic is also shown in Figure 5.15, where the FFH-MFSK demodulator is identical to that discussed in Section 1.3.3, except that clipped combining is performed as expressed by Equations (1.35) and (1.30) [71]. After FFH-MFSK demodulation and derivation of soft information discussed in Section 5.3.1, the *a posteriori probabilities* (APP) SISO unity rate decoder and the outer decoder perform iterative decoding, as shown in Figure 5.15.

The MI transfer characteristics of the unity-rate decoder recorded for various values of precoder memory are shown in Figure 5.16. It can be seen that the as the precoder's memory is increased, the EXIT curves become steeper. Moreover, in contrast to the demodulator, the rate-1 decoder's EXIT curves do indeed reach the $(1,1)$ point in Figure 5.16, implying that the precoder allows the iterative decoding to converge to an arbitrarily low BER. In our subsequent analysis, we opt for a memory 3 precoder.

**VLC decoding:** Since $N_v$ number of separate VLC encoders are employed in the transmitter, $N_v$ number of separate VLC decoders are employed in the corresponding receiver seen in Figure 5.15. In parallel to the composition of the bit-based transmission frame $\mathbf{u}$ from $N_v$ number of VLC components, the *a priori* LLRs $\Lambda_{V,a}(\mathbf{u})$ are decomposed into $N_v$ number of components, as shown in Figure 5.15. This is achieved with the aid of the explicit side information that we assume for conveying the number of bits $\mathcal{I}^n$ in each transmission frame component $\mathbf{u^n}$. Each of the $N_v$ number of VLC decoders is provided with the *a priori* LLR sub-frame $\Lambda_{V,a}(\mathbf{u^n})$ and in response it generates the *a posteriori* LLR sub-frame $\Lambda_{V,p}(\mathbf{u^n})$, $n \in [1 \dots N_v]$. These *a posteriori* LLR sub-frames are concatenated in order to provide the *a posteriori* LLR frame $\Lambda_{V,p}(\mathbf{u})$, as shown in Figure 5.15.

During the final decoding iteration, $N_v$ number of bit-based MAP VLC sequence estimation processes are invoked instead of single-class APP SISO VLC decoding, as shown in Figure 5.15. In this case, each transmission frame component $\mathbf{u^n}$ is estimated from the corresponding *a priori* LLR frame component $\Lambda_{V,a}(\mathbf{u^n})$.

**System parameter design and Results:** Next we characterise the IrVLC- and VLC-based schemes with the aid of EXIT charts. We opted to employ $N_v = 16$ component VLC codebooks $\{\mathbf{VLC}^n\}_{n=1}^{N_v}$ having approximately equally spaced coding rates in the range $[0.2, 0.95]$ in our proposed IrVLC-FFH-MFSK scheme. In each case, we employ a Variable Length Error Correcting (VLEC) codebook [189] that is tailored to the source symbol values' probabilities of occurrence described above. By contrast, in the VLC scheme, we employ just $N_v = 1$ VLC codebook, which is identical to the VLC codebook $\mathbf{VLC}^{10}$ of the IrVLC scheme, having a coding rate of $R = 0.5$. Note that this coding rate results in an average interleaver length of $J \cdot E/R$ bits. In Figure 5.17 we provide the inverted EXIT curves that characterise the bit-based APP SISO VLC decoding of the above-mentioned VLC codebooks, together with the rate-1 decoder's EXIT curves at $E_b/N_0$ values of 5.7 and 5.9 dB, assuming an interference-free, uncorrelated Rayleigh fading channel.

Figure 5.17 also shows the inverted EXIT curve of the IrVLC scheme. This was obtained as the appropriately weighted superposition of the $N_v = 16$ component VLC codebooks' inverted EXIT curves, where the weight applied to the inverted EXIT curve of the component VLC codebook $\mathbf{VLC}^n$ is proportional to the specific number of source symbols employed to encode $J^n$ [185]. Using the approach of [185], the values of $\{J^n\}_{n=1}^{N_v}$ given in Figure 5.17 were designed so that the IrVLC coding rate matches that of our regular VLC scheme, namely 0.5. Furthermore, we ensured that the inverted IrVLC EXIT curve did not cross the rate-1 decoder's EXIT curve at $E_b/N_0$ of 5.7dB. We note that only 4 of the 16 VLC components are indeed chosen by the algorithm of [185] to encode a non-zero number of source symbols. As shown in Figure 5.17, the presence of the resultant open EXIT chart tunnel implies that an infinitesimally low BER may be achieved by the IrVLC-FFH-MFSK scheme for $E_b/N_0$ values above 5.7dB. By contrast, an open EXIT chart tunnel is not afforded for $E_b/N_0$ values below 5.9dB in the case of the benchmarker VLC-based scheme.

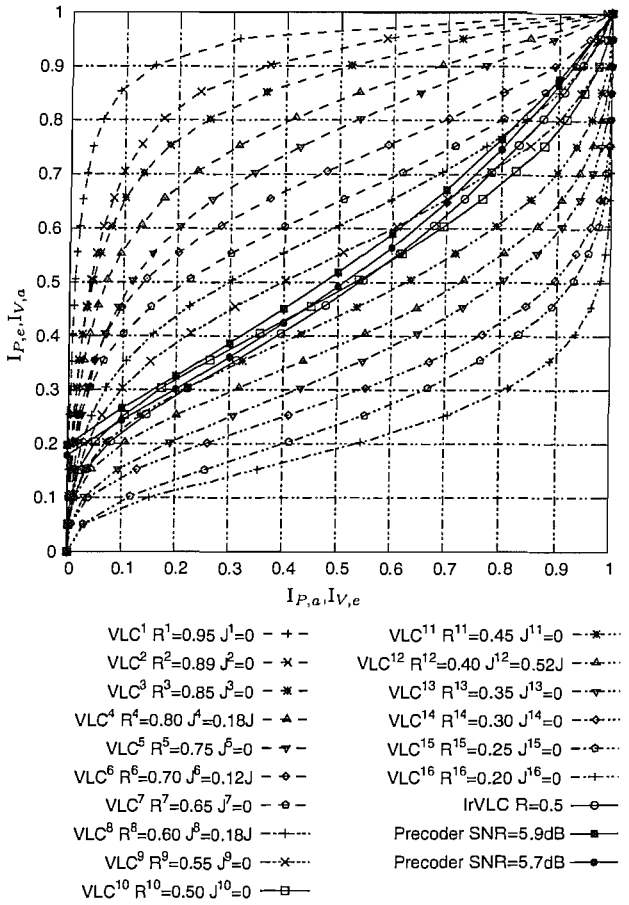


**Figure 5.17:** Inverted VLC EXIT curves and rate-1 decoder's EXIT curves, assuming an interference-free, uncorrelated Rayleigh fading channel.

Analogous to the IrVLC design of Figure 5.17 created for the interference-free channel, we have also designed an IrVLC code for the Rayleigh fading channel contaminated by PBNJ, assuming $E_b/N_J = 10$dB and $\rho = 0.1$. The values of $J^n, n = 1, \ldots, 16$ optimized for this particular jammed channel are $[0\ 0\ 0\ 0.24\ 0\ 0\ 0\ 0.22\ 0\ 0.03\ 0\ 0.5\ 0\ 0\ 0\ 0] \times J$.

The EXIT characteristics were verified by carrying out the ID process of Figure 5.15 and recording the MI values at the output of the inner and outer decoders, as seen in Figure 5.18. We observe that the iterative trajectory more or less follows the EXIT curves of the inner and outer IrVLC decoder, confirming the accuracy of our EXIT chart analysis.

The performance predictions of Figure 5.17 are verified by the BER versus $E_b/N_0$ simulation results of Figure 5.19, where we assume $E_b/N_J = 10$dB and $\rho = 0.1$, when the transmitted signal encounters PBNJ. We observe that, as predicted by the EXIT chart of Figure 5.17, the IrVLC scheme achieves an arbitrarily low BER at $E_b/N_0$ values in excess of 5.7 dB in interference-free channels and at 6.6dB in the channels contaminated by PBNJ. The corresponding $E_b/N_0$ values for the VLC-based scheme are 5.9 and 6.9 dB. We also observe that both of the precoded systems, namely the VLC and the IrVLC-based schemes, yield superior performance compared to the system operating without the precoder, attaining a $E_b/N_0$ gain of approximately 7dB at BER of $10^{-4}$ in the jammed channel. The BER improvement over the system using

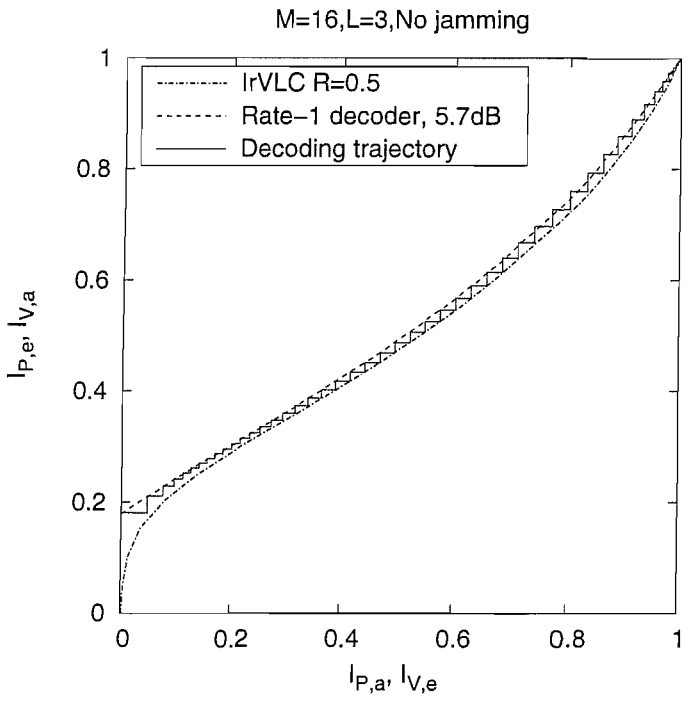


**Figure 5.18:** IrVLC and rate-1 decoder's EXIT curves as well as decoding trajectory, assuming an interference free, uncorrelated Rayleigh fading channel.

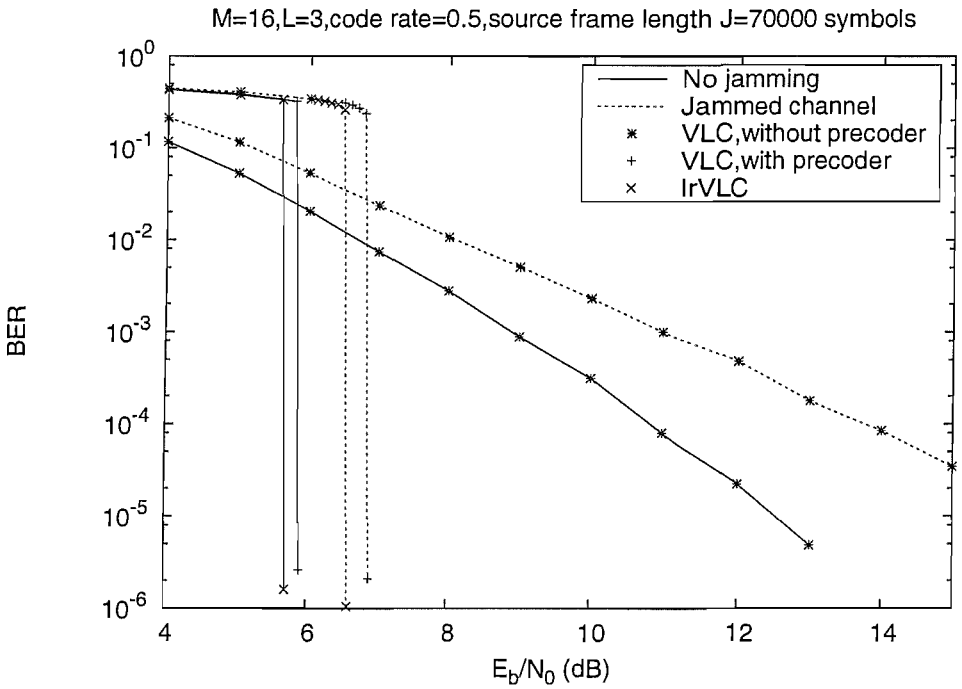


**Figure 5.19:** BER versus $E_b/N_0$ performance of the VLC and IrVLC based schemes, in jammed as well as an interference-free, uncorrelated Rayleigh fading channels. $E_b/N_J = 10$dB and $\rho = 0.1$ is assumed in the jammed channel.

no precoder is achieved at the cost of an increased complexity imposed by the increased number of decoding iterations. For example, the IrVLC-based scheme requires 80 iterations to reach convergence at 6.6dB in the jammed channel. Naturally, the number of iterations can be significantly reduced by raising the $E_b/N_0$

value by as little as 0.1 or 0.2dB.

## 5.5 Soft-SIC Scheme

In Sections 5.3 and 5.4, we investigated the conventional ID assisted FFH-MFSK system using EXIT chart analysis and proposed various means of improving the achievable iterative gain. We demonstrated in Section 5.3 that the iterative gain attained by the FFH-MFSK scheme assisted by conventional ID is not significant, especially at high SNR values and diversity orders. Similarly, the precoded scheme investigated in Section 5.4, although attractive in channels contaminated by PBNJ, does not yield appreciable performance improvements in the presence of MUI. These observations motivate us to employ SISO assisted SIC in FFH-MFSK to combat detrimental effects of MUI.

It is well-known that the SISO decoder provides soft information about the reliability of the encoded bits and hence about the received symbols. Therefore, it is intuitive to surmise that some form of interference cancellation based on the SISO decoder's output may be employed for mitigating the detrimental effects of MUI. In this section, we propose a novel scheme which invokes SIC with the aid of soft output of the decoder. The basic philosophy of this scheme is that the demodulator exploits the soft information fed back by the decoder in order to cancel the interference imposed by reliable symbols. The reliability of the symbols is quantified in terms of the *a posteriori* symbol probabilities at the SISO decoder output. In the subsequent stage of detection and decoding, the interference imposed by symbols declared reliable in the previous stage is removed. The basic principle of the SIC scheme is the same used in [143,194,195] and also exploited in our schemes proposed for uncoded FFH-MFSK in Chapter 4. However, in the context of this soft information based SIC scheme, the SISO decoder assists the demodulator in testing the reliability of the symbols. The reliability test is devised on the principle of Viterbi's RTT [106], although in the context of our soft SIC scheme, the RTT is invoked on the received symbol probabilities instead of on the demodulator's outputs.

We will investigate the proposed concept in the context of two different system configurations, in order to demonstrate that the proposed algorithm is applicable both to binary and non-binary coding scheme, as well as to various types of diversity combining schemes. More specifically, in the first configuration, the FFH-MFSK is convolutionally encoded and the receiver employs SLC. This configuration is identical to the one considered in Section 5.2 and the SIC scheme employing this configuration will be elaborated in Section 5.5.1. The second configuration employs nonbinary low density parity check (LDPC) coding [196–198] and product combining in the receiver. The SIC scheme employed in this configuration is the subject of Section 5.5.2.

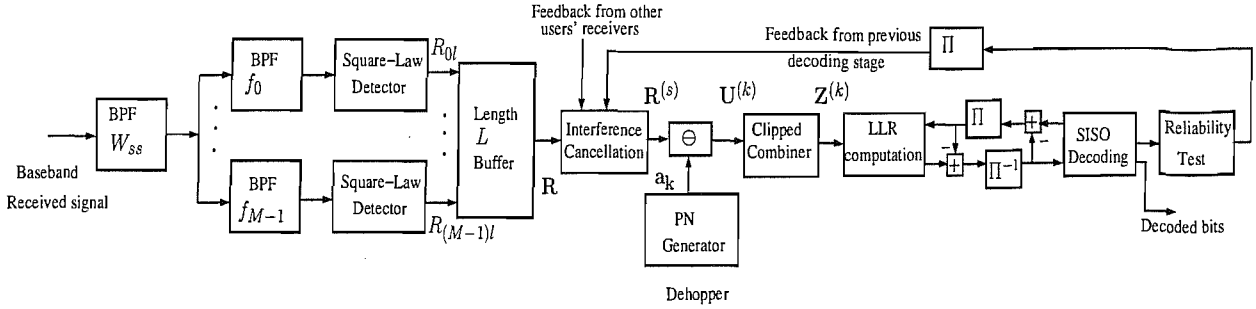


**Figure 5.20:** Block diagram of the FFH-MFSK receiver, corresponding to the $k$th user, $k = 1, 2, \ldots, N_U$, invoking SISO decoding and Soft-SLC-SIC scheme.

### 5.5.1 Soft-SLC-SIC Scheme

Let us now outline the proposed algorithm in the context of the first configuration which we refer to as the Soft-SLC-SIC scheme. The block diagram of the $k$th FFH-MFSK receiver invoking SISO decoding and Soft-SLC-SIC scheme is seen in Figure 5.20. The algorithm is also outlined in the form of a flowchart in Figure 5.21. The system is the same as that described in Section 5.2 and all the assumptions of Section 5.2 apply here, except that the BS receiver employs SIC based MUD.

1) As seen in Figure 5.20, the matrix $\mathbf{R}$ hosting the square-law detector outputs is separately dehopped by each receiver using the corresponding unique user address, resulting in the matrix $\mathbf{U}^{(k)}, k = 1, 2, \ldots, N_U$, for the $k$th user. The dehopping process may be expressed as

$$U_{pl}^{(k)} = R_{nl}, \text{given } p = n \ominus a_k(l), \quad n, p = 0, 1, \ldots, M-1; l = 0, 1, \ldots, L-1. \tag{5.44}$$

2) Clipped combining or SLC is performed on the dehopped signals of Figure 5.20, resulting in $M$ decision variables for each of the users. The clipping operation may be expressed by [48]

$$f(U_{nl}^{(k)}) = \begin{cases} C, & \text{if } U_{nl}^{(k)} \geq C \\ U_{nl}^{(k)}, & \text{otherwise,} \end{cases} \tag{5.45}$$

where $C$ represents an appropriately chosen clipping threshold. The decision variable recorded after clipped combining for the $k$th user is given by [48]

$$Z_n^{(k)} = \sum_{l=0}^{L-1} f(U_{nl}^{(k)}), \qquad n = 0, 1, ..., M-1. \tag{5.46}$$

3) From the diversity combiner outputs of Figure 5.20, the soft information, as derived in Section 5.3, is passed as *a priori* input to the SISO decoder. The extrinsic information $\Lambda_{D,e}^{(k)}$ for the $k$th user is obtained from the *a posteriori* output of the SISO decoder by subtracting the *a priori* input from it, yielding $\Lambda_{D,e}^{(k)} = \Lambda_{D,p}^{(k)} - \Lambda_{D,a}^{(k)}$. The extrinsic information $\Lambda_{D,e}^{(k)}$ is then fed back as the demodulator's

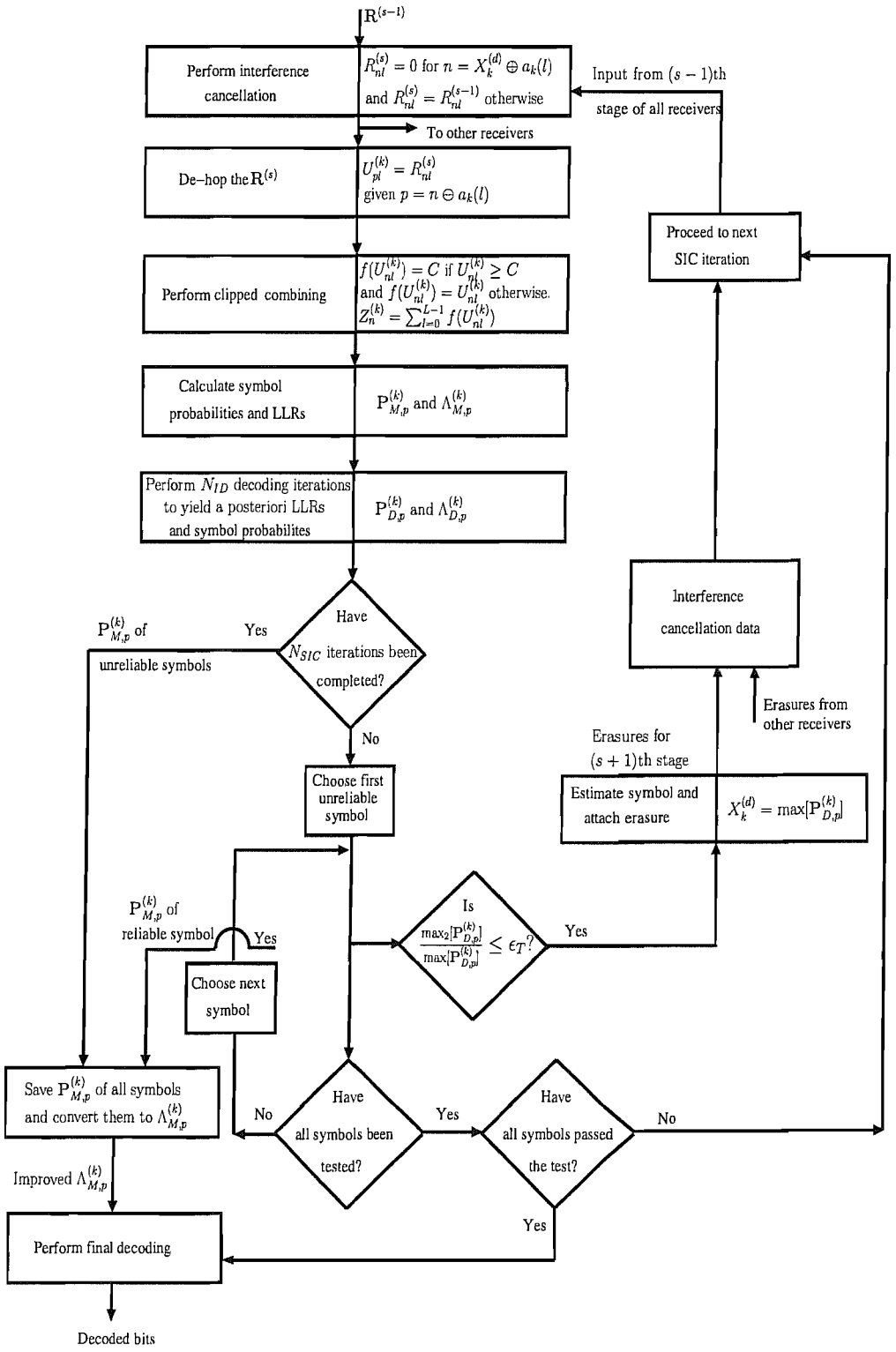


**Figure 5.21:** Flowchart of the Soft-SLC-SIC algorithm, proposed in Section 5.5.1, for the $k$th user, $k = 1, 2, \ldots, N_U$.

*a priori* input $\Lambda_{M,a}^{(k)}$. This ID process between the serially concatenated FFH-MFSK demodulator and the outer SISO decoder may be invoked $N_{ID}$ number of times, $N_{ID} = 0, 1, \ldots$. Upon completing $N_{ID}$ such iterations, the SISO decoder generates the *a posteriori* LLRs $\Lambda_{D,p}^{(k)}$, which are then converted to equivalent bit probabilities and then to symbol probabilities $\mathbf{P}_{D,p}^{(k)}$, using the relation [171]

$$P(X_k = n) = \prod_{i=0}^{b-1} P(b_i), \qquad b_i = (\lfloor \frac{n}{2^i} \rfloor)_2, \tag{5.47}$$

where $(x)_2$ denotes the modulo-2 value of the integer $x$.

4) Next, as seen in Figure 5.20 a reliability test of all users' symbols is carried out. Specifically, if the ratio of the second largest to the largest of the $M$ number of *a posteriori* probabilities $\mathbf{P}_{D,p}^{(k)}$ corresponding to a symbol is less than a predefined threshold $\epsilon_T$, that is, if we have

$$\epsilon^{(k)} = \frac{\max_2 [\mathbf{P}_{D,p}^{(k)}]}{\max [\mathbf{P}_{D,p}^{(k)}]} < \epsilon_T, \tag{5.48}$$

then the symbol is declared reliable, else it is deemed unreliable. Intermediate estimates of the reliable symbols are then generated from the *a posteriori* symbol probabilities using conventional hard decisions. Specifically, if the $k$th user's symbol, $k = 1, 2, \ldots, N_U$ satisfies the reliability test given in the inequality (5.48), then $X_{k(e)}$ is the estimate of the $k$th user's symbol, where $X_{k(e)} = 0, 1, \ldots, M-1$, is the index of the maximum of $\mathbf{P}_{D,p}^{(k)}$. Note that this estimate is performed only for the sake of cancellation of interference, as explained in the following step. The actual decoded bits are obtained at the end of SIC stages through the final hard decoding process. If no user passes the test, we earmark that specific user's symbol for subsequent erasure, which has the lowest value of $\epsilon$. The symbol probabilities $\mathbf{P}_{M,p}^{(k)}$ corresponding to the reliable symbols are stored.

5) If some but not all symbols are declared reliable, we proceed with the $s$th stage of SIC, where $s = 1, 2, \ldots$. We also define $\mathbf{R}^{(s)}$ as the modified form of $\mathbf{R}$ at the $s$th stage, as seen in Figure 5.20. The $s$th stage of the SIC, $s \geq 1$, consists of the following steps:

   (a) The matrix $\mathbf{R}^{(s-1)}$ is modified by partially erasing the elements representing the signals, which correspond to all the symbols that were declared reliable in the $(s-1)$th stage (Step 4). Hence, if $X_{k(e)}$ is the estimated symbol of the $k$th user, then, after interference cancellation, we have

$$R_{nl}^{(s)} = \begin{cases} \delta_c R_{nl}^{(s-1)} & \text{for } n = X_{k(e)} \oplus a_k(l) \\ R_{nl}^{(s-1)} & \text{otherwise,} \end{cases} \tag{5.49}$$

   where $\delta_c$, $0 < \delta_c < 1$, represents a suitably chosen cancellation coefficient.

   (b) Dehopping is performed on the modified received matrix $\mathbf{R}^{(s)}$ as expressed by Equation (5.44) in Step 1 above.

(c) Clipped combining is performed on the new dehopped matrix as expressed by Equations (5.45) and (5.46).

(d) Given the new diversity combiner outputs, the symbol probabilities are derived, as discussed in Section 5.3. Note that in each SIC iteration, corresponding to the symbols already declared reliable, we use the symbol probabilities $\mathbf{P}_{M,p}^{(k)}$ generated during the specific SIC stage in which they were declared reliable. For the remaining unreliable symbols, new values of symbol probabilities are obtained. The symbol probabilities are converted to equivalent bit probabilities and the corresponding LLR values $\Lambda_{M,p}^{(k)}$ are passed to the SISO decoder as its *a priori* input, which generates improved *a posteriori* LLRs $\Lambda_{D,p}^{(k)}$. The *a posteriori* LLRs are then converted to equivalent bit probabilities and then to the symbol probabilities $\mathbf{P}_{D,p}^{(k)}$ [171]. Also note that we have $N_{ID} = 0$ in each of the $s$th SIC iteration, where $s \geq 1$.

(e) Next, the reliability test given in Step 4 and inequality (5.48) above is performed using the new symbol probabilities $\mathbf{P}_{D,p}^{(k)}$ to earmark reliable symbols for subsequent cancellation.

6) The SIC iterations which include Steps 5 (a) to (e) above may be continued until the affordable number $N_{SIC}$ of SIC iterations have been completed, at the end of which, convolutional hard decoding is performed using the symbol probabilities $\mathbf{P}_{M,p}^{(k)}$ and LLRs $\Lambda_{M,p}^{(k)}$ obtained at the end of last SIC iteration.

We refer to this SIC scheme as Soft-SLC-SIC($N_{ID}, N_{SIC}$) in order to emphasize the number of ID and SIC iterations employed. The reason for employing a cancellation coefficient $\delta_c$ in (5.49) is explained in Section 4.4.2.

We note that in the context of the proposed Soft-SLC-SIC scheme, the SISO decoder does not provide soft feedback to the demodulator in the conventional iterative decoding sense [160, 161]; however, the *a posteriori* information from the decoder is used to determine which symbols are reliable, thus effective interference cancellation is facilitated. A difference between the uncoded SLC-SIC scheme proposed in Chapter 4 and the Soft-SLC-SIC scheme is that in the former the detection is carried out on a symbol-by-symbol basis, while in the later, although reliability test is performed on a symbol-by-symbol basis, the final decoding is done on the complete code block after all SIC iterations have been completed.

### 5.5.2 Soft-PC-SIC Scheme

In this section, we extend the idea of SISO assisted SIC to product combining (PC) [44] and employ non-binary LDPC codes [196–200] instead of binary convolutional encoding, which creates a purely symbol-based $M$-ary scheme. More explicitly, the $M$-ary symbols are encoded using LDPC codes over GF($q$). Furthermore, by employing non-binary LDPC coding, we can process symbol probabilities in the receiver, instead of LLRs, which allows us to dispense with conversion from symbol probabilities to LLRs and vice versa. Moreover, since a FFH-MFSK modulated symbol is transmitted in $L$ different frequencies,

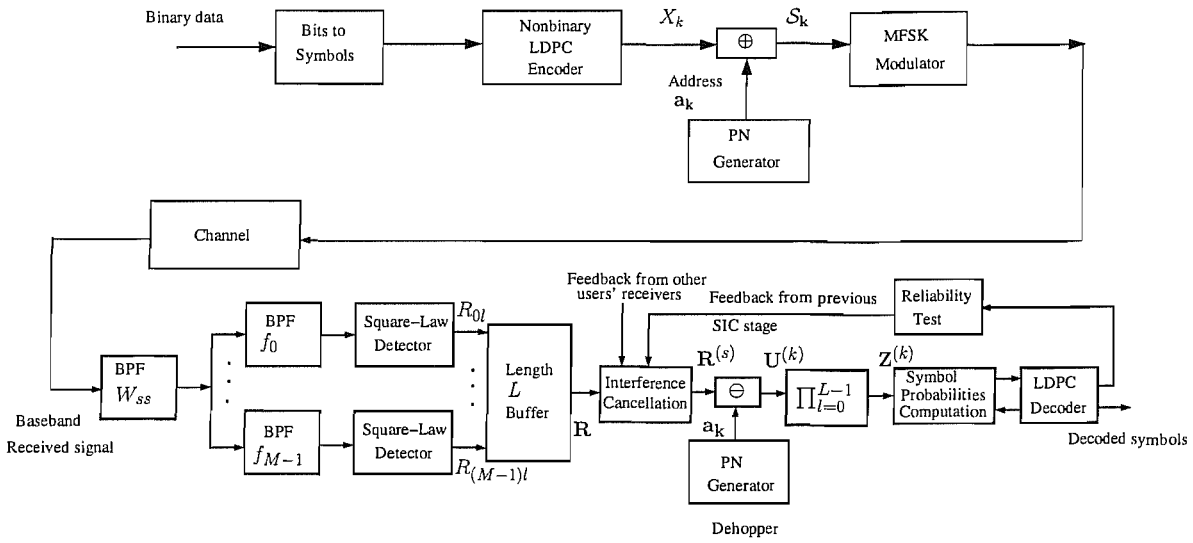


**Figure 5.22:** Block diagram of the FFH-MFSK system for the $k$th user, $k = 1, 2, \ldots, N_U$, employing non-binary LDPC channel coding and Soft-PC-SIC scheme in the receiver.

the channel appears uncorrelated to the transmitted signal and therefore no interleaving of the symbols is needed. Hence, the proposed system is eminently suitable for low-delay applications. Finally, since it is challenging to derive the soft metrics for the PC receiver, we propose a sub-optimum metric for deriving the required symbol probabilities from the diversity combiner's outputs. We will compare the performance of the proposed SIC scheme with that invoking SUD and conventional ID between the SISO decoder and the FFH-MFSK demodulator.

The family of LDPC codes, originally devised by Gallagher [196, 197], have attracted a lot of attention in the last few decades owing to their simple decoding structure and near-capacity performance. In [201] LDPC codes over GF(q) were proposed and have been shown to outperform binary LDPC codes [199]. Nonbinary LDPC codes may be used with $M$-ary and multilevel modulation scheme.

In the transmitter, all users' $M$-ary symbols are encoded by a nonbinary LDPC code [199], as shown in Figure 5.22. The encoded $M$-ary symbols are modulated using a FFH-MFSK modulator as discussed in Section 5.2. All the assumptions made in Section 5.2 also apply.

**Suboptimum Soft Metric:** A number of suboptimum soft metrics have been proposed for the family of noncoherent MFSK based systems [165, 166, 174]. Most of these metrics derive the LLR values from the detectors' outputs. In order to employ a soft metric for our proposed SIC scheme, it should be based on the symbol probabilities rather than on the LLRs, because our test of symbols is based on the symbol probabilities. Hence, we invoke a soft metric which is derived by self-normalization of the diversity combiners' outputs. This soft metric was also discussed in [174, 202], although it has not been employed for the PC receiver before. In the context of this metric, the *a posteriori* symbol probability corresponding to the $n$th PC output of the $k$th user is given by

$$P_{M,p}^{(k)}(X_k = n) = \frac{Z_n^{(k)}}{\sum_{j=0}^{M-1} Z_j^{(k)}}, \qquad n = 0, 1, ..., M-1, \tag{5.50}$$

where $\mathbf{Z}^{(k)}$ represents the set of $M$ PC outputs for the $k$th user, seen in Figure 5.22.

The non-binary LDPC decoder accepts the set of $M$ symbol probabilities $\mathbf{P}_{M,p}^{(k)}$ from the demodulator, subtracts the *a priori* input from its *a posteriori* symbol probabilities $\mathbf{P}_{D,p}^{(k)}$ to yield the extrinsic output, which may be fed back to the demodulator as its *a priori* symbol probabilities, for further assisting the demodulator to improve its soft information output. In conventional ID, this exchange of soft information between the demodulator and decoder may be invoked a number of times [177]. We will refer to this conventional scheme as SUD-ID scheme.

**The SIC algorithm:** Let us now outline our proposed Soft-PC-SIC algorithm. This scheme is identical to the Soft-SLC-SIC scheme except for the product combining instead of the clipped combining and nonbinary LDPC coding replacing the convolutional coding. The algorithm is outlined below:

1) As seen in Figure 5.22, the $M \times L$ order matrix $\mathbf{R}$ is separately dehopped by each receiver using the corresponding unique user address, resulting in the matrix $\mathbf{U}^{(k)}, k = 1, 2, \ldots, N_U$, for the $k$th user. The dehopping process is expressed by Equation (5.44).

2) PC is performed on the dehopped signals of Figure 5.22, resulting in $M$ decision variables for each of the users. The decision variable recorded after PC for the $k$th user is given by [44]

$$Z_n^{(k)} = \prod_{l=0}^{L-1} U_{nl}^{(k)}, \qquad n = 0, 1, ..., M-1. \tag{5.51}$$

3) From the PC outputs of Figure 5.22, the set of $M$ symbols probabilities $\mathbf{P}_{M,p}^{(k)}$, derived using Equation (5.50), are passed as *a priori* input to the SISO decoder. The LDPC decoder and the demodulator may exchange extrinsic symbol probabilities with each other, the extrinsic output of one being used as the *a priori* input for the other. This process may be repeated $N_{ID}$ number of times, at the end of which the LDPC decoder generates the *a posteriori* symbols probabilities $\mathbf{P}_{D,p}^{(k)}$.

4) Next, as seen in Figure 5.22, a reliability test of all users' symbols is carried out. Specifically, if the ratio of the second largest to the largest of the $M$ number of *a posteriori* probabilities $\mathbf{P}_{D,p}^{(k)}$ corresponding to a symbol satisfies Equation (5.48), then the symbol is declared reliable, else it is deemed unreliable. The reliable symbols are estimated from the *a posteriori* symbol probabilities $\mathbf{P}_{D,p}^{(k)}$ using conventional hard decisions, as explained in Section 5.5.1.

5) If some but not all symbols are declared reliable, we proceed with the $s$th stage of SIC, where $s = 1, 2, \ldots$. We also define $\mathbf{R}^{(s)}$ as the modified form of $\mathbf{R}$ at the $s$th stage, as seen in Figure 5.22. The $s$th stage of the SIC, $s \geq 1$, consists of the following steps:

(a) The matrix $\mathbf{R}^{(s-1)}$ is modified by partially erasing the elements representing the signals, which correspond to all the symbols that were declared reliable in the $(s-1)$th stage (Step 4). More specifically, if $X_{k(e)}$ is the estimated symbol of the $k$th user, then, the process of interference cancellation is given by Equation (5.49).

(b) Dehopping is performed on the modified received matrix $\mathbf{R}^{(s)}$ as expressed by (5.44) in Step 1 above.

(c) Product combining is performed on the new dehopped matrix as expressed by Equation (5.51).

(d) Given the new diversity combiner outputs, the symbol probabilities are derived using Equation (5.50). In each SIC iteration, corresponding to the symbols already declared reliable, we use the symbol probabilities $\mathbf{P}_{M,p}^{(k)}$ generated during the specific SIC stage in which they were declared reliable. For the remaining unreliable symbols, new values of symbol probabilities are obtained. The symbol probabilities are passed to the SISO decoder as its *a priori* input, which generates improved *a posteriori* symbol probabilities $\mathbf{P}_{D,p}^{(k)}$ [171]. Also we have $N_{ID} = 0$ in each of the $s$th SIC iteration, where $s \geq 1$.

(e) Next, the reliability test given in Step 4 above is performed using the new symbol probabilities $\mathbf{P}_{D,p}^{(k)}$ in order to earmark reliable symbols for subsequent cancellation.

6) The SIC iterations can be continued until the affordable number $N_{SIC}$ of SIC stages have been completed, following which LDPC hard decoding is performed using the symbol probabilities obtained at the end of last SIC stage.

Analogous to the case of the Soft-SLC-SIC scheme discussed in Section 5.5.1, we refer to this scheme as the Soft-PC-SIC($N_{ID}$,$N_{SIC}$).

### 5.5.3 Simulation Results and Discussion on the SIC Schemes

In this section we present our BER performance results for the the SIC schemes proposed in Sections 5.5.1 and 5.5.2, when they are employed in a FFH-MFSK system operating in a frequency-flat uncorrelated Nakagami-$m$ fading MA channel. We will evaluate these SIC schemes with the aid of comparison with the corresponding scheme employing SUD.

We commence our performance analysis with the Soft-SLC-SIC scheme of Section 5.5.1. In our simulations, optimum clipping thresholds $C$ and the test thresholds $\epsilon$, defined in Section 5.5.1, have been employed. Furthermore, unless otherwise stated, we employ the system parameter values listed in Table 5.2. Finally, since the optimum cancellation threshold values vary with the fading channel conditions which are not known in the context of the system considered, we opt for employing fixed cancellation thresholds for various ranges of SNR values. Specifically, we employ $\delta_c = 0.2$ for $E_b/N_0 < 5$dB, $\delta_c = 0.15$ for $5 \leq E_b/N_0 \leq 10$dB and $\delta_c = 0.1$ for $E_b/N_0 > 10$dB.

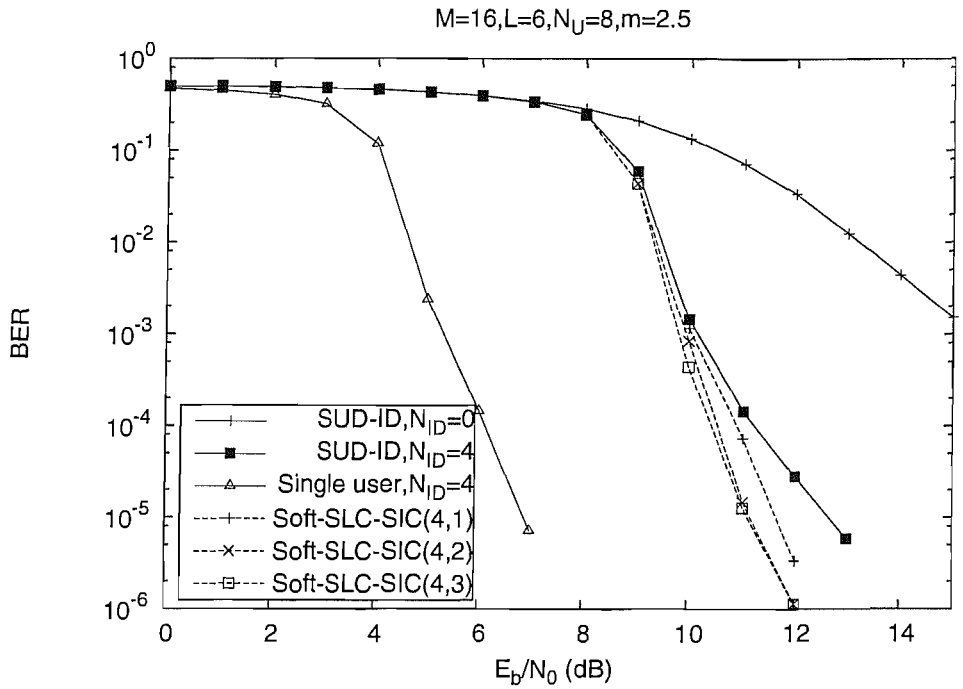


**Figure 5.23:** BER versus $E_b/N_0$ performance of the Soft-SLC-SIC and SUD-ID schemes employed in FFH-MFSK SLC receiver communicating over a Nakagami-$m$ fading MA channel.

In Figure 5.23, the BER versus SNR performance of the SUD-ID scheme, which was discussed in Section 5.3, is compared with that of the proposed Soft-SLC-SIC scheme invoking various number of SIC iterations $N_{SIC}$ following $N_{ID} = 4$ conventional iterations. In this figure we assume $L = 6$, $M = 16$, Nakagami fading parameter of $m = 2.5$ and $N_U = 8$. Also shown is the performance of the SUD-ID scheme in a single-user or interference-free scenario, employing identical system parameters, except that $L = 3$ is used because we discovered that no further diversity gain is achieved in interference-free channel beyond this diversity order. Figure 5.23 demonstrates that by employing the Soft-SLC-SIC scheme, the BER performance can be improved over the SUD-ID scheme employing $N_{ID} = 4$ conventional iterations. Specifically, in the 2nd SIC iteration, shown by the curve labeled as Soft-SLC-SIC(4,2), a gain of approximately 1.5dB is achievable over the SUD-ID scheme with $N_{ID} = 4$ iterations at BER= $10^{-5}$. Furthermore, as seen in Figure 5.23, the third SIC iteration yields negligible performance improvement. Hence, in the next result we opt for using the Soft-SLC-SIC(4,2) configuration. We also observe that the Soft-SLC-SIC(4,2) scheme's performance is inferior to the single-user performance by approximately 4dB at BER= $10^{-5}$.

The SUD-ID and the Soft-SLC-SIC schemes are compared in terms of their BER versus number of users performance in Figure 5.24, where we assume two different channel conditions, one characterised by Nakagami fading parameter of $m = 5$, while the other scenario assumes $m = 1$ which is equivalent to Rayleigh fading. We observe that the Soft-SLC-SIC scheme's performance is superior to that of the SUD-ID scheme using $N_{ID} = 4$ iterations especially at low values of $N_U$, where the SUD-ID scheme suffers from an error floor because the iterative gain drops at lower values of $N_U$. We also observe in Figure 5.24 that when the fading becomes less severe, as characterised by $m = 5$, the difference between the BER

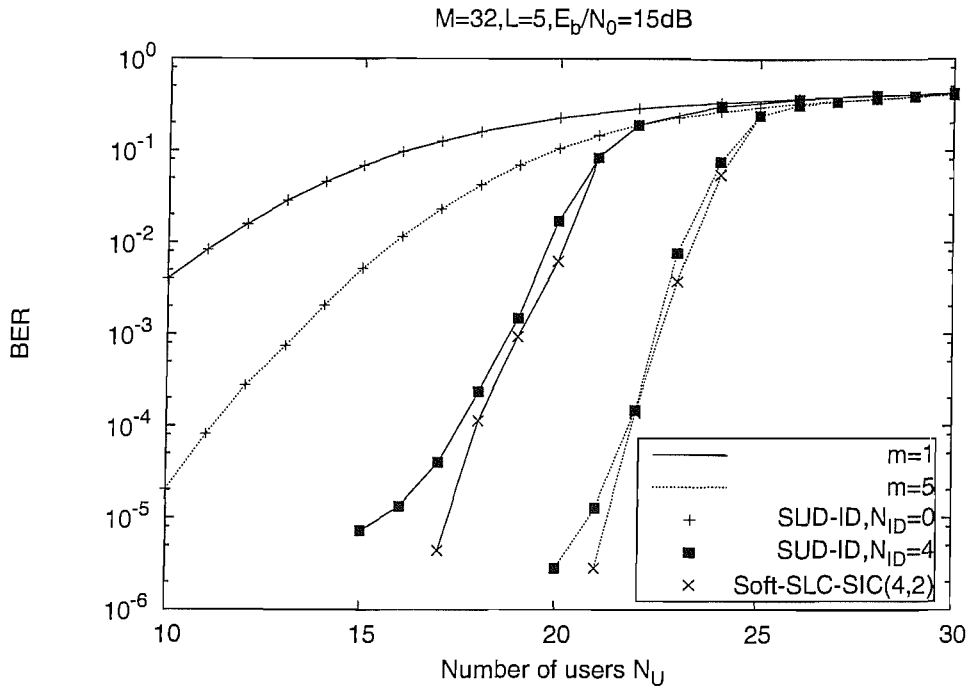


**Figure 5.24:** BER versus number of users performance of the Soft-SLC-SIC and SUD-ID schemes employed in FFH-MFSK SLC receiver communicating over a Nakagami-$m$ fading MA channel.

performance of the two schemes becomes less significant. This observation indicates that the proposed scheme is particularly useful under conditions of severe fading.

Let us now focus our attention on the performance of the Soft-PC-SIC scheme proposed in Section 5.5.2. We have invoked LDPC code constructed over GF(16) and consequently results are shown for $M = 16$ only. Unless otherwise stated, we employ the parameter values listed in Table 5.3 for the simulations on the Soft-PC-SIC scheme.

Note that in our discussion we represent the number of internal iterations of the LDPC decoder as $N_{IN}$ and the number of iterations between the decoder and the demodulator in the context of conventional ID as $N_{ID}$, while the number of SIC iterations is denoted as $N_{SIC}$. Moreover, it has been found that $\delta_c = 0.3$, which was defined in Section 4.4.2 yields optimum results for a wide range of SNR values in the context of the Soft-PC-SIC scheme.

| Channel code | LDPC code over GF(16) |
|---|---|
| Code rate $R_c$ | 0.5 |
| Modulation order $M$ | 16 |
| Code clock length | 24000 bits (6000 4-bits symbols) |

**Table 5.3:** List of parameters values used in the simulation results of Figures 5.25 to 5.29.

We commence with the Soft-PC-SIC(0,$N_{SIC}$) configuration to highlight the effect of SIC iterations only. Figure 5.25 shows the BER versus SNR performance of the Soft-PC-SIC and SUD-ID scheme, assuming

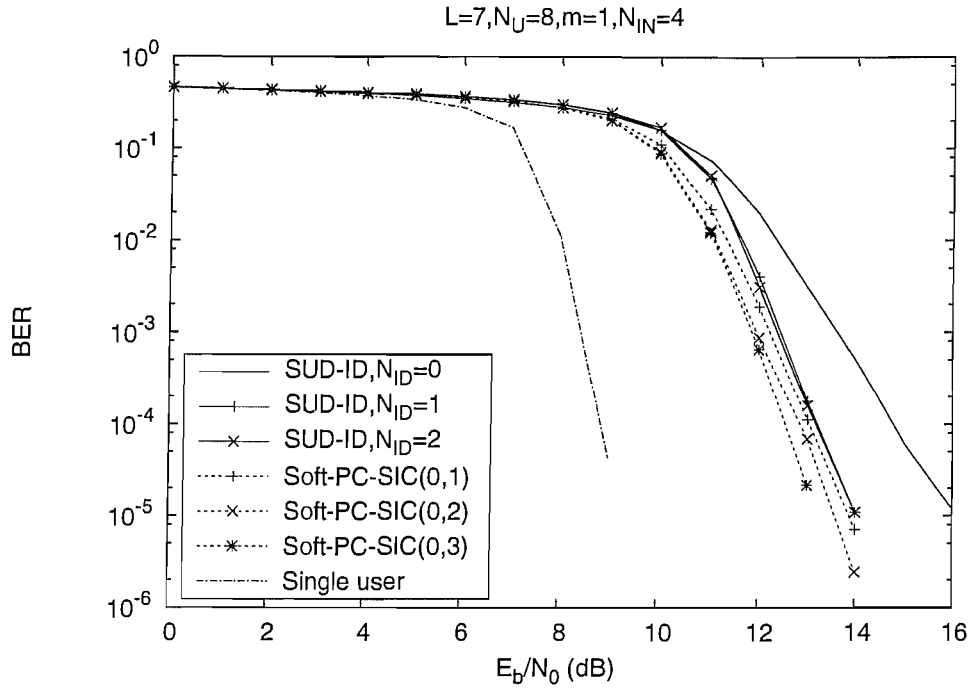


**Figure 5.25:** BER versus $E_b/N_0$ performance of non-binary LDPC coded FFH 16-ary FSK PC receiver communicating over a Rayleigh fading channel, assuming various LDPC, outer and SIC iterations.

$L = 7$ and $N_U = 8$ as well as Rayleigh fading associated with Nakagami paremeter of $m = 1$. As a benchmarker, the single user (interference-free) performance of the FFH-MFSK scheme with $N_{ID} = 1$ is also included. The results of Figure 5.25 demonstrate that at our target BER of $10^{-5}$, the Soft-PC-SIC scheme yields approximately 3dB gain compared to the SUD-ID system using $N_{ID} = 0$ iteration, and about 1dB gain over that using $N_{ID} = 2$ iterations. We also note that the conventional ID process results in no iterative gain after $N_{ID} = 1$ iteration. This is because in the absence of interleaver not much iterative gain is obtained. By contrast, the Soft-PC-SIC scheme yields BER improvements even in the $N_{SIC} = 3$ iterations. Therefore, in the subsequent discussions, unless otherwise specified, we employ $N_{SIC} = 3$ of the SIC scheme and $N_{ID} = 1$ of the SUD-ID scheme.

In Figure 5.26, we consider the BER versus SNR performance of the two schemes considered for various values of the Nakagami parameter $m$. As expected, upon increasing $m$, the performance of both systems improves, although the SNR gain is not significant. This might be because the soft information employed, given by Equation (5.50), does not take into account the channel conditions. Moreover, we observe in Figure 5.26 that the performance difference between the SUD and the SIC scheme is retained for all $m$ values considered.

In Figure 5.27, we consider the BER versus number of users performance of the schemes under consideration, where we assume $L = 5$, Nakagami parameters of $m = 1$ and 10 as well as $E_b/N_0 = 15$dB. We observe that the Soft-PC-SIC scheme performs significantly better than the SUD-ID scheme in terms of supporting more users at a given BER value.

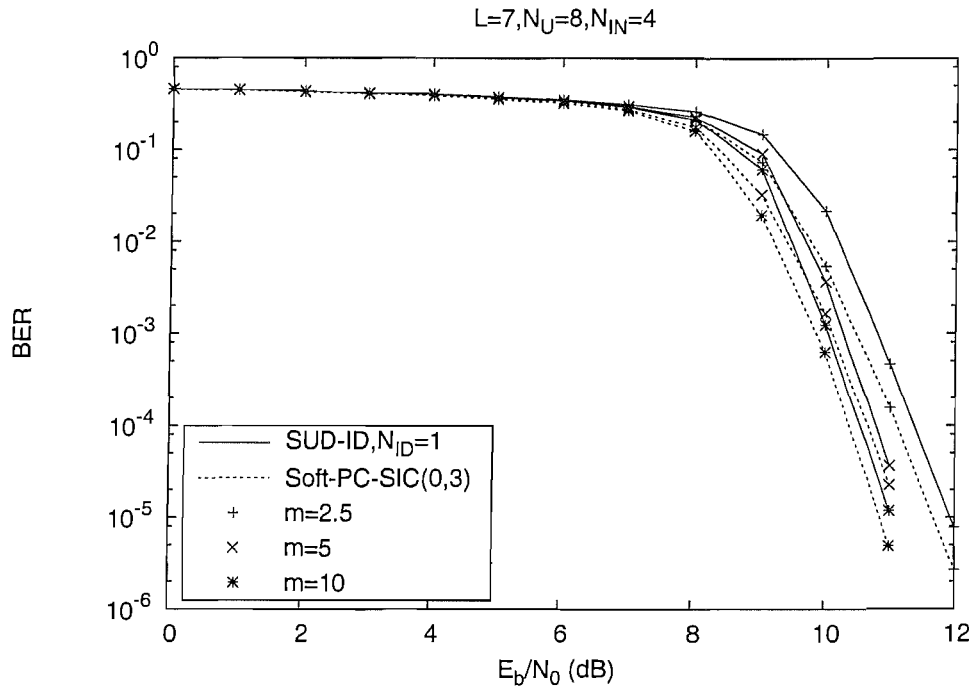


**Figure 5.26:** BER versus $E_b/N_0$ performance of non-binary LDPC coded FFH 16-ary FSK PC receiver communicating over a Nakagami-$m$ fading channel, assuming various $m$ values.

In Figure 5.28, we demonstrate the performance gains attained by the proposed Soft-PC-SIC scheme for various number of LDPC iterations. We assume a Nakagami parameter of $m = 2.5$, while the remaining system parameters are the same as in Figure 5.25. We observe that upon increasing the number of LDPC iterations, further BER improvements are yielded by the SIC scheme, indicating that as expected an increased number of LDPC iterations results in an improved *a posteriori* output of the SISO decoder, thereby assisting in the SIC operations. Hence, at the cost of increased complexity incurred in invoking more LDPC iterations, a combination of LDPC and SIC iterations can yield improved BER performance.

Finally, in Figure 5.29, we show the BER versus SNR performance of the Soft-PC-SIC(1,3) configuration in comparison with those of the other configurations considered in this study. It can be seen that the Soft-PC-SIC(1,3) outperforms the Soft-PC-SIC(0,3) configuration. We conclude that, assisted by $N_{ID} = 1$ outer iteration, the SIC scheme is further improved and now yields a gain of nearly 1 dB over the SUD-ID scheme and of about 0.5 dB over the Soft-PC-SIC(0,3) arrangement at BER of $10^{-5}$. However, we also note that when $N_{IN} = 12$ LDPC iterations are employed, the difference between the Soft-PC-SIC(0,3) and the Soft-PC-SIC(1,3) arrangements is not significant. The reason for this is that when employing a higher number of LDPC's inner iterations, the decoder's *a posteriori* output is sufficiently improved thereby rendering the additional outer iteration nearly insignificant.

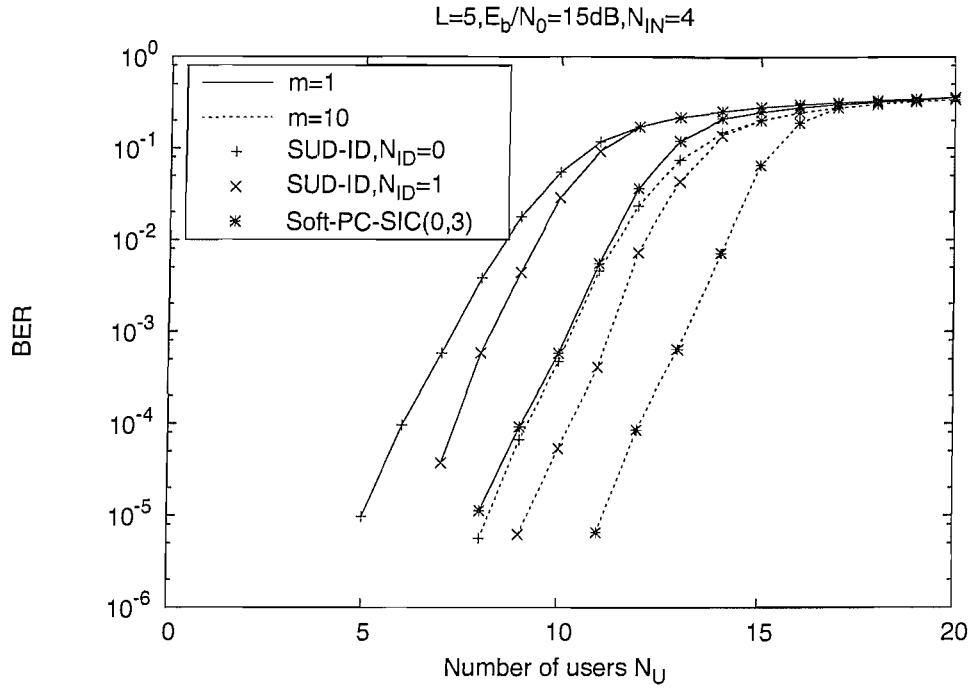


**Figure 5.27:** BER versus number of users performance of non-binary LDPC coded FFH 16-ary FSK PC receiver communicating over a Nakagami-$m$ fading channel, assuming various $m$ values.

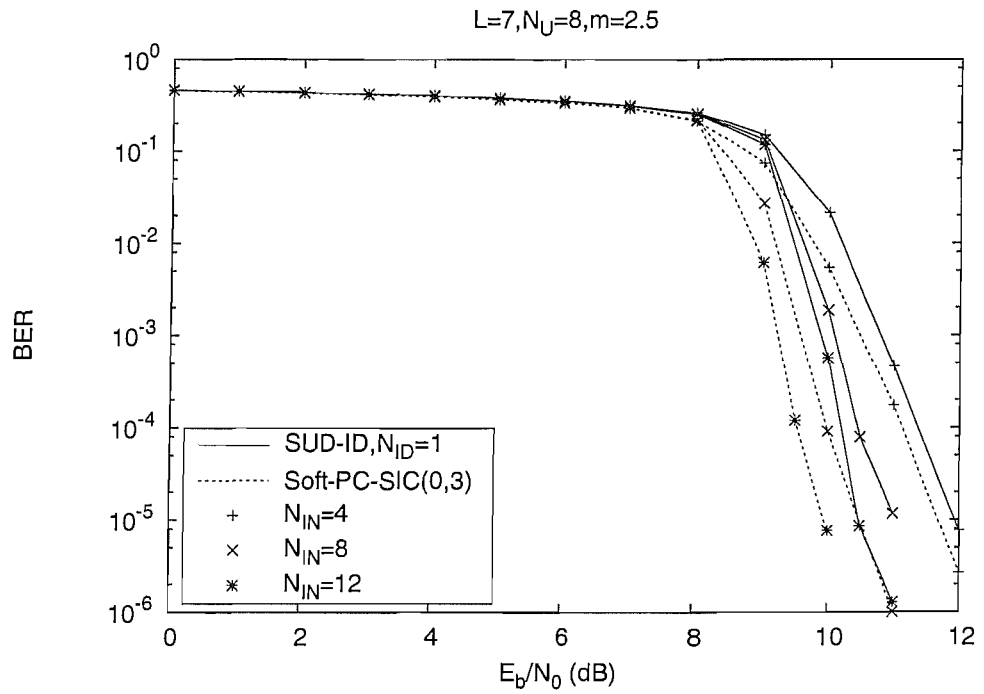


**Figure 5.28:** BER versus $E_b/N_0$ performance of non-binary LDPC coded FFH 16-ary FSK PC receiver communicating over a Nakagami-$m$ fading channel, assuming various number of LDPC iterations $N_{IN}$.

## 5.6 Conclusion

We have investigated ID-assisted FFH-MFSK invoking SLC as well as binary convolutional coding and derived the soft information to be passed from the demodulator to the channel decoder, when operating

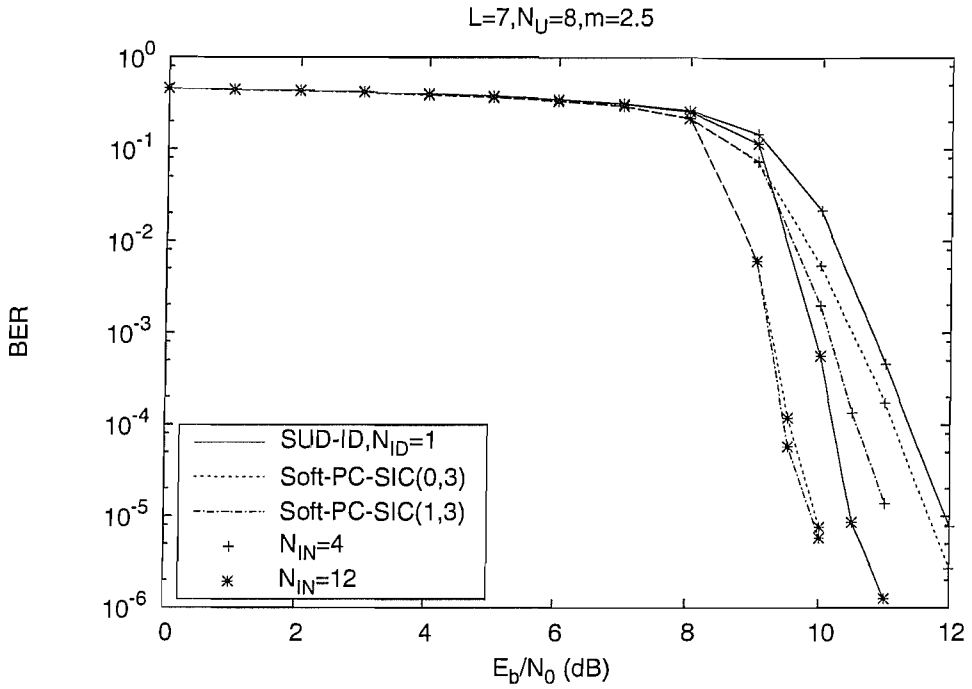


**Figure 5.29:** BER versus $E_b/N_0$ performance of non-binary LDPC coded FFH 16-ary FSK PC receiver communicating over a Nakagami-$m$ fading channel, using the SUD-ID and two configurations of the Soft-PC-SIC scheme.

in Nakagami-$m$ fading MA channels. We employed EXIT charts to gain insights into the parameters that influence the achievable iterative gain, as well into the convergence behaviour of the ID scheme. We also proposed a novel MUD scheme that invokes SIC in conjunction with SISO decoding. The contributions and conclusions of this chapter are summarised below:

1) The soft information derived in Section 5.3 to assist SDD of the coded scheme is based on the assumption of an interference-free channel and linear combining. It may, therefore, be termed as sub-optimal for the scenario considered, which assumes clipped combining aided detection over MA channels. However our results shown in Figures 5.9 to 5.10 demonstrate that useful performance improvements may be achieved over a HDD based scheme, despite using this sub-optimal soft information. The soft information has been derived for the Nakagami-$m$ channels, which cater for a wide range of fading conditions.

2) Our EXIT charts depicted in Figures 5.4 to 5.8 provide interesting insights. More specifically, we found that NSC codes are more suitable than RSC codes for serial concatenation with MFSK based schemes. Secondly, iterative gain is generally low for MFSK based system but it improves upon increasing the modulation order $M$, although it drops at high SNR values. Likewise, a higher diversity order yields better performance but it results in a lower iterative gain. Finally, increased number of users deteriorates the attainable performance, but results in a higher iterative gain. Some of the EXIT chart predictions were also verified by our BER results.

3) We also discovered in Section 5.4 that by employing a unity-rate precoder in the convolutionally encoded FFH-MFSK, the EXIT curve of the corresponding unity-rate decoder can be tailored to a great extent to match that of an outer decoder. We demonstrated this by serially concatenating a precoder assisted FFH-MFSK with both a VLC and an IrVLC coding scheme achieving arbitrarily low BERs at low SNR values in a Rayleigh fading channel contaminated with PBNJ. Our simulation results showed that the precoder aided VLC and IrVLC schemes yield an SNR gain of more than 3dB over the system not employing a precoder. Furthermore, the IrVLC scheme yields a further gain of up to 0.3dB over the VLC scheme.

4) We demonstrated our SIC algorithm by implementing it in two types of configurations. In the first configuration, a Soft-SLC-SIC scheme was proposed in Section 5.5.1 which invoked clipped combining (SLC) in convolutionally encoded FFH-MFSK. Our BER results shown in Figures 5.9 to 5.11 demonstrate that the SUD-ID scheme suffers from error floor in the high-SNR region and when $N_U$ becomes low. By contrast, the proposed Soft-SLC-SIC scheme is capable of significantly enhancing the achievable performance of the FFH-MFSK receiver, as seen in Figures 5.23 and 5.24. The Soft-SIC scheme invoking only $N_{SIC} = 2$ iterations yields a gain of nearly 1.5dB over the conventional SUD-ID scheme, at BER of $10^{-5}$. The performance gain achieved by the proposed Soft-SLC-SIC scheme is attained at the cost of increased complexity, which, however, is quite modest since only 2 $N_{SIC}$ iterations are needed over and above the conventional $N_{ID}$ iterations. Some additional complexity is also incurred because the MUD requires the FFH addresses of all users. However, this does not constitute a serious challenge at the BS receiver.

   The second configuration of the proposed SIC scheme, referred to as the Soft-PC-SIC scheme, was investigated in Section 5.5.2. It consisted of nonbinary LDPC coded FFH-MFSK employing product combining and SISO assisted SIC in the receiver. Our results shown in Figures 5.25 to 5.28 demonstrate that the proposed Soft-SIC scheme is capable of substantially enhancing the achievable performance of the FFH-MFSK receiver. Our Soft-PC-SIC scheme outperforms the conventional SUD-ID scheme and yields iterative gain for up to three SIC iterations, while the conventional SUD scheme yields no further BER improvement after the first outer iteration. An advantage of this particular configuration is that no symbol interleaving is necessary, rendering the system eminently suitable for low-latency applications, such as voice transmission.

The performance of the schemes discussed in this chapter have been summarised in Tables 5.4 and 5.5.

| Detection Scheme (Convolutional coded) | Spectral efficiency $\eta$ (Bits/s/Hz) | | | | | |
|---|---|---|---|---|---|---|
| | $m = 1$ | | | $m = 5$ | | |
| | BER=$10^{-3}$ | BER=$10^{-4}$ | BER=$10^{-5}$ | BER=$10^{-3}$ | BER=$10^{-4}$ | BER=$10^{-5}$ |
| SUD-ID, $N_{ID} = 0$ | 0.27 | 0.22 | 0.175 | 0.41 | 0.344 | 0.29 |
| SUD-ID, $N_{ID} = 4$ | 0.584 | 0.54 | 0.487 | 0.734 | 0.687 | 0.662 |
| Soft-SLC-SIC(4,2) | 0.594 | 0.562 | 0.537 | 0.74 | 0.69 | 0.675 |

**Table 5.4:** Comparison of the spectral efficiencies, in bits/sec/Hz, achieved by the SUD and SIC schemes corresponding to BERs of $10^{-3}$, $10^{-4}$ and $10^{-5}$, when employed in convolutionally encoded FFH-MFSK communicating over Nakagami-$m$ fading MA channels assuming $E_b/N_0 = 15$dB. The spectral efficiencies are computed using Equation (4.4) and the various parameter values are extracted from Figure 5.24.

| BER | Convolutional coded | | | Nonbinary LDPC coded | | | | | |
|---|---|---|---|---|---|---|---|---|---|
| | | | | 4 LDPC iter | | | 12 LDPC iter | | |
| | SUD-ID | | Soft-SLC-SIC | SUD-ID | | Soft-PC-SIC | SUD-ID | | Soft-PC-SIC |
| | $N_{ID} = 0$ | $N_{ID} = 4$ | (4,2) | $N_{ID} = 0$ | $N_{ID} = 4$ | (1,3) | $N_{ID} = 0$ | $N_{ID} = 4$ | (1,3) |
| $10^{-3}$ | 14.5 | 9.9 | 9.6 | 11.6 | 10.9 | 10.3 | 10.2 | 9.4 | 9.2 |
| $10^{-5}$ | NA | 12.2 | 10.7 | 13.3 | 11.8 | 11.1 | 11.3 | 10.6 | 9.8 |

NA means "Not achieved".

**Table 5.5:** Comparison of the $E_b/N_0$ values in dBs required by various schemes in order to achieve BERs=$10^{-3}$ and $10^{-5}$ when employed in FFH-MFSK communicating over Nakagami-$m$ fading MA channels, assuming $M = 16$, $L = 7$, $N_U = 8$ and $m = 2.5$. The $E_b/N_0$ values are extracted from Figures 5.23, 5.26 and 5.29.

Chapter 6

# Summary and Future Work

In this thesis, numerous techniques have been investigated that may be employed both in FFH and SFH systems to combat jamming and multi-user interference. In this chapter, we summarize our findings, highlighting the novel aspects of the work. Furthermore, we briefly discuss a number of aspects of FFH systems, where future research work can be potentially carried out.

## 6.1 Summary and Novelty

**Chapter 1** of this thesis provided an overview of the basic philosophy of frequency hopping and a comparative study of various diversity combining techniques used in FFH-MFSK operating in various jamming and fading conditions. This chapter was based on a study of the state-of-the-art and on simulation results characterising the more popular diversity combining schemes proposed in the published literature. Study of the open literature about this area and our simulations results given in Section 1.5 demonstrate that:

1) Most of the non-linear diversity combining methods used in FFH-MFSK provide a valuable performance gain in comparison to SFH (characterised by $L = 1$, implying no diversity) and to the linear diversity combining method, when the receiver operates in an AWGN channel under the influence of jamming. This performance gain is achieved by virtue of the various operations performed in the non-linear diversity combining schemes to suppress the degrading effects of the jamming. Our results summarised in Tables 1.5, 1.6 and 1.7 demonstrate that using a self-normalization based combining scheme results in a signal-to-jammer-ratio (SJR) gain of up to 1.8dB when encountering partial band noise jamming (PBNJ) and a gain of up to 4.3dB when combatting multitone jamming (MTJ) over the SFH system at BER of $10^{-2}$. By contrast, the performance of the linear combiner based receiver deteriorates upon increasing the diversity order in AWGN channels.

2) At low SNR or SJR values, noncoherent combining losses dominate the diversity gain. Hence, the diversity gain manifests itself only beyond a certain value of $E_b/N_J$, as seen in Figures 1.10 to 1.13.

3) Increasing the modulation order of the MFSK system improves the performance of FFH-MFSK receivers, although when combatting MTJ, a high value of $M$ ($M \geq 8$) increases the detrimental effects of the jamming as well, as seen in Figures 1.18 and 1.19. Thus, when operating under MTJ, a suitable modulation order, for example 4 or 8, has to be chosen [66].

4) The performance of the self-normalization based combining scheme is poor in Rayleigh fading conditions, as seen in Figures 1.11, 1.13 to 1.15, 1.17 to 1.19, 1.21 and 1.22. This is a consequence of the normalization operation performed in the NED receiver on the received signals. Consequently, in Rayleigh fading, using linear combining is a better option than self-normalization combining for a wide range of system parameter values.

In **Chapter 2**, the performance of RS-coded SFH-MFSK systems using various EI schemes was investigated, when communicating over Rayleigh fading channels in the presence of $n = 1$-band MTJ. More specifically, we considered the OTT, the RTT and the MO-RTT based EI schemes [99, 106]. This work may be viewed as an extension of the study reported in [99]. However, our contribution in Chapter 2 is novel in the sense that while the RS-coded SFH-MFSK system was assumed to be interfered by PBNJ in [99], we focused our attention on the operation of the system when combatting MTJ. We have derived closed form expressions for the relevant statistics involved in EI using the above-mentioned schemes. Thus, the BER calculation and subsequent performance evaluation of the system is facilitated. Our analytical results demonstrate that:

1) Using error-and-erasures decoding (EED) based on one of the considered EI schemes a SJR gain of up to 3.5 dB can be achieved over the error-control-only (ECO) decoding at the BER of $10^{-4}$, as seen in Table 2.2.

2) As observed in Table 2.3, under the conditions considered, MO-RTT can yield a maximum SJR gain of 1.8dB over the RTT based scheme at BER of $10^{-5}$, while the performance of OTT is very close to that of the MO-RTT arrangement. However, with suitable choice of the modulation order and code rates, all three schemes are capable of attaining approximately similar performance, with a $E_b/N_J$ difference of less than 0.5dB between them.

3) The considered schemes may be categorized into the family of low complexity schemes. Moreover, while the OTT and the RTT involve similar levels of complexity, the MO-RTT has twice the complexity of the other two.

In **Chapter 3**, a novel BER analysis technique designed for product combining (PC) scheme used in the FFH-MFSK system was proposed. This method employs Mellin transform [118], which is a convenient tool for determining the PDF of a product of random variables. Our method proposed in Chapter 3 allows for the first time the derivation of the PDF of PC outputs in semi-closed form and hence facilitates the analysis of FH $M$-ary FSK receivers using PC in conjunction with $M > 2$. The analysis was performed assuming

both an interference-free Rayleigh fading channel as well as for system contaminated by PBNJ. The Mellin transform method has been found to be attractive since it can find application wherever the PDF of a product of random variables is involved.

In **Chapter 4**, we focused our attention on the multiple access (MA) capability of FFH. Both single-user and multi-user detection were considered. Some of the presented simulation results are novel in the sense that we have provided a comparative analysis of a range of diversity combining techniques when employed in FFH-MA system. As evidenced by our simulations results given in Figures 4.7 to 4.11 and summarised in Table 4.3, we found in the context of single-user detection (SUD) that:

1) Clipped or soft limiter combining (SLC) yields the best performance amongst the schemes considered, whereas the HLMV scheme conventionally considered in FFH-MA systems [93, 143, 146] attains a comparable performance to SLC only when the SNR is sufficiently high (in excess of 25dB).

2) Both SLC and HLMV combining require estimation of the received SNR in order to set appropriate thresholds. By contrast, the PC receiver and the OS-NED are two attractive design options, since they do not require any side information, although their performance is inferior to the SLC scheme.

Two novel successive interference cancellation (SIC) techniques were also been proposed in Chapter 4. One of the proposed schemes invokes the SLC, while the other uses PC in the first stage and SLC in the subsequent SIC stages. Although the basic philosophy governing these schemes is based on the method proposed in [143], the proposed schemes are novel since they perform multistage detection of the symbols based on reliability tests using the RTT [106]. Our simulation results given in Figures 4.17 to 4.21 and summarised in Tables 4.3 and 4.4 demonstrated that

1) The proposed SIC schemes yield an attractive BER performance improvement as compared to Fiebig's scheme [143], which is considered to be a benchmark SIC scheme for FFH-MFSK systems in the published literature. Our results summarised in Table 4.4 show that the proposed schemes are capable of yielding an SNR gain of up to 7.4dB over Fiebig's scheme [143] at a BER of $10^{-4}$. The spectral efficiencies of various SUD and SIC schemes for uncoded FFH-MFSK have been summarised in Table 6.1.

2) The proposed schemes have an attractive low complexity. As seen in Table 4.2 on average the proposed schemes do not impose an additional complexity, quantified in terms of the number of SIC iterations involved, despite outperforming Fiebig's scheme [143].

Finally in **Chapter 5**, iterative decoding designed for FFH-MFSK is investigated assuming various fading and multiple access (MA) channels. More specifically, we have investigated the serial concatenation of the FFH-MFSK demodulator with a soft-input-soft-output (SISO) decoder. Our findings and the novel contributions in this chapter are:

| Detection Scheme | Spectral efficiency $\eta$ (Bits/s/Hz) | |
|---|---|---|
| | BER=$10^{-3}$ | BER=$10^{-4}$ |
| **Uncoded SUD** | | |
| HLMV | 0.0625 | 0.014 |
| SLC | 0.109 | 0.028 |
| **Uncoded SIC** | | |
| Fiebig's scheme | 0.12 | 0.016 |
| SLC-SIC | 0.195 | 0.117 |
| **ID-based SUD** | | |
| SUD-ID, $N_{ID} = 0$ | 0.27 | 0.22 |
| SUD-ID, $N_{ID} = 4$ | 0.584 | 0.54 |
| **ID-based SIC** | | |
| Soft-SLC-SIC(4,2) | 0.594 | 0.562 |

**Table 6.1:** Comparison of the spectral efficiencies, in bits/sec/Hz, achieved by various SUD and SIC schemes corresponding to BERs of $10^{-3}$ and $10^{-4}$ when employed in uncoded and coded FFH-MFSK communicating over Nakagami-$m$ fading MA channels, assuming $m = 1$ and $E_b/N_0 = 15$dB. The values have been extracted from Tables 4.3 and 5.4.

1) A sub-optimal soft information generated by the demodulator and passed to the outer decoder was derived for both Rayleigh as well as Nakagami-$m$ fading channels. It was shown that the derived soft information yields useful performance gain over the hard decision decoding based scheme. Thus, our contribution in this context is novel since it facilitates the soft decision decoding (SDD) of FFH-MFSK in MA channels.

2) The convergence behaviour of iteratively decoded FFH-MFSK is investigated with the aid of Extrinsic Information Transfer (EXIT) charts. This is a major contribution, allowing us to determine the parameters that influence the attainable iterative gain, thereby leading to techniques that may be employed to improve it. We demonstrated the benefits of EXIT chart based analysis by employing a precoder-assisted FFH-MFSK scheme in serial concatenation with an IrVLC scheme. This beneficially matched concatenation, which was facilitated by employing EXIT charts, leads to an infinitesimally low BERs at low SNR values and a gain of up to 7dB over the system dispensing with a precoder at a BER of $10^{-4}$ in a Rayleigh fading channel contaminated by PBNJ, as seen in Figure 5.19.

3) Finally, a novel SIC scheme that operates in conjunction with the SISO decoder is proposed in this chapter. This scheme is similar in principle to the ones proposed in Chapter 4. However, it exploits the SISO decoder's output to test the reliability of the symbols. We demonstrated the efficacy of the proposed idea by implementing it in two different configurations: one based on SLC and binary convolutional codes, while the other using PC and nonbinary LDPC codes. Our simulation

results demonstrate that this scheme significantly enhances the MA capability of the FFH system. As summarised in Table 5.5, the first configuration yields an SNR gain of up to 1.5 dB with only two additional SIC iterations, while the second configuration yields an SNR gain of up to 0.8 dB over the corresponding SUD scheme with three additional iterations at BER of $10^{-5}$. The spectral efficiencies of various SUD and SIC schemes employed in soft decision decoded FFH-MFSK have also been shown in Table 6.1.

## 6.2 Future Work

In this section, we briefly discuss a few future research ideas.

### 6.2.1 A Novel UWB system using Multi-Stage FFH

A research area that is related to frequency hopping and is attracting lot of scientific and commercial attention at the time of writing is constituted by the ultra-wideband (UWB) communication system. The UWB signal can be considered to be a specific type of spread spectrum signal since it is in the form of sub-nanosecond duration pulses and occupies a high bandwidth [203, 204]. Typically, UWB signals are carrier-less, need low transmission power and have very low spectral density. Such characteristics lend the UWB system with attractive properties such as low power consumption for indoor communication, low probability of intercept and reduced interference to and from other narrow band transmitters. Moreover, transmissions in the form of very narrow pulses allows the multipath signals to be resolved on the order of nanosecond, thereby providing an effective anti-fading measure.

In [24], an alternative UWB system using multistage FFH was proposed that communicates using narrowband signals instead of pulses. The proposed system uses residue number system (RNS) [24] to generate frequency hopping patterns in multiple bands and the resulting hopping bandwidth is very wide, making the system analogous to a classical UWB system. The purpose of using RNS based FFH in the proposed UWB system is to ensure that the high number of users supported can be divided into a number of reduced-size subgroups. By virtue of allocating multiple users to small FH groups, the proposed system guarantees reduced interference among various users and thus significantly improved BER performance.

The block diagram of this multi-stage (MS)/UWB FFH-MA transmitter is shown in Figure 6.1. In this figure, following the MFSK modulation stage, an FH unit modulates the signal to be transmitted. As seen in Figure 6.1(b), the FH unit is composed of $S$ FH stages, in each of which, the incoming signal is multiplied by a unique frequency. The transmitted signal for the $k$th user, $k = 1, 2, \ldots, N_U$, during the $l$th hop may be expressed as

$$s_k(t) = \sqrt{2P} \cos \left[ \sum_{s=1}^{S} f_{s,i_s,l}^{(k)} + f_{m,l}^{(k)} \right], \tag{6.1}$$

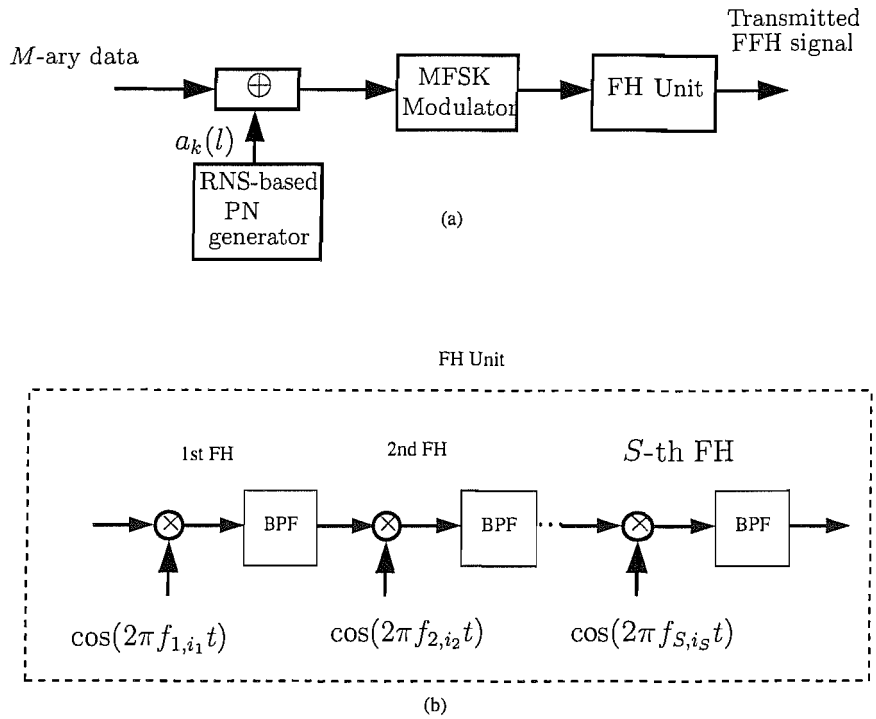


**Figure 6.1:** Schematic of the FFH transmitter employing multi-stage frequency hopping, for the $k$th user, proposed in [24].

where $P$ is the transmitted power, $f^{(k)}_{s,i_s,l}$ is the FH frequency corresponding to the $i$th transmitted symbol and the $l$th hop in the $s$th stage of the multi-stage FH system, and $f^{(k)}_{m,l}$ is the MFSK frequency during the $l$-th hop. In the proposed MS/UWB FFH-MA transmission system [24], the total spread spectrum bandwidth $W_{ss}$ is divided into $m_S$ number of frequency bands, each of which is assigned a frequency from the stage $S$ frequency set. The bandwidth allocated to each stage $S$ frequency band is given by $W_S = W_{ss}/m_S$. Next, each frequency band in the $S$-th stage is further divided into $m_{S-1}$ number of frequency bands, each of which being assigned a frequency from the stage $S-1$ frequency set and each having a bandwidth $W_{S-1} = W_S/m_{S-1}$. This division of frequency bands is continued until the $s = 1$-th stage with $m_1$ number of frequency tones and a bandwidth given by $W_1 = W_2/m_1$. The frequencies at the $S$ number of stages are activated according to the $S$ number of residue digits of a corresponding residue sequence in the RNS. As part of our future work, we will study the RNS in detail. As seen in Equation (6.1), the transmitted frequency during the $l$-th hop of a symbol is sum of the frequencies chosen from all the $S$ stages, as well as the MFSK frequency.

In our future research, we will investigate this novel alternative UWB [24] system in conjunction with various diversity combining and SIC schemes, in order to further enhance its performance and thus design a system capable of supporting very large number of users.

### 6.2.2 Space-Frequency Diversity using FFH-Assisted DSTBC System

In recent years, space diversity or antenna diversity for use in wireless communication systems has attracted lot of attention. It is typically implemented using multiple transmit and/or receive antennas. If the spacing between arrays of antennas in the transmitter or receiver are more than a few wavelengths, then signals transmitted using individuals antennas can be assumed to be uncorrelated with each other. In the receiver, the uncorrelated signals can be combined. Lack of correlation amongst various signal replicas ensures that not all signals experience the same intensity of fading. Hence, detrimental effects of fading channel are considerably reduced.

A number of multiple input multiple output (MIMO) systems, as the systems invoking space diversity are often referred to, have been proposed in the literature. The classic approach is to use multiple receiver antennas and exploit Maximum Ratio Combining (MRC) of the received signals for the sake of improving the system's performance [89, 90]. However, the performance improvement of MRC is achieved at the cost of increasing the complexity of the Mobile Stations. Alternatively, MRC may be employed at the Base Stations (BSs), which support numerous MSs. While this scheme provides diversity gain for the BSs' receivers, the MSs cannot benefit from it.

Employing multiple transmitters, rather than receiver antennas at the BSs constitutes a further design option in this context. Since transmitter diversity techniques are proposed for employment at the BSs, it is possible to enhance the system's integrity by upgrading the BSs. Alamouti [205] introduced an attractive scheme, which uses two transmitters in conjunction with an arbitrary number of receivers for communications in non-dispersive Rayleigh fading channels. Tarokh [206] generalized Alamouti's scheme to an arbitrary number of transmitters. These schemes introduced space-time block codes (STBC), which show remarkable encoding and decoding simplicity, while achieving a good performance. In the context of a two transmitters and single receiver configuration of the Alamouti's scheme, both space and time diversity are invoked. Specifically, during one symbol duration two separate symbols $x_1$ and $x_2$ are transmitted from the two antennas; in the next symbol duration, 'appropriately transformed' replicas of the same symbols as transmitted in the previous duration are transmitted using the two antennas. In the receiver, a suitable decoding algorithm combines the signals from the two symbol durations and the detection decision is based on maximum likelihood principle.

Alamouti's scheme [205] requires the knowledge of the channel state information (CSI) to estimate the fading coefficients induced by the channel. When CSI is not reliable, which is the case when fading is not sufficiently slow owing to high MS speeds, then a differential form of STBC, which was proposed by Tarokh [207], can be applied. It is referred to as the D-STBC scheme and is similar to the Alamouti's STBC scheme, except that the transmitted symbols are differentially encoded in the transmitter and differentially decoded in the receiver. Although the performance achieved using Differential-STBC is inferior to that of the coherent STBC, the former offers the advantage of a less complex system, obviating the need of estimating the CSI. However, an increased diversity order can only be achieved by employing an increased

number of transmit antennas, which results in an increased complexity.

In contrast to the above-mentioned spatial diversity schemes, FFH schemes aim for achieving frequency and time diversity by hopping to independently faded carriers during a single transmitted symbol duration. The achievable diversity gain in context of FFH may be limited by the available bandwidth. Therefore, it is beneficial to design a combined DSTBC and FFH aided system, which is potentially capable of combining the achievable spatial and frequency diversity. This specific system configuration is particularly attractive, since FFH systems are non-coherent by nature [2], prohibiting the estimation of channel state information during each hop duration, since the hop duration may be extremely low compared to the symbol duration. Therefore, coherently detected STBC cannot be applied in conjunction with non-coherently detected FFH. Hence, differentially encoded modulation schemes, such as differential phase shift keying (DPSK), have been used in conjunction with FFH [18, 49].

#### 6.2.2.1 Proposed FFH Assisted DSTBC System

We consider a wireless communication system invoking multiple transmit antennas at the Base Station (BS) and an arbitrary number of receive antennas at the Mobile Station (MS). The block diagram of a system that may be designed to amalgamate the advantages of FFH and STBC is shown in Figure 6.2. The system shown in this figure employs two transmit and one receive antenna, although the concept can be applied to arbitrary number of receive antennas. As shown in Figure 6.2, the output of a standard D-STBC encoder consisting of a constellation mapper, a differential symbol calculation block and the encoder is modulated by a FFH modulator. The D-STBC encoder operates on the principle as explained in [207]. First, the information symbols are mapped on to constellation symbols defined by

$$\mathcal{A} = \frac{e^{j2\pi k/M}}{\sqrt{2}}, \quad , k = 0, 1, \ldots, M-1, \tag{6.2}$$

where $M = 2^b$, $b$ is the number of bits per symbol and $j = \sqrt{-1}$. We will restrict our attention to the binary case only, although higher order phase shift keying (PSK) schemes and quadrature amplitude modulation (QAM) are also supported by the scheme. Hence, in the context of the system under consideration, we have $M = 2$ and the information bits may have two values only, i.e. $k = 0, 1$. Note that the division by $\sqrt{2}$ in Equation (6.2) is done so that the total transmitted power from the two antennas is 1.

Let $x^1(2t+1)$ and $x^2(2t+1)$ denote the differentially encoded symbols during the symbol period $(2t+1)$. These symbols are calculated based on both the symbols transmitted during the interval $(2t-1)$ and the incoming PSK symbols denoted by $\mathcal{S}_i$, where $i$ represents the transmit antenna index. This process can be expressed as [207]

$$\begin{aligned}(x^1(2t+1), x^2(2t+1)) = \mathcal{S}_1(x^1(2t-1), x^2(2t-1)) \\ +\mathcal{S}_2(-x^{2*}(2t-1), x^{1*}(2t-1)),\end{aligned} \tag{6.3}$$

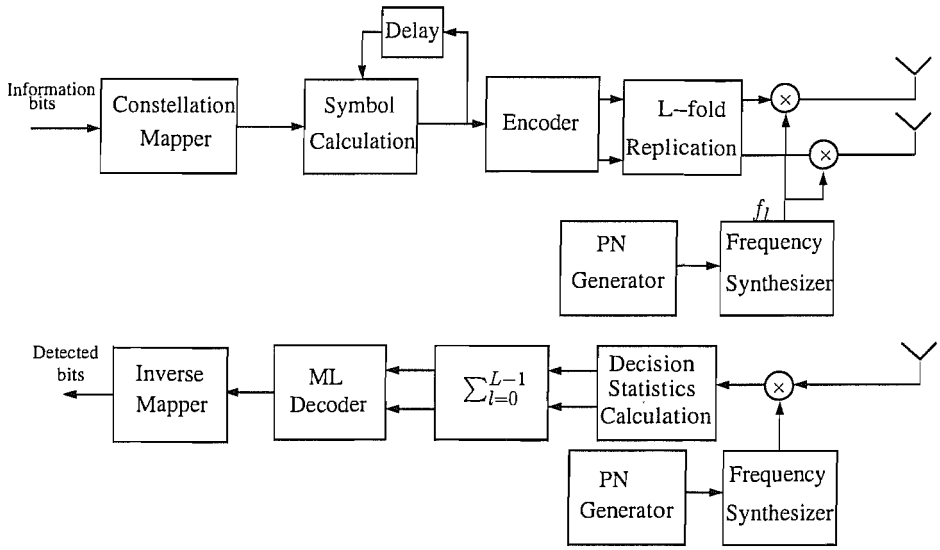


**Figure 6.2:** Schematic of the FFH assisted D-STBC system using $T = 2$ transmitter antennas and $L$-order frequency diversity.

**Table 6.2:** Transmission of symbols $x^1(t)$ and $x^2(t)$ using the transmit antennas $Tx_1$ and $Tx_2$ and $L$ FFH hops, where $x^i(t,l)$ denotes the replica of the $i$th symbol transmitted at time $t$ during the $l$th hop, $l = 0, 1, \ldots, L-1$ and $i = 1, 2$

| | Hop 1 $f_0$ | Hop 2 $f_1$ | $\cdots$ $\cdots$ | Hop $L$ $f_{L-1}$ |
|---|---|---|---|---|
| $Tx_1$ | $x^1(t,0)$ | $x^1(t,1)$ | $\cdots$ | $x^1(t,L-1)$ |
| $Tx_2$ | $x^2(t,0)$ | $x^2(t,1)$ | $\cdots$ | $x^2(t,L-1)$ |

where $*$ denotes the complex conjugate.

Next, a conventional STBC encoder is used, which obeys the $G_2$ transmission matrix and transmits the differential encoded symbols in time slots $(2t+1)$ and $(2t+2)$ according to

$$G_2(x^1(2t+1), x^2(2t+1)) = \begin{bmatrix} x^1(2t+1) & x^2(2t+1) \\ -x^{2*}(2t+1) & x^{1*}(2t+1) \end{bmatrix}. \tag{6.4}$$

The FFH modulator, discussed in Chapter 1, is characterised by $T_h = T_s/L$, where $L$ is the number of hops per symbol, $T_h$ is the hop duration, while $T_s$ is the symbol duration. Thus, during each hop duration one copy of the encoded symbols is transmitted using a different frequency. This arrangement is shown for arbitrary symbols $x^1(t)$ and $x^2(t)$ in Table 6.2, where $x^i(t,l)$ denotes the replica of the $i$th symbol transmitted at time $t$ during the $l$th hop, $l = 0, 1, \ldots, L-1$ and $i = 1, 2$. Note that during any of the hops, the same frequency is used for both symbols to be transmitted using antennas 1 and 2. Thus, if symbols $x^1(2t+1)$ and $x^2(2t+1)$ are input to the FFH modulator, then the signals transmitted during the $l$th hop at

time $(2t+1)$ and $(2t+2)$ may be expressed as

$$\begin{aligned} s^1(2t+1,l) &= \sqrt{2P}x^1(2t+1,l)e^{j2\pi f_l(2t+1)t+\phi_l}, \\ s^2(2t+1,l) &= \sqrt{2P}x^2(2t+1,l)e^{j2\pi f_l(2t+1)t+\phi_l}, \\ s^1(2t+2,l) &= -\sqrt{2P}x^{2*}(2t+1,l)e^{j2\pi f_l(2t+2)t+\phi_l}, \\ s^2(2t+2,l) &= \sqrt{2P}x^{1*}(2t+1,l)e^{j2\pi f_l(2t+2)t+\phi_l}, \end{aligned} \tag{6.5}$$

where $P$ denotes the power of the encoded symbols, $f_l(t)$ is the FFH frequency in the $l$th hop of the symbol at time $t$, while $\phi_l$ is the phase induced by the FFH.

In the receiver shown in Figure 6.2, the signals received by a single antenna are dehopped by the FFH demodulator. It is assumed that the FFH demodulator is perfectly frequency aligned with the FFH modulator. The dehopped received signals during the $l$th hop at time $(2t+1)$ are given by

$$r(2t+1,l) = h_{1,l}s^1(2t+1,l) + h_{2,l}s^2(2t+1,l) + n_{2t+1,l}, \tag{6.6}$$

where $h_{m,l}$ denotes the path gain from the $m$th transmit antenna to the receiver antenna during the $l$th hop, $n_{2t+1,l}$ is the corresponding complex Additive White Gaussian Noise (AWGN) and we have $m = 1, 2$ in the scenario considered. Following dehopping, the detection decision statistics $\tilde{S}_1(l)$ and $\tilde{S}_2(l)$ generated for the $l$th hop of the transmitted PSK symbols using the DSTBC decoder at symbol interval $(2t+1)$ are computed [207], as shown in Figure 6.2, namely

$$\begin{aligned} \tilde{S}_1(l) &= r(2t+1,l)r^*(2t-1,l) + r(2t,l)r^*(2t+2,l) \\ &= (|h_{1,l}|^2 + |h_{2,l}|^2)S_1 + \tilde{N}_1 \\ \tilde{S}_2(l) &= r(2t+1,l)r^*(2t,l) - r(2t-1,l)r^*(2t+2,l) \\ &= (|h_{1,l}|^2 + |h_{2,l}|^2)S_2 + \tilde{N}_2, \end{aligned} \tag{6.7}$$

where $\tilde{N}_1$ and $\tilde{N}_2$ are the combined noise vectors. Once $L$ decision statistics corresponding to one symbol duration have been computed, they are summed over the $L$ corresponding hops to generate the resultant decision statistics as seen in Figure 6.2.

We assume that the phase $\phi_l$ induced by FFH, as expressed in Equation (6.5), is approximately the same for a particular hopping frequency. In other words, for a particular value of $l = 0, 1, \ldots, L-1$, $\phi_l$ is the same during all symbol intervals. This might be an over-simplifying assumption but has been stipulated for ease of analysis. Under the above assumption, the resultant decision statistics for a particular pair of symbols can be obtained by the summation of the decision statistics for all hops and may be expressed as

$$\tilde{S}_1 = \sum_{l=0}^{L-1} \tilde{S}_1(l) \qquad \tilde{S}_2 = \sum_{l=0}^{L-1} \tilde{S}_2(l). \tag{6.8}$$

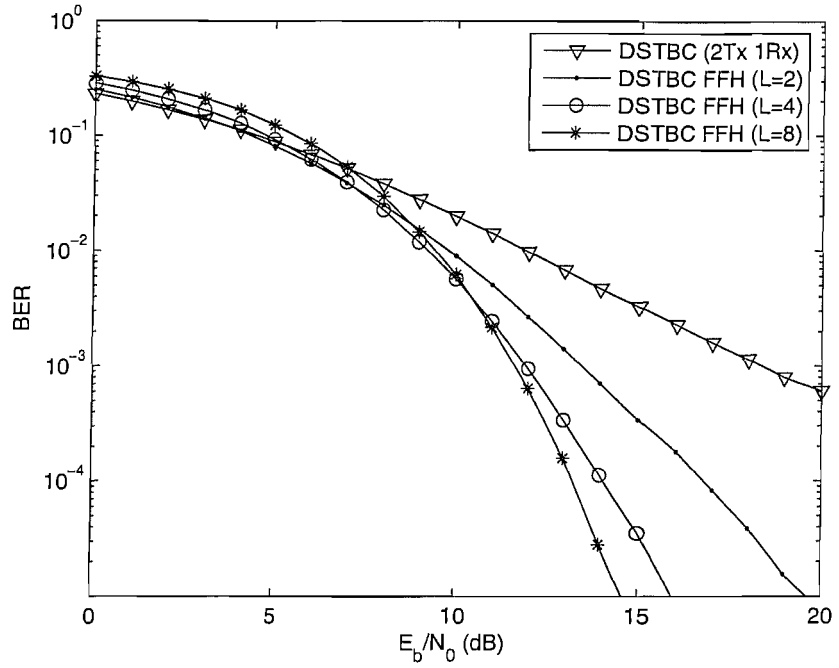


**Figure 6.3:** BER performance of the FFH assisted DSTBC system employing two transmit and one receive antenna, when communicating over correlated Rayleigh fading channels having $f_d = 10^{-2}$ and assuming various orders of frequency diversity $L$.

DSTBC system, the total achievable diversity order is given by $(I \times L)$, where $I$ is the number of transmit antennas. Thus, without invoking a high number of transmit antennas for attaining a high spatial diversity, the proposed system is capable of achieving a high overall diversity gain.

### 6.2.2.2 Simulation Results and Discussion

In this section, we characterise the achievable performance of the FFH aided DSTBC system using our simulation results. In Figure 6.3, the performance of a DSTBC scheme employing two transmit and one receive antenna, assisted by a FFH arrangement using $L = 2, 4$ and 8 hops per symbol has been shown, when communicating over Rayleigh fading channels experiencing a relatively fast fading having a normalized doppler frequency of $f_d = 10^{-2}$. As seen in Figure 6.3, the performance of the DSTBC system dispensing with FFH shows an error floor in the high-SNR region. This is because the differential decoding scheme ideally requires the fading to be constant for four consecutive DSTBC symbol time slots. Thus, when the fading envelope is rapidly fluctuating, this condition cannot be satisfied and hence encountering an error floor is inevitable. However, when frequency diversity is introduced, the above-mentioned error floor can be essentially eliminated, despite the fading envelope's fluctuation experienced during the consecutive time slots.

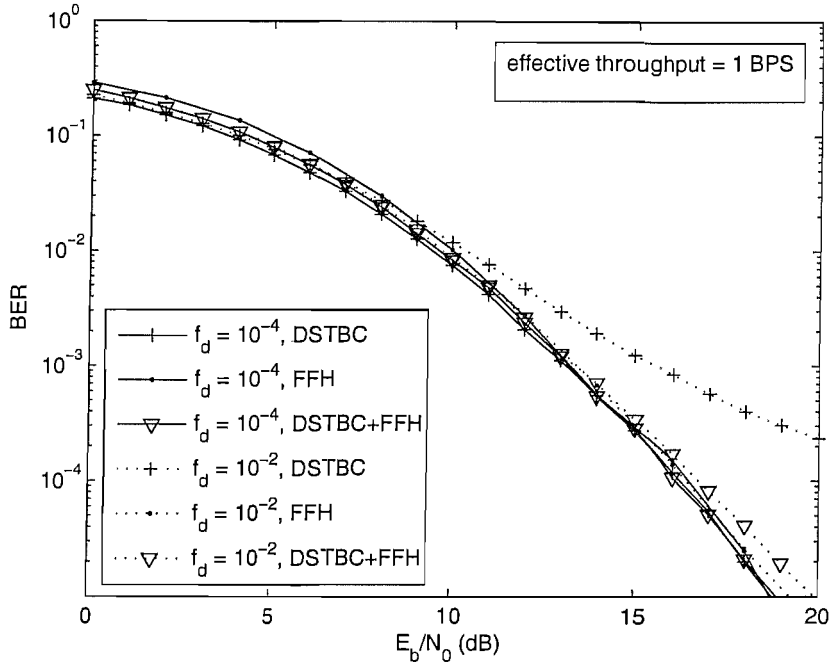


**Figure 6.4:** BER performance comparison of the three systems having a total diversity of $D_{total} = 4$ and an effective throughput of 1BPS, when communicating over correlated Rayleigh fading channels, having both $f_d = 10^{-2}$ and $10^{-4}$.

If we fix the system's total diversity order to $D_{total} = T \times L = 4$, three alternative systems, namely the DSTBC ($T = 4$, $L = 1$), the FFH ($T = 1$, $L = 4$) and the DSTBC + FFH ($T = 2$, $L = 2$) arrangements, may be designed corresponding to different combinations of spatial and frequency diversity. Figure 6.4 explicitly demonstrates that for slow fading having a normalized Doppler frequency of $f_d = 10^{-4}$ all the systems exhibit a similar performance. However, when the fading becomes moderately fast, such as $f_d = 10^{-2}$, the DSTBC system, which requires the fading envelope to be constant for eight consecutive time slots, degrades more significantly than the others. Therefore, we may conclude that the FFH assisted DSTBC system is capable of supporting higher vehicular speeds than the pure DSTBC system having the same diversity order, when considering a fixed transmission rate. A more detailed comparison of the three systems can be found in Table 6.3.

We will extend the work proposed in this section by considering the system communicating in channels contaminated by jamming and multi-user interference.

### 6.2.3 Other Areas of Future Research

Some further areas of future research have been outlined below:

1) In Section 5.4, we demonstrated the benefits of employing a precoder in channel encoded FFH-MFSK. We showed that by using an IrVLC [188] scheme having suitable code rates assigned to different fractions of the source symbols stream, the EXIT curve of the corresponding outer decoder may be

**Table 6.3:** Comparison of various system parameters for the three systems, having a total diversity order $D_{total} = 4$

| Parameter | System | | |
|---|---|---|---|
| | DSTBC | FFH | DSTBC+FFH |
| $T^{\triangledown}$ | 4 | 1 | 2 |
| $L^{\triangle}$ | 1 | 4 | 2 |
| Degradation* | at $f_d > 10^{-3}$ | at $f_d > 10^{-2}$ | at $f_d > 10^{-2}$ |
| Complexity$^{\clubsuit}$ | 4 | 1 | 2 |
| Bandwidth$^{\heartsuit}$ | $A$ | $4A$ | $2A$ |
| Spatial correlation | affected if $\Delta T^{\diamond} < \lambda/2$ | not affected | affected if $\Delta T < \lambda/2$ |
| Frequency correlation | not affected | affected if $\Delta f^{\diamond\diamond} < B_c^{**}$ | affected if $\Delta f < B_c$ |

$^{\triangledown}$ T is the number of transmit antennas. $^{\triangle}$ L is number of hops per symbol. * Degradation is in BER when compared to performance at $f_d = 10^{-4}$. $^{\clubsuit}$ Complexity is measured by the number of transmit antennas. $^{\heartsuit}$ $A$ denotes the bandwidth of the narrowband DSTBC system. $^{**}B_c$ is the channel coherence bandwidth. $^{\diamond}\Delta T$ is the antenna spacing. $^{\diamond\diamond}\Delta f$ is the frequency spacing.

matched to that of the unity-rate decoder, thus creating a narrow convergence tunnel in the EXIT plane and consequently achieving arbitrarily low BERs at low SNR values. In Section 5.4.2, we focused on the extrinsic MI exchange between the inner unity-rate decoder and the outer IrVLC decoder. A natural extension to this concept is the 3-stage MI exchange between the demodulator, the inner unity-rate decoder and the outer IrVLC decoder. This 3-stage iterative decoding scheme is likely to be more beneficial in terms of useful extrinsic information exchange. The concept is shown in Figure 6.5. The 3-stage concatenation may be analyzed using 3-D EXIT charts or resorting to 2-D EXIT charts by treating the demodulator and the unity-rate decoder as a combined module [186].

2) The concept of Irregular codes [185–187] may also be applied to the FFH modulator, which may be deemed as an $L$-order repetition code. It is logical to expect that by employing variable diversity orders for particular fractions of the input symbol stream, a so-called *Irregular FFH* may be designed. By suitable choice of the input stream fractions and the code rates, the resultant EXIT curve of the demodulator, or alternatively of the unity-rate decoder, may be further improved by facilitating a match with that of the outer decoder at even lower SNR values. Thus, a performance very close to the capacity of the FFH-MFSK scheme may be achieved. In this context, the concept of repeat-accumulate (RA) codes is relevant [208–211]. An RA encoder may be viewed as a serial concatenation of a rep-

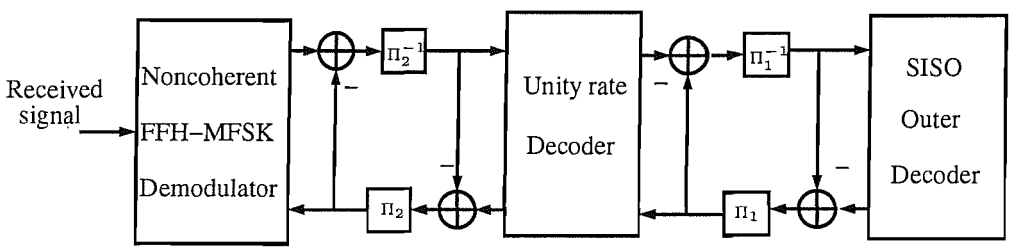


**Figure 6.5:** Schematic of the 3-stage serial concatenation among FFH-MFSK demodulator, a unity-rate decoder and an outer decoder.

etition code and a unity-rate convolutional code. RA codes have been shown to be turbo-like codes using very simple encoders [208,211]. Furthermore, an irregular RA code may be designed by incorporating an irregular repetition code [208], which is similar to our concept of a FFH modulator using variable number of hops per symbol.

# Bibliography


[1] I. Gradshteyn and I. M. Ryzhik, *Tables of integrals, series and products.* London: Academic Press, 1965.

[2] R. E. Ziemer and R. L. Peterson, *Digital communications and spread spectrum systems.* New York: Mcmillan Inc., 1985.

[3] M. K. Simon, J. K. Omura, R. A. Scholtz, and B. K. Levitt, *Spread spectrum communications: Volume I.* Maryland, USA: Computer Science Press Inc., 1985.

[4] M. K. Simon, J. K. Omura, R. A. Scholtz, and B. K. Levitt, *Spread spectrum communications: Volume II.* Maryland, USA: Computer Science Press Inc., 1985.

[5] M. K. Simon, J. K. Omura, R. A. Scholtz, and B. K. Levitt, *Spread spectrum communications: Volume III.* Maryland, USA: Computer Science Press Inc., 1985.

[6] T. S. Rappaport, *Wireless Communications: Principles and Practice, 2nd Edition.* USA: Prentice Hall, 2002.

[7] G. R. Cooper, R. W. Nettleton, and D. R. Grybos, "Cellular land-mobile radio: Why spread spectrum?," *IEEE Communications Magazine*, vol. 17, pp. 17–24, March 1979.

[8] P. Jung, P. W. Baier, and A. Steil, "Advantages of CDMA and spread spectrum techniques over FDMA and TDMA in cellular mobile radio applications," *IEEE Transactions on Vehicular Technology*, vol. 42, pp. 357–364, August 1993.

[9] D. T. Magill, F. D. Natali, and G. P. Edwards, "Spread-spectrum technology for commercial applications," *IEEE Proceedings*, vol. 82, pp. 572–584, April 1994.

[10] P. R. Chang and C. F. Lin, "Design of spread spectrum multicode CDMA transport architecture for multimedia services," *IEEE Journal on Selected Areas in Communication*, vol. 18, pp. 99–111, January 2000.

[11] R. L. Pickholtz, L. B. Milstein, and D. L. Schilling, "Spread spectrum for Mobile Communications," *IEEE Transactions on Vehicular Technology*, vol. 40, pp. 313–322, May 1991.

[12] N. Abramson, "Multiple access in wireless digital networks," *IEEE Proceedings*, vol. 82, pp. 1360–1370, September 1994.

[13] R. Kohno, R. Meidan, and L. B. Milstein, "Spread spectrum access methods for wireless communications," *IEEE Communications Magazine*, vol. 33, pp. 58–67, Januray 1995.

[14] H. Ekstrom, A. Furuskar, J. Karlsson, M. Meyer, S. Parkvall, J. Torsner, and M. Wahlqvist, "Technical solutions for the 3G long-term evolution," *IEEE Communications Magazine*, vol. 44, pp. 38–45, March 2006.

[15] D. Torrieri, "Future army mobile multiple-access communications," in *IEEE Military Communications Conference, 1997. Milcom 97.*, vol. 5, pp. 650–654, November 1997.

[16] P. K. Lee and J. A. Rudin, "Spectrum efficient A/J waveform for 21st century HF communications," in *IEEE Military Communications Conference, 1998. Milcom 98.*, vol. 2, pp. 376–380, October 1998.

[17] L. B. Jocic, S. A. Hovanessian., J. K. Kreng, and M. D. Schultz, "Adapting commercial satellites to military communication needs," in *Proceedings of the IEEE Aerospace Applications Conference.*, vol. 3, pp. 389–401, February 1996.

[18] G. R. Cooper and R. W. Nettleton, "A spread-spectrum technique for high-capacity mobile communications," *IEEE Transactions on Vehicular Technology*, vol. VT-27, pp. 264 – 275, November 1978.

[19] A. Ephremides, J. E. Wieselthier, and D. J. Baker, "A design concept for reliable mobile radio networks with frequency hopping signaling," *Proccedings of IEEE*, vol. 75, pp. 56–73, January 1987.

[20] J. C. Haartsen, "The Bluetooth radio system," *IEEE Personal Communications Magazine*, vol. 7, pp. 28–36, February 2000.

[21] J. H. G. Jr. and M. B. Pursley, "A comparison of slow-frequency-hop and direct-sequence spread-spectrum communications over frequency-selective fading channels," *IEEE Transactions on Communications*, vol. 47, pp. 732 – 741, May 1999.

[22] D. J. Torrieri, "Mobile frequency-hopping CDMA systems," *IEEE Transactions on Communications*, vol. 48, pp. 1318–1327, August 2000.

[23] M. B. Pursley, "Frequency-hop transmission for satellite packet switching and terrestrial packet radio networks," *IEEE Transactions on Information Theory*, vol. 32, pp. 652–667, September 1986.

[24] L. L. Yang and L. Hanzo, "Residue number system assisted fast frequency-hopped synchronous utlra-wideband spread-spectrum mutiple-access: a design alternative to impulse radio," *IEEE Journal on Selected Areas of Communications*, vol. 20, pp. 1652–1663, December 2002.

[25] J. S. Min and H. Samueli, "Analysis and design of a frequency-hopped spread-spectrum transceiver for wireless personal communications," *IEEE Transactions on Vehicular Technology*, vol. 49, pp. 56–73, September 2000.

[26] S. Swales, D. J. Purle, T. Busby, and M. Beach, "The application of frequency hopping CDMA for future universal Personal Communications Systems," in *IEEE 2nd International Conference on Universal Personal Communications, 1993.*, vol. 2, pp. 960–964, October 1993.

[27] M. I. Mandell and R. J. McEliece, "A comparison of CDMA and frequency hopping in a cellular environment," in *IEEE 1st International Conference on Universal Personal Communications Conference, 1992. ICUPC 92.*, vol. 2, pp. 07.01/1 – 07.01/5, October 1992.

[28] S. C. Swales, T. Busby, D. J. Purle, M. A. Beach, and J. P. McGeehan, "A comparison of CDMA techniques for third generation mobile radio systems," in *IEEE 43rd Vehicular Technology Conference, 1993.*, pp. 424–427, May 1993.

[29] H. E. Gamal and E. Geraniotis, "Comparing the capacities of FH/SSMA and DS/CDMA networks," in *The Ninth IEEE International Symposium on Personal, Indoor and Mobile Radio Communications, 1998.*, vol. 2, pp. 769–773, September 1998.

[30] J. H. G. Jr., D. L. Noneaker, and M. B. Pursley, "A comparison of slow-frequency-hop and direct-sequence spread-spectrum packet communications over doubly-selective fading channels," *IEEE Transactions on Communications*, vol. 50, pp. 1236 – 1239, May 2002.

[31] L. L. Yang and L. Hanzo, "Multicarrier DS-CDMA: a multiple access scheme for ubiquitous broadband wireless communications," *IEEE Communications Magazine*, vol. 41, pp. 116 – 124, October 2003.

[32] T. Vlachos and E. Geraniotis, "Performance study of hybrid spread-spectrum random-access communications," *IEEE Transactions on Communications*, vol. 39, pp. 975 – 985, June 1991.

[33] P. Varzakas and G. S. Tombras, "Spectral efficiency for a hybrid DS/FH code-division multiple-access system in cellular mobile radio," *IEEE Transactions on Vehicular Technology*, vol. 50, pp. 131–1327, November 2001.

[34] J. G. Proakis, *Digital communications*. Singapore: Mcgraw-Hill, 2001.

[35] J. S. Lee, R. H. French, and L. E. Miller, "Probability of error analyses of a BFSK frequency-hopping system with diversity under partial-band jamming intereference-Part I: Performance of square-law

linear combining soft decision receiver," *IEEE Transaction on Communications*, vol. COM-32, pp. 645–653, June 1984.

[36] J. S. Lee, L. E. Miller, and Y. K. Kim, "Probability of error analyses of a BFSK frequency-hopping system with diversity under partial-band jamming intereference-Part II: Performance of square-law nonlinear combining soft decision receivers," *IEEE Transaction on Communications*, vol. COM-32, pp. 1243–1250, December 1984.

[37] L. E. Miller, J. S. Lee, and A. P. Kadrichu, "Probability of error analyses of a BFSK frequency-hopping system with diversity under partial-band jamming intereference-Part III: Performance of square-law self-normalizing soft decision receiver," *IEEE Transaction on Communications*, vol. COM-34, pp. 669–675, July 1986.

[38] J. S. Bird and E. B. Felstead, "Anti-jam performance of fast frequency-hopped NCFSK-An overview," *IEEE Journal on Selected Areas in Communications*, vol. SAC-4, pp. 216–233, March 1986.

[39] R. C. Robertson and T. T. Hara, "Error probabilities of a fast frequency-hopped FSK receiver with self-normalization combining in a Rician fading channel with partial-band intereference," *IEEE Journal on Selected Areas in Communications*, vol. 10, pp. 714–723, May 1992.

[40] R. C. Robertson and K. Y. Lee, "Performance of a fast frequency-hopped MFSK receiver with linear and self-normalization combining in a Rician fading channel with partial-band intereference," *IEEE Journal on Selected Areas in Communications*, vol. 10, pp. 731–741, May 1992.

[41] K. C. Teh, A. C. Kot, and K. H. Li, "FFT based self-normalising receiver for FFH spread spectrum system," *IEE Proceedings on Communications*, vol. 145, pp. 99–104, April 1998.

[42] K. C. Teh, A. C. Kot, and K. H. Li, "Multitone jamming rejection of FFH/BFSK spread spectrum system over fading channels," *IEEE Transactions on Communications*, vol. 46, pp. 1050–1057, November 1998.

[43] K. C. Teh, A. C. Kot, and K. H. Li, "Performance analysis of FFH/BFSK product combining receivers under multitone jamming," *IEEE Transactions on Vehicular Technology*, vol. 48, pp. 1946–1953, November 1999.

[44] T. A. Gulliver, E. B. Felstead, R. E. Ezers, and J. S. Wright, "A unified approach to time diversity combining of fast frequency hopped NCMFSK - anti-jam processing," in *IEEE Military Communications Conference, MILCOM '94*, vol. 2, pp. 415–420, October 1994.

[45] Y. S. Shen and S. L. Su, "Performance analysis of an FFH/BFSK receiver with ratio-statistic combining in a fading channel with multitone interference ," *IEEE Transactions on Communications*, vol. 51, pp. 1643–1648, October 2003.

[46] K. A. Hamdi and L. Pap, "Multiple-Access Capability of Synchronous FHSS Wireless Networks: An Analysis of the Effects of the Spacing Between Hopping Carriers," *IEEE Transactions on Communications*, vol. 55, pp. 593–604, March 2007.

[47] H. K. Choi and S. W. Kim, "Frequency-hopped multiple-access communication with nonorthogonal BFSK in Rayleigh fading channels," *IEEE Transactions on Communications*, vol. 46, pp. 1478–1483, November 1998.

[48] O. C. Yue, "Maximum likelihood combining for noncoherent and differentially coherent frequency hopping multiple access systems," *IEEE Transactions on Information Theory*, vol. IT-28, pp. 631–639, July 1982.

[49] R. W. Nettleton and G. R. Cooper, "Performance of a frequency-hopped differentially modulated spread-spectrum receiver in a Rayleigh fading channel," *IEEE Transactions on Vehicular Technology*, vol. VT-30, pp. 14 – 29, February 1981.

[50] M. K. Simon and A. Polydoros, "Coherent Detection of Frequency-Hopped Quadrature Modulations in the Presence of Jamming–Part I: QPSK and QASK Modulations," *IEEE Transactions on Communications*, vol. 29, pp. 1644–1660, November 1981.

[51] W. G. Phoel, "Iterative demodulation and decoding of frequency-hopped PSK in partial-band jamming," *IEEE Journal on Selected Areas in Communications*, vol. 23, pp. 1026–1033, May 2005.

[52] R. C. Robertson and T. T. Ha, "Error probabilties of fast frequency-hopped MFSK receiver with noise-normalization combining in a fading channel with partial-band intereference," *IEEE Transactions on Communications*, vol. 40, pp. 404–412, February 1992.

[53] R. C. Robertson, H. Iwasaki, and M. Kragh, "Performance of a fast frequency-hopped non-coherent MFSK receiver with non-ideal adaptive gain control," *IEEE Transactions on Communications*, vol. 46, pp. 104–114, January 1998.

[54] G. Li, Q. Wang, V. Bhargava, and L. J. Mason, "Maximum-likelihood diversity combining in partial-band noise," *IEEE Transactions on Communications*, vol. 46, pp. 1569–1574, December 1998.

[55] S. L. March and J. A. Ritcey, "Performance of an order statistics based diversity combining frequency hopping BFSK system in partial band jamming environment," in *IEEE Proceedings of Pacific Rim Conference on Communications, Computer and Signal Processing*, pp. 107–110, June 1989.

[56] K. C. Teh, A. C. Kot, and K. H. Li, "Partial band jamming rejection of FFH/BFSK with product combining receiver over a Rayleigh-fading channel," *IEEE Communications Letters*, vol. 1, pp. 64–66, May 1997.

[57] T. C. Lim, W. He, and K. Li, "Rejection of partial-band noise jamming with FFH/BFSK product combining receiver over Nakagami-fading channel," *IEEE Communications Letters*, vol. 34, pp. 960 – 961, May 1998.

[58] C.-L. Chang and T.-M. Tu, "Performance analysis of FFH/BFSK product-combining receiver with partial-band jamming over independent Rician fading channels," *IEEE Transactions on Wireless Communications*, vol. 4, pp. 2629–2635, November 2005.

[59] G. Huo and M. S. Alouini, "H-functions and BER analysis of FFH/BFSK with product combining over partial-band jammed Rayleigh fading channels," in *IEEE Vehicular Technology Conference, VTC Fall 2001*, vol. 4, pp. 2374–2378, October 2001.

[60] G. Huo and M. S. Alouini, "BER evaluation of FFH/BFSK with product combining over partial-band jammed Rayleigh fading channels," in *IEEE Military Communications Conference, MILCOM '2000*, vol. 2, pp. 774–778, October 2000.

[61] G. Huo and M. S. Alouini, "Another look at the BER performance of FFH/BFSK with product combining over partial-band jammed Rayleigh fading channels," *IEEE Transactions on Vehicular Technology*, vol. 50, pp. 1203–1215, September 2001.

[62] R. C. Robertson, R. John F, and T. T. Ha, "Error probabilities of fast frequency-hopped FSK with ratio-statistics combining in a fading channel with partial band interference," in *IEEE Military Communications Conference, MILCOM '92*, vol. 3, pp. 865–869, October 1992.

[63] K. C. Teh, A. C. Kot, and K. H. Li, "Error probabilities of FFH/BFSK self-normalizing receivers in a Rician fading channel with multitone jamming," *IEEE Transactions on Communications*, vol. 4, pp. 305–308, February 2000.

[64] K. C. Teh, A. C. Kot, and K. H. Li, "Performance analysis of FFH/BFSK product combining receivers with multitone jamming over Rician fading channels," in *Proceedings of the IEEE Vehicular Technology Conference, Spring 2000*, vol. 2, (Tokyo, Japan), pp. 1508–1512, May 2000.

[65] J. Wang and C. Jiang, "Analytical study of FFH systems with square-law diversity combining in the presence of multitone interference," *IEEE Transactions on Communications*, vol. 48, pp. 1188–1196, July 2000.

[66] C. Jiang and J. Wang, "Performance analysis of FFH/MFSK receivers with self-normalization combining in the presence of multitone jamming," *IEEE Transactions on Vehicular Technology*, vol. 51, pp. 1120–1127, September 2002.

[67] J. J. Chang and L. S. Lee, "An exact performance analysis of the clipped diversity combining receiver for FH/MFSK systems against a band multitone jammer," *IEEE Transactions on Communications*, vol. 42, pp. 700–710, February/March/April 1994.

[68] T. A. Gulliver and E. B. Felstead, "Moment methods for diversity combining of fast frequency hopped non-coherent MFSK," in *IEEE Military Communications Conference, MILCOM '93*, vol. 1, pp. 192–197, October 1993.

[69] T. A. Gulliver and E. B. Felstead, "Nonparametric diversity combining for fast frequency hopping," in *IEEE Military Communications Conference, MILCOM '95*, vol. 1, pp. 60–64, November 1995.

[70] G. L. Orr and B. F. Rice, "Effect of multitone jammers on error rates of fast-hopped MFSK signals with no side information," in *IEEE Military Communications Conference, MILCOM '94*, vol. 3, pp. 801–805, October 1994.

[71] K. C. Teh, A. C. Kot, and K. H. Li, "FFT-based clipper receiver for fast frequency-hopping spread-spectrum system," in *Proceedings of the IEEE Symposium on Circuits and Systems*, vol. 4, pp. 305–308, May-June 1998.

[72] R. E. Ezers, E. B. Felstead, T. A. Gulliver, and J. S. Wright, "An analytical method for linear combining with application to FFH NCFSK receivers," *IEEE Journal on Selected Areas in Communications*, vol. 11, pp. 454–464, April 1993.

[73] Y. Han and K. C. Teh, "Maximum-likelihood receiver with side information for asynchronous FFH-MA/MFSK systems over Rayleigh fading channels," *IEEE Communications Letters*, vol. 10, pp. 435–437, June 2006.

[74] Y. Han and K. C. Teh, "Performance study of suboptimum maximum-likelihood receivers for FFH/MFSK systems with multitone jamming over fading channels," *IEEE Transactions on Vehicular Technology*, vol. 54, pp. 82–90, January 2005.

[75] B. K. Levitt, "FH/MFSK performance in multitone jamming," *IEEE Journal on Selected Areas in Communications*, vol. SAC-3, pp. 627–643, September 1985.

[76] R. C. Robertson and J. F. Sheltry, "Multiple tone interference of frequency-hopped non-coherent MFSK signals transmitted over Rician fading channels," *IEEE Transactions on Communications*, vol. 44, pp. 867–875, July 1996.

[77] Z. Yu, T. T. Tjhung, and C. C. Chai, "Independent multitone jamming of FH/MFSK in Rician channels," *IEEE Transactions on Communications*, vol. 49, pp. 2006–2015, November 2001.

[78] P. J. Crepeau, "Performance of FH/BFSK with generalized fading in worst-case partial-band gaussian interference," *IEEE Transactions on Selected Areas of Communications*, vol. 8, pp. 884–886, June 1990.

[79] T. A. Gulliver and E. B. Felstead, "Anti-jam by fast FH NCFSK - myths and realities," in *IEEE Military Communications Conference, MILCOM '93*, vol. 1, pp. 187–191, October 1993.

[80] V. A. Aalo and J. Zhang, "Performance analysis of maximal ratio combining in the presence of multiple equal-power cochannel interferers in a Nakagami fading channel," *IEEE Transactions on Vehicular Technology*, vol. 50, pp. 497–503, March 2001.

[81] C. R. C. M. daSilva and M. D. Yacoub, "Bit error analysis of equal gain combining reception for Nakagami fading channels: an exact formulation," *Electronics Letters*, vol. 36, pp. 1147–1149, June 2000.

[82] Q. T. Zhang, "Exact analysis of postdetection combining for DPSK and NFSK systems over arbitrarily correlated Nakagami channels," *IEEE Transactions on Communications*, vol. 46, pp. 1459–1467, June 1998.

[83] N. C. Beaulieu and A. A. Abu-Dayya, "Analysis of equal gain diversity on Nakagami fading Channels," *IEEE Transactions on Communications*, vol. 39, pp. 225–234, February 1991.

[84] U. Charash, "Reception through Nakagami fading multipath channels with random delays," *IEEE Transactions on Communications*, vol. 39, pp. 657–670, April 1979.

[85] G. L. Turin, "On optimal diversity reception, II," *IEEE Transactions on Communications*, vol. 10, pp. 22–31, March 1962.

[86] G. L. Turin, "On optimal diversity reception," *IEEE Transactions on Information Theory*, vol. 7, pp. 154–166, July 1961.

[87] D. G. Brennan, "Linear diversity combining techniques," *IEEE Proceedings*, vol. 91, pp. 331–356, February 2003.

[88] M. K. Simon and M. S. Alouini, "A unified approach to the probability of error for noncoherent and differentially coherent modulations over generalized fading channels," *IEEE Transactions on Communications*, vol. 46, pp. 1625–1638, December 1998.

[89] J. Zhang, E. K. P. Ching, and I. Kontoyiannis, "Unified spatial diversity combining and power allocation schemes for CDMA systems," in *IEEE Global Telecommunications Conference, 2000. GLOBECOM '00.*, vol. 3, pp. 1365–1369, Nov-Dec 2000.

[90] M. A. Beach, S. C. Swales, A. Bateman, D. J. Edwards, and J. P. McGeehan, "A diversity combining antenna array for land mobile satellite communications," in *IEEE Vehicular Tecnology Conference, 1989*, vol. 2, pp. 749–756, May 1989.

[91] D. J. Goodman, P. S. Henry, and V. K. Prabhu, "Frequency-hopped multilevel FSK for mobile radio," *Bell System Technical Journal*, vol. 59, pp. 1257–1275, September 1980.

[92] I. Z. Maljevic and M. I.Dukic, "Comparison of FFH FSK nonlinear combining receivers in a fading channel with partial-band interference," in *IEEE Proceedings of 4th International Symposium on Spread Spectrum and Applications, 1996*, vol. 3, pp. 1273–1277, September 1996.

[93] G. Einarsson, "Address assignment for a time-frequency-coded, spread-spectrum system," *Bell System Technical Journal*, vol. 59, pp. 1241–1255, September 1980.

[94] J. Joo, H. Kang, K. Kim, and K. Kim, "Analysis of asynchronous FFH-MA systems with a hard-limited combining in Rayleigh fading," *IEEE Communications Letters*, vol. 9, pp. 295–297, April 2005.

[95] L. ping Zhu, Y. Yao, and Y.-S. Zhu, "Antijam performance of FFH/BFSK with noise-normalization combining in a Nakagami-m fading channel with partial-band interference," *IEEE Communications Letters*, vol. 10, pp. 429–431, June 2006.

[96] Y. T. Su and L. der Jeng, "Antijam capability analysis of RS-coded slow frequency hopped system," *IEEE Transactions on Communications*, vol. 48, pp. 270–281, February 2000.

[97] Y. T. Su and C. Y. Hsiao, "On the detection of a class of fast frequency-hopped multiple access signals," *IEEE Journal on Selected Areas of Communications*, vol. 19, pp. 2151–2164, November 2001.

[98] E. D. Spilchen and T. A. Gulliver, "Diversity combining for $M$-ary fast frequency hopping in a multiple access Rayleigh fading channel," in *IEEE Military Communications Conference, MILCOM '96*, vol. 3, pp. 893–897, October 1996.

[99] L. L. Yang and L. Hanzo, "Low Complexity Erasure Insertion in RS-Coded SFH Spread-Spectrum Communications with Partial-band Interference and Nakagami-m Fading," *IEEE Transactions on Communications*, vol. 50, pp. 914–924, June 2002.

[100] W. E. Stark, "Coding for frequency-hopped spread-spectrum communication with partial-band interference-part I: capacity and cutoff rate," *IEEE Transactions on Communications*, vol. COM-33, pp. 1036–1044, October 1985.

[101] W. E. Stark, "Coding for frequency-hopped spread-spectrum communication with partial-band interference-part I: coded performance," *IEEE Transactions on Communications*, vol. COM-33, pp. 1045–1057, October 1985.

[102] J. H. Kang and W. E. Stark, "Iterative estimation and decoding for FH-SS with slow Rayleigh fading," *IEEE Transactions on Communications*, vol. 48, pp. 2014 – 2023, December 2000.

[103] H. E. Gamal and E. Geraniotis, "Iterative channel estimation and decoding for convolutionally coded anti-jam FH signals," *IEEE Transactions on Communications*, vol. 50, pp. 321–331, February 2002.

[104] J. H. G. Jr. and C. J. Langford, "Iterative demodulation and decoding for a mobile packet system with parallel concatenated trellis-coded modulation," in *IEEE Aerospace Conference Proceedings*, pp. 3.1355–3.1360, 2002.

[105] Q. Zhang and T. Le-Ngoc;, "Turbo product codes for FH-SS with partial-band interference," *IEEE Transactions on Wireless Communications*, vol. 1, pp. 513–520, July 2002.

[106] A. J. Viterbi, "A robust ratio-threshold technique to mitigate tone and partial band jamming in coded MFSK systems," in *IEEE Proceedings of Military Communications Conference Record*, pp. 22.4.1–22.4.5, October 1982.

[107] C. W. Baum and M. B. Pursley, "Bayesian methods of erasure insertion in frequency-hop communication with partial-band interference," *IEEE Transactions on Communications*, vol. 40, pp. 1231–1238, July 1992.

[108] C. W. Baum and M. B. Pursley, "Erasure insertion in frequency-hop communications with fading and partial-band interference," *IEEE Transactions on Communications*, vol. 46, pp. 949 – 956, November 1997.

[109] S. D. Fina, "Bayesian methods for erasure insertion in frequency-hopping multiple access with Rice selective fading," *IEEE Transactions on Communications*, vol. 52, pp. 1616–1620, November 2003.

[110] T. G. Macdonald and M. B. Pursley, "Staggered interleaving and iterative errors-and-erasures decoding for frequency-hop packet radio," *IEEE Transactions on Wireless Communications*, vol. 2, pp. 92 – 98, January 2003.

[111] M. B. Pursley and C. S. Wilkins, "An investigation of relationships between side information and information rate in slow-frequency-hop communications," in *IEEE Military Communications Conference, 1997, MILCOM 97*, vol. 2, pp. 545 – 549, November 1997.

[112] M. B. Pursley and C. S. Wilkins, "A comparison of two methods for erasure generation in frequency-hop communications with partial-band interference and Rayleigh fading," in *Proceedings of IEEE Military Communications Conference, 1996, MILCOM 96*, vol. 1, pp. 85 – 89, October 1996.

[113] G. E. Corazza and S. D. Fina, "On the generation of side information for frequency hopping multiple access in Rice fading," in *IEEE Vehicular Technology Conference, 1997*, vol. 2, pp. 1248–1252, May 1997.

[114] N. Sharma, H. E. Gamal, and E. Geraniotis, "Multiuser demodulation and iterative decoding for frequency-hopped networks," *IEEE Transactions on Communications*, vol. 49, pp. 1437 – 1446, August 2001.

[115] N. Sharma and E. Geraniotis, "Soft multiuser demodulation and iterative decoding for FH/SSMA with a block turbo code," *IEEE Transactions on Communications*, vol. 51, pp. 1561 – 1570, September 2003.

[116] Q. Wang, T. A. Gulliver, V. K. Bhargava, and E. B. Felstead, "Performance of error-erasure-correction decoding of Reed-Solomon codes for frequency-hop communications in multitone jamming," in *IEEE Military Communications Conference, MILCOM '89*, vol. 1, pp. 189–195, October 1989.

[117] L. L. Yang and L. Hanzo, "A residue number system based parallel communication scheme using orthogonal signaling: PartII-Multipath fading channels," *IEEE Transactions on Vehicular Technology*, vol. 51, pp. 1547–1559, November 2002.

[118] I. H. Sneddon, *The use of integral transforms.* New York: Mcgraw-Hill Book Company Inc., 1972.

[119] Y. Han and K. C. Teh, "Error probabilities and performance comparisons of various FFH/MFSK receivers with multitone jamming," *IEEE Transactions on Communications*, vol. 53, pp. 769–772, May 2005.

[120] Y. S. Shen and S. L. Su, "Performance analysis of an FFH/BFSK receiver with product-combining in a fading channel under multitone interference," *IEEE Transactions on Wireless Communications*, vol. 3, pp. 1867–1872, November 2004.

[121] M. D. Springer, *The algebra of random variables.* New York: John Wiley and Sons, 1979.

[122] M. Abramowitz and I. A. Stegun, *Handbook of mathematical functions.* New York: Dover Publications, Inc., 1970.

[123] P. Galambos and I. Simonelli, *Products of Random Variables: Applications to problems of physics and to arithmetical functions.* New York: Marcel Dekker Inc., 2004.

[124] H. Bateman, *Tables of integral transforms, Volume I.* New York: Mcgraw-Hill Book Company Inc., 1954.

[125] S. Lang, *Complex analysis.* New York: Springer-Verlag New York, Inc., 1999.

[126] S. Ahmed, L. L. Yang, and L. Hanzo, "Mellin Transform Based Performance Analysis of Fast Frequency Hopping Using Product Combining," in *Proceedings of the IEEE Vehicular Technology Conference, 2006. VTC Spring, 2006*, vol. 4, pp. 1635– 1639, May 2006.

[127] S. Ahmed, L. L. Yang, and L. Hanzo, "Mellin Transform Based Performance Analysis of FFH M-ary FSK Using Product Combining Against Partial Band Noise Jamming," in *Proceedings of the IEEE Vehicular Technology Conference, 2007. VTC Spring, 2007*, pp. 1901 – 1905, April 2007.

[128] A. M. Mathai, "Products and ratios of generalized gamma variates," *Skandinavisk Aktuarietidskrif*, no. 55, pp. 193–198, 1972.

[129] R. B. Paris and D. Kaminski, *Asymptotics and Mellin-Barnes Integrals.* Cambridge: Cambridge University Press, 2001.

[130] J. Blumlein and S. Kurth, "Harmonic sums and Mellin transforms up to two-loop order," *Physical Review HEP-PH/9810241*, vol. 60, pp. 1–31, June 1998.

[131] Y. Sheng and C. Lejeune, "Invariant pattern recognition using Fourier-Mellin transforms and neural networks," *Journal of Optics*, vol. 22, pp. 223–228, Septemeber-October 1991.

[132] R. J. Sasiela and J. D. Shelton, "Mellin transform methods applied to integral evaluation: Taylor series and asymptotic approximations," *Journal of Mathematical Physics*, vol. 34, pp. 2572–2617, June 1993.

[133] R. Janaswamy, "Analytical Expressions for the Ergodic Capacities of Certain MIMO Systems by the Mellin Transform," in *Conference Record / IEEE Global Telecommunications Conference*, vol. 1, pp. 287–291, 2003.

[134] J. Bertrand, P. Bertrand, and J. P. Ovarlez, "Discrete Mellin transform for signal analysis," in *ICASSP 90. 1990 International Conference on Acoustics, Speech and Signal Processing*, vol. 3, pp. 1603–1606, October 1990.

[135] H. Serretta and M. R. Inggs, "Ship target recognition with the Mellin Transform aided by neural networks," in *Proceedings of the South African Symposium on Communications and Signal Processing, COMSIG, 1998*, pp. 203–208, 1998.

[136] J. S. Lee, J. M. Burke, and J. K. Hammond, "The theoretical prediction, interpretation and computation of the Fourier-Mellin transform applied to sonar classification of ships," in *ICASSP 90. 1990 International Conference on Acoustics, Speech and Signal Processing*, vol. 5, pp. 203–208, 2735-2738 1990.

[137] J. C. Terrillon, D. McReynolds, M. Sadek, Y. Sheng, and S. Akamatsu, "Invariant neural-network based face detection with orthogonal Fourier-Mellin moments," in *Proceedings 15th International Conference on Pattern Recognition. ICPR-2000*, vol. 2, pp. 993–1000, 2000.

[138] A. T. B. Jin, D. N. C. Ling, and O. T. Song, "An efficient fingerprint verification system using integrated wavelet and Fourier-Mellin invariant transform," *Image and Vision Computing*, vol. 22, pp. 503–513, June 2004.

[139] A. D. Sena and D. Rocchesso, "A fast Mellin transform with applications in DAFX," in *7th International Conference on Digital Audio Effects, DAFx'04*, pp. 65–69, October 2004.

[140] T. Irino, R. D. Patterson, and H. Kawahara, "Auditory vocoder: speech resynthesis from an auditory Mellin representation," in *2002 IEEE International Conference on Acoustics, Speech, and Signal Processing*, vol. 2, pp. 1921–1924, 2002.

[141] U. C. Fiebig, "The efficiency of FFH/CDMA systems in a mobile radio environment," in *SUPERCOMM/ICC'94 Conference Record*, vol. 1, pp. 525–529, May 1994.

[142] O. C. Yue, "Performance of frequency-hopping multiple-access multilevel FSK systems with hard-limited and linear combining," *IEEE Transactions on Communications*, vol. COM-29, pp. 631–639, November 1981.

[143] U. C. Fiebig, "Iterative interference cancellation for FFH/MFSK MA systems," in *IEEE Proceedings of International Conference on Communications*, pp. 90–95, December 1996.

[144] K. W. Halford and M. B. Pearce, "Multistage multiuser detection for FHMA," *IEEE Transactions on Communications*, vol. 48, pp. 1550–1562, September 2000.

[145] C. P. Hung and Y. T. Su, "Diversity combining considerations for incoherent frequency hopping multiple access systems," *IEEE Journal on Selected Areas of Communications*, vol. 13, pp. 333–344, February 1995.

[146] U. Timor, "Improved decoding for frequency-hopped multilevel FSK system," *Bell System Technical Journal*, vol. 59, pp. 1839–1855, December 1980.

[147] U. Timor, "Multi-stage decoding of frequency-hopped multilevel FSK system," *Bell System Technical Journal*, vol. 60, pp. 471–483, April 1981.

[148] T. Mabuchi, R. Kohno, and H. Imai, "Multiuser detection scheme based on cancelling cochannel interference for MFSK/FH-SSMA system," *IEEE Journal on Selected Areas of Communications*, vol. 12, pp. 593–604, February 1995.

[149] U. C. Fiebig, "An algorithm for joint detection in fast frequency hopping systems," *IEEE Proceedings on Communications*, vol. 143, pp. 380–388, December 1996.

[150] R. J. Kozick and B. M. Sadler, "Maximum likelihood multi-user detection fast frequency hopping/Multiple frequency shift keying systems," in *IEEE Wireless Communications and Networking Conference*, vol. 1, pp. 67–72, September 2000.

[151] E. V. Maniati, "Multiuser robust detection for frequency hopped signals in non-Rayleigh fading channels," in *IEEE Military Communications Conference, 2003. MILCOM 2003.*, vol. 1, pp. 369–374, October 2003.

[152] R. A. Iltis, J. A. Ritcey, and L. B. Milstein, "Interference rejection in FFH systems using least squares estimation techniques," *IEEE Transactions on Communications*, vol. 38, pp. 2174–2183, December 1990.

[153] S.-Y. Lin, G.-C. Yang, S.-C. Tseng, and C.-F. Hong, "Improved cochannel interference cancellation for MFSK/FH-SSMA systems," *IEEE Journal on Selected Areas in Communications*, vol. 17, pp. 1940 – 1952, November 1998.

[154] K. Hamaguchi, L. L. Yang, and L. Hanzo, "On the performance of multi-stage multi-user detection assisted fast-FH/MFSK," in *Proceedings of IEEE Vehicular Technology Conference, 2003, VTC2003-Spring*, vol. 4, pp. 2798 – 2802, April 2003.

[155] H. Zhang, H. Yang, R. Luo, and H. Wang, "Improved multiuser detector for fast FH/MFSK systems with soft-limiter," in *IEEE International Symposium on Microwave, Antenna, Propagation and EMC Technologies for Wireless Communications, 2005. MAPE 2005.*, vol. 2, pp. 1464–1467, August 2005.

[156] X. Wang, S. Zhu, and D. Sun, "Cochannel interference cancellation for frequency hopped multiple access systems," in *IEEE Eighth International Symposium on Spread Spectrum Techniques and Applications, 2004.*, pp. 42–46, August 2004.

[157] S. ten Brink, "Convergence behavior of iteratively decoded parallel concatenated codes," *Electronics Letters*, vol. 35, pp. 1117 – 1119, June 1999.

[158] S. ten Brink, "Convergence of iterative decoding," *IEEE Transactions on Communications*, vol. 49, pp. 1727 – 1737, October 2001.

[159] P. C. P. Liang and W. E. Stark, "Algorithm for joint decoding of turbo codes and M-ary orthogonal modulation," in *IEEE International Symposium on Information Theory, 2000*, p. 191, June 2000.

[160] M. C. Valenti, E. Hueffmeier, B. Bogusch, and J. Fryer, "Towards the capacity of noncoherent orthogonal modulation: BICM-ID for turbo coded NFSK," in *IEEE Conference on Military Communications, 2004. MILCOM 2004*, vol. 3, pp. 1549 – 1555, October-November 2004.

[161] M. C. Valenti and S. Cheng, "Iterative demodulation and decoding of turbo-coded M-ary noncoherent orthogonal modulation," *IEEE Journal on Selected Areas inCommunications*, vol. 23, pp. 1739 – 1747, September 2005.

[162] J. Hagenauer, "Forward error correcting for CDMA systems," in *IEEE 4th International Symposium on Spread Spectrum Techniques and Applications Proceedings, 1996*, vol. 2, pp. 566 – 569, September 2001.

[163] H. V. Poor, "Iterative multiuser detection," *IEEE Signal Processing Magazine*, vol. 21, pp. 81 – 88, January 2004.

[164] L. Hanzo, L.-L. Yang, E.-L. Kuan, and K. Yen, *Single- and Multi-Carrier DS-CDMA: Multi-User Detection, Space-Time Spreading, Synchronisation, Networking and Standards*. New York: John Wiley and Sons, England, 2003.

[165] Y. T. Su and R. C. Chang, "Performance of fast FH/MFSK Signals in jammed binary channels," *IEEE Transactions on Communications*, vol. 42, pp. 2414 – 2422, July 1994.

[166] B. M. Peric, M. R. Souryal, E. Larsson, and B. R. Vojcic, "Soft Decision Metrics for Turbo-coded FH M-FSK Ad Hoc Packet Radio Networks," in *IEEE 61st Vehicular Technology Conference, Spring 2005*, vol. 2, pp. 724 – 727, May-June 2005.

[167] N. Chayat, "Turbo codes for incoherent M-ary orthogonal signaling," in *Nineteenth Convention of Electrical and Electronics Engineers in Israel, 1996.*, vol. 3, pp. 471–474, November 1996.

[168] A. Rahman and K. Elhakeem, "Concatenated combined modulation and coding of frequency hopping multiaccess systems," *IEEE Transactions on Selected Areas in Communications*, vol. 8, pp. 650 – 662, May 1990.

[169] C. D. Frank and M. B. Pursley, "Concatenated coding for frequency-hop spread-spectrum with partial-band interference," *IEEE Transactions on Communications*, vol. 44, pp. 589 – 596, May 1996.

[170] M. D. Theodoss and R. C. Robertson, "Performance of the FFH/BFSK self-normalized receiver with convolutional coding and soft decision decoding over Rician fading channels with partial-band noise interference," in *IEEE Military Communications Conference, 1996. MILCOM '96*, vol. 2, pp. 436–441, October 1996.

[171] U. C. Fiebig, "Soft-decision and erasure decoding in fast frequency-hopping systems with convolutional, turbo, and Reed-Solomon codes," *IEEE Transactions on Communications*, vol. 47, pp. 1646 – 1654, November 1999.

[172] C. Durand, J. Boutros, and E. Bejjani, "Forward error correction of FSK alphabets for noncoherent transmissions over AWGN channel," *IEEE Communications Letters*, vol. 4, pp. 318–320, October 2000.

[173] A. Pouttu, "Performance simulations of coded slow frequency hopping M-ary FSK with sub-optimal soft decision metrics in partial band interference," in *Seventh IEEE International Symposium on Personal, Indoor and Mobile Radio Communications, 1996*, vol. 3, pp. 1097 – 1101, October 1996.

[174] Y. Kim and K. Cheun, "Performance of soft metrics for convolutional coded asynchronous fast FHSS-MA networks using BFSK under Rayleigh fading," *IEEE Transactions on Communications*, vol. 51, pp. 5 – 7, January 2003.

[175] D. Park and B. G. Lee, "Iterative decoding in convolutionally and turbo coded MFSK/FH-SSMA systems," in *IEEE International Conference on Communications, ICC 2001*, vol. 9, pp. 2784 – 2788, June 2001.

[176] J. S. G. Panaro, "Simplified Soft-Output Demapper for Bit-Interleaved Coded Orthogonal Modulation," in *International Conference on Wireless and Mobile Communications, 2006. ICWMC '06.*, pp. 71–71, June 2006.

[177] L. Hanzo, T. H. Liew, and B. L. Yeap, *Turbo Coding, Turbo Equalisation and Space-Time Coding for Transmission over Fading Channels.* England: John Wiley and Sons, England, 2002.

[178] J. Hagenuaer, "The turbo principle in mobile communications," in *International Symposium on Information Theory and Its Applications*, (Xi'an, China), October 2002.

[179] A. Ashikhmin, G. Kramer, and S. ten Brink, "Extrinsic information transfer functions: model and erasure channel properties," *IEEE Transactions on Information Theory*, vol. 49, pp. 445 – 454, November 2004.

[180] G. Lechner, J. Sayir, and I. Land, "Optimization of LDPC Codes for Receiver Frontends," in *IEEE International Symposium on Information Theory. ISIT 2006*, pp. 2388 – 2392, July 2006.

[181] W. E. Ryan and A. Ghrayeb, "Precoder design for concatenating convolutional codes with intersymbol interference channels," in *IEEE Wireless Communications and Networking Conference, 2000. WCNC 2000*, vol. 3, pp. 1013 – 1018, September 2000.

[182] W. E. Ryan, "Concatenated codes for class IV partial response channels," *IEEE Transactions on Communications*, vol. 49, pp. 445 – 454, March 2001.

[183] R. Y. S. Tee, S. X. Ng, and L. Hanzo, "Precoder-aided iterative detection assisted multilevel coding and three-dimensional EXIT-chart analysis," in *IEEE Wireless Communications and Networking Conference, 2006. WCNC 2006*, vol. 3, pp. 1322–1326, April 2006.

[184] D. Divsalar, S. Dolinar, and F. Pollara, "Serial concatenated trellis coded modulation with rate-1 inner code," in *IEEE Global Telecommunications Conference, 2000. GLOBECOM '00.*, vol. 2, pp. 777 – 782, November-December 2000.

[185] M. Tüchler and J. Hagenauer, "EXIT charts of irregular codes," in *Conference on Information Sciences and Systems*, (Princeton, NJ), pp. 748–753, March 2002.

[186] J. Wang, S. X. Ng, A. Wolfgang, L.-L. Yang, S. Chen, and L. Hanzo, "Near-capacity three-stage MMSE turbo equalization using irregular convolutional codes," in *International Symposium on Turbo Codes*, (Electronic publication, Munich Germany), April 2006.

[187] L. Hanzo, L. L. Yang, A. Q. Pham, and J. Wang, "An Iterative Detection Aided Irregular Convolutional Coded Wavelet Videophone Scheme Using Reversible Variable-Length Codes and Map Equalization," in *IEEE Vehicular Technology Conference, VTC Spring 2007*, pp. 2404 – 2408, April 2007.

[188] R. G. Maunder, J. Wang, S. X. Ng, L.-L. Yang, and L. Hanzo, "Iteratively Decoded Irregular Variable Length Coding and Trellis Coded Modulation," in *(to appear in) IEEE Workshop on Signal Processing Systems*, (Shanghai, China), October 2007.

[189] V. Buttigieg and P. G. Farrell, "Variable-length error-correcting codes," *IEE Proceedings on Communications*, vol. 147, pp. 211–215, August 2000.

[190] V. B. Balakirsky, "Joint source-channel coding with variable length codes," in *IEEE International Symposium on Information Theory*, (Ulm, Germany), p. 419, June 1997.

[191] R. Bauer and J. Hagenauer, "On variable length codes for iterative source/channel decoding," in *Data Compression Conference*, (Snowbird, UT), pp. 273–282, March 2001.

[192] R. Bauer and J. Hagenauer, "Iterative source/channel-decoding using reversible variable length codes," in *Data Compression Conference*, (Snowbird, UT, USA), pp. 93–102, 2000.

[193] S. Lloyd, "Least squares quantization in PCM," *IEEE Transactions on Information Theory*, vol. 28, no. 2, pp. 129–137, 1982.

[194] S. Ahmed, L. L. Yang, and L. Hanzo, "Successive Interference Cancellation in Clipped and Product Combining aided FFH Multi-User Systems," in *Proceedings of the IEEE Vehicular Technology Conference, 2006.*, vol. 5, pp. 2188–2192, May 2006.

[195] S. Ahmed, S. X. Ng, L. L. Yang, and L. Hanzo, "Iterative Decoding and Soft Interference Cancellation in Fast Frequency Hopping Multiuser System Using Clipped Combining," in *Proceedings of the IEEE Wireless Communications and Networking Conference, WCNC 2007.*, pp. 723 – 728, March 2007.

[196] R. G. Gallager, *Low Density Parity Check Codes - No. 21 in Research Monograph Series.* Cambridge, Mass.: MIT Press, 1963.

[197] R. G. Gallager, "Low-density parity-check codes," *IRE Transactions on Information Theory*, vol. 8, pp. 21–28, January 1962.

[198] D. J. C. MacKay and R. M. Neal, "Near Shannon limit performance of low density parity check codes," *Electronics Letters*, vol. 32, August 1996.

[199] F. Guo and L. Hanzo, "Low complexity non-binary LDPC and modulation schemes communicating over MIMO channels," in *Proceedings of IEEE Vehicular Technology Conference, 2004, VTC2004-Fall*, vol. 2, pp. 1294 – 1298, September 2004.

[200] A. Bennatan and D. Burshtein, "Design and analysis of nonbinary LDPC codes for arbitrary discrete-memoryless channels," *IEEE Transactions on Information Theory*, vol. 52, pp. 549 – 583, February 2006.

[201] M. C. Dabey and D. Mackay, "Low-density parity check codes over GF(q)," *IEEE Communications Letters*, vol. 2, pp. 165 – 167, June 1998.

[202] K. Cheun and W. E. Stark, "Performance of robust metrics with convolutional coding and diversity in FHSS systems under partial-band noise jamming," *IEEE Transactions on Communications*, vol. 41, pp. 200 – 209, January 1993.

[203] M. Win and R. Scholtz, "Ultra-wide bandwidth time-hopping spread-spectrum impulse radio for wireless multiple-access communications," *IEEE Transactions on Communications*, vol. 48, pp. 679–689, April 2000.

[204] M. Win and R. Scholtz, "Evaluation of an ultra-wide-band propagation channel," *IEEE Transactions on Communications*, vol. 50, pp. 561–570, May 2002.

[205] S. M. Alamouti, "A simple transmit diversity technique for wireless communications," *IEEE Journal on Selected Areas of Communications*, vol. 16, pp. 1451–1458, October 1998.

[206] V. Tarokh, H. Jafarkhani, and A. R. Calderbank, "Space-time block codes from orthogonal designs," *IEEE Transactions on Information Theory*, vol. 45, pp. 1456 – 1467, July 1999.

[207] V. Tarokh and H. Jafarkhani, "A differential detection scheme for transmit diversity," *IEEE Journal on Selected Areas of Communications*, vol. 18, pp. 1169 – 1174, July 2000.

[208] S. J. Johnson and S. R. Weller, "Constructions for irregular repeat-accumulate codes," in *International Symposium on Information Theory, 2005. ISIT 2005*, vol. 2, pp. 179–183, September 2005.

[209] F. Peng, M. Yang, and W. E. Ryan, "Simplified eIRA code design and performance analysis for correlated Rayleigh fading channels," *IEEE Transactions on Wireless Communications*, vol. 5, pp. 720 – 725, April 2006.

[210] A. Roumy, S. Guemghar, G. Caire, and S. Verdu, "Design methods for irregular repeat-accumulate codes," *IEEE Transactions on Information Theory*, vol. 50, pp. 1711 – 1727, August 2004.

[211] A. Abbasfar, D. Divsalar, and K. Yao, "Accumulate-Repeat-Accumulate Codes," *IEEE Transactions on Communications*, vol. 55, pp. 692 – 702, April 2007.

# Index

## O



## P



## Q



## R



## S



## U



## V

# Author Index

## D



## E



## F



## G

## H



## I



## J

## K



## L

## R



## S

## T



## V



## W



## X



## Y

## Z